

Copyright  
by  
Young Jae Choi  
2007

**The Dissertation Committee for Young Jae Choi Certifies that this is the approved  
version of the following dissertation:**

**Reliability Assessment of Foundations for Offshore Mooring Systems  
under Extreme Environments**

**Committee:**

---

Robert B. Gilbert, Supervisor

---

Kenneth H. Stokoe II

---

Jorge G. Zornberg

---

Lance Manuel

---

Larry W. Lake

**Reliability Assessment of Foundations for Offshore Mooring Systems  
under Extreme Environments**

**by**

**Young Jae Choi, B.E., M.S.**

**Dissertation**

Presented to the Faculty of the Graduate School of

The University of Texas at Austin

in Partial Fulfillment

of the Requirements

for the Degree of

**Doctor of Philosophy**

**The University of Texas at Austin**

**August 2007**

## **Dedication**

This dissertation is dedicated to my faithful family  
Yoon Ki Choi, Gui Ja Kim, Mi Kyung Choi, Kyung Min Choi and Yun Seo Choi

more to my lovely wife and son

Sang Hyun Lee

Joshua Ji-Wan Choi

most to my God who has guided and helped me

## **Acknowledgements**

From the bottom of my heart, I would like to express my sincere gratitude to my advisor, Dr. Robert Gilbert, for his valuable guidance and support throughout my doctoral study. I am not able to express my appreciation in a single word. I am also sincerely grateful to Drs. Kenneth Stokoe, Jorge Zornberg, Lance Manuel and Larry Lake for reviewing the dissertation.

I am indebted to Sanyam Dangayach for his assistance and valuable contributions throughout the early stage of this research and to the Offshore Technology Research Center for providing financial support for this study.

I want to thank administrative staff Teresa Tice-Boggs and Chris Trevino from the Geotechnical Engineering Center.

Special thanks are also expressed to John McCartney for his valuable help with technical writing and Kenneth Kniss for his generous encouragement during the final stage of writing.

Sincere gratitude is also expressed to the Korean student fellows in geotechnical engineering for their continuous encouragement and emotional help during the last five years.

Finally, I would like to express my deep and sincere gratitude to my parents Yoon Ki Choi and Gui Ja Kim, my wife Sang Hyun Lee, my son Joshua Ji-wan Choi, and my

sisters Mi Kyung Choi and Kyung Min Choi for their patience, encouragement, and their unlimited love and support throughout my graduate study. Without their continuous prayers to God, I could not have made this dissertation.

Young Jae Choi

The University of Texas at Austin

August, 2007

# **Reliability Assessment of Foundations for Offshore Mooring Systems under Extreme Environments**

Publication No. \_\_\_\_\_

Young Jae Choi, Ph.D.

The University of Texas at Austin, 2007

Supervisor: Robert B. Gilbert

Mooring systems for floating facilities that are used offshore to produce oil and gas, consisting of individual mooring lines and foundations, are currently designed on the basis of individual components and on a case-by-case basis. The most heavily loaded line and anchor are checked under extreme loading conditions (hurricane and loop current) with the system of lines intact and with one line removed. However, the performance of the entire mooring system depends more directly on the performance of the system of lines and foundations rather than on the performance of a single component.

In this study, a floating production system design originally developed by the industry consortium, DeepStar, was chosen for study. The mooring system was designed for three different nominal water depths: 1000, 2000 and 3000 m. It is a classic spar with steel mooring lines in 1000 m of water and polyester mooring lines in deeper depths.

Based on simulated results of loads on mooring lines and foundations using a numerical model, reliability analyses were conducted using representative probabilistic descriptions of the extreme met-ocean conditions, hurricanes and loop currents, in the

Gulf of Mexico. The probability of failure of individual mooring line components during a 20-year design life is calculated first, followed by that of a complete mooring line which consists of top and bottom chains, a steel cable or polyester rope at the middle and a suction caisson foundation, and finally that of the mooring system.

It is found that foundations have failure probabilities that are more than an order of magnitude smaller than those for lines under extreme loading. Mooring systems exhibit redundancy in that the failure of the most heavily loaded component during an extreme event does not necessarily lead to failure of the system. The system reliability and redundancy are greater for the taut versus semi-taut systems and is greater for designs governed by loop current versus hurricane events. Although this study concerns about the mooring systems of a classical spar, the methodology of the reliability analysis and the conclusions made in this study may have important implications to the other deepwater mooring systems.



## Table of Contents

List of Tables .....	xiii
List of Figures .....	xvi
Chapter 1: Introduction .....	1
1.1 Motivation for Research .....	1
1.2 Objectives and Approach of Research .....	3
1.3 Organization of Dissertation .....	4
Chapter 2: Offshore Structure and Generic Soil Profile in the Gulf of Mexico used in this Study .....	6
2.1 Introduction .....	6
2.2 Description of the Study Spar and Mooring System .....	8
2.3 Generic Soil Profile in the GOM .....	14
2.4 Summary .....	14
Chapter 3: Mooring Line and Offshore Foundation Loads under Extreme Environmental Loadings .....	16
3.1 Introduction .....	16
3.2 Methods of Estimating Environmental Loads on the Study Spar .....	16
3.2.1 Aerodynamic (wind) loads .....	17
3.2.2 Wave and current loads .....	17
3.2.3 Analysis model for estimating mooring line loads – COUPLE6D .....	18
3.3 Characterization of Environmental Loading Conditions .....	20
3.3.1 Sea state parameters .....	21
3.3.2 Example of loading history of mooring lines during a hurricane event .....	23
3.3.3 Example of loading history of mooring lines during a loop current event .....	26
3.3.4 Probability distribution used for Hurricanes .....	29
3.3.5 Probability distribution used for Loop currents .....	30
3.4 Methodology for Probability Distribution of Maximum Line Loads .....	38

3.4.1 Step 1: Relationship between the maximum load and the sea state.....	40
3.4.1.1 Theoretical background for probability distribution of maximum loads.....	40
3.4.1.2 Estimation of the maximum load in a given sea state.....	41
3.4.1.3 Examples of Step 1 .....	43
3.4.2 Step 2: Reliability contours for probabilities of non-exceedance storm events for a specified design life.....	45
3.4.2.1 Relationship between storm frequency and storm severity .....	45
3.4.2.2 Probability of exceedance during a storm.....	47
3.4.2.3 Example of Step 2.....	49
3.4.3 Step 3: Probability distributions for maximum loads .....	51
3.5 Uncertainty in Line Loads .....	56
3.5.1 Uncertainty in model parameters .....	56
3.5.2 Total uncertainty in maximum line loads .....	60
3.6 Line Load.....	61
3.7 Foundation Load.....	64
3.7.1 Interaction among mooring lines, caisson and seabed soils .....	65
3.7.2 Parametric study on padeye loads.....	67
3.7.3 Relationship between loads at the padeye and at the mudline.....	68
3.7.4 Design foundation loads .....	73
3.7.5 Bias and c.o.v values for foundation loads .....	74
Chapter 4: Models for Line and Foundation Capacities .....	78
4.1 Introduction.....	78
4.2 Line Capacity.....	78
4.2.1 Factored loads for design.....	78
4.2.2 Models for line capacity.....	81
4.2.2.1 Model for chain.....	83
4.2.2.2 Model for wire and polyester ropes .....	85
4.2.2.3 Comparison of probability distributions for capacities of the mostly loaded mooring line .....	86
4.3 Foundation Capacity .....	90
4.3.1 Factored loads for design.....	90

4.3.2 Model for estimating axial capacity of a suction caisson in normally consolidated clay.....	94
4.3.3 Model for estimating lateral capacity of a suction caisson in normally consolidated clay .....	96
4.3.4 Model for estimating combined capacity at padeye in normally consolidated clay.....	98
4.3.4.1 Theoretical background on calculating combined capacity at padeye .....	99
4.3.4.2 Effect of design parameters and soil properties on the combined capacity at Padeye .....	104
4.3.4.3 Simplified model for estimating combined capacity at padeye	106
4.3.5 Model for estimating combined capacity at mudline.....	112
4.4 Design Chart for Capacities of Suction Caissons .....	121
4.5 Bias and c.o.v Values for the Predicted Foundation Capacities .....	124
4.6 Lower Bound Foundation Capacity .....	127
4.7 Probabilistic Description of Foundation Capacities .....	128
Chapter 5: Framework for Reliability Analysis.....	130
5.1 Introduction.....	130
5.2 Framework for Component Reliability Calculations.....	130
5.2.1 Assessment of probability of failure with general distributions .....	130
5.2.2 Assessment of probability of failure with normal or lognormal distributions.....	132
5.2.3 Relationship between the median and mean factors of safety .....	136
5.2.4 Mooring line reliability .....	137
5.3 Reliability Assessment for Distributions with a Lower Bound .....	139
5.4 Examples of Component Reliability .....	140
5.5 Framework for System Reliability Calculations.....	144
5.5.1 Definition of system failure .....	144
5.5.2 System reliability calculation.....	144
5.5.3 System redundancy .....	147
5.6 Examples of System Reliability .....	149

Chapter 6: Results and Comparisons of Reliability Analysis of the Study Spar under Extreme Environmental Conditions.....	151
6.1 Introduction.....	151
6.2 Bias and c.o.v values for foundations .....	151
6.3 Component Reliability .....	153
6.4 Effect of Lower Bound Capacity on Reliability .....	159
6.5 Effect of Factor of Safety on Reliability.....	162
6.6 System Reliability .....	165
6.7 Comparison of Results to Industry Targets .....	173
6.8 Comparisons of the Actual Performances of Floating Systems in Hurricanes.....	179
6.8.1 Noble Jim Thompson.....	180
6.8.2 Deepwater Nautilus.....	184
6.8.3 Comparisons of the predicted vs. actual performances of deepwater facilities.....	187
6.9 Summary .....	187
Chapter 7: Summary, Conclusions and Implications.....	189
7.1 Summary .....	189
7.2 Conclusions.....	192
7.3 Implications of this Research.....	193
References.....	195
Vita .....	203

## List of Tables

Table 2.1: Main specification of the study spar .....	9
Table 2.2: Mooring system specifications .....	9
Table 2.3: Design information for hurricane and current dominant conditions .....	10
Table 3.1: Parameters characterizing Type II and Weibull distributions depending on loop current frequencies.....	37
Table 3.2: Annual median values for $H_s$ and $T_p$ .....	37
Table 3.3: Sea states used in the numerical model for the case of loop current .....	38
Table 3.4: Summary of the percentile loads at fairlead and mudline in 1,000 m, 2,000 m and 3,000 m under a hurricane event.....	55
Table 3.5: Summary of the percentile loads at fairlead and mudline in 1,000 m, 2,000 m and 3,000 m under a loop current event (Type II distribution).....	55
Table 3.6: Summary of the percentile loads at fairlead and mudline in 1,000 m, 2,000 m and 3,000 m under a loop current event (Weibull Distribution).....	56
Table 3.7: Sensitivity of expected maximum load to model parameters- Line No. 8 (1,000 m).....	59
Table 3.8: Nominal line load at the fairlead in three water depths under hurricane conditions .....	62
Table 3.9: Nominal line load at the fairlead in three water depths under loop current conditions .....	63
Table 3.10: Comparison of the ratio of median to nominal design line loads in three water depths under different environmental conditions.....	64
Table 3.11: Nominal foundation load at the padeye in three water depths under hurricane conditions.....	73

Table 3.12: Nominal foundation load at the padeye in three water depths under loop current conditions.....	73
Table 3.13: Comparison of the ratio of median to design foundation loads in three water depths under different environmental conditions.....	74
Table 3.14: Summary of the percentile loads at padeye in 1,000 m, 2,000 m and 3,000 m under a hurricane event.....	75
Table 3.15: Summary of the percentile loads at padeye in 1,000 m, 2,000 m and 3,000 m under a loop current event (Type II distribution) .....	76
Table 3.16: Summary of the percentile loads at padeye in 1,000 m, 2,000 m and 3,000 m under a loop current event (Weibull distribution) .....	76
Table 4.1: Comparison of factors of safety for mooring line design for intact and damaged conditions used in different design codes.....	79
Table 4.2: Nominal line capacity and design governing case under hurricane conditions.....	81
Table 4.3: Nominal line capacity and design governing case under loop current conditions.....	81
Table 4.4: Nominal foundation capacity at the padeye and design governing case under hurricane conditions with an intact factor of safety of 2.0 .....	91
Table 4.5: Nominal foundation capacity at the padeye and design governing case under hurricane conditions with an intact factor of safety of 2.5 .....	91
Table 4.6: Nominal foundation capacity at the padeye and design governing case under hurricane conditions with an intact factor of safety of 3.0 .....	92
Table 4.7: Nominal foundation capacity at the padeye and design governing case under loop current conditions with an intact factor of safety of 2.0 .....	92

Table 4.8: Nominal foundation capacity at the padeye and design governing case under loop current conditions with an intact factor of safety of 2.5 .....	93
Table 4.9: Nominal foundation capacity at the padeye and design governing case under loop current conditions with an intact factor of safety of 3.0 .....	93
Table 4.10: Contribution of each component to total axial uplift capacity ( $L/d = 6$ ) .....	95
Table 4.11: Contribution of a friction coefficient to ultimate lateral load ( $L_i = 0.67 L$ ) ...	98
Table 5.1: Probability of failure for a case of $FS_{\text{median}} = 4$ using Equation 5.4 .....	133
Table 5.2: Probability of failure for a case of $FS_{\text{median}} = 4$ using Equation 5.5 .....	134
Table 5.3: Relationship between reliability index, reliability and probability of failure.	135
Table 5.4: Comparison of reliabilities of foundations subject to uplift failure vs combined failure modes in 1,000 m of water under a hurricane event.....	141
Table 6.1: Bias and c.o.v values for the heavily loaded mooring line in study spar in hurricane and current conditions.....	152
Table 6.2: Bias and c.o.v values for the foundation for study spar in hurricane and current conditions.....	152

## List of Figures

Figure 1.1: Offshore Structures (from Mineral Management Services, <a href="http://www.mms.gov">www.mms.gov</a> ).....	2
Figure 2.1: Example of a typical spar in 3,000 m of water (Image taken from website: <a href="http://www.ocsbbs.com">http://www.ocsbbs.com</a> ) .....	7
Figure 2.2: Example of suction caissons (from Andersen et al., 2005) .....	7
Figure 2.3: Spread mooring system .....	10
Figure 2.4: Schematic graphs (a) for spread of a mooring line system (Photo courtesy of Dr.Gilbert) and (b) comparing a catenary mooring system and a taut mooring system (Image taken from Murff and Young, 2007).....	11
Figure 2.5: Relative directions among a loop current, wave and wind under a hurricane condition .....	12
Figure 2.6: The profile of current velocity for a mooring system analysis during a hurricane event.....	12
Figure 2.7: Relative directions among a loop current, wave and wind under a loop current condition .....	13
Figure 2.8: The profile of current velocity for three different water depths during a loop current event .....	13
Figure 2.9: Soil boring at study spar site in the Gulf of Mexico .....	14
Figure 3.1: Example of wave frequency spectrum for a storm event ( $H_s=9.32$ m, $T_p=$ 12.64 sec) .....	23
Figure 3.2: Time-varying loads of the most heavily loaded line at the fairlead in 1,000 m ( $H_s = 12.5$ m and $T_p=14.4$ sec).....	24
Figure 3.3: Time-varying loads of the most heavily loaded line at the fairlead in 2,000 m ( $H_s = 12.5$ m and $T_p=14.4$ sec).....	24



Figure 3.4: Time-varying loads of the most heavily loaded line at the fairlead in 3,000 m ( $H_s = 12.5$ m and $T_p = 14.4$ sec).....	25
Figure 3.5: Comparison of tensions and angles at the mudline in three different water depths for intact case during a hurricane event ( $H_s = 12.5$ m and $T_p = 14.4$ sec) .....	26
Figure 3.6: Time varying line load vs. angle at the mudline (with $V_{c_{max}} = 2.0$ m/s in a 2000-m water depth) during a loop current event.....	27
Figure 3.7: Time-varying angle and load on line No. 1 at the mudline (with $V_{c_{max}} = 2.0$ m/s in a 2000-m water depth) during a loop current event .....	28
Figure 3.8: Comparison of tensions and angles at the mudline in three different water depths for intact case during a loop current event ( $V_{c_{max}} = 2.0$ m/s) .....	28
Figure 3.9: The profile of current velocity factor (non-dimensional) during a loop current .....	31
Figure 3.10: CDFs for the maximum current velocity with different return periods of 6, 12 and 16 months: (a) Type II distribution; (b) Weibull distribution. ....	35
Figure 3.11: Inverse CDFs with different event occurrence frequencies: (a) for the Type II distribution; (b) for the Weibull distribution; (c) Comparison of the Type II and Weibull distributions with $v = 1/\text{year}$ .....	36
Figure 3.12: Expected values for the mean of the maximums for 5, 10, 15, 20, 30, 45, 60, 90, and 180 minute durations for ten separate three hour storms for mooring line No. 8 at 1000 m water depth for a sea state with $H_s = 9.32$ m and $T_p = 12.64$ s .....	42
Figure 3.13: Standard deviation for the mean of the maximums for different durations for 10 three hour storms for mooring line No. 8 for a sea state with $H_s = 9.32$ m and $T_p = 12.64$ s .....	43

Figure 3.14: Expected maximum load (in kN) during a 3-hour storm for 1,000-m water depth.....	44
Figure 3.15: Expected maximum load (in kN) during a 3-hour storm for 2,000-m water depth.....	44
Figure 3.16: Expected maximum load (in kN) during a 3-hour storm for 3,000-m water depth.....	45
Figure 3.17: Relationship between storm frequency and severity for T=1 year and 20 years .....	46
Figure 3.18: $H_s$ - $T_p$ annual reliability contours due to hurricanes in the Gulf of Mexico ..	50
Figure 3.19: $H_s$ - $T_p$ reliability contours due to hurricanes for a 20 year design life .....	51
Figure 3.20: Superposition of Figures 3.14 and 3.19 for spar in 1,000 m of water .....	53
Figure 3.21: Lognormal probability plot of mooring line load for 1,000 m water depth ..	53
Figure 3.22: Superposition of Figures 3.15 and 3.19 for spar in 2,000 m of water .....	54
Figure 3.23: Superposition of Figures 3.16 and 3.19 for spar in 3,000 m of water .....	54
Figure 3.24: Sensitivity of the maximum load to the variation in model parameters in the case of hurricanes and 1,000 m water depth. ....	59
Figure 3.25: Comparison of coefficient of variation values for individual components of uncertainty in hurricane loads for the study spar.....	60
Figure 3.26: Expected maximum line loads at the fairlead in a 3-hour sea state vs. line number for design hurricane event .....	62
Figure 3.27: Expected maxima of line loads in a 100-year loop current event .....	63
Figure 3.28: (a) Inverse catenary mooring line below mudline; (b) Chain-soil interaction below mudline (Note: N.T.S) .....	65
Figure 3.29: Parametric study for loads and angle at the padeye .....	68

Figure 3.30: Relationship between tension in chain at padeye and tension in chain at mudline for suction caisson foundation; nominal water depth of 1,000 m...	70
Figure 3.31: Relationship between angle of chain at padeye (subtended to horizontal) and tension in chain at mudline for suction caisson foundation; nominal water depth of 1,000 m .....	70
Figure 3.32: Relationship between vertical force at padeye and tension in chain at mudline for suction caisson foundation; nominal water depth of 1,000 m...	71
Figure 3.33: Comparison of tension at mudline and vertical component at padeye for line No. 8 in 1,000-m water depth during a 3-hr storm event.....	71
Figure 3.34: Relationship between normalized vertical force at padeye and normalized tension at mudline in 1,000 m water depth during a 3-hr storm event.....	72
Figure 3.35: Relationship between normalized vertical component at padeye and normalized tension at mudline in 3,000 m water depth. ....	72
Figure 4.1: (a) A typical mooring line (Image from <a href="http://www.ocsbbs.com">http://www.ocsbbs.com</a> )-top; (b) schematic of a mooring line-bottom (N.T.S) .....	82
Figure 4.2: Comparison of probability density function for tension strength of the chain segments and individual chain link (for 1000-m water depth under hurricane condition) .....	87
Figure 4.3: Comparison of probability density functions for line capacities of the line components (1000-m water depth under hurricane condition): (a) coefficient of variation for wire rope =0.15; (b) coefficient of variation for wire rope =0.05 .....	89

Figure 4.4: Plasticity model for suction caissons (a) failure mechanism assumed by Murff and Hamilton (1993); and (b) simplified analysis by Aubeny et al., (2001) (after Aubeny et al., 2003).....	97
Figure 4.5: Failure mechanism adopted for simplified model by Aubeny et al., (2001)...	98
Figure 4.6: Suction caisson rigid body motions under inclined loading (after Aubeny et al., 2003b) .....	100
Figure 4.7: Effect of load attachment point (padeye) on total load capacity .....	101
Figure 4.8: Example of interaction curve for capacity of suction caissons .....	103
Figure 4.9: Effect of aspect ratio on combined capacity at padeye .....	103
Figure 4.10: Effect of skin friction on combined capacity at the padeye of a suction caisson ( $L/d = 6$ and $d = 4$ m) .....	105
Figure 4.11: Effect of end bearing factors on combined capacity at the padeye of a suction caisson ( $L/d = 6$ and $d = 4$ m).....	105
Figure 4.12: Effect of shear strength rate with depth on combined capacity at the padeye of a suction caisson ( $L/d = 6$ and $d = 4$ m) .....	106
Figure 4.13: Normalized interaction curve for a suction caisson with $L/d = 6$ .....	107
Figure 4.14: Comparison of the normalized and theoretical interaction curves for a suction caisson with $L/d = 6$ .....	108
Figure 4.15: Interaction diagram showing wave load (line No. 8) and predicted capacity at the padeye of the suction caisson in 1,000 m of water .....	109
Figure 4.16: Interaction diagram showing wave load (line No. 8) and predicted capacity at the padeye of the suction caisson in 2,000 m of water .....	110
Figure 4.17: Interaction diagram showing wave load (line No. 8) and predicted capacity at the padeye of the suction caisson in 3,000 m of water .....	110

Figure 4.18: Comparison of the normalized and theoretical curves for ultimate total load at the padeye for a suction caisson with $L/d = 6$ .....	111
Figure 4.19: Interaction curves for capacity at the mudline vs. padeye in 1,000 m water depth.....	114
Figure 4.20: Effect of skin friction on combined capacity at the mudline of a suction caisson ( $L/d = 6$ and $d = 4$ m) .....	115
Figure 4.21: Effect of end bearing factors on combined capacity at the mudline of a suction caisson ( $L/d = 6$ and $d = 4$ m).....	115
Figure 4.22: Effect of shear strength rate with depth on combined capacity at the mudline of a suction caisson ( $L/d = 6$ and $d = 4$ m) .....	116
Figure 4.23: Comparison of the normalized and theoretical interaction curves for a suction caisson with $L/d = 6$ .....	117
Figure 4.24: Comparison of the normalized and theoretical curves for ultimate total load at the mudline for a suction caisson with $L/d = 6$ .....	118
Figure 4.25: Interaction diagram showing wave load (line No. 8) and predicted capacity at the mudline of the suction caisson in 1,000 m of water .....	119
Figure 4.26: Interaction diagram showing wave load (line No. 8) and predicted capacity at the mudline of the suction caisson in 2,000 m of water .....	120
Figure 4.27: Interaction diagram showing wave load (line No. 8) and predicted capacity at the mudline of the suction caisson in 3,000 m of water .....	120
Figure 4.28: Design chart for lateral (top) and vertical (bottom) resistances of caisson foundations in normally consolidated clay (in case of $N_c = 9$ ).....	122
Figure 4.29: Design chart for lateral (top) and vertical (bottom) resistances of caisson foundations in normally consolidated clay (in case of $\alpha = 1$ ).....	123

Figure 4.30: Design chart for total resistances at the mudline of caisson foundations in normally consolidated clay (in case of $\alpha = 1$ and $N_c = 9$ ).....	124
Figure 4.31: Measured versus predicted axial capacity for model tests on suction caissons in normally consolidated clays (from Najjar 2005).....	126
Figure 4.32: Calculated lower-bound versus measured axial capacity for suction caissons in normally consolidated clays (from Najjar 2005).....	128
Figure 4.33: Mixed lognormal distribution for foundation capacity with a lower-bound.....	129
Figure 5.1: Example of probability distributions for caisson load and capacity .....	131
Figure 5.2: Component reliability from Equation 4.5.....	136
Figure 5.3: Comparison of probabilities of failure of foundations subject to uplift failure vs. combined failure modes in 1,000 m of water under a hurricane event.....	142
Figure 5.4: Example of reliabilities of individual components for most heavily loaded line of the study spar under hurricane conditions .....	143
Figure 5.5: Example of complete line reliability of most heavily loaded line of the study spar under hurricane conditions .....	143
Figure 5.6: Probabilities of sea state and failure for mooring line No. 8.....	146
Figure 5.7: Expected maximum load at fairlead for mooring lines Nos. 8 and 9 plotted against the significant wave height.....	147
Figure 5.8: Mooring system redundancy factor.....	149
Figure 5.9: Example of system reliability of station keeping in 20-yr design life at three water depths under hurricane loading.....	150
Figure 6.1: Reliability of components for the most heavily loaded line (No. 8) during hurricane events .....	155

Figure 6.2: Complete line reliability of the mostly heavily loaded line during hurricane events .....	155
Figure 6.3: Effect of proof load on the reliabilities of the mostly heavily loaded mooring line in three water depths for the hurricane condition.....	157
Figure 6.4: Comparison of total line and anchor reliability of No. 8 with two different coefficients of variation in rope capacity for hurricane conditions .....	157
Figure 6.5: Comparison of failure probability of the components of the study spar under hurricane vs. loop current conditions in 1,000-m water depth .....	158
Figure 6.6: Comparison of total line and anchor reliability of the study spar under hurricane vs. loop current conditions in 1000-m water depth .....	159
Figure 6.7: Effect of lower-bound capacity on probability of foundation failure (study spar in 2,000-m water depth) .....	160
Figure 6.8: Effect of lower-bound capacity of foundation on probability of failure of foundation No. 8 in three water depths for the case of $FS_{\text{intact}}=2.5$ and $FS_{\text{damage}}=2.0$ for hurricane loading.....	161
Figure 6.9: Effect of coefficient of variation in line load on reliability of total line .....	162
Figure 6.10: Effect of factors of safety on reliabilities of total line and its components in 2,000-m water depth with hurricane loading.....	163
Figure 6.11: Effect of factors of safety on reliabilities of total line in three water depths for hurricane loading .....	164
Figure 6.12: Variation in the probability of failure of foundation No. 8 with a lower bound ratio of 0.43 for hurricane loading .....	165
Figure 6.13: Comparisons of probabilities of failure of any line and the mostly loaded line in design life for three water depths under hurricane loading .....	166

Figure 6.14: Comparisons of probabilities of failure of any line and the mostly loaded line in design life under hurricane versus loop current loading.....	167
Figure 6.15: Conditional probability of failure of line No. 9 given that line No. 8 has failed at three water depths under hurricane loading.....	169
Figure 6.16: Redundancy factor for the study systems at three water depths for hurricane loading .....	169
Figure 6.17: Redundancy factor for the study systems in 1000 m of water under hurricane and current conditions.....	170
Figure 6.18: Redundancy factor for the study systems in 2000 m of water under hurricane and current conditions.....	170
Figure 6.19: Redundancy factor for the study systems in 3000 m of water under hurricane and current conditions.....	171
Figure 6.20: System reliability of station keeping in 20-yr design life at three water depths under hurricane loading.....	171
Figure 6.21: System reliability of station keeping in 20-yr design life at three water depths under loop current loading (Weibull).....	172
Figure 6.22: Effect of probability of one line missing on system reliability of station keeping in 20-yr design life in 1000-m water depth under hurricane loading condition .....	173
Figure 6.23: Reliability for study spar foundation versus design factor of safety (20-year design life).....	175
Figure 6.24: Comparison of target reliability and total line reliability of the mostly loaded line in three water depths in a design life of 20 years for hurricane conditions.....	177



Figure 6.25: Comparison of target reliability with reliabilities of the semi-taut system and the taut systems in a design life of 20 years for current conditions (Weibull) .....	178
Figure 6.26: Nobel Jim Thompson (Image from <a href="http://www.rigzone.com">www.rigzone.com</a> ) .....	181
Figure 6.27: Mooring line pattern during Hurricane Ivan for Nobel Jim Thompson (Sharples 2004) .....	182
Figure 6.28: Diagrams showing the most probable sequence of line failure in order from (1) through (6) (Sharples 2004).....	183
Figure 6.29: Deepwater Nautilus (Image from <a href="http://www.rigzone.com">www.rigzone.com</a> ) .....	185
Figure 6.30: Mooring line pattern during Hurricane Ivan for Deepwater Nautilus (Sharples 2004) .....	185
Figure 6.31: Diagrams showing the most probable sequence of line failure in order from (1) through (8) (Sharples 2004).....	186

## **Chapter 1: Introduction**

### **1.1 MOTIVATION FOR RESEARCH**

The offshore industry has been moving to deeper waters to extend the search for oil and gas because of the high demand on energy worldwide. This tendency results in the evolution of the early offshore structures, such as the fixed and/or compliant tower structures designed for shallow depths, to new types of the offshore structures that are floating facilities in deeper depths of water (Figure 1.1). The deepwater floating structures include Tension Leg Platforms (TLPs), Spars, Semi-submersibles, and Floating Production Storage and Offloading (FPSO) systems. These deepwater offshore structures are anchored to foundations in the seafloor using mooring lines. Suction caisson foundations have been used for the deepwater structures as an alternative to driven piles in order to reduce installation costs. Compared to driven piles for the shallow offshore structures, suction caisson foundations have one primary difference: the foundation is subject to high tension loads due to environmental conditions while the driven piles are mainly in compression. Despite the wide use of suction caisson foundations, they have not been fully studied in terms of their design and reliability.

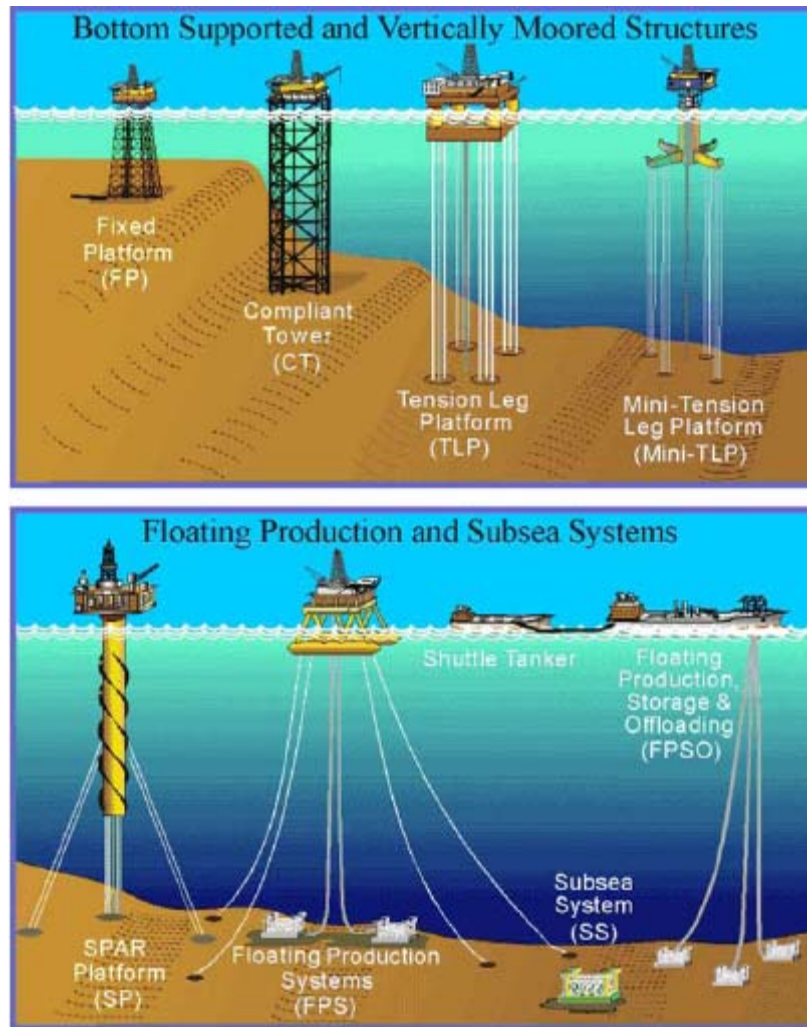


Figure 1.1: Offshore Structures (from Mineral Management Services, [www.mms.gov](http://www.mms.gov))

The design of suction caisson foundations is largely performed on a case-by-case basis following design guidelines such as those developed by the American Petroleum Institute (API PR-2A 2002). There have been few published works (e.g., Gilbert et al., 2005) which investigate the effect of using different factors of safety for design on the reliability of these foundations. Many researchers (e.g., Bruen et al., 1991; Banon et al., 1994; Larsen 1996; Larsen and Mathisen, 1996; Ahilan et al., 1996; Goodwin et al., 1999; Snell et al., 1999; Siddiqui and Ahmad, 2000) have focused on the reliability of

mooring lines, excluding the foundation component. Very little work (e.g., Clukey et al., 2000) has been performed on the reliability of offshore foundations for the deepwater structure systems. The effect of different design factors of safety on the reliabilities of the individual components has not been studied in detail.

Mooring systems for floating production systems, consisting of individual mooring lines and anchors, are currently designed on the basis of individual components. The most heavily loaded line and anchor are checked under extreme loading conditions (hurricane and loop current) with the system of lines intact and with one line removed. However, the performance of the floating production system depends more directly on the performance of the system of lines and anchors rather than on the performance of a single line or anchor.

Moreover, in the aftermath of Hurricanes Ivan (2004), Katrina (2005) and Rita (2005), several Mobile Offshore Drilling Units (MODUs) were set adrift tens of miles from their original locations. Failure of the system was found to initiate with failure of the most heavily loaded mooring line. The remaining mooring lines then failed in succession due to the excessive environmental loadings, resulting in failure of the complete station-keeping system. However, failure of a single component, even though it may be the most critically loaded one, does not necessarily mean collapse of the entire system. Instead, failure of an offshore structure occurs in a systematic way. Therefore, it is of interest to understand how individual components are related to the performance of the whole system for offshore structures.

## **1.2 OBJECTIVES AND APPROACH OF RESEARCH**

This study has two main goals: (1) to investigate the relationship between component and system performances of offshore foundation and its mooring systems of a

spar that is representative of existing practical technology in the Gulf of Mexico and (2) to assess the level of conservatism in the current design procedures of offshore foundations by comparing the predicted and actual performances of offshore deepwater mooring systems that experienced hurricanes, including Hurricanes Ivan, Katrina and Rita. These goals are achieved through the following tasks:

1. Investigate environmental loadings on offshore foundation and its mooring line for floating production systems under hurricane-dominated and loop-current-dominated conditions.
2. Study capacities of mooring lines and suction caisson foundations during extreme environmental conditions.
3. Adapt a methodology for reliability analysis to evaluate the performance of components in a mooring system as well as the performance of the entire system.
4. Perform reliability assessment for the mooring system of a spar under the extreme environmental conditions.
5. Investigate the impact on system and component reliabilities due to the mooring line configuration, water depth, metocean conditions and factors of safety.

### **1.3 ORGANIZATION OF DISSERTATION**

A study spar and its mooring systems chosen for this research are described in detail in Chapter 2. The relationship between foundation loads and met-ocean conditions are investigated in Chapter 3. A methodology for establishing probabilistic descriptions of foundation loads is also discussed in Chapter 3. Further, probabilistic distributions for foundation loads are developed using this methodology and uncertainty in the foundation load is discussed. Models for mooring line and foundation capacities

under extreme environmental loading conditions are described in Chapter 4. Axial, lateral and combined capacities for suction caissons are studied in this chapter. A probabilistic representation for foundation capacity is adopted for reliability analysis. Uncertainty in foundation capacity is also addressed in detail. The framework for quantifying component and system reliabilities is introduced in Chapter 5. Results from a reliability analysis of the mooring system for the study spar are presented and analyzed in Chapter 6. The predicted results are compared with the actual performance of offshore deepwater mooring systems that experienced hurricanes, including Hurricanes Ivan, Katrina and Rita in this chapter. Finally, a summary of the major conclusions obtained from this research is presented in Chapter 7.

## **Chapter 2: Offshore Structure and Generic Soil Profile in the Gulf of Mexico used in this Study**

### **2.1 INTRODUCTION**

To fulfill the research objectives mentioned in Chapter 1, a deepwater spar was selected to provide a practical context for this research. This section includes a description of the main characteristics of the study spar, as well as a description of a generic soil profile representative of the conditions in the Gulf of Mexico in which the spar may be deployed. The study spar is representative of existing practical technology and design practice for deepwater floating production systems in the Gulf of Mexico. An example of a typical spar is shown in Figure 2.1. The study spar was originally developed by an industry consortium named “DeepStar”. DeepStar is a joint industry development project focused on advancing technologies to meet its member deepwater business needs ([www.deepstar.org](http://www.deepstar.org)). The floating production system is supported by suction caissons. An example of suction caisson foundations is shown in Figure 2.2.

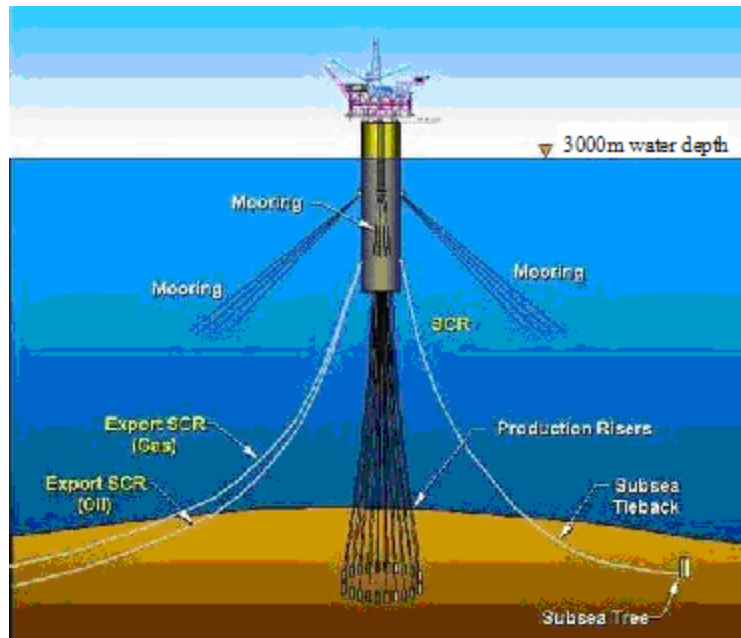


Figure 2.1: Example of a typical spar in 3,000 m of water (Image taken from website: <http://www.ocsbbs.com>)



Figure 2.2: Example of suction caissons (from Andersen et al., 2005)



## 2.2 DESCRIPTION OF THE STUDY SPAR AND MOORING SYSTEM

The study spar serves as the “theme structure” of Offshore Technology Research Center (OTRC) in water depths of 1,000, 2,000, and 3,000 m (nominally, 3,000, 6,000, and 10,000 ft). The main characteristics of the study spar and its mooring systems are given in Tables 2.1 and 2.2. The differences between the three mooring systems are mainly the length and material of mooring lines (Table 2.2). The mooring lines in 1,000-m water depth are the traditional combination of steel chain-wire-chain, while those in 2,000 and 3,000-m water depths are the integration of steel chain-polyester rope-steel chain. The mooring systems deployed in all water depths consist of fourteen omnidirectional spread mooring lines as depicted in Figure 2.3. Figure 2.4a gives an idea of the spread of the mooring systems on the sea floor.

The foundation for each mooring line is a suction caisson with a length-to-diameter ( $L/d$ ) ratio ranging from 5 to 7 in normally consolidated soils. Suction caissons are closed-top steel tubes that are lowered to the seafloor, allowed to penetrate the soil under their own weight, and then pushed to their final penetration using suction (e.g., Luke et al. 2003). Each mooring line is connected to a padeye that is located at about two-thirds of the penetration depth below the mudline. In 1,000-m of water, the study spar is moored by a semi-taut system while it is moored by taut systems in deeper waters (Table 2.2). The extreme water depths require that mooring line systems shift from catenary systems to taut systems. Figure 2.4b schematically compares a catenary mooring system with a taut mooring system indicating that the difference in line angles of the two different systems at the mudline is quite noticeable.

Design information for hurricane and loop current dominant conditions is shown in Table 2.3. Relative direction among a loop current, wind and wave and a loop

current profile are shown in Figures 2.5 and 2.6 (under a hurricane condition) and in Figures 2.7 and 2.8 (under a loop current condition).

Table 2.1: Main specification of the study spar

Displacement	53600 metric ton
Total displacement	220640 metric ton
Diameter	37 m
Length	215 m
Draft	198 m
Hard tank depth	67 m
KB	165 m
KG	140 m
KG (based on total displacement)	96 m
Radius of gyration	Pitch=67 m, yaw=8.7 m
Drag force coefficient	1.16
Wind force coefficient	2.672 (kN/(m/sec) <sup>2</sup> )
Center of pressure	220 m ABL

Table 2.2: Mooring system specifications

Water depth	1,000 m	2,000 m	3,000 m
Mooring type	Steel semi taut	Poly taut	Poly taut
Mooring pattern	14 point taut-leg omni-directional spread	14 point taut-leg omni-directional spread	14 point taut-leg omni-directional spread
Mooring line composition	Platform section 76 m x 13.3 cm K4 Studless chain	Platform section 91 m x 11.7 cm K4 Studless chain	Platform section 91m x 13cm K4 Studless chain
	Riser section 975 m x 13.7 cm Sheathed Wire	Middle section 2377 m x 21 cm Polyester	Middle section 4054 m x 23 cm Polyester
	Ground section 350 m x 13.3 cm K4 Studless chain	Ground section 122 m x 11.7 cm K4 Studless chain	Ground section 122m x 13cm K4 Studless chain
Fairlead location	91 m ABL	91 m ABL	91 m ABL
Pretension	3025 kN	2357 kN	2890 kN

Table 2.3: Design information for hurricane and current dominant conditions

	Hurricane Dominant	Current Dominant
Significant wave height ( $H_s$ )	12.2 m	6.1 m
Peak spectral period ( $T_p$ )	14 sec	11 sec
Wave spectra	Jonswap ( $\gamma = 2.5$ )	Jonswap ( $\gamma = 2$ )
Wave direction	270° (West)	90° L of Loop current
Current direction	30° R of waves	90° (East)
Wind direction	30° L of waves	collinear with waves
Wind speed (1-hr)	41.1 m/s @10m	22.4 m/s @10m
Wind spectra	refer to API RP 2A-WSD, paragraph 2.3.2b	
Wind profile	refer to API RP 2A-WSD, paragraph 2.3.2b	
Storm surge & tide	0 m	0 m
Current speed (below surface)		
0	1.1 m/sec	2.1 m/sec
60 m	1.1 m/sec	2.1 m/sec
90 m	0.1 m/sec	2.1 m/sec
244 m	0.1 m/sec	0.9 m/sec
Seabed	0.1 m/sec	0 m/sec

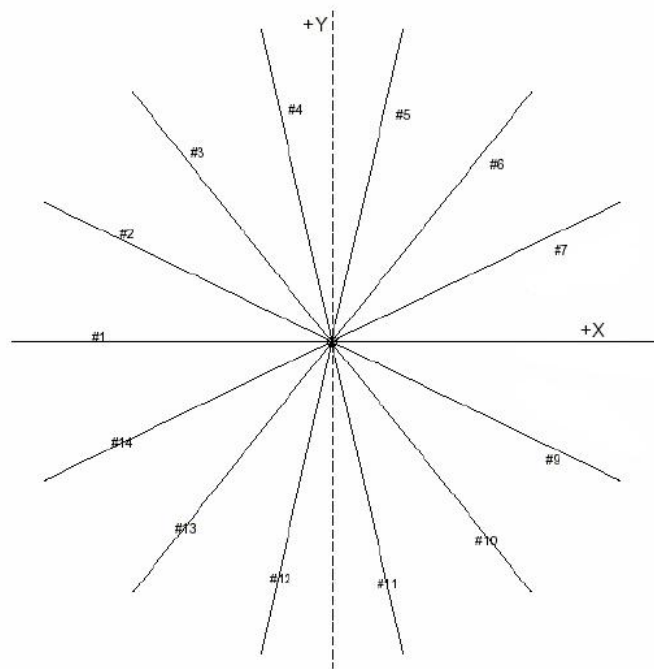
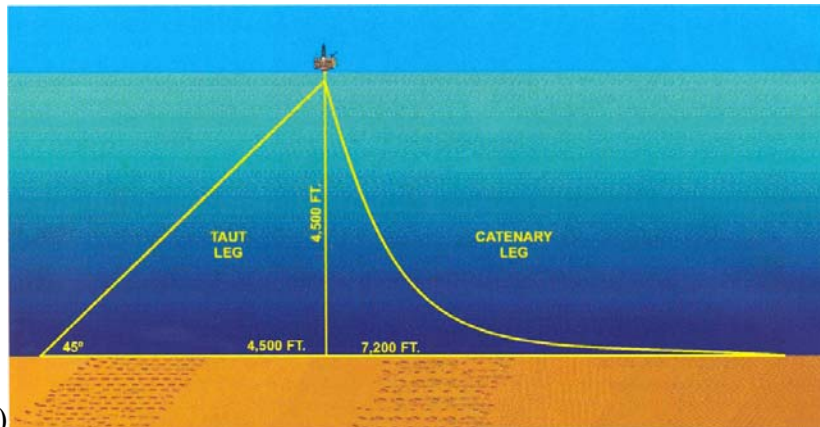


Figure 2.3: Spread mooring system



a)



b)

Figure 2.4: Schematic graphs (a) for spread of a mooring line system (Photo courtesy of Dr. Gilbert) and (b) comparing a catenary mooring system and a taut mooring system (Image taken from Murff and Young, 2007)

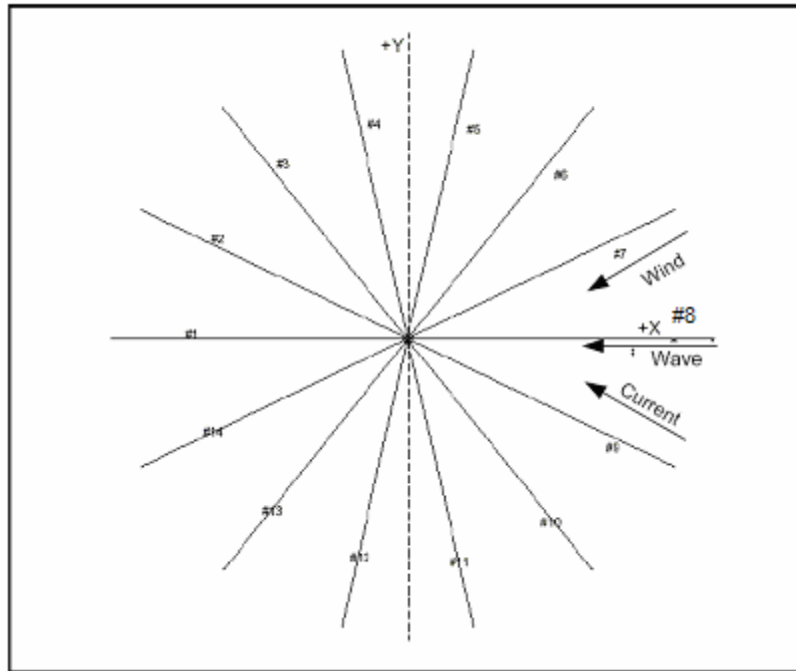


Figure 2.5: Relative directions among a loop current, wave and wind under a hurricane condition

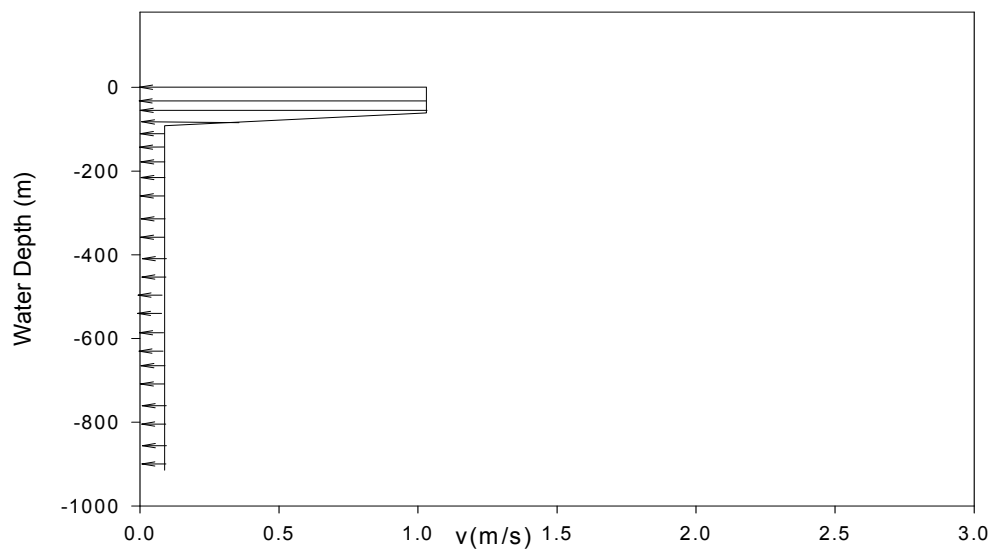


Figure 2.6: The profile of current velocity for a mooring system analysis during a hurricane event

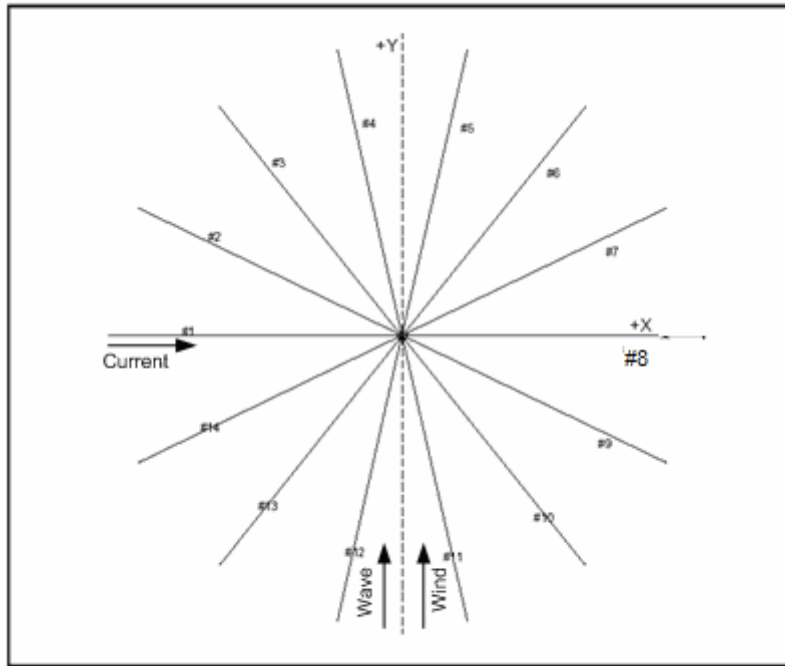


Figure 2.7: Relative directions among a loop current, wave and wind under a loop current condition

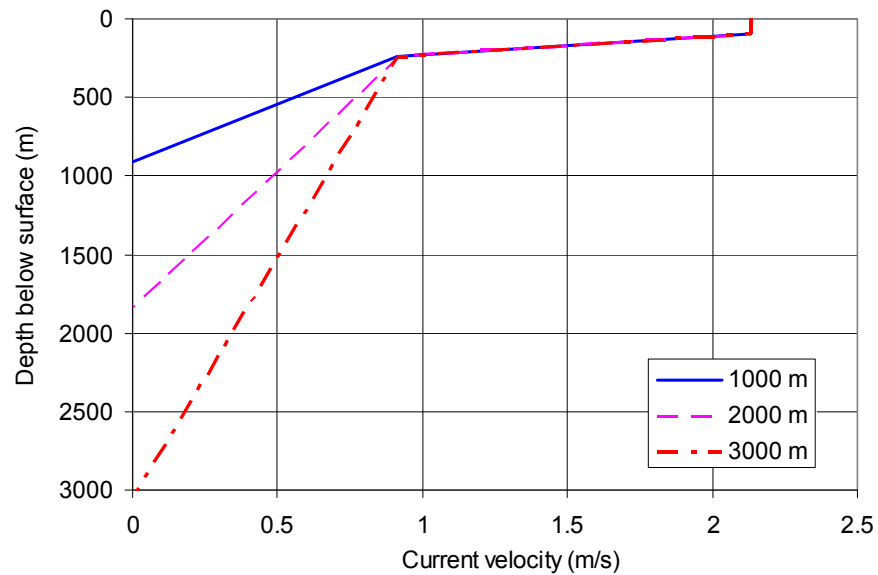


Figure 2.8: The profile of current velocity for three different water depths during a loop current event

### 2.3 GENERIC SOIL PROFILE IN THE GOM

Figure 2.9 shows a generic soil profile from the Gulf of Mexico consisting of soft clay deposits. Typical clays in the Gulf of Mexico are normally and slightly overconsolidated, with plastic limit (PL) of about 25 and liquid limit (LL) of approximately 70 (Gilbert and Murff, 2001). The undrained shear strength is 4 kPa at the mudline and it increases with increasing depth at a rate 1.3 kPa/m. Since this profile is representative of conditions currently being encountered for deepwater application in the GOM, this generic soil profile and soil type have been used for designing suction caissons subjected to extreme environmental loadings and identifying uncertainties in the suction caisson loads in later sections of this dissertation.

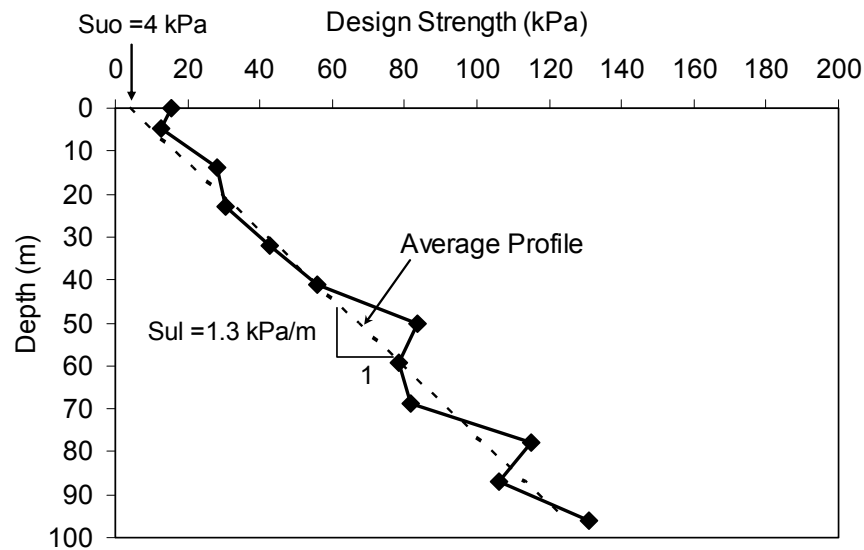


Figure 2.9: Soil boring at study spar site in the Gulf of Mexico

### 2.4 SUMMARY

For this research, the study spar consisting of 14 omni-directional mooring lines in three different water depths, i.e. 1,000 m, 2,000 m and 3,000 m, is adopted and studied

under extreme environmental loading conditions: hurricane and loop current dominated conditions. The differences between the three mooring systems are mainly the length and material of mooring lines. The main characteristics of the study spar are described in this chapter.



## **Chapter 3: Mooring Line and Offshore Foundation Loads under Extreme Environmental Loadings**

### **3.1 INTRODUCTION**

In this chapter, the effect of environmental loadings on offshore foundations for floating structures is investigated for a given set of sea states using a hydrodynamic model to find the relationships between foundation loads and the set of sea states. A methodology is utilized to find the environmental loads on the offshore foundation in a probabilistic manner. The predicted loads for the study spar are then assessed. This work establishes environmental loads in a probabilistic manner to be used subsequently in reliability analyses.

### **3.2 METHODS OF ESTIMATING ENVIRONMENTAL LOADS ON THE STUDY SPAR**

According to API RP 2A guidelines (API 2002), as indicated in Equation 3.1, the total met-ocean environmental loads on an offshore structure can be divided into three major parts: 1) wave, 2) current and 3) wind. The major parts are very briefly explained in the following sections. Readers should consult other references for more details on the methods (Choi et al., 2006; Bea and Mortazavi, 1996).

$$F = F_{Wave} + F_{Current} + F_{Wind} \quad (3.1)$$

### 3.2.1 Aerodynamic (wind) loads

The computation of wind force is based on the empirical formula recommended by API RP-2A,

$$F_{wind} = \frac{1}{2} C_s \rho_a V_a^2 A \quad (3.2)$$

where  $\rho_a$  is the mass density of air,  $C_s$  is the wind velocity pressure (or shape) coefficient,  $V_a$  is the total wind velocity for an appropriate time interval and  $A$  is the projected area of an offshore structure above the sea level. The pressure coefficient and the location of center of wind pressure are determined based on the corresponding wind-tunnel tests. The wind pressure coefficient is also a function of air turbulence, structural geometry and surface roughness.

However, in general, wind forces acting on the study spar are not as significant as wave forces acting on the offshore structure (API 1997b).

### 3.2.2 Wave and current loads

In order to estimate wave and current loads on the offshore structure, the Morison equation is used as a basic equation in Equation 3.3. This force is composed of two components: an inertia component ( $F_i$ ) and a drag component ( $F_d$ ). The inertia component is related to the acceleration of an ideal fluid around the structure body while the drag component is related to the horizontal undisturbed fluid velocity around the body.

$$F = F_i + F_d = C_m \rho V \frac{du}{dt} + \frac{1}{2} C_d \rho A u |u| \quad (3.3)$$

where  $C_m$  is the inertia coefficient,  $\rho$  is the mass density of fluid,  $V$  is the volume of the body,  $du/dt$  is the fluid acceleration,  $C_d$  is the drag coefficient,  $A$  denotes the projected area of the body normal to the flow direction, and  $u$  is the horizontal velocity of water at a particular point on the submerged portion of the structure element. The horizontal velocity of water depends on the height of wave crest. Although extremely simple, the Morison equation has been used for many years by researchers and engineers to calculate the wave forces on marine structures such as spars and fixed platforms. Choi et al., (2006) discusses more details of the application of the Morison equation used for the study spar.

### **3.2.3 Analysis model for estimating mooring line loads – COUPLE6D**

To simulate mooring line loads at the fairlead and mudline under hurricane and loop current dominated conditions, a numerical model (COUPLE6D), which was developed by the Ocean Engineering Program of Texas A&M University, is used for this research. The Loads on the mooring system of the study spar under hurricane and loop current dominated events in the Gulf of Mexico (GOM) are derived from the numerical model. In COUPLE6D, two basic computational parts are involved: one for evaluating the loads on the hull due to the specified conditions of wave, current and wind and the other for computing the loads and dynamics of the mooring system, i.e., how the restoring force is transferred between the various mooring lines.

Using the Morison equation, the nonlinear wave forces on the theme spar is calculated because the diameter of the hull of the study spar is much smaller than the typical incident wavelength. Figures 2.5 and 2.7 show the relative directions among the wave, current and wind forces for hurricane and loop current dominated simulations,

respectively. Loop current profiles for the two different dominated conditions are represented by a surface current velocity that diminishes with water depth as shown in Figures 2.6 and 2.8.

In the second part of the COUPLE6D program, using a nonlinear Finite Element Method (FEM), the code, known as CABLE3D, for computing dynamics of the mooring/tendon/riser system is programmed (Ma and Webster, 1994). The computation in the original CABLE3D assumes infinitesimal elongation of a slender rod. Because large elongation of slender components, such as springs and polyester ropes are often, respectively, used in a model test and a prototype mooring system, CABLE3D was extended to allow for large elongation in a mooring line to achieve accurate simulation (Chen et al., 2002).

These two independent codes are coupled together in the time domain by using a Newmark- $\beta$  method. This coupling involves matching the forces and displacements of a mooring/tendon/riser system and the joints where the mooring system connects to the spar hull (it is called “fairlead”). The outcome from the program is a three hour storm simulation consisting of load and motion responses. The load responses include line loads from each individual mooring line at the fairlead and at the mudline. The motion responses are in all six degrees of freedom for the hull.

In the current version of COUPLE, both magnitude and direction of current velocity are the input and assumed to be steady. The magnitude of current velocity decays with depth. However, for cases where unsteady currents are considered, it can be incorporated into the program without principal difficulties. For the case of the study spar, considering that the diameter of the spar, the velocities of waves and currents may change along its axis, the total wave and current loads on the spar in the numerical model, CABLE6D, are computed through the numerical integration of the corresponding loads

over many segments along its longitudinal axis. In addition to computing the wave/current/wind loads on a moored floating structure (hull), the dynamic 6-DOF (degree of freedom) behavior of the mooring/tendon/riser system should be computed which is combined with the first computation by matching the forces and displacements of the mooring/tendon/riser system and the related hull at their joints following prescribed connection condition. For more details about COUPLE6D, refer to Ding et al., (2003) and Choi et al., (2006).

### **3.3 CHARACTERIZATION OF ENVIRONMENTAL LOADING CONDITIONS**

To estimate environmental loadings on an offshore structure, the sea state parameters, i.e., significant wave height ( $H_s$ ), peak spectral period ( $T_p$ ), surface current velocity ( $V_c$ ), and wind velocity ( $V_w$ ), must be provided. The four parameters,  $H_s$ ,  $T_p$ ,  $V_c$ , and  $V_w$ , shall be referred to as met-ocean parameters.

Two different types of extreme sea states in the Gulf of Mexico, namely, hurricanes (storms) and loop currents, are considered in this study. Conventional practice for a deepwater mooring system deployed in the Gulf of Mexico is to design it to be able to accommodate the impact of either a 100-year hurricane or loop current. In a reliability analysis, the occurrence of a particular storm or loop current near the location of the spar during its 20-year life span is modeled by a probability distribution function.

In this section, each of the sea state parameters affecting environmental loadings on the structure for a given storm or loop current event is first addressed. The probability distribution functions used for the occurrence of a storm or loop current are then described.

### 3.3.1 Sea state parameters

Significant wave height ( $H_s$ ) is defined as a value which is approximately equal to the mean of the highest one-third waves on the structure. It is estimated from the wave frequency spectrum using Equation 3.4 below because it cannot be measured directly during a storm event.

$$\frac{S(\omega)}{H_s^2 T_1} = \frac{0.11}{2\pi} \left( \frac{\omega T_1}{2\pi} \right)^{-5} \exp \left[ -0.44 \left( \frac{\omega T_1}{2\pi} \right)^4 \right]$$
$$T_1 = 2\pi m_0 / m_1 \quad (3.4)$$

$$H_s = 4\sqrt{m_0} \quad \text{and} \quad m_k = \int_0^\infty \omega^k S(\omega) d\omega$$

where:  $T_1$  is a mean wave period,  $S(\omega)$  is the spectral density which is proportional to the square of the amplitude (along the y-axis) in the wave frequency spectrum. More strictly speaking, the above equation is valid for cases where the wave frequency is a narrow-banded spectrum and the wave elevation follows a Gaussian distribution (Faltinsen, 1990). Figure 3.1 shows the normalized amplitude versus the frequency for a sample storm event. The Fourier amplitude spectrum describes the amplitude of any frequency in the loading history. The JONSWAP (Joint North Sea Wave Project) spectrum is an omni-directional wave power spectrum used especially for the theme spar. In this spectrum, waves from all directions contribute to the tension load in the mooring lines. However, the waves apply an overall resultant force on the structure in a particular direction. The waves themselves are the major source of environmental forces on offshore structures in wind-driven sea states, like hurricanes (API RP-2A 2002).

Peak spectral period ( $T_p$ ) can be calculated by inversing the most dominant (or peak) frequency on the wave frequency spectrum as indicated in Equation 3.5.

$$T_p = \frac{1}{f_p} \quad (3.5)$$

where  $f_p$  is the peak spectral frequency corresponding to the largest amplitude in the wave frequency spectrum.

Surface current velocity ( $V_c$ ) represents the effect of ocean currents associated with waves during a storm event. Wind speed ( $V_w$ ) represents the effect of winds associated with waves during a storm event. Note that both current velocity and wind have their directions associated with them. For design purpose, the wind speed is based on an elevation of 10 meters above still water level.

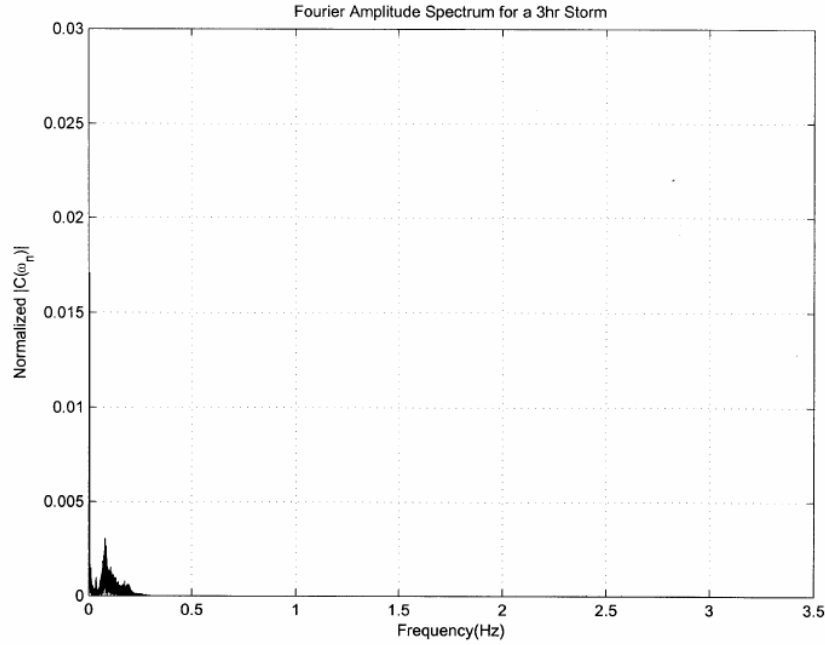


Figure 3.1: Example of wave frequency spectrum for a storm event ( $H_s=9.32$  m,  $T_p=12.64$  sec)

### 3.3.2 Example of loading history of mooring lines during a hurricane event

As an example of calculating hurricane loadings given a set of met-ocean parameters, a hurricane loading history for three hour duration of a storm event developed by the Texas A&M research team using the numerical load model, CABLE6D is shown in Figure 3.2. The length of a time step in these numerical simulations was 0.16 sec in 1,000 m water depth and 0.32 sec in 2,000 m and 3,000 m water depths. The maximum tension of each individual mooring line occurs at its fairlead. Time-varying loading histories of the mostly heavily loaded line, i.e. No. 8 (Figure 2.5), at the fairlead in 1,000 m, 2,000, and 3,000 m water depths are presented in Figures 3.2 to 3.4.



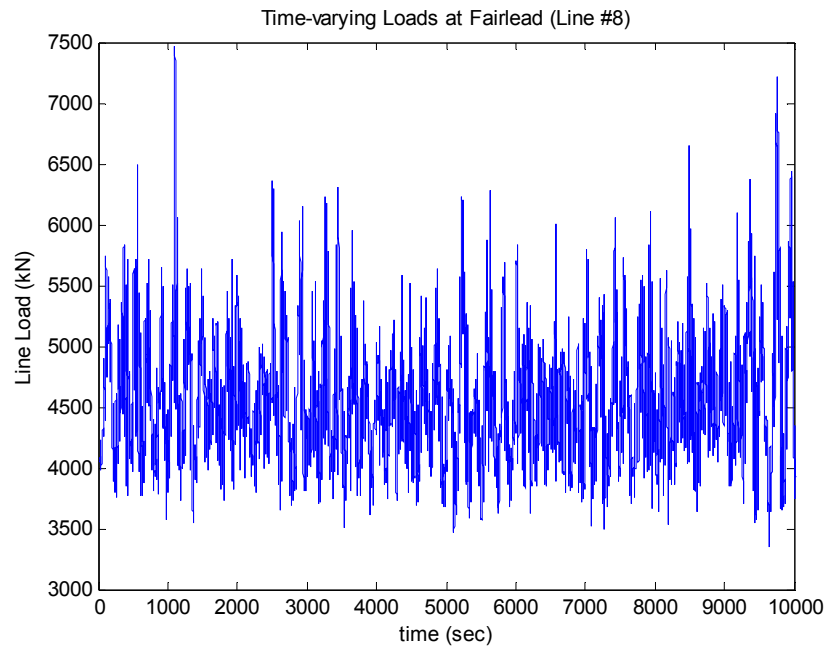


Figure 3.2: Time-varying loads of the most heavily loaded line at the fairlead in 1,000 m ( $H_s = 12.5$  m and  $T_p = 14.4$  sec)

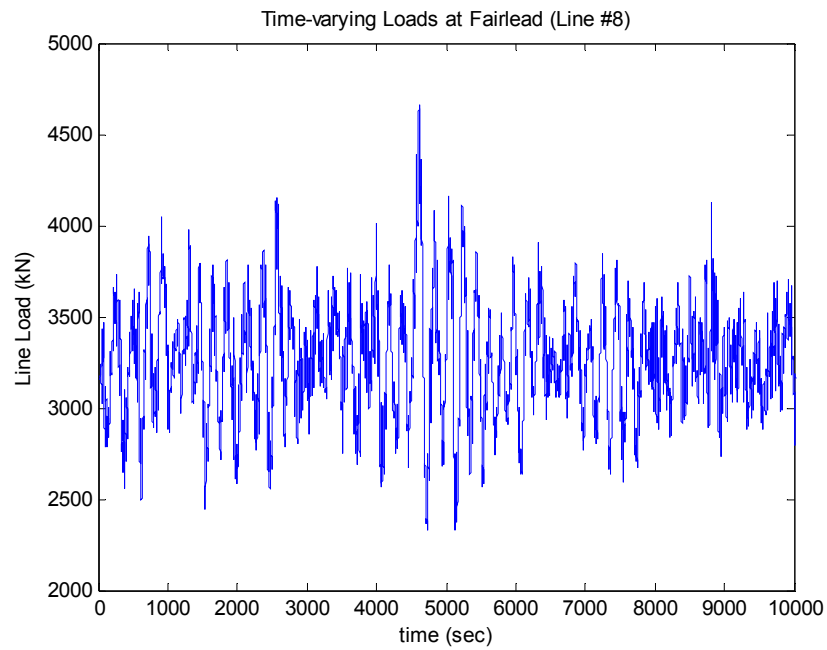


Figure 3.3: Time-varying loads of the most heavily loaded line at the fairlead in 2,000 m ( $H_s = 12.5$  m and  $T_p = 14.4$  sec)

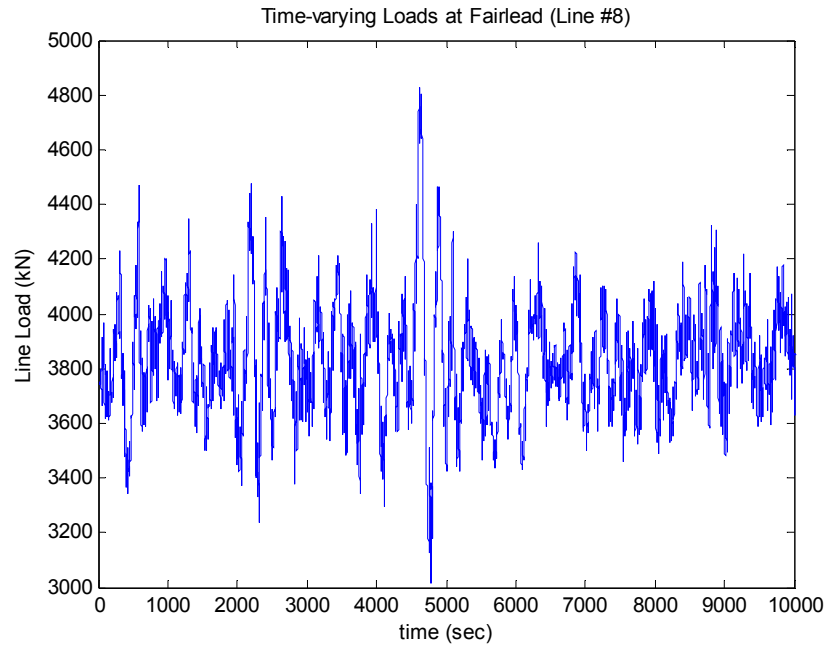


Figure 3.4: Time-varying loads of the most heavily loaded line at the fairlead in 3,000 m ( $H_s = 12.5$  m and  $T_p = 14.4$  sec)

The line loads on No. 8 and corresponding angles at the mudline during the hurricane event with the same sea states as for Figures 3.2 to 3.4 in three different water depths are compared and plotted in Figure 3.5. In this case, all mooring lines are intact. The different behaviors between the semi-taut system in 1,000 m of water and the taut systems in 2,000 m and 3,000 m of water are well illustrated in this figure. The taut systems have a constant angle at the mudline of about  $35^\circ$  while the semi-taut system has a range from  $11^\circ$  to  $26^\circ$ .

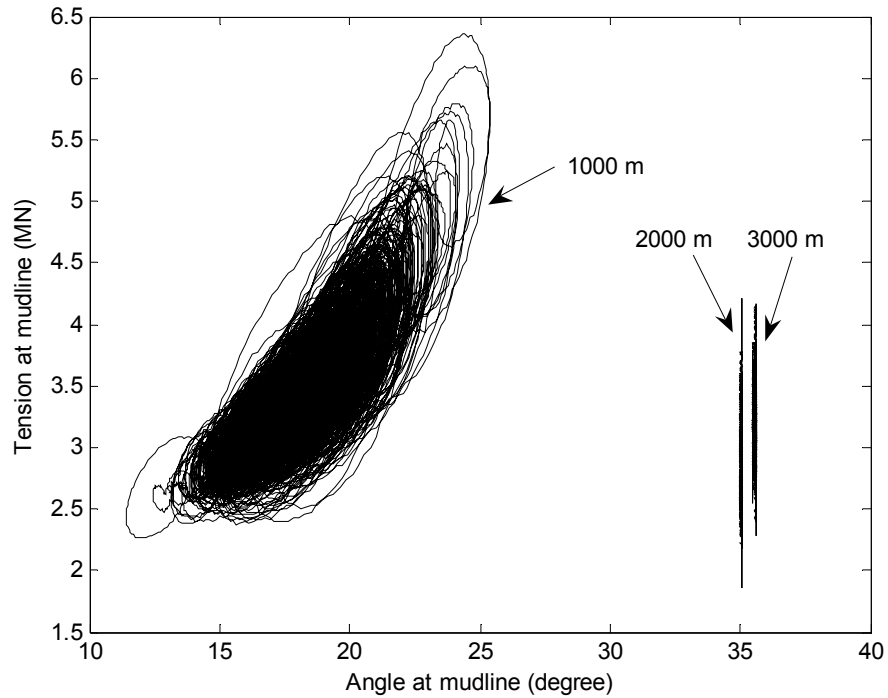


Figure 3.5: Comparison of tensions and angles at the mudline in three different water depths for intact case during a hurricane event ( $H_s = 12.5$  m and  $T_p = 14.4$  sec)

### 3.3.3 Example of loading history of mooring lines during a loop current event

As an example of simulating loop current loadings given a set of met-ocean parameters, the time-varying loads and the corresponding angles of fourteen mooring lines at the mudline during a loop current dominated event are shown in Figure 3.6. Note that during a loop current event the most heavily loaded mooring line is line No. 1 (Figure 2.7). The variation in the line load and angle at the mudline is much smaller for the loop current event than that for the hurricane event. Since the change in the angle and load on line No. 1 is negligible, the load and angle at the mudline may be considered as static values. This behavior is also reflected in the time variation in the angle and

loads at the mudline (Figure 3.7), and in the relationship between tension and angle (Figure 3.8). Because different simulations for the same sea state result in different maximums, these time-varying loading histories have to be processed to obtain a statistical description of maximum load in the mooring lines for a specified sea state and duration. This work is explained in the following sections.

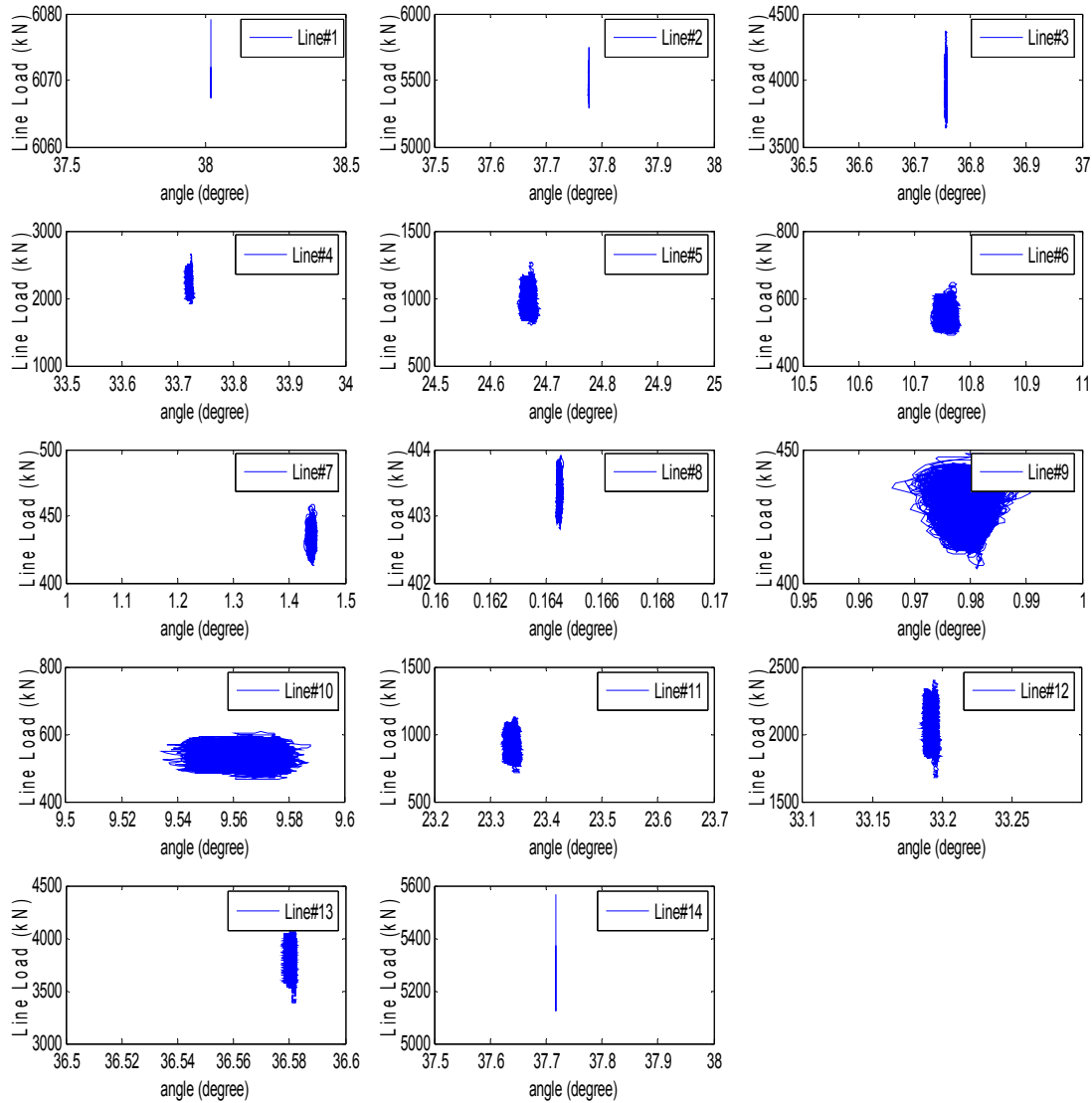


Figure 3.6: Time varying line load vs. angle at the mudline (with  $V_{c_{max}} = 2.0$  m/s in a 2000-m water depth) during a loop current event

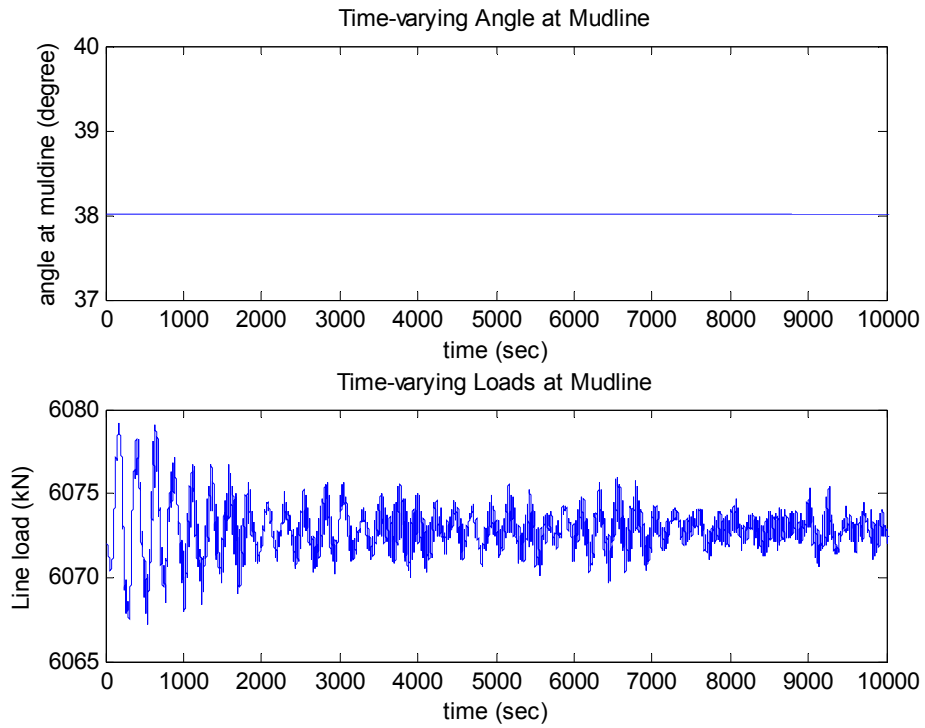


Figure 3.7: Time-varying angle and load on line No. 1 at the mudline (with  $V_{c_{max}} = 2.0$  m/s in a 2000-m water depth) during a loop current event

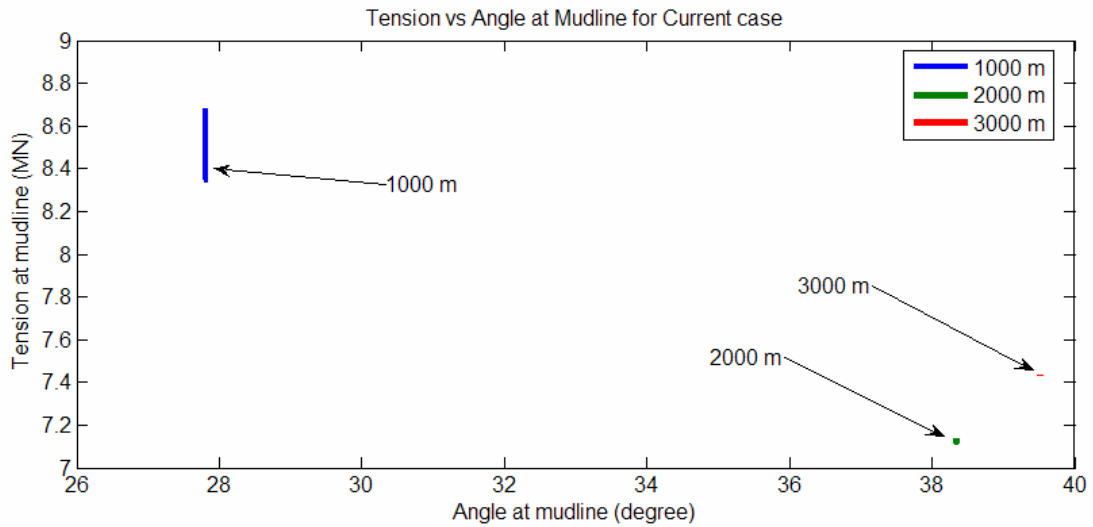


Figure 3.8: Comparison of tensions and angles at the mudline in three different water depths for intact case during a loop current event ( $V_{c_{max}} = 2.0$  m/s)

### 3.3.4 Probability distribution used for Hurricanes

Based on the GUMSHOE data base (Banon et al., 1991), a probabilistic distribution for the met-ocean parameters characterizing a storm in the Gulf of Mexico was adopted from Winterstein and Kumar (1995). The database is an oceanographic database for Gulf of Mexico and comprises of hindcasts for 100 historical hurricanes in the Gulf of Mexico, which is modeled by a joint probability distribution of significant wave height ( $H_s$ ) and peak period ( $T_p$ ). While the model is recently being updated based on data from recent hurricanes in 2004 and 2005, an older but publicly available model is used here since the focus is on the methodology and on relative rather than absolute results. The probabilistic distribution for each of the met-ocean parameters is described below.

1. The significant wave height ( $H_s$ ) has been modeled as a truncated Weibull distribution:

$$\text{Probability}[H_s > h] = \begin{cases} 0 & \text{if } h < h_{\min} \\ \exp \left[ \left( \frac{h_{\min}}{h_0} \right)^\gamma - \left( \frac{h}{h_0} \right)^\gamma \right] & \text{if } h \geq h_{\min} \end{cases} \quad (3.6)$$

where:  $h_{\min} = 8.00$  m,  $h_0 = 6.42$  m, and  $\gamma = 2.29$

2. The peak spectral period ( $T_p$ ) is modeled as a conditional normal distribution with a c.o.v. of 0.06 and a mean value that depends on  $H_s$ :

$$E[T_p | H_s] = 5.39 H_s^{0.382} \quad (3.7)$$

where:  $H_s$  is in meters and  $T_p$  is in seconds.

3. The surface current velocity ( $V_c$ ) is modeled as a linear function of  $H_s$ :

$$V_c \text{ (fps)} = 0.056 H_s \text{ (ft)} + 1.0625 \quad (3.8)$$

4. The one hour mean wind speed ( $V_w$ ) at 10 m above the sea surface is also modeled as a linear function of  $H_s$ :

$$V_w \text{ (mph)} = 1.895 H_s \text{ (ft)} + 18.316 \quad (3.9)$$

As indicated in the equations above, the hurricane is characterized by two parameters, i.e.,  $H_s$  and  $T_p$  because  $V_c$  and  $V_w$  are linear functions of  $H_s$ . For simplicity, it is assumed that the relative directions of wave, wind and current in all simulated hurricanes remain the same. With respect to the mooring systems, their relative orientations are depicted in Figure 2.5 and summarized in Table 2.3. Furthermore, hurricanes at the spar location in the Gulf of Mexico were assumed to occur independently with an annual rate of occurrence,  $\nu$ , of 0.1 per year, which is a typical rate (Winterstein and Kumar, 1995).

### **3.3.5 Probability distribution used for Loop currents**

As depicted in Figure 2.7 and summarized in Table 2.3, two major assumptions associated with the direction of loop currents and the occurrence of loop currents are made for simulating the mooring line loads under a loop current event. The direction of the loop current is always normal to that of winds and waves. The occurrence of loop currents in the Gulf of Mexico is assumed to be independent of the winds and waves. A non-dimensional velocity profile in a loop current, which is typical of what is being

assumed in analyses at present (Ward 2005), is used in our simulation and depicted in Figure 3.9. Therefore, the primary variable describing a loop current is the maximum velocity at the free surface.

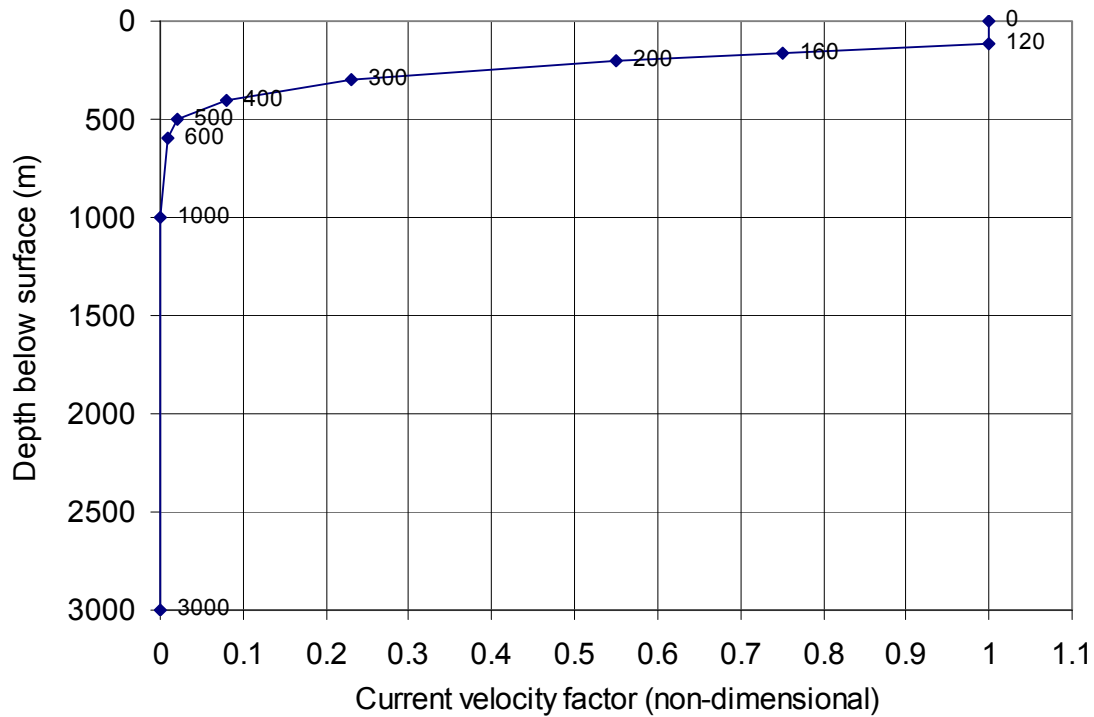


Figure 3.9: The profile of current velocity factor (non-dimensional) during a loop current

The probability distribution for the maximum velocity due to a loop current for the mooring systems in a 20-year design life is developed based on the following three assumptions recommended by Ward (2005).

- (1) The 100-year current surface velocity is equal to 2.1 m/sec
- (2) The 10-year current surface velocity is 1.9 m/sec



- (3) The occurrence frequencies for loop-current events range from one for every 6 to 17 months.

Therefore, the cumulative distribution function (CDF) for the maximum current velocity for an exposure time of 20 years can be derived for a given distribution form. Since no established distribution about the maximum velocity is available at present, the maximum current velocity with a specified duration is assumed to follow either a Type II distribution or a Weibull (Type III) distribution in this work. Thus both distributions have been used in this study.

Let  $H(y)$  be the probability that the maximum current velocity is greater than a specific current velocity value of  $y$  and  $F(y)$  is denoted as the probability that the maximum current velocity during an event is less than or equal to  $y$ .  $H(y)$  and  $F(y)$  for both Type II and Weibull distributions can be expressed as follows:

$$\text{For Type II, } F_{II}(y) = P(V_c \leq y) = \exp[-(u/y)^k] \quad (3.10a)$$

$$H_{II}(y) = P(V_c > y) = 1 - \exp[-(u/y)^k] \quad (3.10b)$$

$$\text{For Weibull, } F_{III}(y) = P(V_c \leq y) = 1 - \exp[-(y/\alpha)^\beta] \quad (3.11a)$$

$$H_{III}(y) = P(V_c > y) = \exp[-(y/\alpha)^\beta] \quad (3.11b)$$

where  $(u, k)$  and  $(\alpha, \beta)$  are the parameters characterizing Type II and Weibull distributions, respectively, and  $V_c$  is the maximum current velocity at the free surface. CDFs for the annual maximum current velocity can be estimated using  $H(y)$  combined with a Poisson process.

$$\begin{aligned} F_{II, T=1}(y) &= P(\text{annual } V_c \leq y) = \exp[-\nu H_{II}(y)] \\ F_{III, T=1}(y) &= P(\text{annual } V_c \leq y) = \exp[-\nu H_{III}(y)] \end{aligned} \quad (3.12)$$

where  $\nu$  is the occurrence frequency for loop current events. With specified 100-year and 10-year current velocities, the parameters of  $(u, k)$  and  $(\alpha, \beta)$  can be estimated as follows. A 100-year current velocity of 2.1 m/sec will not be exceeded with probability of 0.99 ( $=1-1/100$ ) in any year (for Type II case).

$$F_{II, T=1}(2.1 \text{ m/sec}) = 0.99 = \exp[-\nu(1 - \exp\{-(u/2.1)^k\})] \quad (3.13)$$

Similarly, the likelihood that a 10-year current velocity will not be exceeded can be calculated as follows:

$$F_{II, T=1}(1.9 \text{ m/sec}) = 0.9 = \exp[-\nu(1 - \exp\{-(u/1.9)^k\})] \quad (3.14)$$

In the same manner, for the Weibull distribution, we have the following relations.

$$F_{III, T=1}(2.1 \text{ m/sec}) = 0.99 = \exp[-\nu \exp\{-(2.1/\alpha)^\beta\}] \quad (3.15)$$

$$F_{III, T=1}(1.9 \text{ m/sec}) = 0.90 = \exp[-\nu \exp\{-(1.9/\alpha)^\beta\}] \quad (3.16)$$

The Type II distribution parameters  $u$  and  $k$  can be calculated from Equations 3.13 and 3.14, while the Weibull distribution (Type III) parameters  $\alpha$  and  $\beta$  can be calculated from Equations 3.15 and 3.16. Lastly, the maximum current velocity distribution for an exposure of 20 years ( $T = 20$ ) can be described using the Poisson process.

$$F_{II, T=20}(y) = P(V_{\text{current}} \text{ in 20 years} \leq y) = \exp[-\nu T \{1 - \exp(-(u/y)^k)\}] \quad (3.17)$$

$$F_{III, T=20}(y) = P(V_{\text{current}} \text{ in 20 years} \leq y) = \exp[-\nu T \exp\{-(y/\alpha)^\beta\}] \quad (3.18)$$

Ranges of parameters characterizing the cumulative distributions of the maximum current velocity were considered and are summarized in Table 3.1. The resulting CDFs for different occurrence rates for loop currents are shown in Figures 3.10 and 3.11. Based on the results in these figures, there is little effect of the occurrence frequency on the maximum current velocity distributions for both distributions over a wide range of current velocities. Accordingly, a nominal frequency of one loop current per year will be used hereafter. However, as expected from an extreme distribution, the data in Figure 3.11c indicates a more significant difference in behavior for the two distributions near the upper tail between Type II and Weibull distributions. In Figure 3.11, the inverses of the standard normal CDF values,  $\Phi^{-1}(\text{CDF})$ , of 1 and 4 correspond to CDF values of about 0.84 and 0.9997, respectively. Accordingly, the probability that the maximum current velocity is less than or equal to 2.1 m/sec in a 20-year design life has a CDF value of about 0.84 for both cases. However, the maximum current velocities corresponding to a probability of 0.9997 are about 2.5 m/sec for the Weibull distribution and 3.1 m/sec for the Type II distribution, indicating a greater impact of the distribution choice at higher maximum current velocities. Due to uncertainty at present in the most appropriate distributional form for the current velocity, the reliability analysis described in Chapter 6 is conducted using both the Type II and Weibull distributions.

The associated storm (winds and waves) during a loop-current event were assumed to be independent of the current velocity. For simplicity, therefore, the associated values of  $H_s$  and  $T_p$  during a loop current event can be assumed equal to the annual median values obtained from a weather buoy (Station No. 42001, <http://www.ndbc.noaa.gov/maps/WestGulf.shtml>) at a representative deepwater location in the Gulf of Mexico. The buoy is currently deployed in 3246-m depth of water.

Using the annual standard meteorological data for 2002, 2003 and 2004, which can be downloaded from the National Data Buoy Center ([www.ndbc.noaa.gov](http://www.ndbc.noaa.gov)), the annual median values for  $H_s$  and  $T_p$  were estimated and are summarized in Table 3.2. The values of 1.0 m and 6.2 sec for  $H_s$  and  $T_p$ , respectively, were used for simulating the time-varying loads in the mooring lines under a loop current event. The sea states used in the numerical simulation for the case of a loop current event are summarized in Table 3.3.

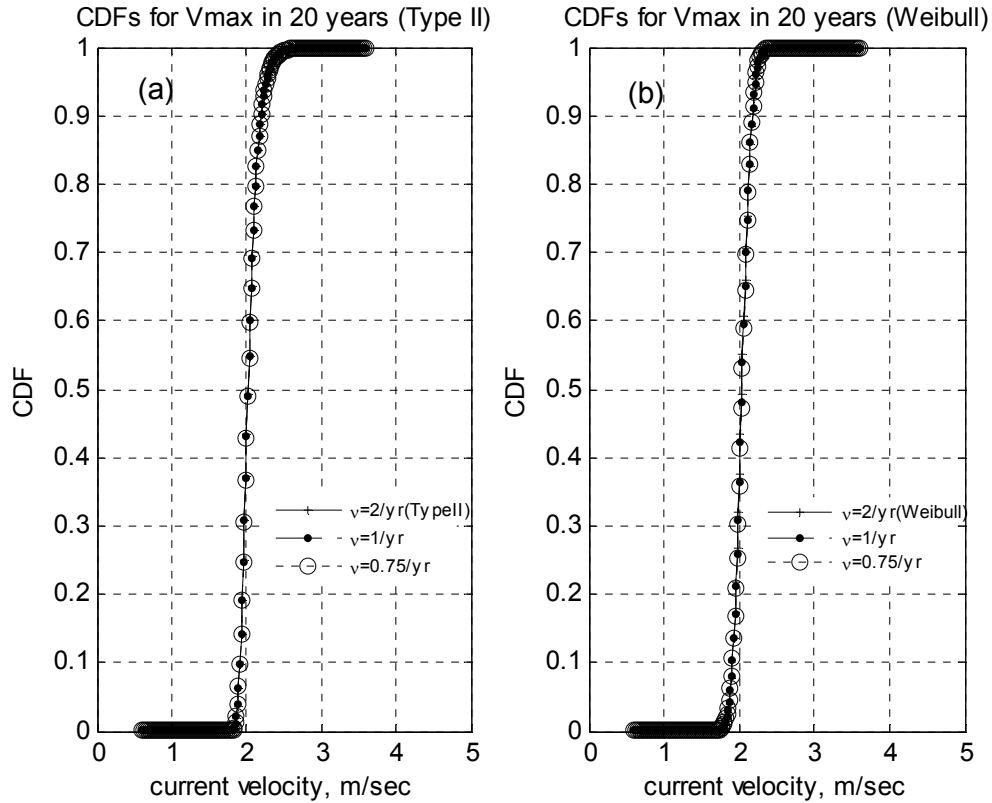


Figure 3.10: CDFs for the maximum current velocity with different return periods of 6, 12 and 16 months: (a) Type II distribution; (b) Weibull distribution.

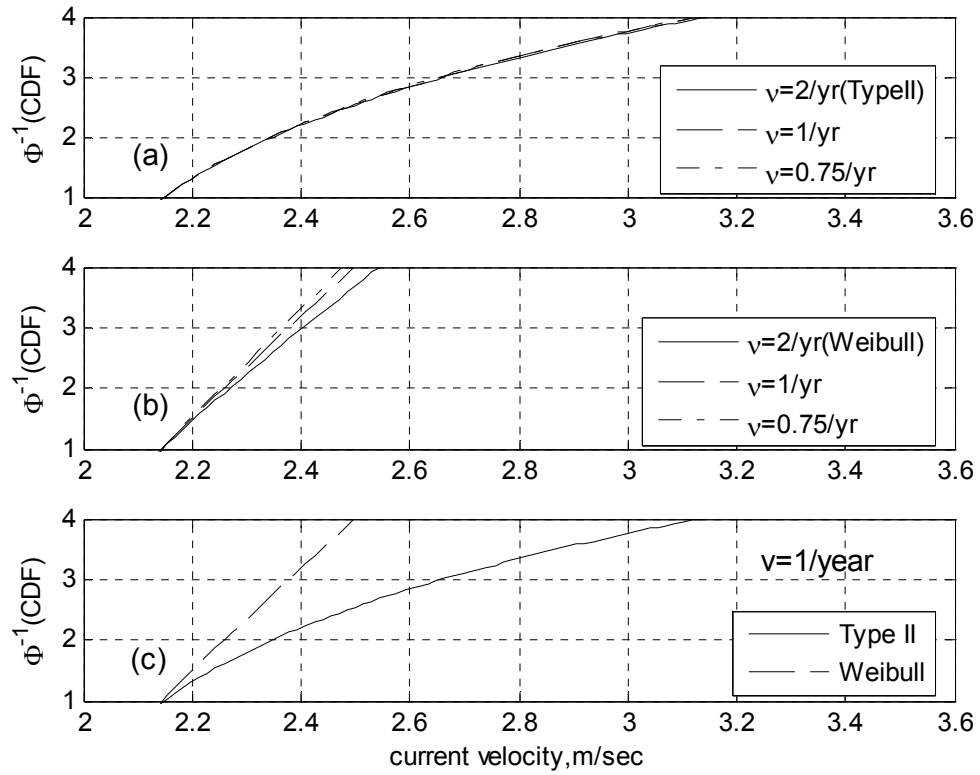


Figure 3.11: Inverse CDFs with different event occurrence frequencies: (a) for the Type II distribution; (b) for the Weibull distribution; (c) Comparison of the Type II and Weibull distributions with  $v=1/\text{year}$

Table 3.1: Parameters characterizing Type II and Weibull distributions depending on loop current frequencies

Loop Current Frequency, $\nu$ (times/year)	CDF for maximum current during event			
	Type II		Weibull	
	$u$	$k$	$\alpha$	$\beta$
2	1.69	22.53	1.58	5.57
1.5	1.71	22.61	1.63	6.02
1.2	1.73	22.7	1.67	6.42
1	1.74	22.78	1.7	6.79
0.86	1.76	22.86	1.73	7.14
0.75	1.77	22.95	1.75	7.47

Table 3.2: Annual median values for  $H_s$  and  $T_p$

Year	$H_s$ (m)	$T_p$ (sec)	$V_w$ (m/s)
2002	0.97	6.25	3.1
2003	1.04	6.25	2.84
2004	0.98	6.25	2.93

Table 3.3: Sea states used in the numerical model for the case of loop current

No.	$H_s$ (m)	$T_p$ (sec)	$V_w$ (m/s)	Jonswap ( $\gamma$ )	$V_{c_{max}}$ (m/s)	Percentile (%)	Assumption
1	1	6.2	3	2.75	2.04	50	Weibull
2	1	6.2	3	2.75	2.18	90	
3	1	6.2	3	2.75	2.22	95	
4	1	6.2	3	2.75	2.3	99	
5	1	6.2	3	2.75	2.39	99.9	
6	1	6.2	3	2.75	2.46	99.99	
7	1	6.2	3	2.75	2.53	99.999	
8	1	6.2	3	2.75	2.02	50	Type II
9	1	6.2	3	2.75	2.2	90	
10	1	6.2	3	2.75	2.27	95	
11	1	6.2	3	2.75	2.43	99	
12	1	6.2	3	2.75	2.69	99.9	
13	1	6.2	3	2.75	2.98	99.99	
14	1	6.2	3	2.75	3.3	99.999	

Notes:  $V_w$  is the wind speed at 10 m above sea level;  $\gamma$  is the JONSWAP sharp factor;  $V_{c_{max}}$  is the maximum current velocity.

### 3.4 METHODOLOGY FOR PROBABILITY DISTRIBUTION OF MAXIMUM LINE LOADS

In this section, the methodology to establish a probability distribution of the expected maximum loads during extreme environment events is presented. This methodology as proposed by Winterstein and Kumar (1995) and applied previously to this study spar by Dangayach (2004) consists of the following steps:

1. Establish a relationship between the median value of the maximum load and the sea state, which is characterized by the significant wave height ( $H_s$ ) and the peak spectral period ( $T_p$ );
2. Develop reliability contours for probabilities of non-exceedance environmental events for a specified design life for different combinations of the significant wave height ( $H_s$ ) and peak spectral period ( $T_p$ ); and
3. Develop a distribution for the expected maximum load by combining the results from steps 1 and 2.

In Step 2, an additional part may be added associated with a joint probability distribution of the met-ocean parameters. Using the joint PDF, the probability of occurrence of a storm event of a given met-ocean environment can be estimated. The methodology may be used to determine the probability distribution for the maximum load at any connection points, i.e., at the fairlead, at the mudline or at the padeye of the anchor, and for different configurations, such as a damaged mooring system.

One advantage to the proposed methodology is that it will accommodate any change in the met-ocean probabilistic representations very easily because this methodology decouples the responses of a structure (step 1) from the probabilistic descriptions of sea states (step 2) that change for hurricanes that are analyzed. For example, they may be changing due to new information from Hurricanes Ivan, Katrina, and Rita or due to other reasons later. Each of the three steps for the methodology is described in the following sections.



### 3.4.1 Step 1: Relationship between the maximum load and the sea state

In this step, a relationship between the median value of the maximum load and the sea state is developed. Tension load simulations of the mooring anchor system were generated from a three-hour simulation made by the COUPLE program for a given sea state. These simulations were then processed as follows to estimate the expected maximum load value and its standard deviation in that sea state.

#### 3.4.1.1 Theoretical background for probability distribution of maximum loads

From a theoretical perspective, if the time-varying loads are assumed to be stationary according to a Gaussian process, then the maximum load in a storm duration  $T$ ,  $S_{\max,T}$ , can be expressed as follows:

$$S_{\max,T} = \mu_{S(t)} + Y(T)\sigma_{S(t)} \quad (3.19)$$

where  $Y(T)$  is defined as a peaking factor and  $\mu_{S(t)}$  and  $\sigma_{S(t)}$  are the mean and standard deviation of the time-varying load. Furthermore, the mean and the standard deviation of the peaking factor,  $Y(T)$ , are given by (Vanmarcke 1983):

$$\mu_{Y(T)} = \sqrt{2 \ln \nu_o^+ T} + \frac{0.577}{\sqrt{2 \ln \nu_o^+ T}} \quad (3.20)$$

$$\sigma_{Y(T)} = \frac{\pi}{6} \frac{1}{\sqrt{2 \ln \nu_o^+ T}} \quad (3.21)$$

where  $\nu_o^+$  is the mean up-crossing rate, i.e. the rate at which the load time curve crosses the mean value in the upward direction (related to the frequency of variations).

As seen in Equations 3.20 and 3.21, the mean for the maximum load will be related proportionally to the square root of the natural logarithm of the storm duration (T) for a Gaussian process while the standard deviation for the maximum load varies proportionally with the inverse of the square root of the natural logarithm of the storm duration. This relationship is true as long as the second term on the right hand side of Equation 3.20 does not contribute significantly to the expected value of Y (generally < 5%) and is negligible.

#### ***3.4.1.2 Estimation of the maximum load in a given sea state***

While the time series for tension loads are not strictly Gaussian, we explain the applicability of using the form of the relationship in Equations 3.20 and 3.21. In order to apply this theory, the 3-hour storm simulations were divided into 5, 10, 15, 20, and 30 minute intervals. The maximum load values were then selected from each interval and the sample mean and standard deviation were calculated for each set (e.g., the sample mean of the 36 maximum values corresponding to a 5-minute interval).

The results of this processing on ten 3-hour storm simulations of the same sea state for mooring line No. 8 at the fairlead are shown in Figures 3.12 and 3.13. As expected by the theory, the mean value for the maximum increases approximately proportionally to the square root of the natural logarithm of the storm duration (Equation 3.20 and Figure 3.12). This result is useful because a single 3-hour storm simulation, which is the industry standard, can be used to estimate the mean value for the maximum load in a 3-hour storm by processing the simulation in smaller intervals. Otherwise, it would be necessary to estimate the mean value from a single point (there is only one maximum in a 3-hour simulation), which would not be reliable, or running many 3-hour simulations. The expected maximum value of the storm loads for a three hour storm

obtained by this approach is 5033000 N (Figure 3.12). The standard deviation for the maximum is seen to be more or less constant with time duration of the storms, and equal approximately to 250,000 N (Figure 3.13). Therefore, the coefficient of variation (standard deviation divided by mean) for the maximum load on line No. 8, which represents the variability between 3-hour storm events, is roughly 250,000 N/5,033,000 N or 0.05.

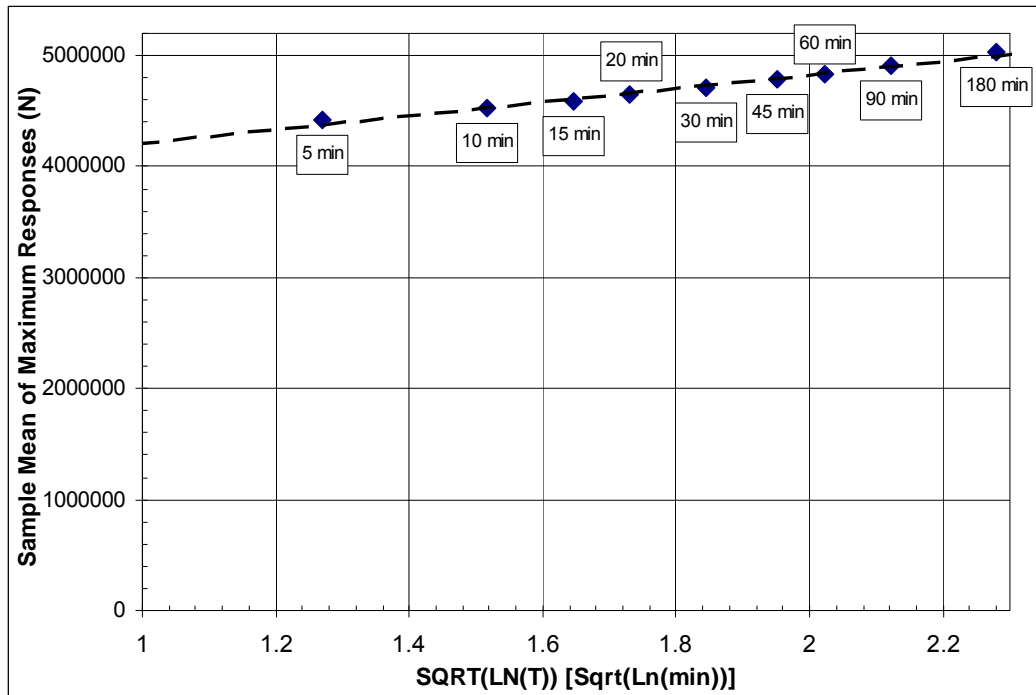


Figure 3.12: Expected values for the mean of the maximums for 5, 10, 15, 20, 30, 45, 60, 90, and 180 minute durations for ten separate three hour storms for mooring line No. 8 at 1000 m water depth for a sea state with  $H_s = 9.32$  m and  $T_p = 12.64$  s

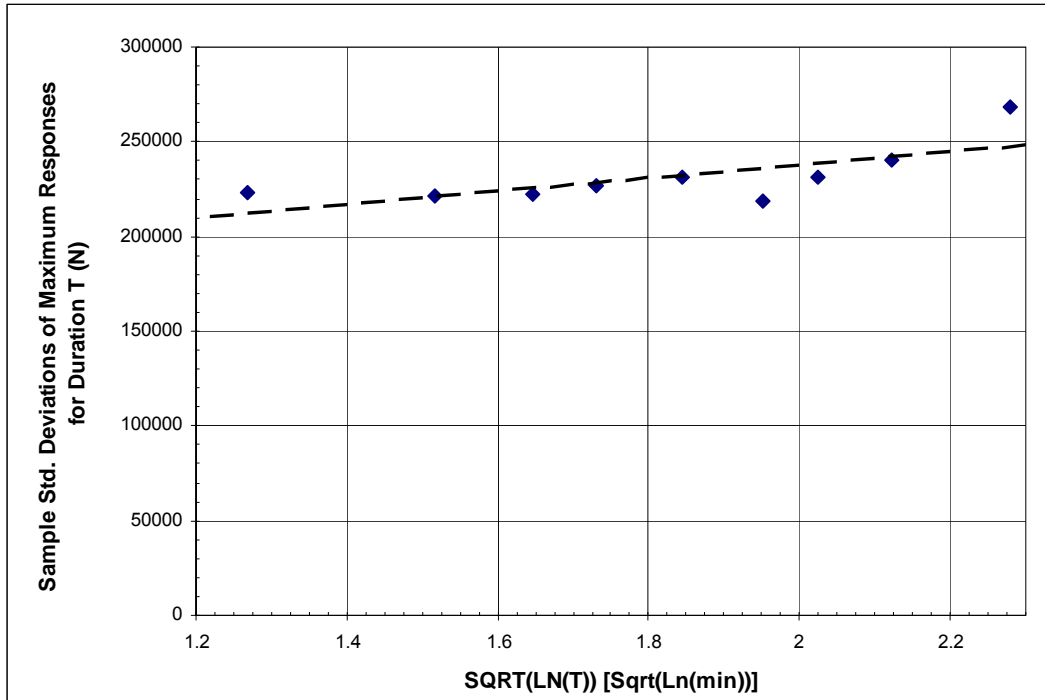


Figure 3.13: Standard deviation for the mean of the maximums for different durations for 10 three hour storms for mooring line No. 8 for a sea state with  $H_S = 9.32$  m and  $T_p = 12.64$  s

#### 3.4.1.3 Examples of Step 1

Three hour storm simulations (generating loading history of the structure) were carried out for a number of sea states and the expected maximum loads during a 3-hour storm were estimated using the approach depicted on Figure 3.12. Figures 3.14 to 3.16 show examples of the results of this analysis for the study spars in 1,000 m, 2,000 m, and 3,000 m water depths. The expected maximum load contours on this plot have a nearly vertical trend, indicating that the loads on this structure during a storm event depend mostly on the significant wave height of the sea state.

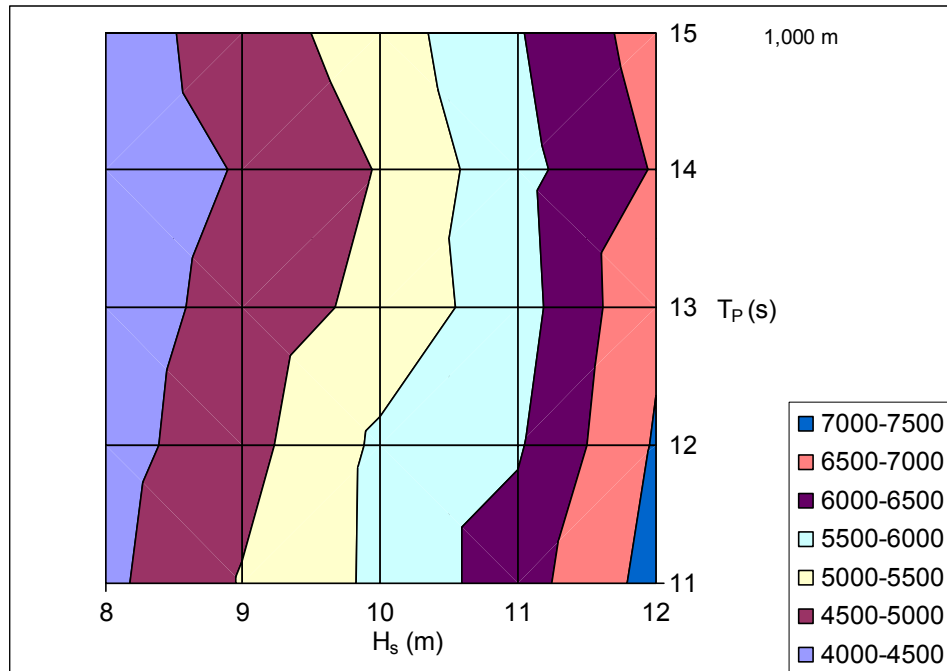


Figure 3.14: Expected maximum load (in kN) during a 3-hour storm for 1,000-m water depth

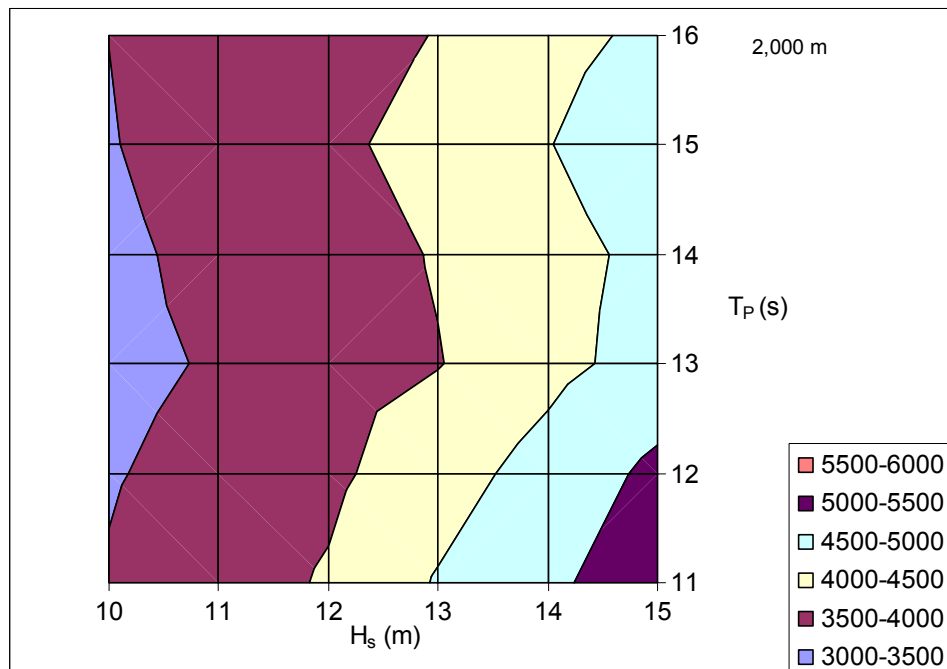


Figure 3.15: Expected maximum load (in kN) during a 3-hour storm for 2,000-m water depth

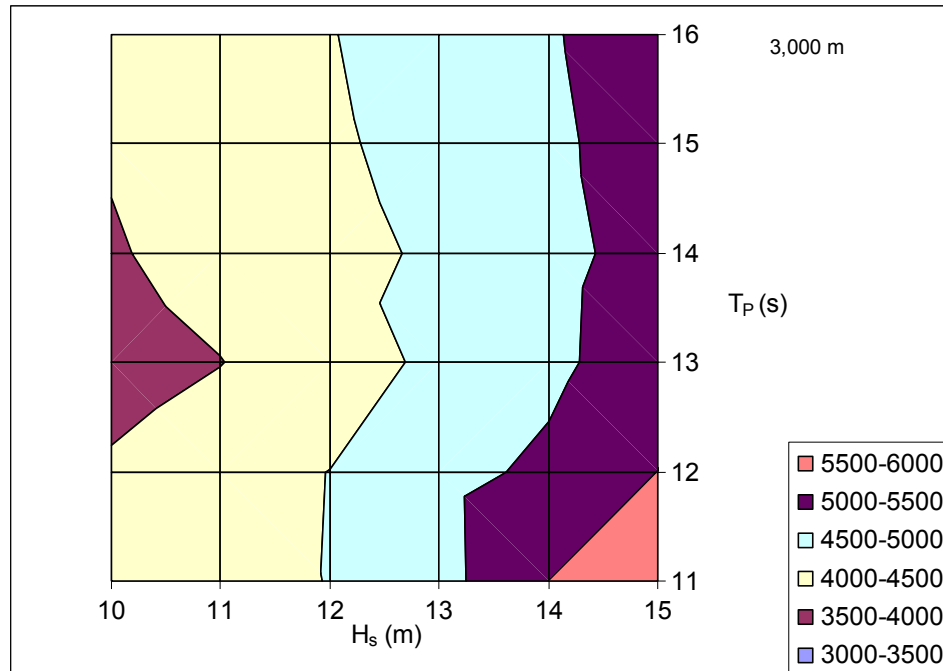


Figure 3.16: Expected maximum load (in kN) during a 3-hour storm for 3,000-m water depth

### 3.4.2 Step 2: Reliability contours for probabilities of non-exceedance storm events for a specified design life

The main purpose of this step is to develop return period contours for different combinations of the significant wave height and peak spectral period. A relationship between storm frequency and storm severity is first developed, and then the probability distribution for the occurrence of different storm event is developed.

#### 3.4.2.1 Relationship between storm frequency and storm severity

Hurricanes in the Gulf of Mexico are assumed to occur independently with an annual rate of occurrence,  $\nu$ , of 0.1 per year (Winterstein and Kumar, 1995). Thus within a period of 'T' years, the expected number of storms that the structures will experience is  $\nu T$ . The return period for a storm of a given magnitude is the expected

time between storms of that magnitude. Also, for a given return period,  $T_R$ , the annual probability,  $p_{T=1\text{yr}}$  that a storm of at least that severity will occur in any given year is  $1/T_R$ . For example, the 100-year storm has an annual probability of exceedance of 0.01 ( $= 1/100$ ) per year. Let  $p_{\text{storm}}$  be the probability that a storm severity will be exceeded during a storm event. If storms are assumed to follow a Poisson process, the probability of exceedance in a period of 'T' years can be calculated as (Ang and Tang, 1975)

$$\begin{aligned} p_T &= \exp(-\nu T p_{\text{storm}}) \\ p_{T=1\text{year}} &= \exp(-\nu * 1\text{year} * p_{\text{storm}}) \\ p_{T=20\text{year}} &= \exp(-\nu * 20\text{year} * p_{\text{storm}}) \end{aligned} \quad (3.22)$$

As an example, using Equation 3.22, the relationship between storm frequency and storm severity for  $T=1$  year and  $T=20$  years given  $\nu=0.1$  is shown in Figure 3.17.

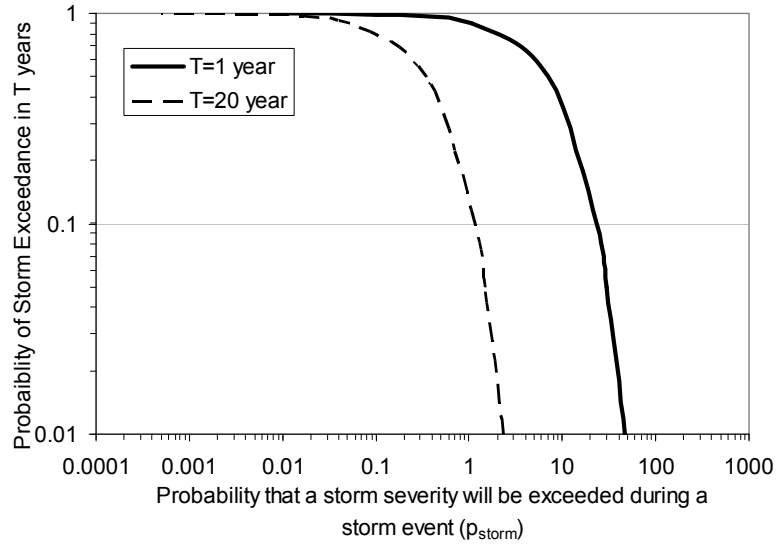


Figure 3.17: Relationship between storm frequency and severity for  $T=1$  year and 20 years

### 3.4.2.2 Probability of exceedance during a storm

From Equations 3.6, 3.7 and 3.22, a joint probability distribution of  $H_s$  and  $T_p$  can be developed that includes both the likelihood of different combinations of  $H_s$  and  $T_p$  in a hurricane as well as the frequency of hurricanes (Winterstein and Kumar, 1995). This joint probability distribution is expressed as a reliability contour using a technique named the inverse First Order Reliability Method (FORM), as described by Winterstein and Kumar (1995).

Let  $p_{\text{storm}}$  be the probability of exceedance during a storm, which is related to the sea state, i.e.,  $H_s$  and  $T_p$ . To find all possible combinations of  $H_s$  and  $T_p$ , the inverse FORM technique involves the following steps:

1. For a given value of  $p_{\text{storm}}$ , a reliability index,  $\beta$ , can be calculated using:

$$\beta = \left| \Phi^{-1}(p_{\text{storm}}) \right| \quad (3.23)$$

where  $\Phi^{-1}(\cdot)$  is the inverse of the standard normal cumulative distribution function (Ang and Tang, 1984). The failure plane in the standard normal space defines the boundary between an exceedance event and a non-exceedance event. Physically,  $\beta$  is represented as the radius of a circle in a standard normal space.

2. Consider a 2-dimensional hypersphere of radius equal to the reliability index in a 2-dimensional space describing the two independent standard normal random variables,  $U_1$  and  $U_2$ , the circle represented by  $U_1^2 + U_2^2 = \beta^2$  can be described using polar coordinates as follows:



$$U_1 = U_{H_s} = \beta \cos \theta \quad (3.24)$$

$$U_2 = U_{T_p} = \beta \sin \theta \quad (3.25)$$

3. Using Equations 3.24 and 3.25, equivalent polar forms in the standard normal space are converted to the parameter  $H_s$  and  $T_p$  in the original space with  $\beta$  and angle  $\theta$  varying 0 to 360 degrees to represent all possible combinations of  $H_s$  and  $T_p$  that have a joint PDF value of  $p_{\text{storm}}$ . The polar coordinates can then be converted back to their original  $H_s$  and  $T_p$  space using the Rosenblatt transformation (Rosenblatt, 1952). This is achieved by the following equations:

$$\text{CDF}(H_s) = \Phi(U_{H_s}) = \Phi(\beta \cos \theta) \quad (3.26)$$

$$\text{CDF}(T_p | H_s) = \Phi(U_{T_p}) = \Phi(\beta \sin \theta) \quad (3.27)$$

where CDF is the cumulative distribution function and  $T_p | H_s$  is the conditional event of a particular value of  $T_p$  given a value of  $H_s$ .

4. Once the CDF values of  $H_s$  and  $T_p$  above, the combination of  $H_s$  and  $T_p$  that produce a specified probability of exceedance,  $p_{\text{storm}}$  are then obtained by the following equations:

$$H_s = h_0 \left[ \left( \frac{h_{\min}}{h_0} \right)^\gamma - \text{Ln}(1 - \text{CDF}(H_s)) \right]^{1/\gamma} \quad (3.28)$$

$$E[T_p | H_s] = 5.39 H_s^{0.382} \quad (3.29)$$

$$\sigma_{T_p | H_s} = c.o.v. [T_p | H_s] E[T_p | H_s] \quad (3.30)$$

$$T_p = \Phi^{-1}(\text{CDF}(T_p | H_s)) \sigma_{T_p | H_s} + E[T_p | H_s] \quad (3.31)$$

These equations are derived using Equations 3.6 to 3.7 along with the definition of standard deviation (equal to mean multiplied by coefficient of variation).

5. From Equations 3.28 to 3.31, reliability contours can be plotted describing the joint probability distribution that corresponds to a specified failure plan with an exceedance probability of  $p_{\text{storm}}$ .

Details of the inverse reliability procedure and its applications can be found in many references (e.g., Li and Foschi, 1998; Saranyasontorn and Manuel, 2004; Murty and Naikan, 1996; Minguez et al., 2005).

#### ***3.4.2.3 Example of Step 2***

Using the information from the previous two sections, the reliability contours for varying return periods are derived and plotted in Figure 3.18. For each contour in this figure, the volume of the joint probability distribution outside of a tangent line to the contour has a constant value (e.g., Winterstein and Kumar, 1995). For the 50-year contour, the constant value of probability is 1/50 in a one-year period. For the 100-year contour, this probability is 1/100 in a one-year period. These contours, which will be referred to as annual reliability contours, are useful because they express the distribution for  $H_s$  and  $T_p$  in terms related to the return periods specified in the design guidelines.

One noteworthy aspect of the contours on Figure 3.18 is that the 100-year event with the maximum  $H_s$  value corresponds to the 100-year  $H_s$ . Based on these contours, derived from the GUMSHOE data base (Winterstein and Kumar, 1995 and Banon et al., 1991), the 100-year  $H_s$  value is 11.7 m. GUMSHOE is an oceanographic database for

the Gulf of Mexico and comprises of hindcasts for 100 historical hurricane events in the Gulf of Mexico. However, the typical 100-year value in the API code (Table 2.3) and the value used in the design of this spar is 12.5 m. Therefore, either the value used in the code is a bit conservative or the probability distributions developed by Winterstein and Banon based on GUMSHOE are slightly unconservative. In any event, the estimate for 100 year value will be changing in light of recent hurricanes.

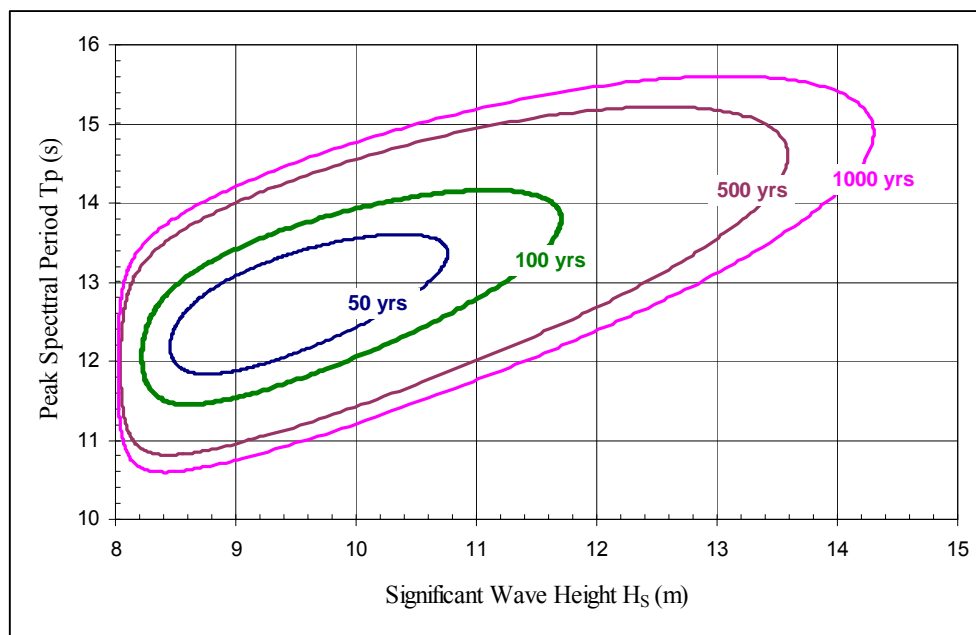


Figure 3.18:  $H_s$ - $T_p$  annual reliability contours due to hurricanes in the Gulf of Mexico

For the reliability analysis, we are concerned about the response of the structure to storms occurring during its design life. The design life of the theme spar was taken to be 20 years. Therefore, the annual reliability contours have been converted (assuming storm occurrences follow a Poisson process) into 20-year reliability contours on Figure 3.19. Here, the probability of being outside of a tangent line along the contour in a 20-year period corresponds to complement of the percentile. For example, this probability is 5 percent for the contour labeled 95th percentile.

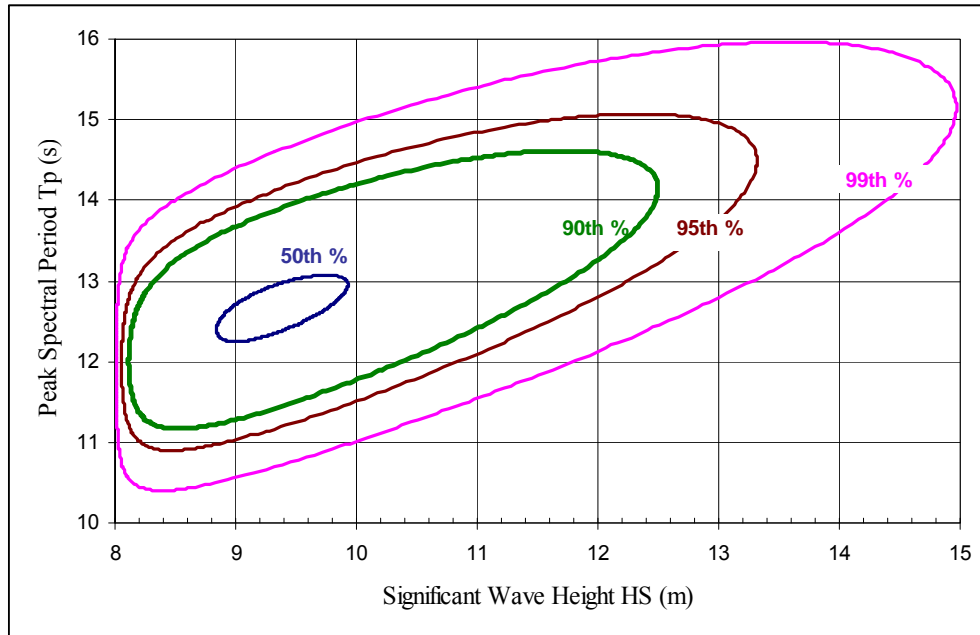


Figure 3.19:  $H_s$ - $T_p$  reliability contours due to hurricanes for a 20 year design life

### 3.4.3 Step 3: Probability distributions for maximum loads

A probability distribution for the maximum line loads in a 20-year design life can be obtained by combining the information on the maximum line load during a given 3-hour storm (Step 1) with the probability distribution for the occurrence of different storm events (Step 2). In the following subsections, the probability distributions for maximum loads are shown and discussed for the study spars.

Figure 3.20 combines Figures 3.14 and 3.19 and shows the load contours and the  $H_s$ - $T_p$  likelihood contours on the same graph. Figure 3.20 can be used to establish the probability distribution for the expected maximum load: the 50th percentile value is 5,144 kN; the 90th percentile value is 7,158 kN; and the 95th percentile value is 7,512 kN. A lognormal distribution provides a reasonable and convenient fit to these percentiles as shown in Figure 3.21. The lognormal distribution is characterized by two

parameters:  $\lambda$ , which is the natural logarithm of the median value for the expected maximum load, and  $\zeta$ , which is approximately the coefficient of variation for the load. Figure 3.21 show an example of how these parameters are determined with the percentile loads available above. The solid line in the plot is a linear regression line with the following equation:

$$\Phi^{-1}(p_{T=20\text{years}}) = 4.1737LN(\mu_{X(T=20\text{years}})) - 35.678 \quad (3.32)$$

For a lognormal distribution, Equation 3.32 is equal to:

$$\Phi^{-1}(p_{T=20\text{years}}) = \frac{1}{\zeta}LN(\mu_x) - \frac{\lambda}{\zeta} \quad (3.33)$$

From Equations 3.32 and 3.33,  $\zeta$  turns out to be 0.24 ( $=1/4.1737$ ) and  $\lambda$  equals 8.54829 ( $=35.678/4.1737$ ). Therefore, the median value for the mean maximum load is equal to 5,144 kN and the coefficient of variation (c.o.v.) is about 0.25. In comparison to the c.o.v. in the maximum line load in a given sea state, 0.05, the c.o.v. in the maximum load due to uncertainty in the occurrence of different sea states, 0.25, is significantly larger and therefore dominant.

Figure 3.22 combines Figures 3.15 and 3.19 and shows each of three percentile values for spar in 2,000 m of water, while Figure 3.23 combines Figures 3.16 and 3.19 and indicates them for spar in 3,000 m of water.

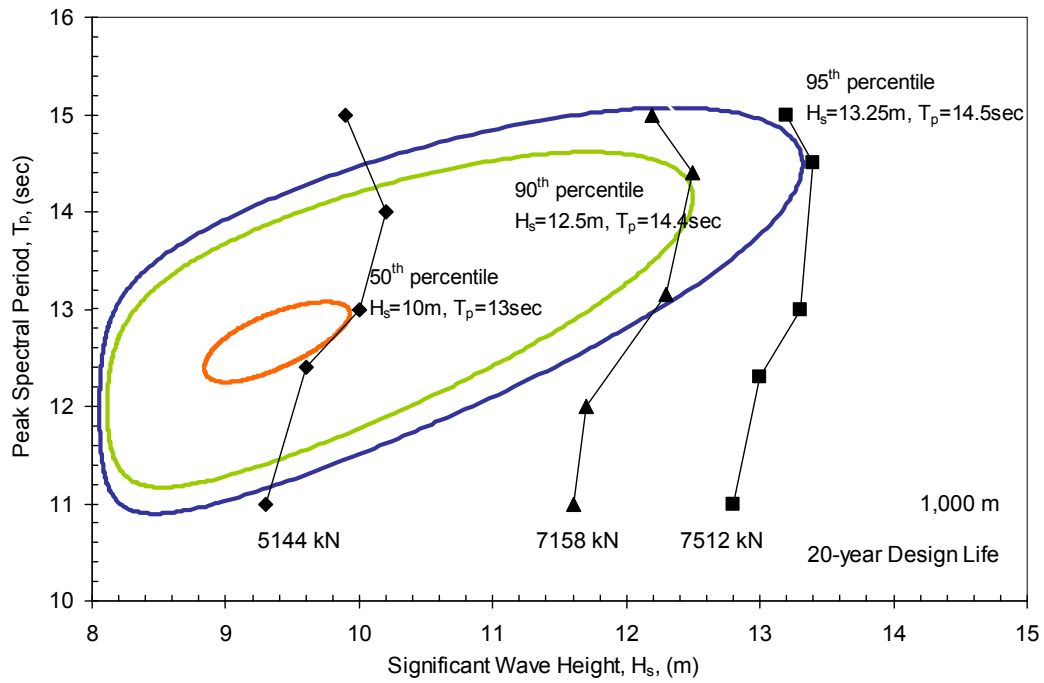


Figure 3.20: Superposition of Figures 3.14 and 3.19 for spar in 1,000 m of water

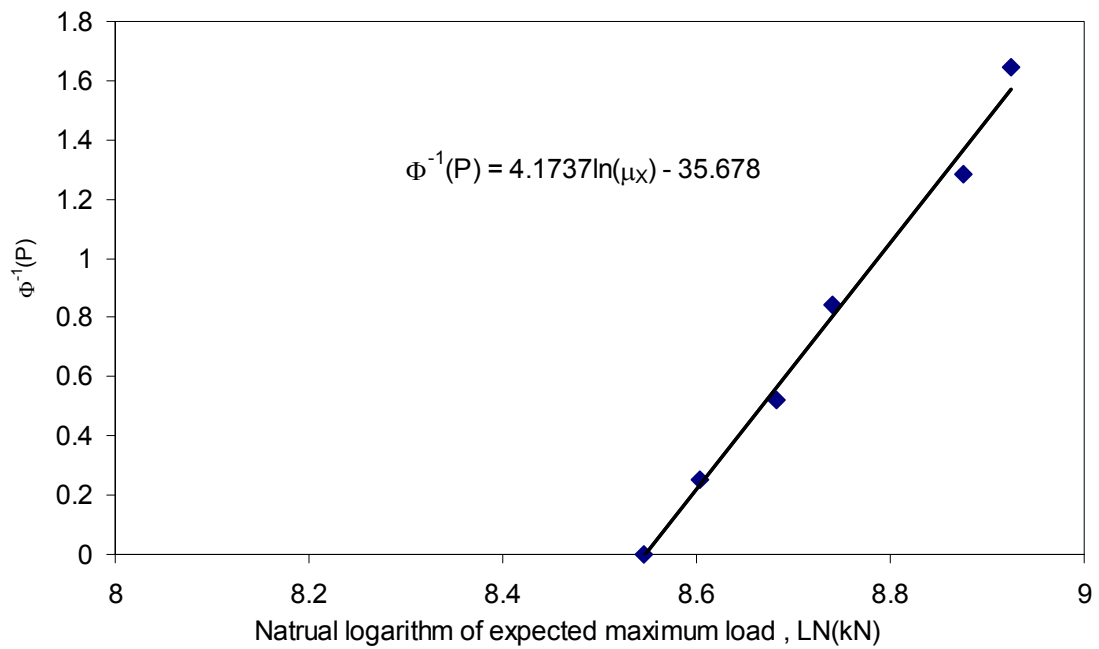


Figure 3.21: Lognormal probability plot of mooring line load for 1,000 m water depth

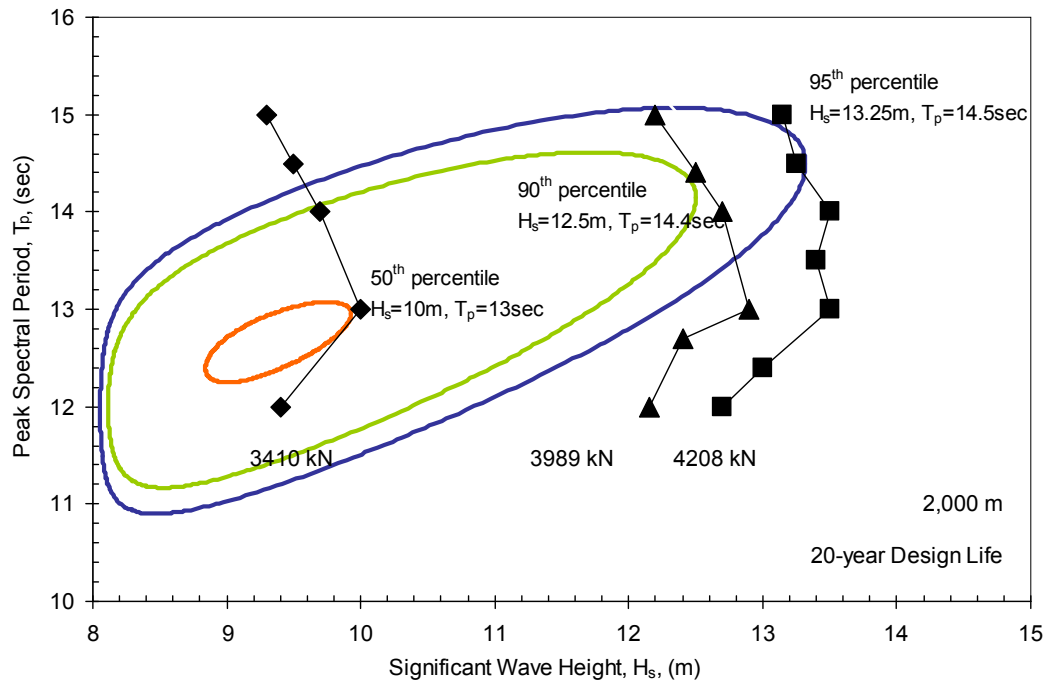


Figure 3.22: Superposition of Figures 3.15 and 3.19 for spar in 2,000 m of water

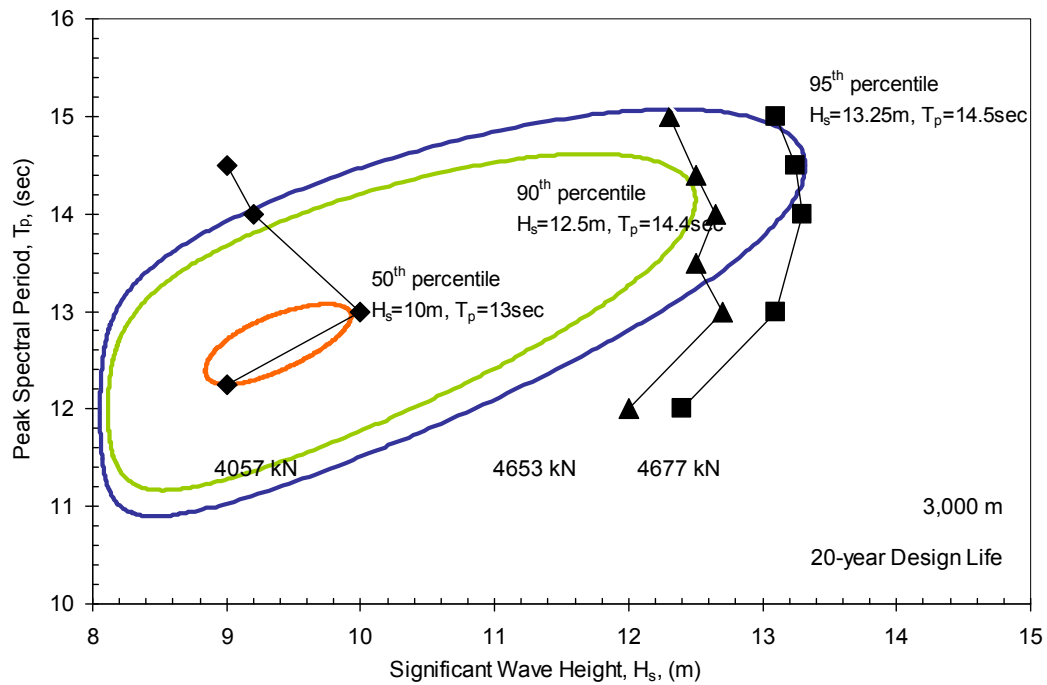


Figure 3.23: Superposition of Figures 3.16 and 3.19 for spar in 3,000 m of water

With the methodology described above, three percentile loads and corresponding coefficients of variation in loads at fairlead and mudline for the study spar in three different water depths are derived. The results are summarized in Tables 3.4 to 3.6 for the most heavily loaded line during hurricane, loop current (Type 2 distribution) and loop current (Weibull distribution), respectively.

Table 3.4: Summary of the percentile loads at fairlead and mudline in 1,000 m, 2,000 m and 3,000 m under a hurricane event

Hurricane	Water depth (m)					
	1,000		2,000		3,000	
	Fairlead	Mudline	Fairlead	Mudline	Fairlead	Mudline
50%	5144	4052	3410	2963	4057	3398
90%	7158	6063	3989	3547	4653	4020
95%	7512	6430	4208	3770	4677	4035
c.o.v	0.25	0.30	0.13	0.14	0.10	0.12

Note: All loads are based on the mostly heavily loaded line.

All loads are in kN.

Table 3.5: Summary of the percentile loads at fairlead and mudline in 1,000 m, 2,000 m and 3,000 m under a loop current event (Type II distribution)

Current (Type2)	Water depth (m)					
	1,000		2,000		3,000	
	Fairlead	Mudline	Fairlead	Mudline	Fairlead	Mudline
50%	8528	7368	6535	6077	7058	6376
90%	9791	8626	7592	7134	8115	7433
95%	10335	9168	8053	7596	8576	7894
c.o.v	0.11	0.13	0.12	0.13	0.11	0.13

Note: All loads are based on the mostly heavily loaded line.

All loads are in kN.



Table 3.6: Summary of the percentile loads at fairlead and mudline in 1,000 m, 2,000 m and 3,000 m under a loop current event (Weibull Distribution)

Current (Weibull)	Water depth (m)					
	1,000		2,000		3,000	
	Fairlead	Mudline	Fairlead	Mudline	Fairlead	Mudline
50%	8634	7474	6622	6164	7146	6463
90%	9656	8491	7475	7017	7998	7316
95%	9982	8816	7749	7292	8273	7591
c.o.v	0.09	0.10	0.10	0.10	0.09	0.10

Note: All loads are based on the mostly heavily loaded line.

All loads are in kN.

### 3.5 UNCERTAINTY IN LINE LOADS

The maximum line load in the 20-year design life of the structure is not known with certainty due to variability in the sea state conditions and uncertainty in the model used to predict the line loads. In this section, uncertainty in the maximum line loads is addressed.

#### 3.5.1 Uncertainty in model parameters

In addition to uncertainty in the environmental conditions (Table 3.4), there is also uncertainty in the loads due to uncertainty in the numerical model used to predict loads. The five most significant model parameters affecting the response of the structure are the drag force coefficient,  $C_D$ , the added mass coefficient,  $C_M$ , the VIV lifting force coefficient,  $C_L$ , Strouhal number,  $S_t$ , and the shape coefficient due to wind loads,  $C_S$ . Since the exact values for these model parameters are not known for the study spar, a first-order analysis was conducted to determine how significant this source

of uncertainty is on the maximum line load. This work was primarily performed by Dangayach (2004) and summarized here.

To study the effect of the parameters on the maximum load, each of these parameters was varied keeping the values of other parameters fixed. The storm simulations were carried out for the sea state:  $H_s = 9.32$  m and  $T_p = 12.64$  s. The sensitivity of the maximum load to each parameter was calculated. Sensitivity factors,  $S_i$ , defined as a percentage change in the maximum load due to a percentage change in the parameter  $i$ , were calculated using the following equations.

$$\Delta\mu_{Xi} = \frac{\mu_{Xi+D} - \mu_{Xi-D}}{\mu_X} (\%) \quad (3.34)$$

$$S_i(\%) = \Delta\mu_{Xi} / 2D \quad (3.35)$$

where  $\Delta\mu_{Xi}$  is the percentage change in the maximum load value in a three-hour storm simulation due to variation in the physical parameter  $i$ ;  $D$  is an amount of change in % in parameter  $i$ ,  $\mu_{Xi+D}$ , the maximum load at the fairlead of line No. 8 when the value of parameter  $i$  is increased by  $D$  %,  $\mu_{Xi-D}$  the maximum load at the fairlead of line No. 8 when the value of parameter  $i$  is decreased by  $D$  % and  $\mu_X$  is the maximum load at the fairlead of line No. 8 when none of the parameter values is changed. The sensitivity factors of the expected maximum loads for mooring line No. 8 at the fairlead in 1,000 m water are summarized in Table 3.7 and also depicted in Figure 3.24.

Assuming that the errors for each parameter are additive and statistically independent, the c.o.v in the maximum load can be estimated as follows,

$$\Omega_{\mu_X}^2 \cong \sum_{\forall \text{ model\_parameters}} S_i^2 \Omega_i^2 \quad (3.36)$$

where  $\Omega_i$  is the c.o.v. for parameter,  $i$ . The c.o.v. value for an individual parameter was conservatively assumed to be one half of the range selected to represent the possible values. For example, a  $\pm 10\%$  change range was used for the study of the sensitivity of  $C_D$ , and thus a c.o.v. of 0.05 was assumed for  $C_D$ . The resulting c.o.v. in the load,  $\Omega_{\mu x}$ , was estimated to be 0.02 based on Equation 3.36. Therefore, the predicted maximum loads in the mooring lines are relatively insensitive to the parameters in the numerical model in comparison to the uncertainty in the met-ocean conditions. In order to be conservative, a value of 0.05 was assigned to represent model uncertainty in the predicted loads for both hurricane and loop current events.

Table 3.7: Sensitivity of expected maximum load to model parameters- Line No. 8 (1,000 m)

Case	Variation in the parameter(s)	Max load at fairlead for line #8 (N)	Sensitivity of load to change in parameter
1	No variation in parameter values	4840210	--
2	$C_D$ increased by 10 %	4877470	6.80%
3	$C_D$ decreased by 10 %	4811730	
4	$C_M$ increased by 10 %	4875330	6.90%
5	$C_M$ decreased by 10%	4808660	
6	$C_L$ increased by 25 %	4876520	2.60%
7	$C_L$ decreased by 25 %	4814550	
8	$S_t$ increased by 10 %	4784930	-11%
9	$S_t$ decreased by 10 %	4898350	
10	$C_S$ increased by 20 %	5001770	18%
11	$C_S$ decreased by 20 %	4652030	

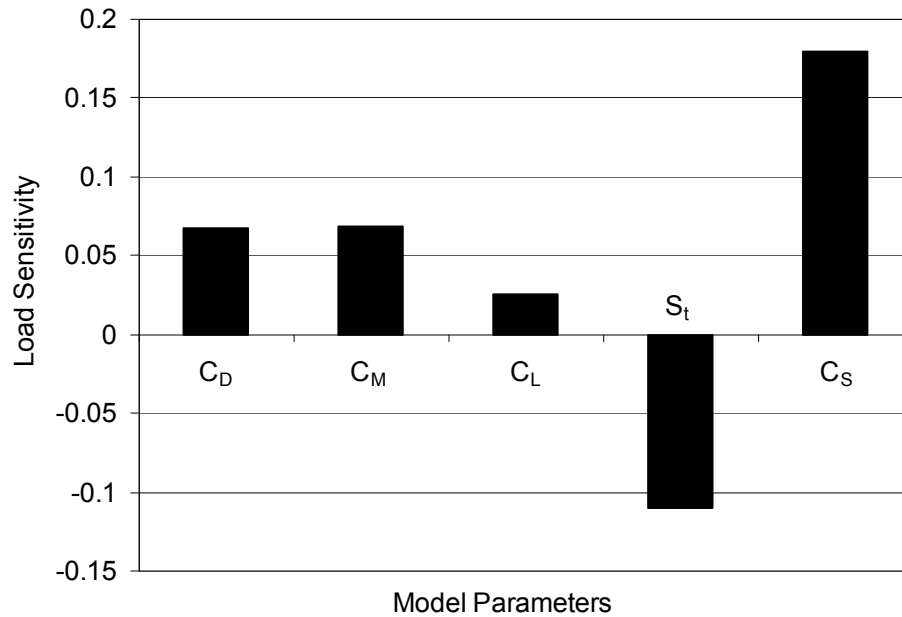


Figure 3.24: Sensitivity of the maximum load to the variation in model parameters in the case of hurricanes and 1,000 m water depth.

### 3.5.2 Total uncertainty in maximum line loads

Total uncertainty in the loads acting on the study spar arises from three sources: 1) the uncertainty due to extreme environmental events that the study spar experience during its lifetime (Section 3.4.3); 2) the inherent randomness in loads from one event to another (Section 3.4.1); and 3) the uncertainty due to numerical model used to estimate loads on the structures (Section 3.5.1). In terms of the model uncertainty, it can be concluded that the predicted maximum loads in the mooring lines are relatively insensitive to the model parameters used for COUPLE6D. The reason for this small model uncertainty is that the line loads are dominated by pre-tension versus environmental loads. The inherent randomness associated with storm events is also significantly small compared to the uncertainty due to different sea state conditions. These three sources of uncertainty are depicted in Figure 3.25. From Figure 3.25, it is realized that the uncertainty due to the metocean environment is the dominant source of uncertainty for this structure.

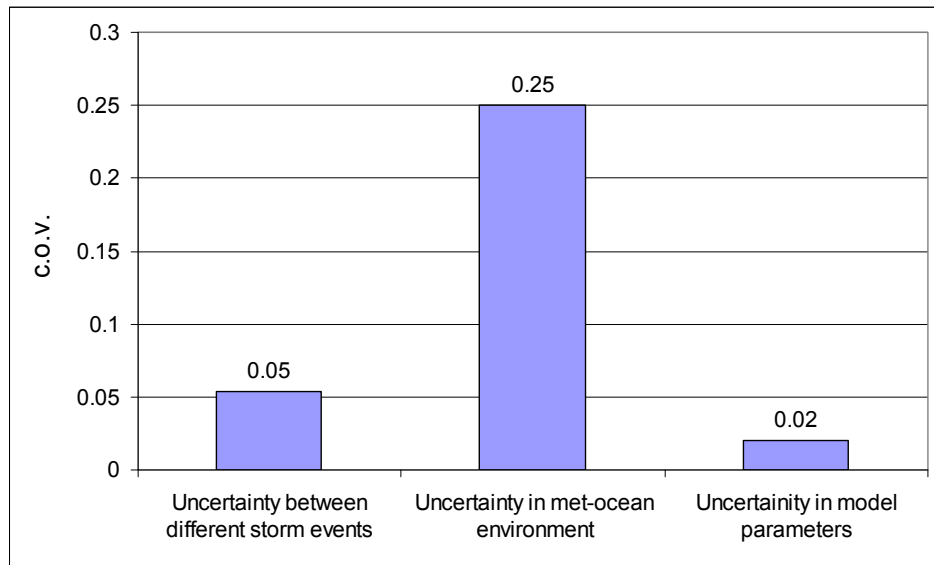


Figure 3.25: Comparison of coefficient of variation values for individual components of uncertainty in hurricane loads for the study spar

### 3.6 LINE LOAD

The expected maximum line loads during a 3-hr hurricane event were estimated using Gaussian approximation for the time series. The line loads at the fairlead are shown on Figure 3.26 and summarized in Table 3.8 for the design hurricane event. Both intact and damaged conditions in three different water depths are shown in Figure 3.26. “Intact” and “Damaged” conditions are design criteria established in the API guidelines (e.g., API RP 2SK 1997) to represent different states of the structure that should be considered in a design. According to API RP 2SK, an intact condition is referred to as the condition in which “all mooring lines are intact” while a damaged condition is referred to as the condition in which “the vessel settles at a new equilibrium position after a mooring line breakage”.

The variation in the loads for both intact and damaged conditions is larger for the 1,000-m water depth than for the other water depths. The loads are shared more evenly between the lines in the taut mooring systems (2,000 and 3,000 m water depths), particularly in the damage cases. This same information is shown on Figure 3.27 and in Table 3.9 for the design loop current event. Table 3.10 provides a summary of the nominal design loads for the most heavily loaded lines compared to the median loads in a 20-year design life due to hurricanes or loop currents.

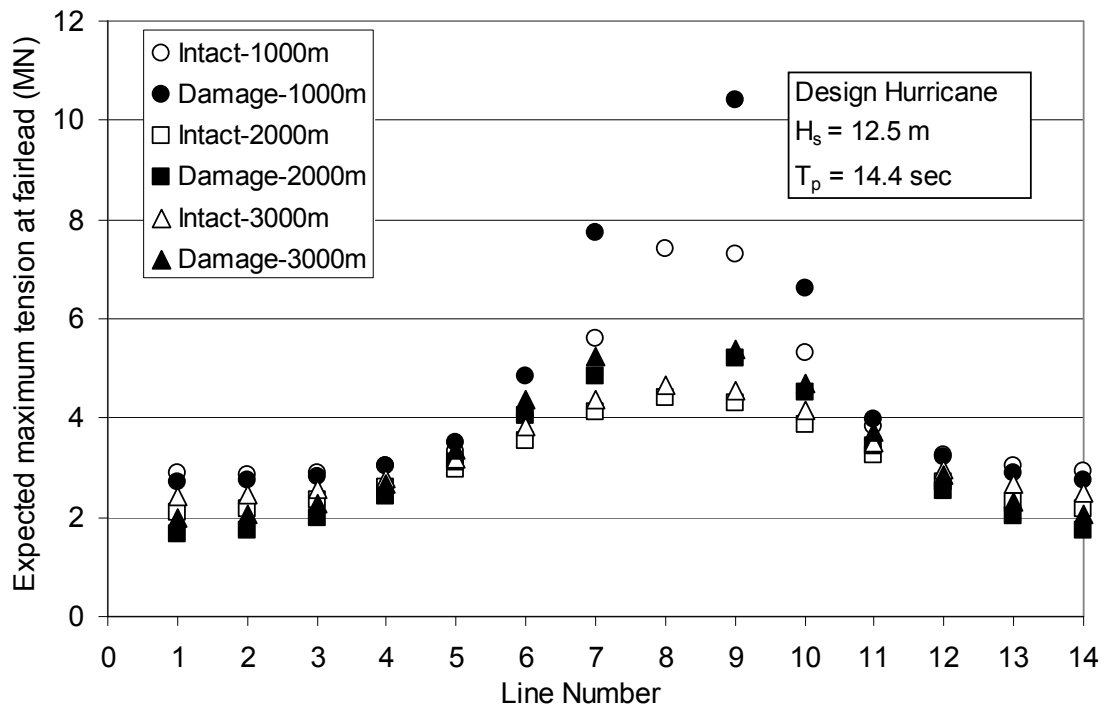


Figure 3.26: Expected maximum line loads at the fairlead in a 3-hour sea state vs. line number for design hurricane event

Table 3.8: Nominal line load at the fairlead in three water depths under hurricane conditions

Water Depth (m)	Mooring Condition	Nominal Line Load (kN)
1,000	Intact	7157
	Damage	10293
2,000	Intact	3990
	Damage	4679
3,000	Intact	4653
	Damage	5400

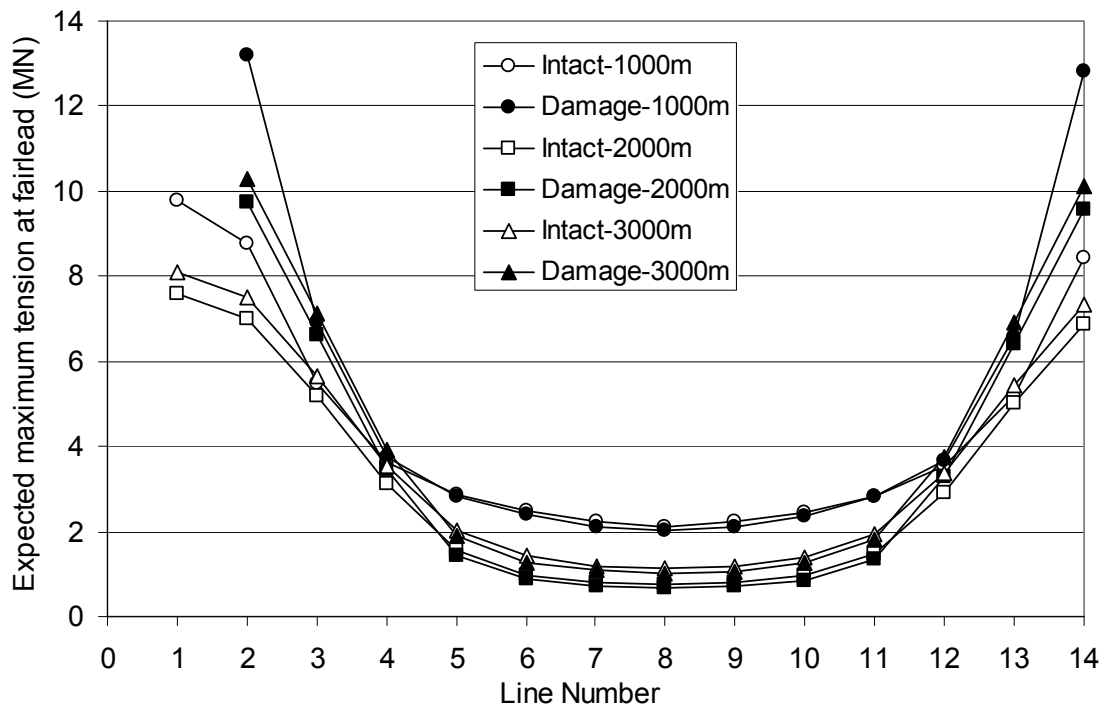


Figure 3.27: Expected maxima of line loads in a 100-year loop current event

Table 3.9: Nominal line load at the fairlead in three water depths under loop current conditions

Water Depth (m)	Mooring Condition	Nominal Line Load (kN)
1,000	Intact	9554
	Damage	13442
2,000	Intact	7210
	Damage	9434
3,000	Intact	7735
	Damage	9972



Table 3.10: Comparison of the ratio of median to nominal design line loads in three water depths under different environmental conditions

Environmental Condition	Water depth (m)	$\text{load}_{\text{median}}/\text{load}_{\text{design}}$
Hurricane	1,000	0.50
	2,000	0.73
	3,000	0.75
Current (Weibull)	1,000	0.70
	2,000	0.72
	3,000	0.72
Current (Type II)	1,000	0.63
	2,000	0.69
	3,000	0.71

### 3.7 FOUNDATION LOAD

The foundation for each mooring line is a suction caisson with a length-to-diameter ratio of 6 and a padeye that is located at two-thirds of the penetration depth below the mudline. The size of a suction caisson used for the mooring systems deployed in different water depths can be determined based on the factored foundation design load which is affected by mooring line loads in the extreme environmental conditions. The details of deriving the size or capacity of the caissons in different water depths will be presented in Chapter 4. In this section, an analytical approximation is presented for calculating the load and its angle at the padeye of a caisson given the properties of the seabed soils and based on the tension in a mooring line and its angle at the mudline. A parametric study on padeye loads is then performed and presented.

### 3.7.1 Interaction among mooring lines, caisson and seabed soils

Figure 3.28a shows conceptually how the line angle varies below the mudline. The loads at the padeye are different in both magnitude and direction from the loads of the corresponding mooring line at the mudline. In general, the foundation load is smaller than the corresponding line loads, and the loading angle at the padeye is greater than the loading angle at the mudline. Soil resistance results in inverse-catenary mooring line shapes as shown in Figure 3.28a. The change in shape and load is due to soil-chain friction acting tangentially to the chain and bearing resistance acting normally to the chain. The soil around the chain is assumed to fail similarly to a strip footing with a loading direction perpendicular to the chain (Degenkamp and Dutta, 1989). Gault and Cox (1974) observed that the soil resistance normal to the chain has little influence on the total load transferred to the padeye but has a greater influence on the direction of a line.

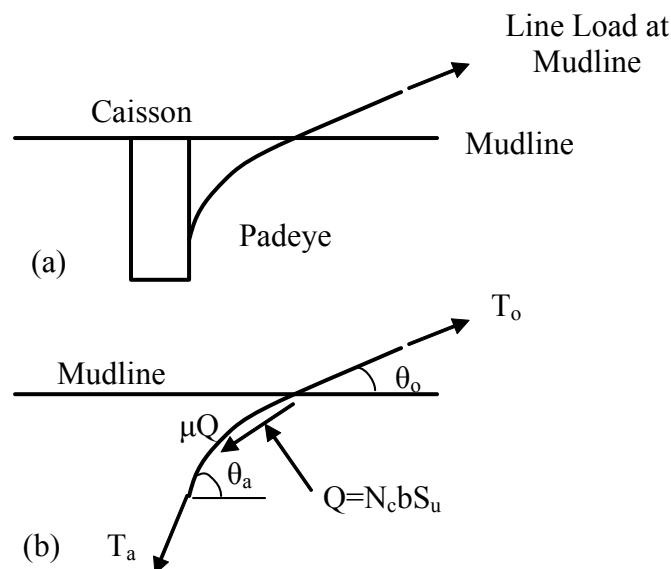


Figure 3.28: (a) Inverse catenary mooring line below mudline; (b) Chain-soil interaction below mudline (Note: N.T.S)

Vivatrat et al., (1982) derived a governing differential equation for the padeye load considering both chain self weight and the tangential soil resistance. The use of a self-weight term in the differential equation made the solution more complicated, so numerical integration of the equation was needed. Accordingly iteration was needed to meet the boundary conditions for the solution to the governing differential equation.

Neubecker and Randolph (1995) proposed an analytical solution for the tension and loading angle at the padeye by neglecting the chain self weight, as the effect of the chain self weight was significant only at shallow embedment depth. The analytical equations are expressed by:

$$\frac{T_a}{2}(\theta_a^2 - \theta_o^2) = DQ_{avg} \quad \text{and} \quad \frac{T_o}{T_a} = \exp(f \cdot \theta_a) \quad (3.37)$$

where  $T_a$  and  $T_o$  are tensions at the padeye and mudline,  $\theta_a$  and  $\theta_o$  are angles at the padeye and mudline respectively,  $D$  is a depth of padeye from mudline,  $Q_{avg}$  is the average normal force to the chain over the depth range below mudline, and  $f$  is a friction coefficient for the seabed soils (Figure 3.28b). Equation 3.37 requires iteration to estimate  $T_a$  and  $\theta_a$ . The normal force per unit length,  $Q$  acting on the chain can be expressed in terms of undrained shear strength as

$$Q = b \cdot N_c \cdot S_u \quad (3.38)$$

where  $b$  is the effective width ( $b=2.5d_b$ ) of bar diameter,  $d_b$ , of a chain,  $N_c$  is a bearing capacity factor ranging from 5.1 at the mudline to 7.6 at a depth of  $z = 2.4b$  and  $S_u$  is the

local undrained shear strength of the soil. The friction coefficient ranges from 0.4 to 0.6.

Although Equation 3.37 also requires iteration to estimate  $T_a$  and  $\theta_a$ , the analytical solution is preferred to the differential solution because there is no need to integrate the governing equation along the length of chain below the mudline. The analytical solution also provides direct insight into chain performance, as discussed in the next section. Once  $T_a$  and  $\theta_a$  are calculated using Equation 3.38 with the load and angle at the mudline, the vertical and horizontal components of  $T_a$  can be determined.

### 3.7.2 Parametric study on padeye loads

A sensitivity analysis was performed to obtain direct insight into padeye loads. Four parameters affecting loads at the padeye are: (1) the undrained shear strength  $S_{uo}$  of soil at the mudline; (2) the rate of strength increase with depth  $S_{ul}$ ; (3) the friction coefficient between soil and chain  $f$ ; and (4) the soil bearing factor  $N_c$ . The sensitivities of the solution for the transferred tension load ( $T_a$ ) and corresponding angle ( $\theta_a$ ) at the padeye, (or vertical component load,  $T_{av}$ , horizontal component load,  $T_{ah}$ , of  $T_a$ , and maximum vertical component load,  $T_{avmax}$ , in a 3-hour storm) to these four variables are shown in Figure 3.29.

The sensitivity study was performed by varying one of the parameters while holding the other three constant. The level of sensitivity of loads and angle to each of the parameters is determined by normalizing the ratio of change in loads and angle with respect to the ratio of change in the parameter. In this figure, a positive increase indicates that an increase in the parameter under consideration causes an increase in the solution value. For example, as  $N_c$  increases, the tension load ( $T_a$ ) at the padeye decreases. The tension load ( $T_a$ ) at the padeye is most sensitive to the friction

coefficient,  $f$ .  $N_c$  is also an important factor because the bearing resistance also affects the angle resulting in change in the vertical and horizontal load at the padeye.

Both  $N_c$  and  $S_{ul}$  have an effect because they are related to the undrained capacity of the strip loading. It is also observed from Figure 3.29 that the friction coefficient has a negative effect on both the vertical component and the horizontal component and all four parameters have a negative effect on  $T_a$  and  $T_{ah}$ .  $N_c$  and  $S_{ul}$  have a greater effect on the angle at the padeye, while the friction coefficient has less of an impact on the angle. In a semi-taut mooring system, a general range of angles at mudline is between  $25^\circ$  and  $35^\circ$ . The angles will increase by  $5^\circ$  to  $10^\circ$  as the mooring chain is getting deeper due mainly to the  $N_c$ , resulting in an increase in  $T_{av}$  but a decrease in  $T_{ah}$ .

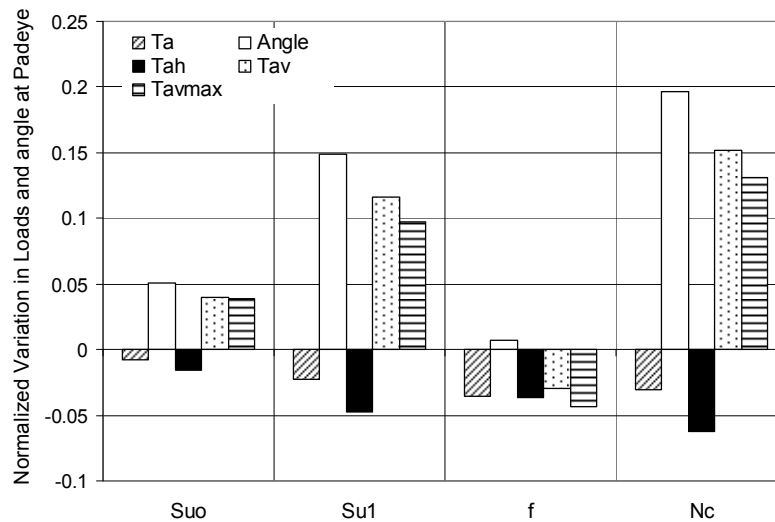


Figure 3.29: Parametric study for loads and angle at the padeye

### 3.7.3 Relationship between loads at the padeye and at the mudline

Figures 3.30 to 3.35 illustrate how the load applied to the foundation is related to the load at the mudline for the mooring system in 1,000 m of water. As the tension in the chain at the mudline increases, the relative tension applied to the padeye increases

(Figure 3.30). The tension in the chain at the padeye is five to ten percent smaller than that at the mudline under the design load of about 6,000 kN for the most heavily-loaded line. The angle of the chain at the padeye decreases as the tension at the mudline increases since higher tension pulls the chain through the soil and decreases the reverse catenary (Figure 3.31). The angle at the padeye is about five to ten degrees steeper than that at the mudline under the design load of about 6,000 kN. The design capacity of the suction caisson is generally governed by its axial capacity for semi-taut and taut mooring systems (e.g., Gilbert and Murff, 2001a). Figure 3.32 shows how the vertical force applied to the foundation is related to the tension and the angle in the chain at the mudline. While the angle of the chain at the padeye becomes less steep with greater tension, the vertical component of the force at the padeye increases with increasing tension (Figure 3.32).

A time series of load during a simulated 3-hour sea state corresponding to the design hurricane event is shown on Figures 3.33 and 3.34. There is a hysteretic relationship between the vertical force at the foundation and the tension in the line (Figure 3.34). However, the maximum vertical force applied to the foundation occurs essentially at the instant when the maximum tension occurs in the chain (Figure 3.34). Therefore, the maximum tension and its associated angle at the mudline can be taken directly from a 3-hour simulation in order to establish the maximum vertical force on the foundation. This finding is illustrated on Figure 3.35, showing a relationship between the normalized loads at the mudline and padeye for the mooring system in 3,000 m of water.

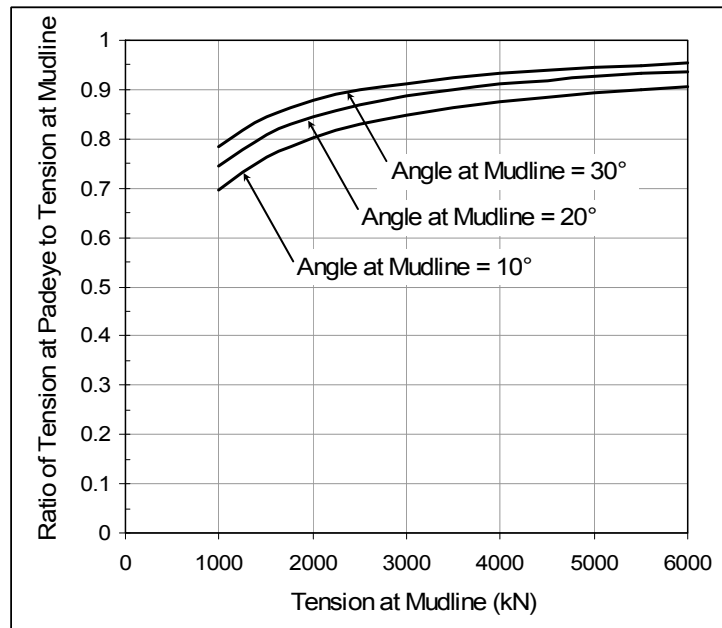


Figure 3.30: Relationship between tension in chain at padeye and tension in chain at mudline for suction caisson foundation; nominal water depth of 1,000 m

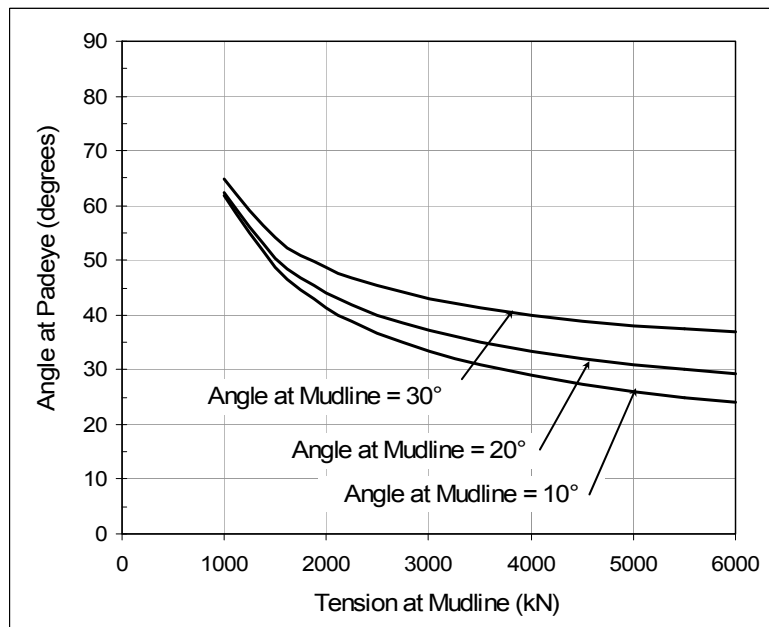


Figure 3.31: Relationship between angle of chain at padeye (subtended to horizontal) and tension in chain at mudline for suction caisson foundation; nominal water depth of 1,000 m

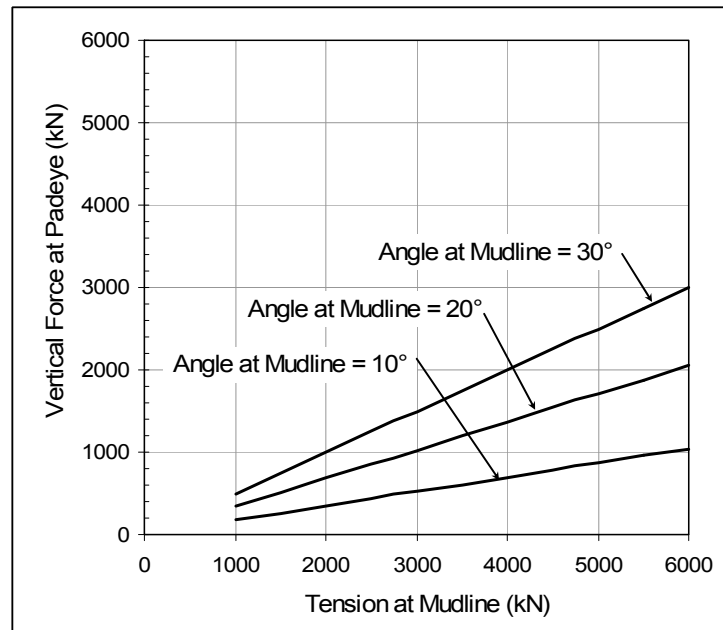


Figure 3.32: Relationship between vertical force at padeye and tension in chain at mudline for suction caisson foundation; nominal water depth of 1,000 m

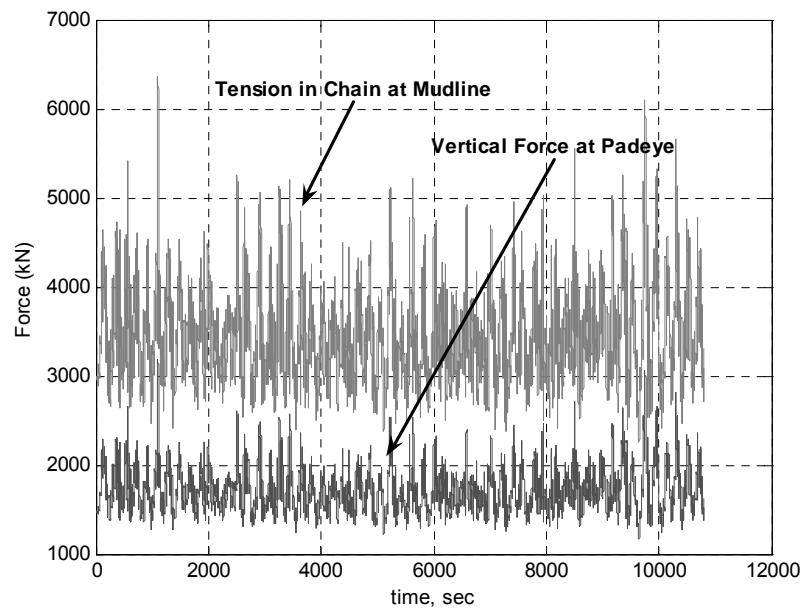


Figure 3.33: Comparison of tension at mudline and vertical component at padeye for line No. 8 in 1,000-m water depth during a 3-hr storm event



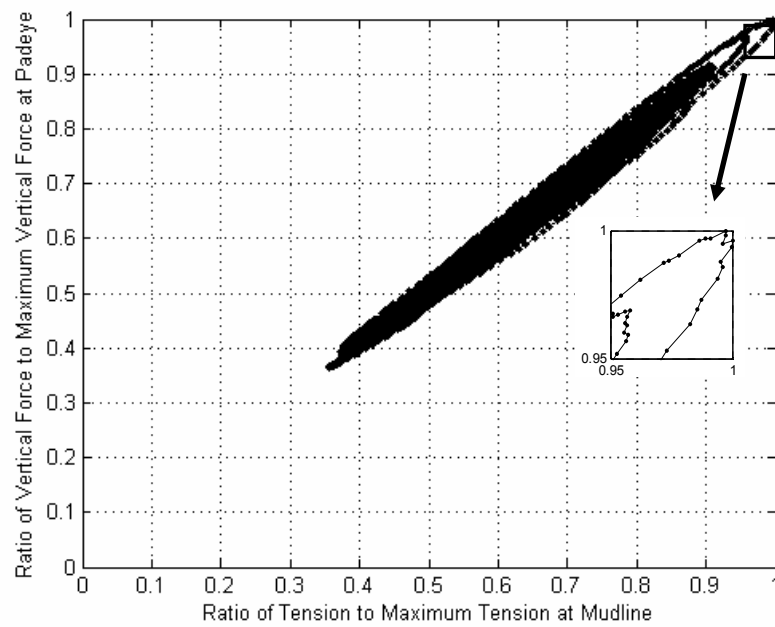


Figure 3.34: Relationship between normalized vertical force at padeye and normalized tension at mudline in 1,000 m water depth during a 3-hr storm event

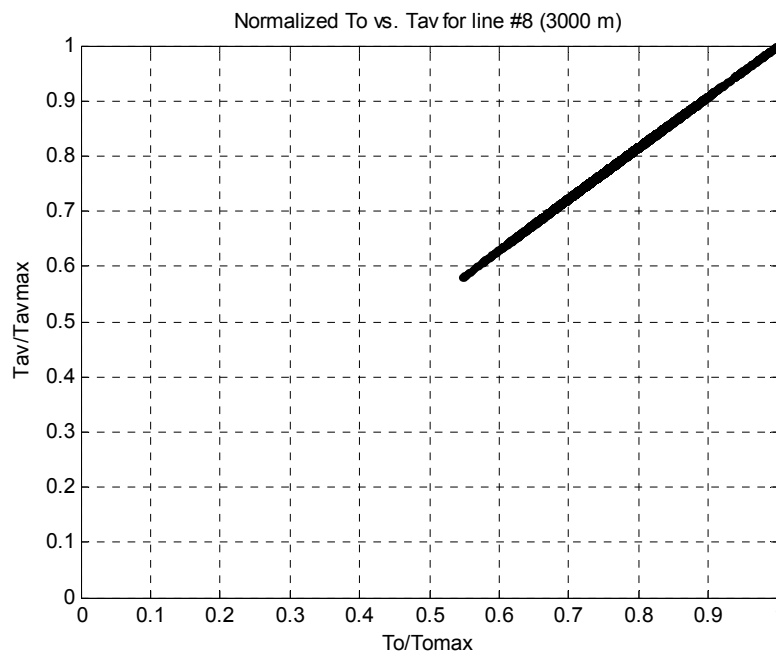


Figure 3.35: Relationship between normalized vertical component at padeye and normalized tension at mudline in 3,000 m water depth.

### 3.7.4 Design foundation loads

The design (or nominal) foundation loads at the padeye are estimated and summarized in Tables 3.11 and 3.12 for the design hurricane event and the design loop current event, respectively. The design sea state is  $H_s = 12.5$  m and  $T_p = 14.4$  sec for a hurricane event and  $V_{\text{cmax}} = 2.1$  m/s at water surface for a loop current event. Table 3.13 provides a summary of the design loads for the most heavily loaded foundations compared to the median loads in a 20-year design life due to hurricanes or loop currents.

Table 3.11: Nominal foundation load at the padeye in three water depths under hurricane conditions

Water Depth (m)	Mooring Condition	Design Foundation Load (kN)
1,000	Intact	3001
	Damage	4833
2,000	Intact	2310
	Damage	2768
3,000	Intact	2625
	Damage	3131

Table 3.12: Nominal foundation load at the padeye in three water depths under loop current conditions

Water Depth (m)	Mooring Condition	Design Foundation Load (kN)
1,000	Intact	4350
	Damage	6423
2,000	Intact	4448
	Damage	5880
3,000	Intact	4728
	Damage	6223

Table 3.13: Comparison of the ratio of median to design foundation loads in three water depths under different environmental conditions

Environmental Condition	Water depth (m)	$\text{load}_{\text{median}}/\text{load}_{\text{design}}$
Hurricane	1,000	0.41
	2,000	0.70
	3,000	0.71
Current (Weibull)	1,000	0.60
	2,000	0.69
	3,000	0.70
Current (Type II)	1,000	0.59
	2,000	0.68
	3,000	0.69

### 3.7.5 Bias and c.o.v values for foundation loads

Using the methodology presented in Section 3.4 and Equation 3.37, the percentile loads in the foundation loads at the padeye are presented in Tables 3.14 to 3.16 for three different water depths. The corresponding coefficients of variation (c.o.v.) are also presented. The uncertainties in foundation loads due to different sea state conditions at the mudline and padeye are essentially the same. This analysis in this section is based on a similar analysis by Gilbert et al. (2005).

Due to several reasons, the coefficients of variation in the spar foundation load (Table 3.14) are smaller than that for a pile in a typical jacket platform, where the c.o.v. values are generally between 0.3 and 0.5 (Tang and Gilbert, 1993). The reasons for smaller uncertainty in the foundation loads on the spar include:

- 1) The line loads are less sensitive to wave height for a spar mooring system in deep water compared to a fixed jacket in shallow water (e.g., Banon and

Harding, 1989), resulting in that variations in the sea states over the design life are less significant for the spar mooring system.

- 2) The mooring system is simpler to model than a jacket, meaning that there is less uncertainty in the loads predicted by the model.
- 3) The spar line loads are dominated by pre-tension versus environmental loads, meaning that variations in the load due to variations in the sea states therefore have a smaller effect on the total line load. This effect of pre-tension is particularly significant for the taut mooring systems (2,000-m and 3,000-m water depths), which consequently have the smallest c.o.v. values (Table 3.14).

Table 3.14: Summary of the percentile loads at padeye in 1,000 m, 2,000 m and 3,000 m under a hurricane event

Hurricane	Water depth (m)					
	1,000		2,000		3,000	
	Padeye	Tav	Padeye	Tav	Padeye	Tav
50%	3700	1959	2736	1940	3175	2229
90%	5744	3001	3322	2310	3797	2625
95%	6111	3157	3545	2451	3814	2643
c.o.v	0.33	0.32	0.16	0.14	0.12	0.11

Note: All loads are based on the mostly heavily loaded line. All loads are in kN.

Padeye load is the total load at padeye. Tav is the vertical component of padeye load

Table 3.15: Summary of the percentile loads at padeye in 1,000 m, 2,000 m and 3,000 m under a loop current event (Type II distribution)

Current (Type2)	Water depth (m)					
	1,000		2,000		3,000	
	Padeye	Tav	Padeye	Tav	Padeye	Tav
50%	7072	3804	5861	4011	6166	4274
90%	8337	4503	6919	4694	7223	4982
95%	8882	4804	7381	4992	7685	5290
c.o.v	0.13	0.14	0.14	0.13	0.13	0.13

Note: All loads are based on the mostly heavily loaded line. All loads are in kN.

Padeye load is the total load at padeye. Tav is the vertical component of padeye load

Table 3.16: Summary of the percentile loads at padeye in 1,000 m, 2,000 m and 3,000 m under a loop current event (Weibull distribution)

Current (Weibull)	Water depth (m)					
	1,000		2,000		3,000	
	Padeye	Tav	Padeye	Tav	Padeye	Tav
50%	7179	3863	5949	4068	6253	4333
90%	8202	4428	6802	4619	7106	4904
95%	8528	4608	7077	4796	7381	5087
c.o.v	0.10	0.11	0.11	0.10	0.10	0.10

Note: All loads are based on the mostly heavily loaded line. All loads are in kN.

Padeye load is the total load at padeye. Tav is the vertical component of padeye load

Table 3.13 provides a summary of the nominal design loads for the most heavily loaded foundations compared to the median loads in a 20-year design life due to the extreme environmental conditions. As shown in Table 3.13, the conservative bias in the median load versus the design load is greater for these spar foundations than for a pile in a typical jacket platform, where the ratio of the median to the design load is between 0.7 and 0.8 (Tang and Gilbert, 1993). This conservative bias is especially significant for the

semi-taut mooring system (1,000-m water depth) due to the effect of removing a line in establishing the design load. The loads are shared more evenly between the lines in the taut mooring systems, which minimizes the impact on each line when one line is removed.

## **Chapter 4: Models for Line and Foundation Capacities**

### **4.1 INTRODUCTION**

The work in this chapter includes the description of methods for estimating the capacity of line and foundation. In addition, the bias factor and coefficients of variation in the estimated capacities are established. Lastly, a discussion on the existence of lower bound capacity is provided. The capacities predicted using the models in this chapter are used as nominal (or design) values of capacity for reliability analyses in Chapter 6.

### **4.2 LINE CAPACITY**

In this section, the models of line capacity, including chain and wire or polyester ropes, are discussed.

#### **4.2.1 Factored loads for design**

For the design cases with intact and damaged conditions, the nominal (design) line capacity is calculated with a factor of safety of 1.67 for intact conditions and 1.25 for damaged conditions (API RP-2SK, 1997). Of the two design conditions, the one providing larger factored line load was considered as the nominal line capacity. The design sea state is  $H_s = 12.5$  m and  $T_p = 14.4$  sec for a hurricane event and  $V_{cmax} = 2.1$  m/s at water surface for a loop current event. A range of factors of safety has actually been used in practice, as shown in Table 4.1. For example, in the semi-taut system where a mooring line composes of top and bottom chains and wire rope, the intact factor of safety ranges from 1.5 to 2.0 while the damaged factor of safety ranges from 1.1 to

1.65. For the taut systems consisting of top and bottom chains and polyester rope, the factor of safety is typically increased by 0 to 20 % in practice because of the lack of field and laboratory experience and as it is a recently adopted technique. For this study, the factors of safety from the most recent published version of API design guideline were used for reliability analyses of the semi-taut and taut mooring systems.

Table 4.1: Comparison of factors of safety for mooring line design for intact and damaged conditions used in different design codes

Material	Factor of Safety		Comment	Reference
	Design Condition	Equivalent FS		
Wire	Intact	1.67	API RP 2SK	API (1997b)
	Damaged	1.25		
	Intact	1.67	API RP-2FPS	Bruen et al. (1991)
	Damaged	1.33		
	Intact	1.7	Calibrated FS based on a target reliability	Goodwin et al. (2000)
	Damaged	1.65		
	Intact	1.5	Intact only (p354)	Larsen (1996)
	Damaged	N/A		
	Intact	1.6	Calibrated FS based on a target reliability	Ahilan et al. (1996)
	Damaged	1.35		
	Intact	1.5	DNV POSMOOR	
	Damaged	1.1		
	Intact	1.85	Lloyds FPS	
	Damaged	1.35		
	Intact	1.65	NMD FPS	
	Damaged	1.25		
	Intact	2	Norwegian Petroleum Directorate (NPD)	
	Damaged	1.4		
	Intact	1.8	IACS	
	Damaged	1.25		
Polyester	Intact Damaged	Increase FSs by ~9 %	American Bureau of Shipping (ABS)	Bhat et al. (2002)
		Increase FSs by 10 %	Det Norske Veritas (DNV)	
		Increase FSs by 20 %	Bureau Veritas (BV)	
		Increase FSs by 0 %	American Petroleum Institute (API)	
		20 % increase	Used for the Mad Dog project (practical example)	Petruska et al. (2005)



The required line capacity was determined for the intact condition and for the damaged condition for the hurricane loading (Table 4.2) and the loop current loading (Table 4.3). The required nominal capacity is equal to the factor of safety multiplied by the nominal load. The governing design condition is then determined by choosing the larger nominal capacity between the two cases, intact and damaged system, in each water depth. The governing condition is indicated in Tables 4.2 and 4.3 for each spar design.

The original spar design developed by DeepStar did not include loop current loading. For the purposes of the reliability analyses, it has been assumed that either the hurricane loading or the loop current loading governs the design. Specifically, it was assumed that hurricane loading governs the design. The reliability was evaluated considering only the occurrence of hurricanes. The reliability analysis considering only the occurrence of loop currents was then repeated by assuming that the loop current loading governs the design. This approach is reasonable providing that the governing loading condition is dominant. Since greater capacities are required for this spar design with loop current loading, it was assumed for convenience that the line capacity could be scaled up without significantly affecting the hydrodynamic response (that is, the larger line weights and diameters needed for the loop current do not affect the load response) while this assumption is not appropriate for actually designing the lines, it is not problematic in the reliability analysis since the structure is hypothetical.

Table 4.2: Nominal line capacity and design governing case under hurricane conditions

Water Depth (m)	Mooring Condition	Factor of Safety	Nominal Line Load (kN)	Nominal Line Capacity (kN)	Governing Condition
1,000	Intact	1.67	7158	11954	
	<b>Damage</b>	<b>1.25</b>	<b>10291</b>	<b>12864</b>	√
2,000	<b>Intact</b>	<b>1.67</b>	<b>3989</b>	<b>6662</b>	√
	Damage	1.25	4679	5849	
3,000	<b>Intact</b>	<b>1.67</b>	<b>4653</b>	<b>7771</b>	√
	Damage	1.25	5403	6754	

Table 4.3: Nominal line capacity and design governing case under loop current conditions

Water Depth (m)	Mooring Condition	Factor of Safety	Nominal Line Load (kN)	Nominal Line Capacity (kN)	Governing Condition
1,000	Intact	1.67	9554	15956	
	<b>Damage</b>	<b>1.25</b>	<b>13442</b>	<b>16802</b>	√
2,000	<b>Intact</b>	<b>1.67</b>	<b>7210</b>	<b>12041</b>	√
	Damage	1.25	9434	11793	
3,000	<b>Intact</b>	<b>1.67</b>	<b>7735</b>	<b>12918</b>	√
	Damage	1.25	9972	12466	

#### 4.2.2 Models for line capacity

Individual mooring lines consist of an upper chain segment, a wire or polyester rope segment and then a lower chain segment. A typical mooring line is shown in Figure 4.1. In this section, capacity models for each of the components of a mooring

line are developed and discussed. The work in this section is primarily based on the work by Choi et al., (2006).

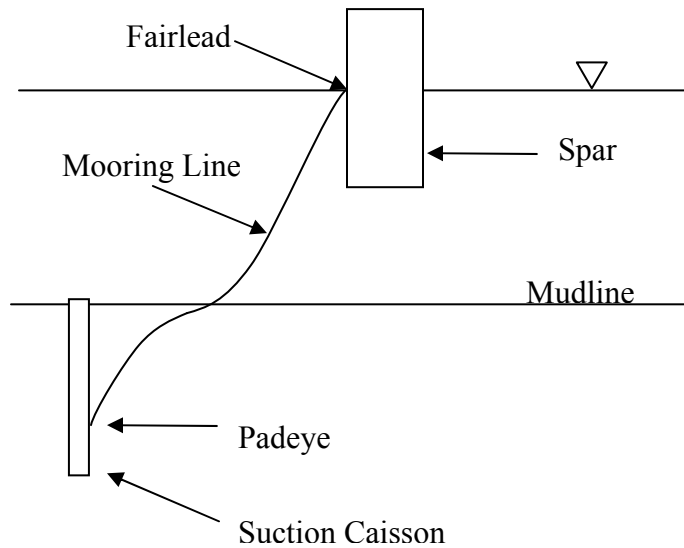


Figure 4.1: (a) A typical mooring line (Image from <http://www.ocsbbs.com>)-top; (b) schematic of a mooring line-bottom (N.T.S)

#### 4.2.2.1 Model for chain

The mooring lines that consist of chain segments are not redundant systems as individual links are connected together in series (Larsen 1996). This implies that if one component link fails, the whole line will fail. Therefore, the final strength of a typical mooring chain depends on the strength of the weakest link (Bush et al., 1992). For practical purposes, the mooring analysis and design are performed based on a test break strength specified by the chain manufacturer (Luo and Ahilan, 1992). A chain strength model proposed by Luo and Ahilan (1992) and Bush et al., (1992) is incorporated in this study as follows:

1. For a single chain link, the probability that line capacity is less than line load (i.e.,  $P(r_i < s)$ ) is expressed as  $F_{r_i}(s)$ . For a line consisting of  $n$  individual components whose distribution functions of the strength are statistically independent, the probability of failure of the line can be expressed as:

$$F_R(s) = P(R < s) = 1 - P(R > s) = 1 - \prod_{i=1}^n (1 - F_{r_i}(s)) \quad (4.1)$$

where  $F_R(s)$  is the cumulative distribution function for the line capacity;  $F_{r_i}(s)$  is the cumulative distribution function of the strength of individual link; and  $n$  is the number of links.

2. From Equation 4.1, if the strength of individual links is statistically independent and identically distributed, then the probability distribution function of the strength of the weakest link out of  $n$  links is given by:

$$F_R(s) = 1 - [1 - F_{r_i}(s)]^n \quad (4.2)$$

3. Based on limited breaking test data, the mean breaking strength ( $\mu_{\text{link}}$ ) of a link is 1.25 times larger than the break test load (BTL), which is set equal to the required nominal capacity of the mooring line (Bush et al., 1992; Luo and Ahilan, 1992).
4. If the material used in mooring systems of high quality is under good quality control, a coefficient of variation ( $\delta_{\text{link}}$ ) of 10 % is considered reasonable given the limited full-scale test data (Bruen et al., 1991; Bush et al., 1992; Luo and Ahilan, 1992).
5. A chain proof load of 70 % of BTL is applied to all links during the manufacturing certification processes. Therefore, in the calculation of the reliability, the proof load is considered as a minimum capacity of the chain segments. If variations in the chain capacity have more to do with handling before and during installation but after testing, then this proof load is not necessarily an appropriate lower bound.
6. During manufacturing of the chain, a test specimen consisting of at least three links is loaded to perform break tests (API, 1997a). Based on this recommendation, the total number of links of the chain segments,  $n$  in Equation 4.1, is divided by 3 to reflect that systems of 3 links are actually tested and essentially comprise a single link for the purpose of reliability.
7. Even though Equation 4.2 is exact solution, there is no closed form solution, which means that numerical integration is required. However, as  $n$  increases infinitely, Equation 4.2 converges to an asymptotic extreme value distribution (Type I smallest for an exponential tail), which may be considered to be accurate as long as  $n$  is large enough (Ang and Tang, 1984). The cumulative

distribution function of the Type I asymptotic form for the distribution of the smallest value is as follows:

$$F_{Y_1}(y_1) = 1 - \exp(-\exp(+\alpha_1(y_1 - u_1))) \quad (4.3)$$

where  $u_1$  and  $\alpha_1$  are the most probable smallest value and an inverse measure of dispersion of initial variate  $X_1$  (i.e.,  $R_i$ ).  $u_1$  and  $\alpha_1$  can be calculated using the equations below:

$$\begin{aligned} u_1 &= F_X^{-1}(1/n) \\ \alpha_1 &= n \cdot f_X(u_1) \end{aligned} \quad (4.4)$$

where  $F_X^{-1}(\cdot)$  is the inverse of CDF of  $X$  and  $f_X(\cdot)$  is the probability density function of  $X$ .

8. The expected value and variance of  $Y_1$  can then be estimated as follows:

$$\begin{aligned} E(Y_1) &= u_1 - \frac{\gamma}{\alpha_1} \\ Var(Y_1) &= \frac{\pi^2}{6\alpha_1^2} \end{aligned} \quad (4.5)$$

where  $\gamma$  is Euler's constant ( $\approx 0.577$ ).

9. With  $E(Y_1)$ ,  $Var(Y_1)$  and line loads, the reliability of the chain segments can be estimated.

Note that the Type I asymptotic distribution has a negative skewness coefficient of -1.1396 which is independent of the parameters  $u_1$  and  $\alpha_1$ .

#### ***4.2.2.2 Model for wire and polyester ropes***

The model for the capacity of the wire and polyester ropes was based on the work of Bruen et al., (1991), Ahilan et al., (1996), Goodwin et al., (1999), Snell et al., (1999)

and Goodwin et al., (2000). The required nominal design capacity is set equal to the Catalog Break Strength (CBS). The capacity is assumed to have a lognormal distribution, with a mean value that is 1.1 times the CBS value and a coefficient of variation equal to either 0.15 or 0.05. The CBS value is equal to the related nominal design capacity. The lower coefficient of variation is adopted from several published papers (e.g., Ahilan et al., 1996; Larsen 1996; Snell et al., 1999; Goodwin et al., 2000). The higher c.o.v value is selected because of the strong possibility that damage to the ropes will occur during the life time of ropes. This may occur due to incidents such as crossed moorings or dropped objects. Damage during such events may result in the reduction in the initial capacity of the ropes. The effect of use of the different coefficients of variation on component and system reliabilities will be studied later. The same model is assumed for both the polyester and the wire rope (Snell et al., 1999).

#### ***4.2.2.3 Comparison of probability distributions for capacities of the mostly loaded mooring line***

Based on the model for individual mooring lines explained in the previous sections, the effect of line length on the total strength of the most heavily loaded mooring line can be investigated as shown in Figure 4.2. The number of the top and bottom chains was estimated using the mooring system specification (Table 2.2) and the corresponding size of the chains from API specification (API 1997a). BTL is equal to the required nominal capacity and the proof test load is set equal to 0.7 of the BTL. It is observed that:

1. As  $n$  increases, the asymptotic distributions shift to lower loads.

2. The mean strength of a chain decreases rapidly with an increasing number of links, resulting in decreasing the reliability of the most heavily loaded line.
3. The bottom chain has considerably smaller capacity than that of a single link because it has so many links.
4. The coefficient of variation decreases with the number of links. However, the difference between the two coefficients of variation for the bottom and top chains is not significant, which indicates that the coefficient of variation does not decrease significantly after a certain number of links.

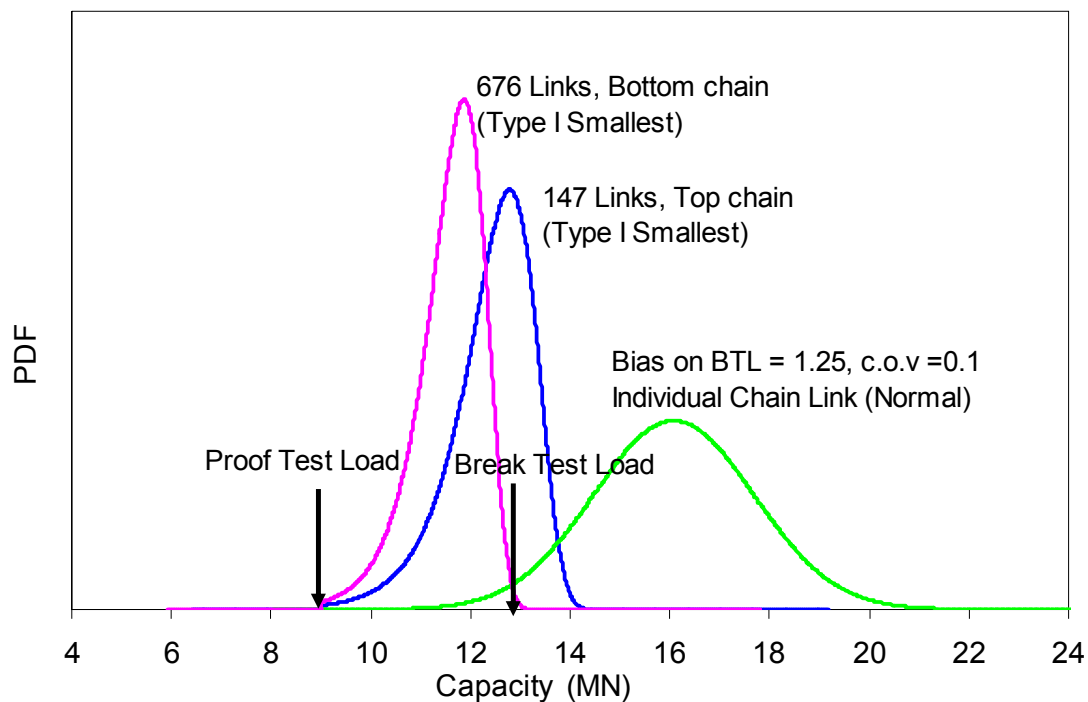


Figure 4.2: Comparison of probability density function for tension strength of the chain segments and individual chain link (for 1000-m water depth under hurricane condition)

Probability density functions for the line capacities of the top and bottom chains and wire rope are compared, as illustrated in Figure 4.3. The line capacities for the top



and bottom chains follow the Type I distribution with a coefficient of variation of about 0.006 and the wire rope has a lognormal distribution with a coefficient of variation of 0.15 (Figure 4.3a) and 0.05 (Figure 4.3b). It is of interest that the shapes of the asymptotic distributions are similar to that of the wire rope distribution. The probabilities of failure of the line components depend largely on the left tail behavior of the three distributions rather than the right tail. Note that the asymptotic form of an extreme distribution does not depend on the exact form of the initial distribution, but depends on the behavior near the tail of the initial distribution in the direction of the extreme (Ang and Tang, 1984). The probability of failure of the wire rope will be much smaller for the case in Figure 4.3b than that in Figure 4.3a. These effects will be compared and verified in the result sections.

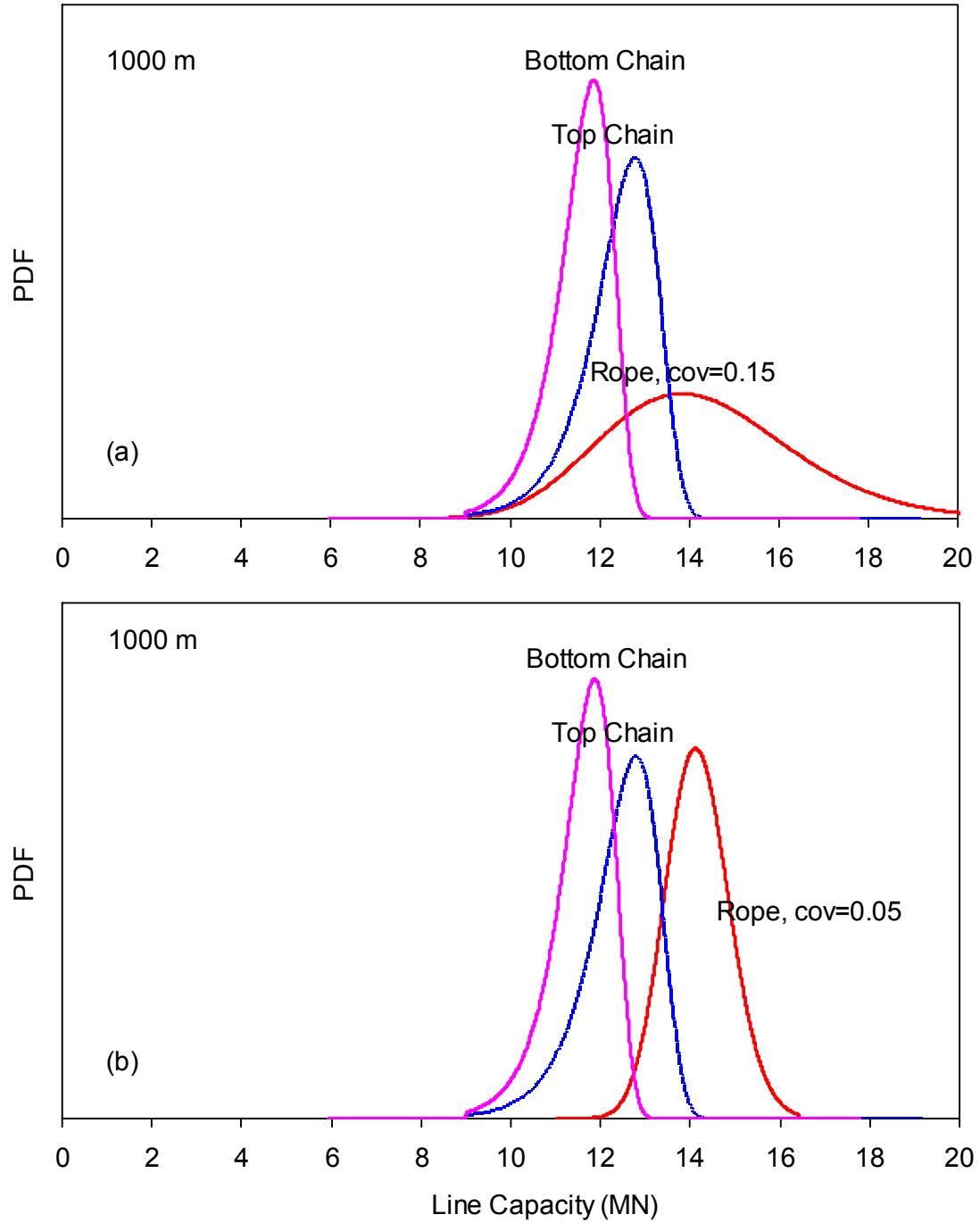


Figure 4.3: Comparison of probability density functions for line capacities of the line components (1000-m water depth under hurricane condition): (a) coefficient of variation for wire rope =0.15; (b) coefficient of variation for wire rope =0.05

### **4.3 FOUNDATION CAPACITY**

Foundation capacity depends on the soil profile, caisson geometry, loading angle at padeye, and the location of the attachment point (i.e., the depth of padeye below the mudline). Due to these factors, failure mechanisms for a suction caisson can be different depending on various combinations of these factors: a pure vertical failure mechanism, a pure horizontal failure mechanism, or an interaction failure mechanism (Clukey et al., 2004). In the following sections, based on the foundation loads discussed in the previous chapter, factored loads for foundation designs are determined for the mooring systems under the hurricane and loop current conditions. The models for estimating axial and lateral capacities and combined capacity are then discussed.

#### **4.3.1 Factored loads for design**

Based on the nominal (or design) foundation loads calculated in the previous chapter, the nominal foundation capacities can be determined with a typical factor of safety ranging from 2 to 3 for intact conditions and 1.5 to 2.5 for damaged conditions. For example, these required nominal capacities at the padeye used for the design of foundations for the study spar are summarized in Tables 4.4 to 4.6 for hurricane conditions and Tables 4.7 to 4.9 for loop current conditions. For hurricane conditions, damaged condition governs for the semi-taut system while intact condition governs for the taut systems. For loop current conditions, intact conditions govern for the taut systems only with a intact factor of safety of 2.0 while, for all other cases, damage conditions govern the design. However, the difference between the nominal capacities for intact and damage conditions is relatively so small that the governing case will be considered to be damage conditions for simplicity.

Table 4.4: Nominal foundation capacity at the padeye and design governing case under hurricane conditions with an intact factor of safety of 2.0

Water Depth (m)	Mooring Condition	Factor of Safety	Nominal Foundation Load (kN)	Nominal Foundation Capacity (kN)	Governing Condition
1,000	Intact	2.0	3002	6005	
	<b>Damage</b>	<b>1.5</b>	<b>4831</b>	<b>7246</b>	√
2,000	<b>Intact</b>	<b>2.0</b>	<b>2309</b>	<b>4617</b>	√
	Damage	1.5	2767	4150	
3,000	<b>Intact</b>	<b>2.0</b>	<b>2624</b>	<b>5249</b>	√
	Damage	1.5	3131	4697	

Table 4.5: Nominal foundation capacity at the padeye and design governing case under hurricane conditions with an intact factor of safety of 2.5

Water Depth (m)	Mooring Condition	Factor of Safety	Nominal Foundation Load (kN)	Nominal Foundation Capacity (kN)	Governing Condition
1,000	Intact	2.5	3002	7506	
	<b>Damage</b>	<b>2.0</b>	<b>4831</b>	<b>9661</b>	√
2,000	<b>Intact</b>	<b>2.5</b>	<b>2309</b>	<b>5771</b>	√
	Damage	2.0	2767	5533	
3,000	<b>Intact</b>	<b>2.5</b>	<b>2624</b>	<b>6561</b>	√
	Damage	2.0	3131	6263	

Table 4.6: Nominal foundation capacity at the padeye and design governing case under hurricane conditions with an intact factor of safety of 3.0

Water Depth (m)	Mooring Condition	Factor of Safety	Nominal Foundation Load (kN)	Nominal Foundation Capacity (kN)	Governing Condition
1,000	Intact	3.0	3002	9007	
	<b>Damage</b>	<b>2.5</b>	<b>4831</b>	<b>12076</b>	√
2,000	<b>Intact</b>	<b>3.0</b>	<b>2309</b>	<b>6926</b>	√
	Damage	2.5	2767	6917	
3,000	<b>Intact</b>	<b>3.0</b>	<b>2624</b>	<b>7873</b>	√
	Damage	2.5	3131	7828	

Table 4.7: Nominal foundation capacity at the padeye and design governing case under loop current conditions with an intact factor of safety of 2.0

Water Depth (m)	Mooring Condition	Factor of Safety	Nominal Foundation Load (kN)	Nominal Foundation Capacity (kN)	Governing Condition
1,000	Intact	2.0	4350	8700	
	<b>Damage</b>	<b>1.5</b>	<b>6423</b>	<b>9634</b>	√
2,000	<b>Intact</b>	<b>2.0</b>	<b>4448</b>	<b>8896</b>	√
	Damage	1.5	5880	8820	
3,000	<b>Intact</b>	<b>2.0</b>	<b>4728</b>	<b>9456</b>	√
	Damage	1.5	6223	9334	

Table 4.8: Nominal foundation capacity at the padeye and design governing case under loop current conditions with an intact factor of safety of 2.5

Water Depth (m)	Mooring Condition	Factor of Safety	Nominal Foundation Load (kN)	Nominal Foundation Capacity (kN)	Governing Condition
1,000	Intact	2.5	4350	10875	√
	<b>Damage</b>	<b>2.0</b>	<b>6423</b>	<b>12846</b>	
2,000	Intact	2.5	4448	11120	√
	<b>Damage</b>	<b>2.0</b>	<b>5880</b>	<b>11761</b>	
3,000	Intact	2.5	4728	11821	√
	<b>Damage</b>	<b>2.0</b>	<b>6223</b>	<b>12446</b>	

Table 4.9: Nominal foundation capacity at the padeye and design governing case under loop current conditions with an intact factor of safety of 3.0

Water Depth (m)	Mooring Condition	Factor of Safety	Nominal Foundation Load (kN)	Nominal Foundation Capacity (kN)	Governing Condition
1,000	Intact	3.0	4350	13050	√
	<b>Damage</b>	<b>2.5</b>	<b>6423</b>	<b>16057</b>	
2,000	Intact	3.0	4448	13344	√
	<b>Damage</b>	<b>2.5</b>	<b>5880</b>	<b>14701</b>	
3,000	Intact	3.0	4728	14185	√
	<b>Damage</b>	<b>2.5</b>	<b>6223</b>	<b>15557</b>	

#### 4.3.2 Model for estimating axial capacity of a suction caisson in normally consolidated clay

If the top cap of a suction caisson is sealed, the axial pullout capacity of the suction caisson anchor is equal to the sum of caisson weight ( $W_c$ ), soil plug weight ( $W_p$ ), external side friction ( $Q_f$ ), reverse end bearing ( $R_c$ ) and overburden ( $Q_o$ ) as shown in Equation 4.6. Detailed equations for each component can be found in VanShaar (2002).

$$R = W_c + W_p + Q_f + R_c - Q_o \quad (4.6)$$

The external side friction is typically calculated under undrained conditions using different values for a friction coefficient,  $\alpha$ , which is a function of the undrained shearing strength of the soil. For normally consolidated clay, an alpha value less than 1.0 is typically used in the design of suction caissons. The reverse end bearing is typically calculated by multiplying the undrained shearing strength at the tip of the suction caisson by an end bearing factor,  $N_c$ . Although there has been some debate over the selection of the end bearing factor, a typical value for  $N_c$  is considered to be 9.0 in the design of suction caissons as recommended in API RP-2A (2002). The API value is based on the conventional bearing capacity theory in clays in which correction factors for shape and depth effects are considered (Skempton 1951; Olson 2005). However, from 1-g model tests and centrifuge model tests, many researchers find that  $N_c$  can be a value greater than 9.0 (e.g., El-Sherbiny et al., 2005; House and Randolph, 2001; Luke et al., 2005). The net reverse end bearing at the tip of a suction caisson can only develop under undrained conditions since typical soils have no “effective stress” tensile strength (Gilbert and Murff, 2001).

Based on the information on the typical design values, contribution of each component to total axial uplift capacity can be found as indicated in Table 4.10. For this table, a length-to-diameter ratio of 6 and the profile of undrained shearing strength for the soil (Figure 2.9) were used along with the typical design values of 0.85 and 9 for  $\alpha$  and  $N_c$ , respectively. The end bearing resistance contributes about 53 % to the total axial capacity while the reverse end bearing account for about 37 % of the total axial capacity. The end bearing resistance is an important value in addition to the skin friction resistance for the axial capacity of suction caisson foundations as indicated in Table 4.10. The submerged self-weight of the suction caisson also affects a small part of the total axial capacity. Plug weight and overburden weight are usually assumed to cancel one another.

Table 4.10: Contribution of each component to total axial uplift capacity ( $L/d = 6$ )

	Diameter of Suction Caissons, ft (m)			
	12 (3.7)	13 (4.0)	14 (4.3)	15 (4.6)
Caisson Weight ( $W_c$ )	12%	12%	11%	10%
Plug Weight ( $W_p$ )	12%	12%	13%	13%
External Side Friction ( $Q_f$ )	52%	53%	53%	53%
Reverse End Bearing* ( $R_c$ )	36%	36%	37%	37%
Overburden ( $Q_o$ )	-13%	-13%	-13%	-13%
Total Axial Capacity	100%	100%	100%	100%

If the top cap is vented, the side friction resistance is assumed on the exterior and interior walls and the end bearing resistance is only assumed along the tip of the caisson wall. In such cases, the reverse end bearing component is small due to the small area of



the tip. However, during the extreme environmental events, it is assumed that the top cap is fully sealed.

In driven pile foundations in cohesive soil, the skin friction component along the embedded depth of the piles provides most of the axial pile capacity, whereas, for the suction caisson foundations, both the skin friction and the end bearing components provide most of the total caisson capacity as indicated in Table 4.10.

#### **4.3.3 Model for estimating lateral capacity of a suction caisson in normally consolidated clay**

Assuming a gap on the back side and a rough interface with the caisson wall, the lateral capacity of a suction caisson was estimated using the plasticity model initially proposed by Murff and Hamilton (1993), modified by Aubeny et al., (2001) and recently updated by Aubeny et al., (2003). The approximate analytical model (Murff and Hamilton, 2003) is based on a collapse mechanism consisting of: (1) a conical wedge near the surface of the soil that is pushed upward by the pile, (2) plane strain horizontal flow of soil around the pile below the conical wedge, and (3) a hemispherical failure surface around the tip as shown in Figure 4.4a. In the original model, the best solution is found by minimizing  $F$  with respect to four optimizing parameters characterizing the kinematics of the failure mechanism. The plasticity model has been widely used in determining the capacity of laterally loaded piles and has been validated by many researchers using numerical solutions and experimental tests (e.g., Aubeny et al., 2001).

However, optimizing four parameters to minimize  $F$  can be difficult. Instead, a simplified model is proposed by Aubeny et al., (2001) as shown in Figures 4.4b and 4.5. In this model, the four optimization parameters are reduced to only one parameter, the depth to the center of rotation,  $L_0$ . This simplified model has some limitations on the

soil profile of linearly increasing shear strength with depth. This profile can be easily found in normally consolidated or lightly overconsolidated clay (Aubeny et al., 2001). The simplified plasticity model for suction caissons has been compared favorably with several finite element analyses, centrifuge model tests (e.g., Clukey and Phillips, 2002) and 1g model tests (e.g., El-Sherbiny et al., 2005). These tests indicate that this model is acceptable for use in designing suction caissons. Details on equations showing the resulting expressions in the forms of the total rates of energy dissipation due to side resistance and at the end of the caisson can be found in Aubeny et al., (2003a and 2003b). Using the updated model, the effect of use of the friction coefficients of 1.0, 0.5 and 0.0 on the ultimate lateral loads are investigated for suction caissons having different aspect ratios of 4 to 8. The lateral capacity increases with increasing the friction coefficient at a relatively constant rate of 13 %.

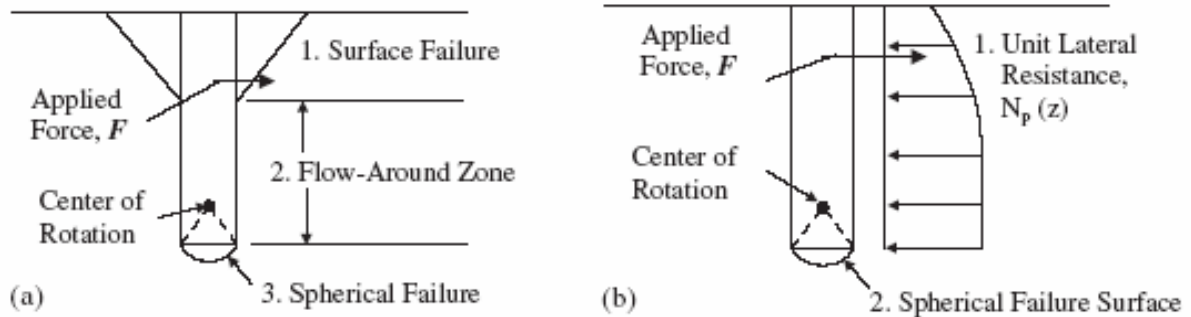


Figure 4.4: Plasticity model for suction caissons (a) failure mechanism assumed by Murff and Hamilton (1993); and (b) simplified analysis by Aubeny et al., (2001) (after Aubeny et al., 2003)

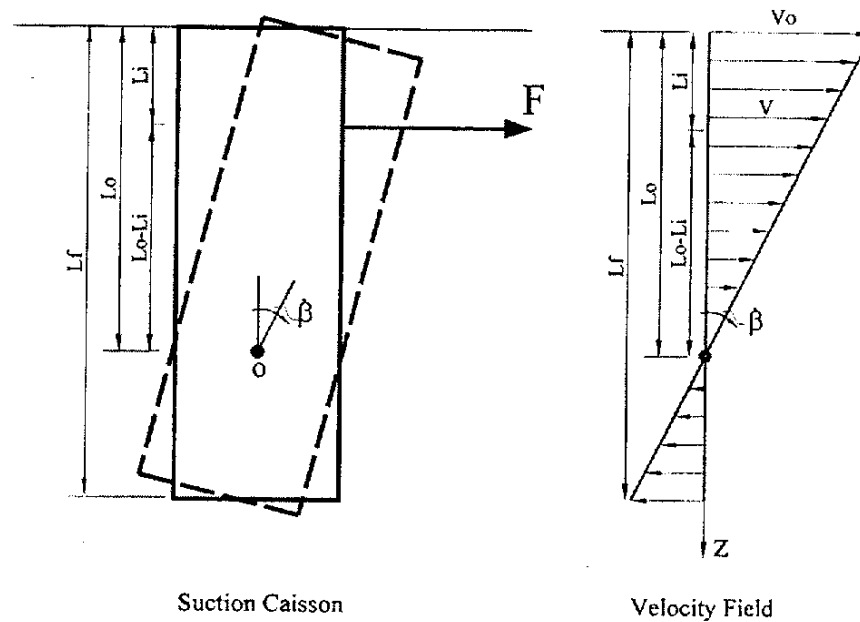


Figure 4.5: Failure mechanism adopted for simplified model by Aubeny et al., (2001)

Table 4.11: Contribution of a friction coefficient to ultimate lateral load ( $L_i = 0.67 L$ )

Aspect Ratio $L/d$	Lateral Capacity (MN)			Ratio of Lateral Capacities w.r.t $\alpha=0$		
	$\alpha=1.0$	$\alpha=0.5$	$\alpha=0.0$			
4	10.1	9.1	8.0	1.26	1.13	1.00
5	14.8	13.3	11.8	1.26	1.13	1.00
6	21.0	18.7	16.6	1.27	1.13	1.00
7	27.4	24.9	21.8	1.26	1.14	1.00
8	35.5	31.3	27.7	1.28	1.13	1.00

#### 4.3.4 Model for estimating combined capacity at padeye in normally consolidated clay

For the mooring systems, suction caissons do not carry purely horizontal or purely vertical load. Instead, it is almost always subject to inclined loading as indicated in Figure 2.3. The ultimate capacity of a suction caisson is expected to be lower than the

resultant of the purely vertical and horizontal capacities because of interaction effects (Randolph and House, 2002). The combined capacity of a suction caisson subject to inclined loading due to environmental loading conditions is discussed in this section. The theoretical background on calculating the combined capacity is first studied. The effects of aspect ratio, design parameters and soil properties on the combined capacity are then investigated. Finally, a simplified equation of the combined capacity given a padeye angle is developed and presented.

#### ***4.3.4.1 Theoretical background on calculating combined capacity at padeye***

Aubeny et al., (2003b) updated their work on lateral resistance (i.e., Aubeny et al., 2001) to account for general loading conditions at the padeye. They used the upper bound analysis by equating the external work performed by applied axial and lateral loads to the energy dissipation from side resistance and from bottom resistance. The upper bound solution is obtained by minimizing  $F$  with respect to two optimization parameters: the center of rotation of the rotating caisson and a parameter,  $\xi$ , relating the magnitude of vertical to horizontal motion (Figure 4.6). In Figure 4.6,  $L_f$  is the embedded length of a caisson,  $d$  is the diameter of the caisson and  $\psi$  is the ultimate loading angle at the padeye of the caisson due to the mooring line (from horizontal). More details on the governing equations that relate the external and internal work can be found in Aubeny et al., (2003a and 2003b). The recently updated analytical method was implemented in an EXCEL spreadsheet program called “SAIL” written by Aubeny et al., (2003a and 2003b). One of the important terms in the model is the skin resistance coefficient, which ranges from unity (full adhesion) to zero (no bonding between the soil and the boundaries of the caisson). This term was only included in the updated

analytical model by Aubeny et al., (2003a). Note that no adhesion means that a gap will form on the backside of the laterally loaded caisson.

The SAIL code has been well verified using centrifuge model tests (e.g. Clukey et al., 2004), finite element analyses (e.g., Aubeny et al., 2003b) and 1-g laboratory tests using two 4-inch diameter prototype caissons in normally consolidated kaolinite (e.g. El-Sherbiny et al., 2005).

It should be noted that during purely vertical loading, the SAIL model is equivalent to the API method. For purely horizontal loading conditions, this model is equivalent to the original model developed by Aubeny et al., (2001) that was described in Section 4.3.3. This model was recommended for caissons with aspect ratio,  $L_f/d$ , greater than 5 (Aubeny et al., 2003b).

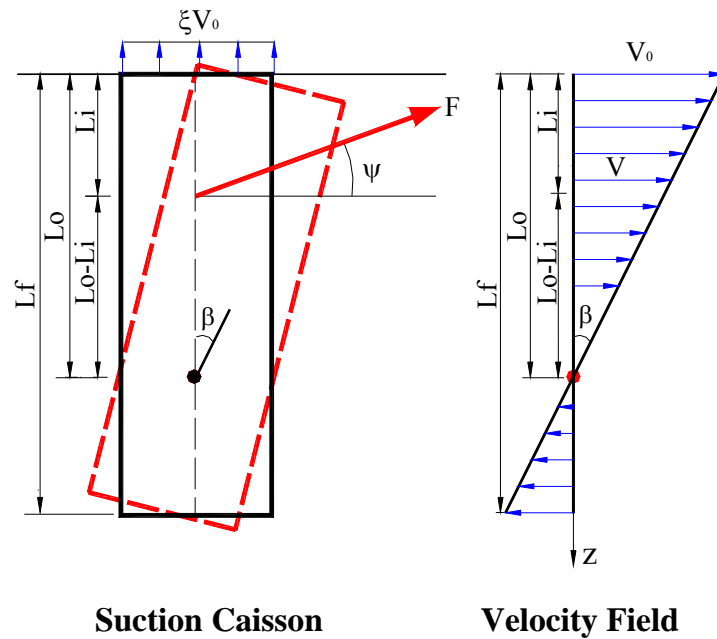


Figure 4.6: Suction caisson rigid body motions under inclined loading (after Aubeny et al., 2003b)

This model (i.e., Aubeny et al., 2003b) is capable of predicting the combined capacity of a suction caisson for different padeye depths, aspect ratios, and undrained

shearing profile that may be constant or varies linearly with depth. The effect of the load attachment point (i.e. padeye) on the predicted ultimate capacity is shown in Figure 4.6. The padeye depth and the predicted capacity for angles ranging from 0 degree to 90 degrees are normalized with respect to the embedded length and the maximum predicted capacity given the geometry of a suction caisson and an undrained shear strength profile. The side friction coefficient,  $\alpha$ , used in Figure 4.7 is 0.9, which is less than unity. The optimum attachment depth ratio is approximately two thirds of the length of the suction caisson. This finding is similar to that of other researchers (Clukey et al., 2003; Aubeny et al., 2003a, b). Accordingly, a padeye depth ratio of 0.67 is used in this study.

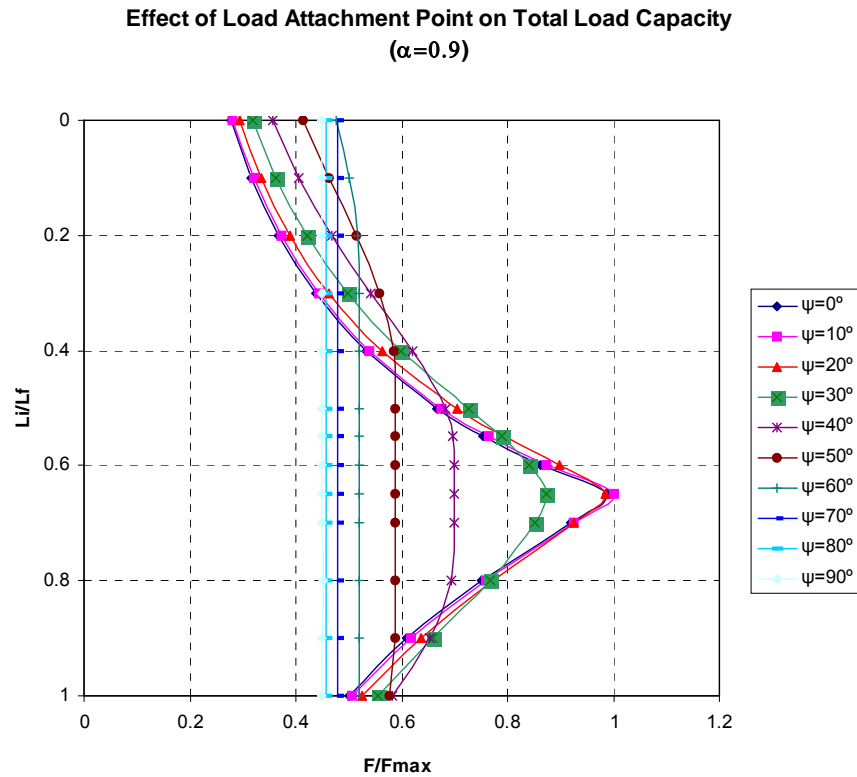


Figure 4.7: Effect of load attachment point (padeye) on total load capacity

From an upper-bound plasticity analysis, Clukey et al., (2000) find that the axial capacity tends to govern the foundation design for suction caissons as the load angle approaches 35 degrees from the horizontal. The result was verified by 1-g model tests by El-Sherbiny et al., (2005). El-Sherbiny et al., (2005) reveals that suction caissons subjected to inclined loads fail only by uplift, as long as the angle at the padeye is greater than about 35 degrees. For the study systems including the semi-taut system under hurricane conditions, the angle at the mudline ranges from 28 and 32 degrees and the padeye angles have a range of 35 to 40 degrees. Hence, foundation design for the study spar will likely be governed by vertical capacity.

The interaction curve for the combined capacities of suction caissons having three different diameters of 3.5 m (11.5 ft), 4 m (13 ft) and 4.3 m (14 ft) with an aspect ratio of 6 is shown in Figure 4.8. For the case where the diameter of the suction caisson is 4.0 m, the pure vertical capacity is about 10.7 MN and the pure horizontal capacity is about 20.9 MN, which is about two times greater than the pure vertical capacity. Likewise, given the geometry of a suction caisson, the design values of the ultimate combined capacity can be obtained from the interaction diagram. The effect for aspect ratios ranging from 4 to 8 on the combined capacity at the padeye is also investigated as shown in Figure 4.9. The combined capacities at the padeye are normalized by the gross tip area of the suction caisson multiplying by undrained shear strength at the tip of the suction caisson. As can be expected, the ultimate lateral load increases with increasing aspect ratios at a higher rate than the ultimate axial load. This plot may be used in preliminary design of a suction caisson in normally consolidated soils subject to inclined loadings.

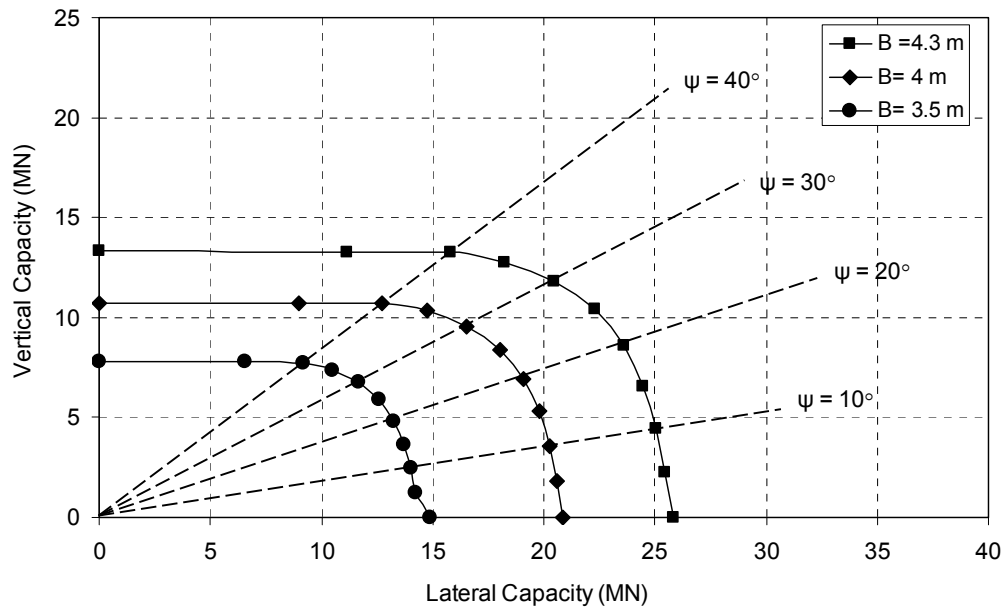


Figure 4.8: Example of interaction curve for capacity of suction caissons

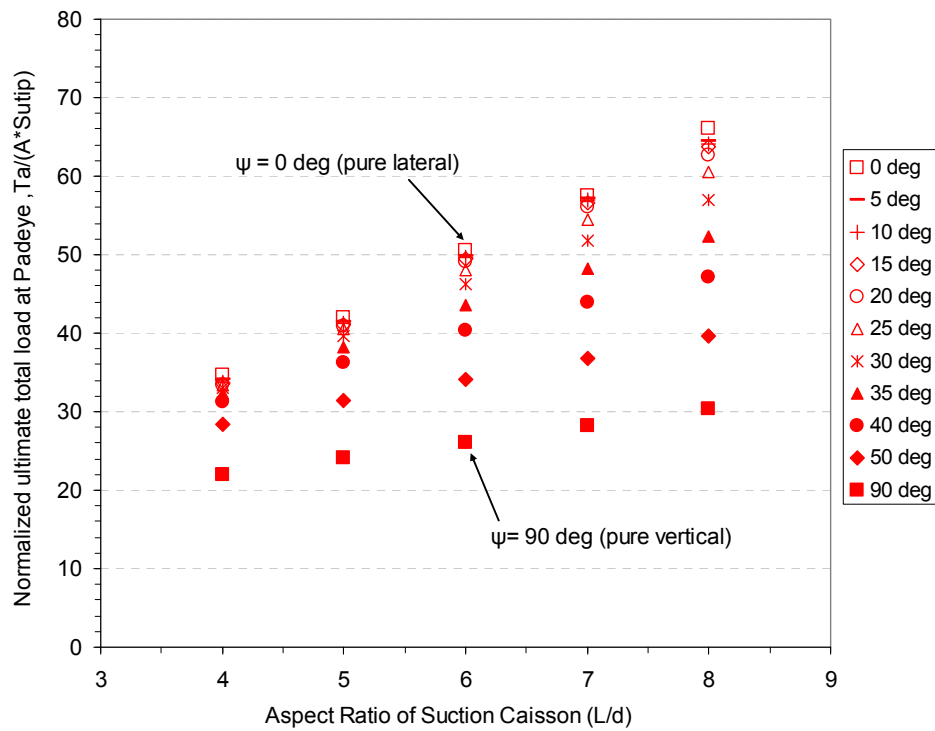


Figure 4.9: Effect of aspect ratio on combined capacity at padeye



#### ***4.3.4.2 Effect of design parameters and soil properties on the combined capacity at Padeye***

The effect of parameters associated with design and soil properties, i.e.  $\alpha$ ,  $N_c$  and  $S_u$  on the combined capacity is investigated as indicated in Figures 4.10 to 4.12, respectively. The side friction coefficient,  $\alpha$ , is varied from 1 to 0.6 in the plots. Similarly, the end bearing factor is varied from 6 to 15. Independent studies deduced a wide range of end bearing factors varying between 6 and 15 (House and Randolph, 2001; Luke 2002; Randolph and House, 2002). A generic soil profile in the Gulf of Mexico includes a shear strength rate with depth of 8 to 10 psf/ft (Gilbert and Murff, 2001a). It is reasonable to expect that for the same aspect ratio and the same padeye depth, the combined capacity will increase with the design and soil parameters. This expectation is confirmed in Figures 4.10 to 4.12. It is of interest that the side friction coefficient affects both lateral and axial capacities essentially evenly while the end bearing factor has no influence on the lateral capacity. The shear strength rate affects the lateral capacity more than the axial capacity as indicated in Figure 4.12.

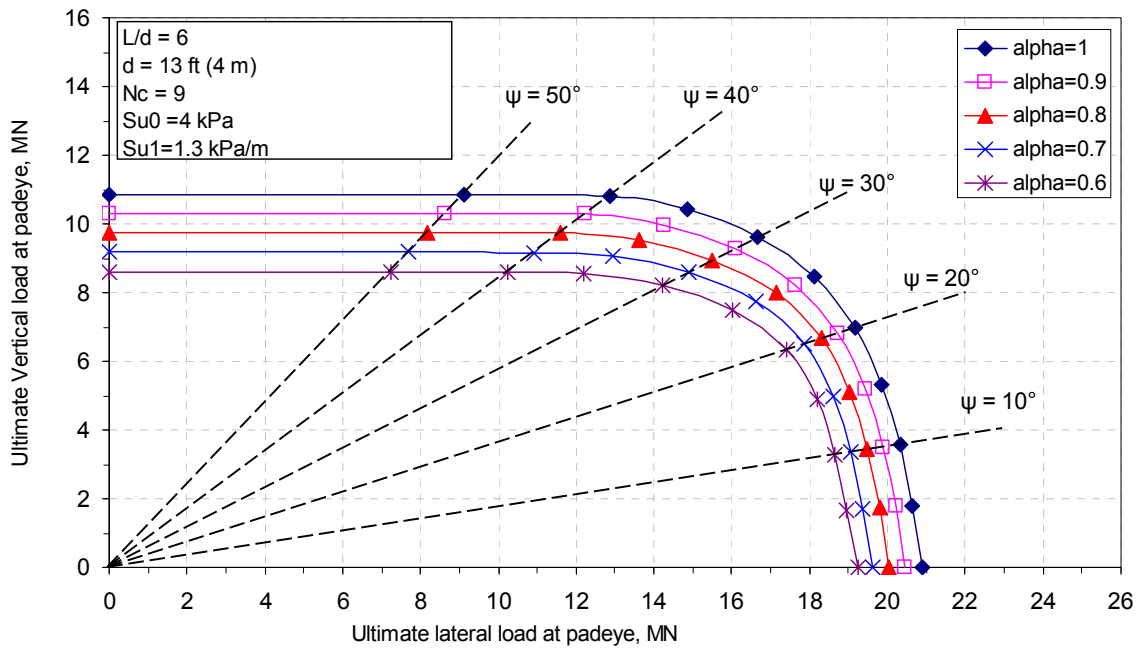


Figure 4.10: Effect of skin friction on combined capacity at the padeye of a suction caisson ( $L/d = 6$  and  $d = 4 \text{ m}$ )

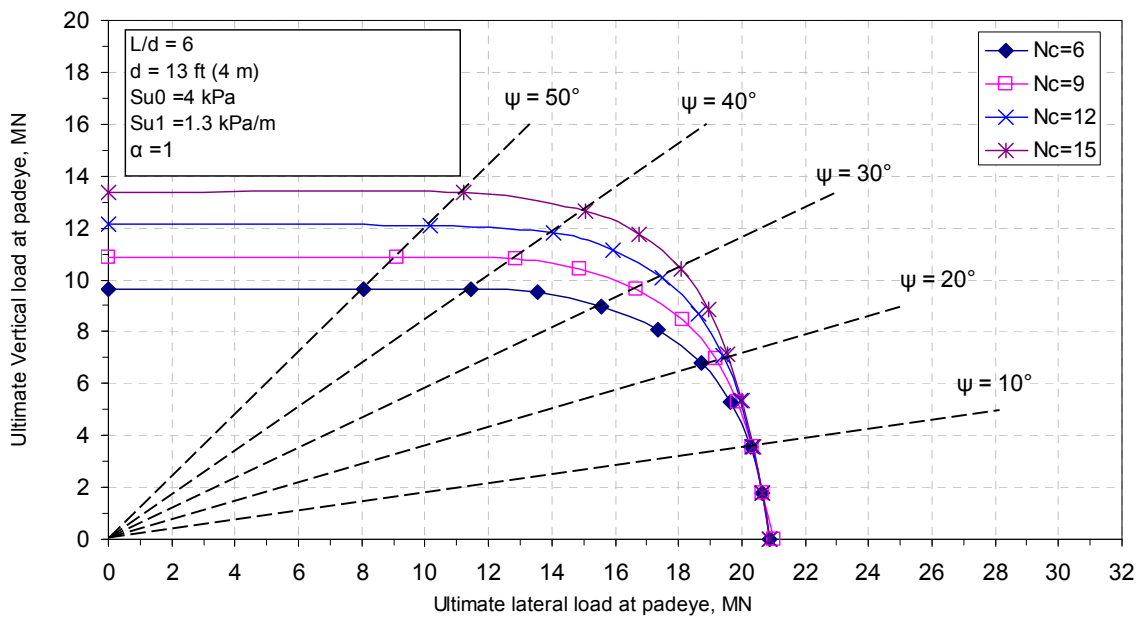


Figure 4.11: Effect of end bearing factors on combined capacity at the padeye of a suction caisson ( $L/d = 6$  and  $d = 4 \text{ m}$ )

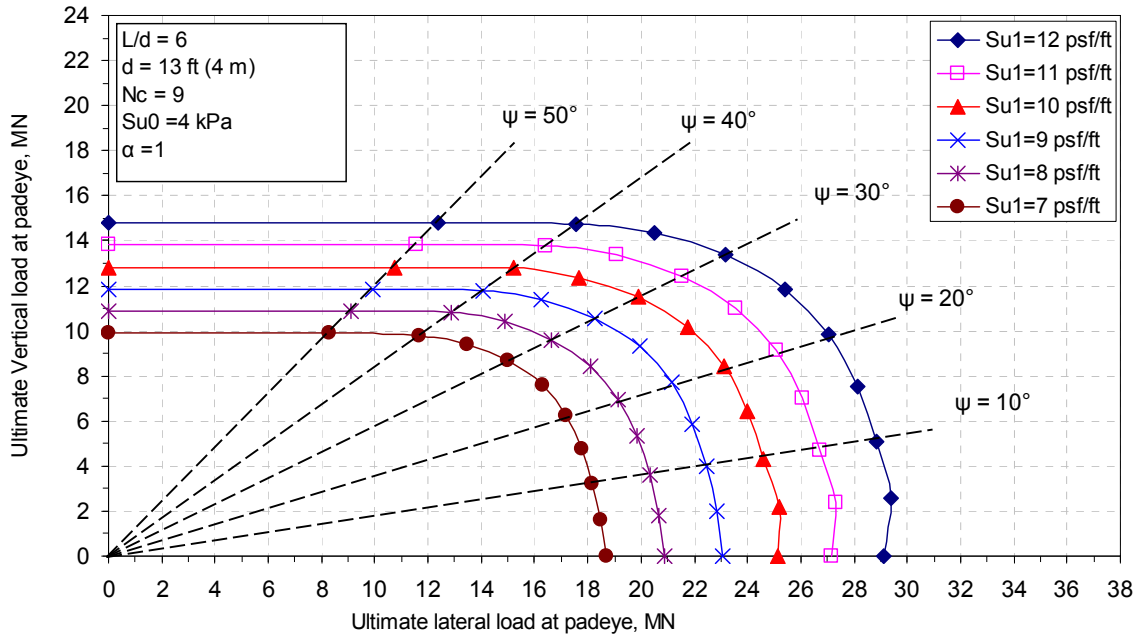


Figure 4.12: Effect of shear strength rate with depth on combined capacity at the padeye of a suction caisson ( $L/d = 6$  and  $d = 4$  m)

#### 4.3.4.3 Simplified model for estimating combined capacity at padeye

It is now common practice for the results of studies of foundations subjected to inclined loadings to be expressed in the form of a yield (or failure) surface for the foundation (e.g., Byrne and Houlsby, 1999; Martin and Houlsby, 2001; Cassidy et al., 2004). A normalized interaction curve is developed for the study spar as shown in Figure 4.13 for the case where  $N_c=9$  and  $\alpha=1$ . The points represent the ultimate total loads at the padeye corresponding to mooring line angles of 0, 5, 10, 15, 20, 25, 30, 35, 40, 50 and 90 degrees from the horizontal. As shown in Figure 4.13, the axial, lateral and inclined capacities of a suction caisson are normalized by multiplying the gross tip area of the suction caisson by the undrained shearing strength at the tip. To generalize the curve accommodating all mooring line angles at the padeye, the normalized points may be approximated using an equation of the form

$$\frac{V}{AS_{utip}} = -0.00013 \exp(0.2408 \frac{H}{AS_{utip}}) + 26.34 \exp(-0.00067 \frac{H}{AS_{utip}}) \quad (4.7)$$

Note that the curve fitting equation was derived using a tool box of curve fitting in MATLAB 7.0 with options of non-linear least squares and Gauss-New method. As may be seen in Figure 4.14, it is observed that the agreement of the curves is excellent.

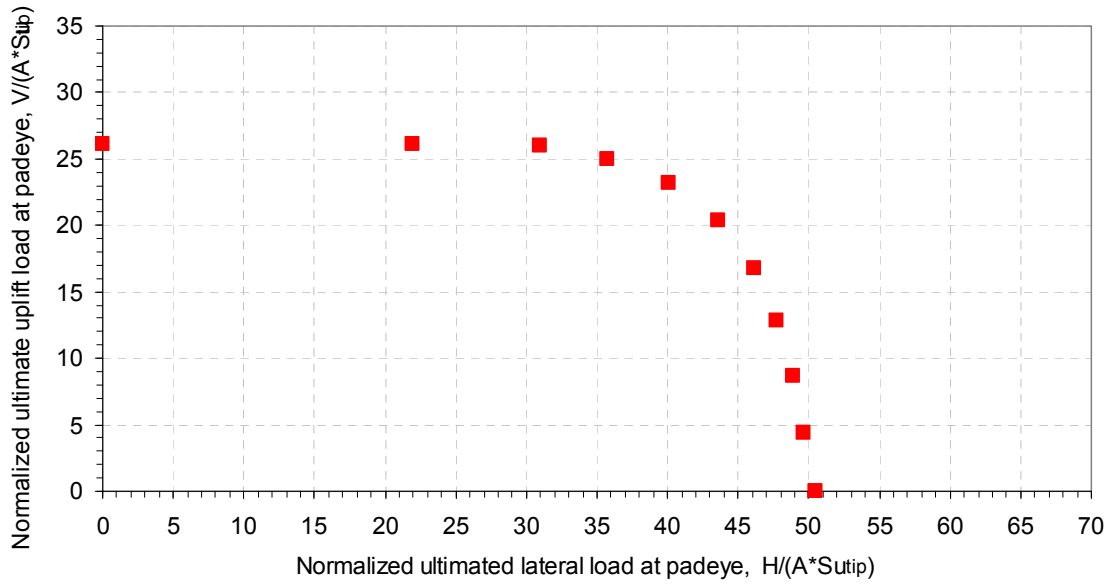


Figure 4.13: Normalized interaction curve for a suction caisson with  $L/d = 6$

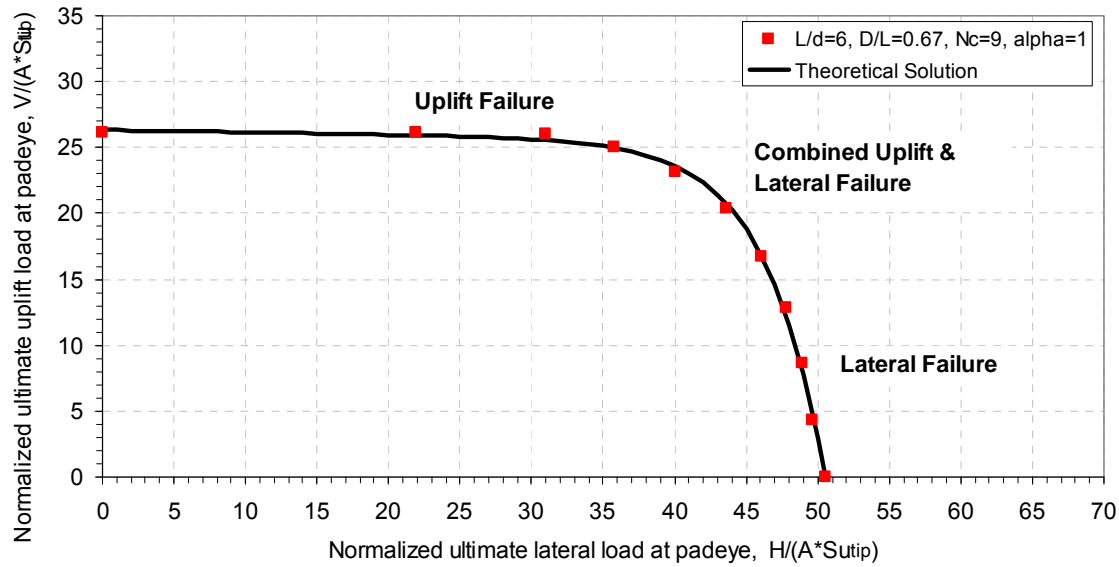


Figure 4.14: Comparison of the normalized and theoretical interaction curves for a suction caisson with  $L/d = 6$

In Figure 4.14, there are three distinct zones of interaction between the uplift load and the lateral load that cause failure. The zone labeled “Uplift Failure” corresponds to an axial failure at the padeye of a suction caisson (that is, the suction caisson pulls out at failure). The zone labeled “Lateral Failure” corresponds to a lateral failure at the padeye due to large lateral loads. The zone labeled “Combined Uplift & Lateral Failure” is a more complicated failure mode where the failure of the suction caisson is due to the interaction between the axial and lateral capacities of the suction caisson.

Figures 4.15 to 4.17 show these interaction curves together with the wave load and predicted capacity at the padeye of the suction caisson in three different water depths. Caisson geometry and design parameters are included in these figures. The blue circle point represents the expected maximum mooring line load at the padeye for the significant wave heights,  $H_s=13.25$  m, 18.3 m and 19.8 m in 1,000 m, 2,000 m and 3,000 m of water, respectively. The interaction diagrams passing through the wave

loads can be derived by reducing the undrained shearing strength at the tip of the suction caisson by a reduction factor (RF) of 0.31, 0.53 and 0.61 in 1,000, 2,000 and 3,000 m of water, respectively. These figures reveal that anchor design is governed by nearly axial failure mechanism in all water depths.

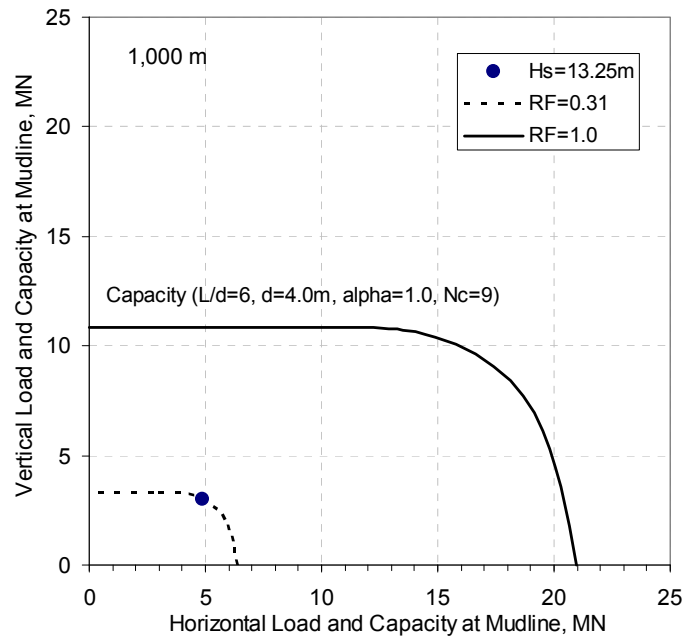


Figure 4.15: Interaction diagram showing wave load (line No. 8) and predicted capacity at the padeye of the suction caisson in 1,000 m of water

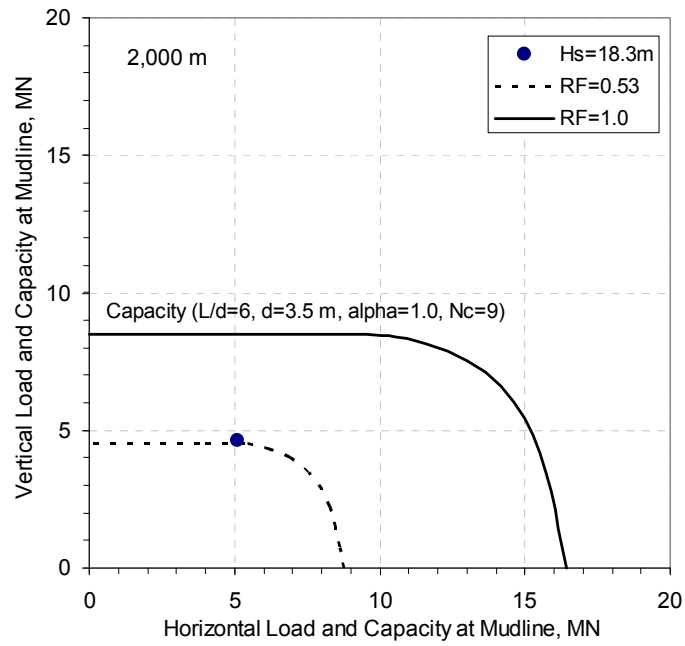


Figure 4.16: Interaction diagram showing wave load (line No. 8) and predicted capacity at the padeye of the suction caisson in 2,000 m of water

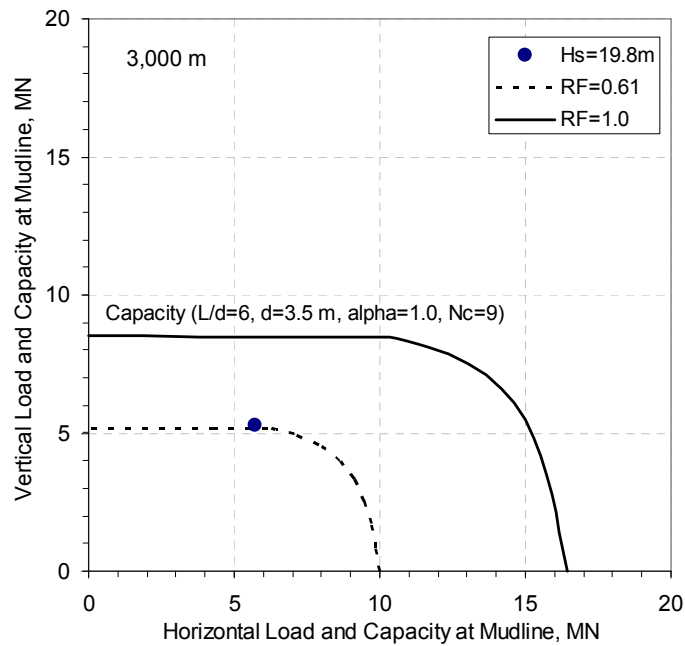


Figure 4.17: Interaction diagram showing wave load (line No. 8) and predicted capacity at the padeye of the suction caisson in 3,000 m of water

Expressing capacity as an ultimate total load corresponding to an angle at the padeye may sometimes be more useful than expressing it as a function of the pure vertical and horizontal capacities. With the curve fitting tool in MATLAB 7.0, a normalized curve in terms of the ultimate total load versus angle at the padeye is developed and shown in Figure 4.18 for the study spar. The curve fitting can be made using an equation of the form

$$\frac{T_a}{AS_{utip}} = -7.02 \times 10^{-5} (angle)^3 - 0.00369 (angle)^2 + 0.0346 (angle) + 50.13 \quad (4.7)$$

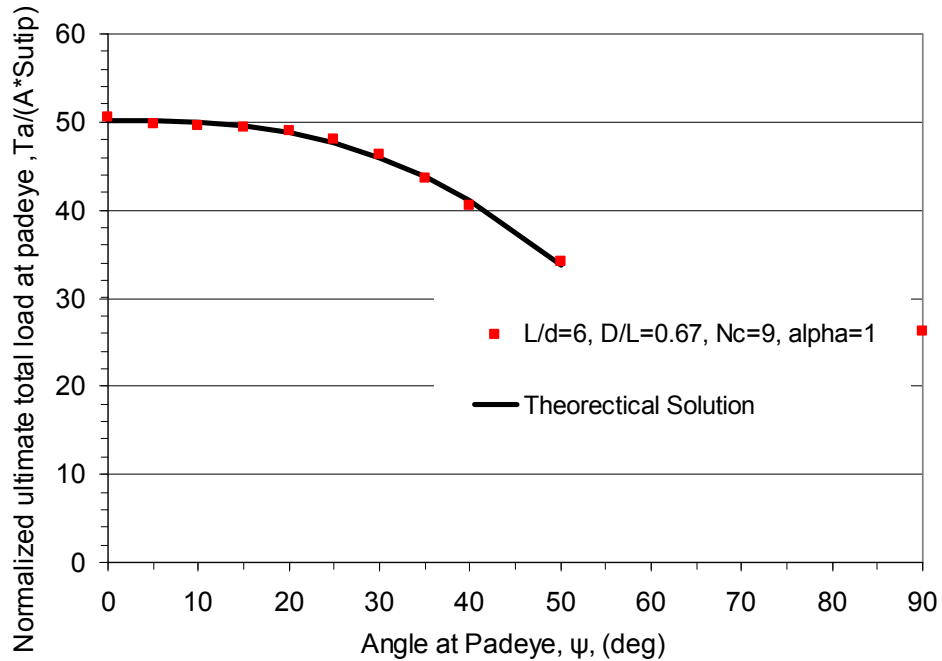


Figure 4.18: Comparison of the normalized and theoretical curves for ultimate total load at the padeye for a suction caisson with  $L/d = 6$

The curve fitting equation was found to work well for a padeye angle less than or equal to 50 degrees. This is because the normalized ultimate total load corresponding to



a loading angle of 90 degrees was excluded in the curve fitting, due to difficulty in deriving a curve fitting equation. However, because the loading angle at the padeye is always less than 50 degrees for the study spar (in all three water depths), this exclusion should not cause a significant discrepancy. The predicted ultimate load at the padeye using Equation 4.7 is considered as a median capacity for the reliability analysis. Note that all of the normalized curves (Figures 4.14 and 4.18) are based on the soil profile shown in Figure 2.9.

#### **4.3.5 Model for estimating combined capacity at mudline**

The load magnitude and angle at the mudline are the output from the numerical hydrodynamic model, i.e., COUPLE6D. The foundation loads at the mudline depend on the environmental sea states and the properties of the superstructure. Therefore, if the capacity of a suction caisson is estimated at the mudline instead of padeye, the reliability analysis of the anchor can be performed in a more convenient way. It is because the anchor load does not depend on the shear strength of soils (i.e., only the anchor capacity depends on the shear strength of soils). In other words, the load and capacity at the mudline can be considered as independent variables; otherwise both load and capacity depend on the soil strength making the reliability analysis more complicated. Therefore, a new interaction relationship focusing on the capacity at the mudline is proposed here by considering the effect of soil friction and bearing resistance against the mooring chain below the mudline as part of the foundation capacity. Using the new interaction curves, critical load combination that will lead to failure of foundation can be estimated.

The procedure for the conversion of the padeye capacity to the mudline capacity is summarized in the following two steps: (1) given the geometry of a suction caisson with a padeye depth ratio of 0.67 and an undrained shear strength profile that varies

linearly with depth, the ultimate load capacity at a padeye angle ranging from 0 to 90 degrees is first calculated using the SAIL program and (2) a new ultimate load capacity at the mudline is obtained by trial and error methods that incorporate the ultimate load capacity at the padeye angle derived from the first step. In the second step, the analytical solution proposed by Neubecker and Randolph (1995) is used as mentioned in Chapter 3. This work was done using a macro the author developed in an Excel spreadsheet.

Figure 4.19 shows an example of combined capacities at the padeye and mudline of a suction caisson having a diameter of 4.0 m and a length-to-diameter ratio of 6 along with mooring line loads of the study spar in 1,000 m water depth. As shown in the figure, the difference between the two interaction curves in the vertical zone is relatively negligible but the gap becomes noticeable as the angle gets closer to the lateral zone, mainly because of the effect of the soil resistances against the mooring chains below the mudline. As the angle of loading approaches horizontal, the contribution of the soil to the ultimate load capacity at the mudline increases with an increase in chain embedment.

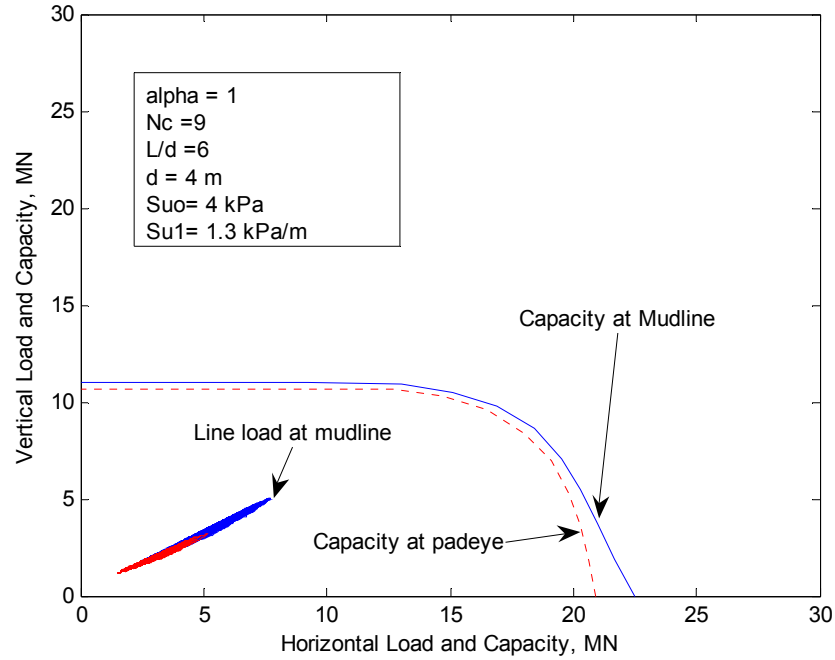


Figure 4.19: Interaction curves for capacity at the mudline vs. padeye in 1,000 m water depth

The effect of the design and soil parameters, i.e.  $\alpha$ ,  $N_c$  and  $S_u$ , on the capacity of the caisson at the mudline is investigated as shown in Figures 4.20 to 4.22, respectively. The combined capacity of the caisson increases with increasing soil parameters. The side friction coefficient affects both the lateral and axial capacities of the caisson in a similar fashion. However, the end bearing factor has no influence on the lateral capacity of the caisson. The rate effect of the shearing strength is greater for the lateral capacity than for the axial capacity, as indicated in Figure 4.22.

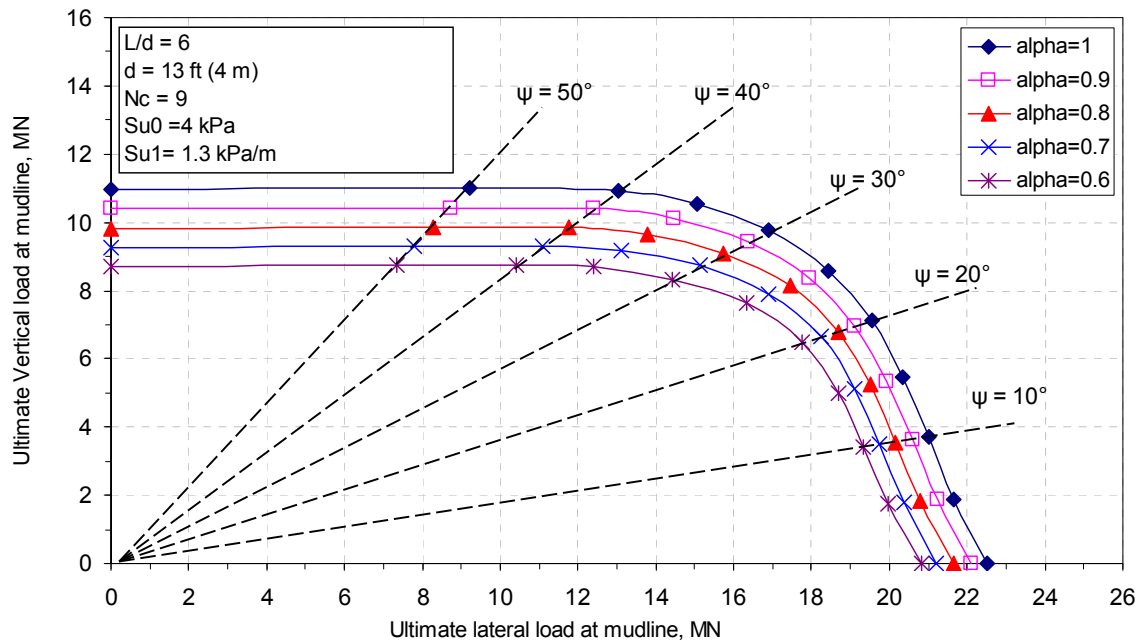


Figure 4.20: Effect of skin friction on combined capacity at the mudline of a suction caisson ( $L/d = 6$  and  $d = 4 \text{ m}$ )

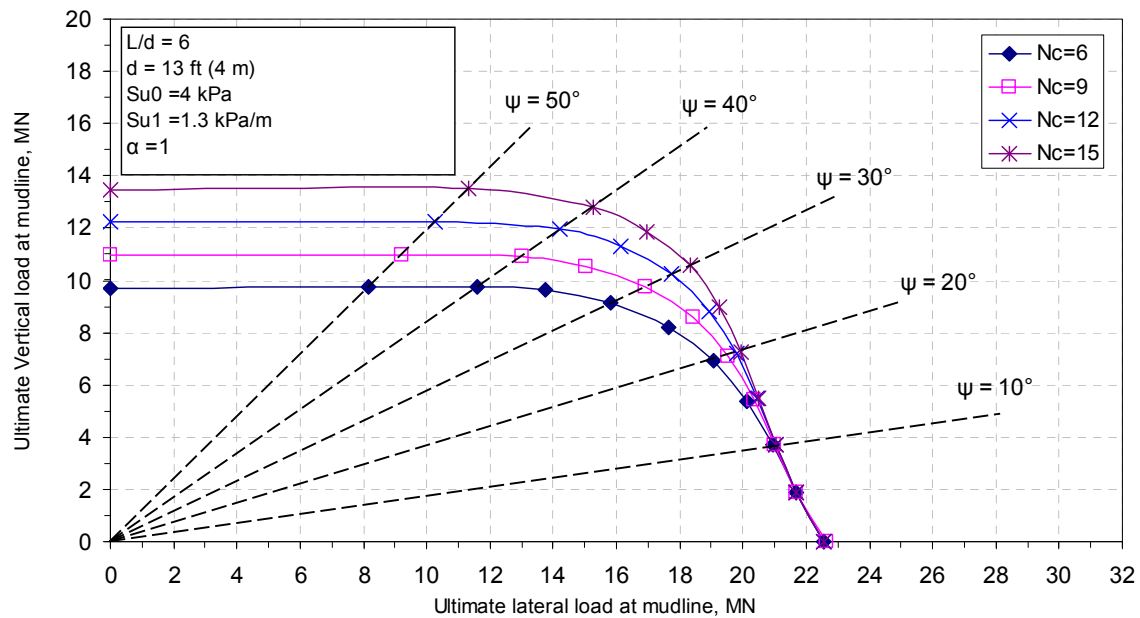


Figure 4.21: Effect of end bearing factors on combined capacity at the mudline of a suction caisson ( $L/d = 6$  and  $d = 4 \text{ m}$ )

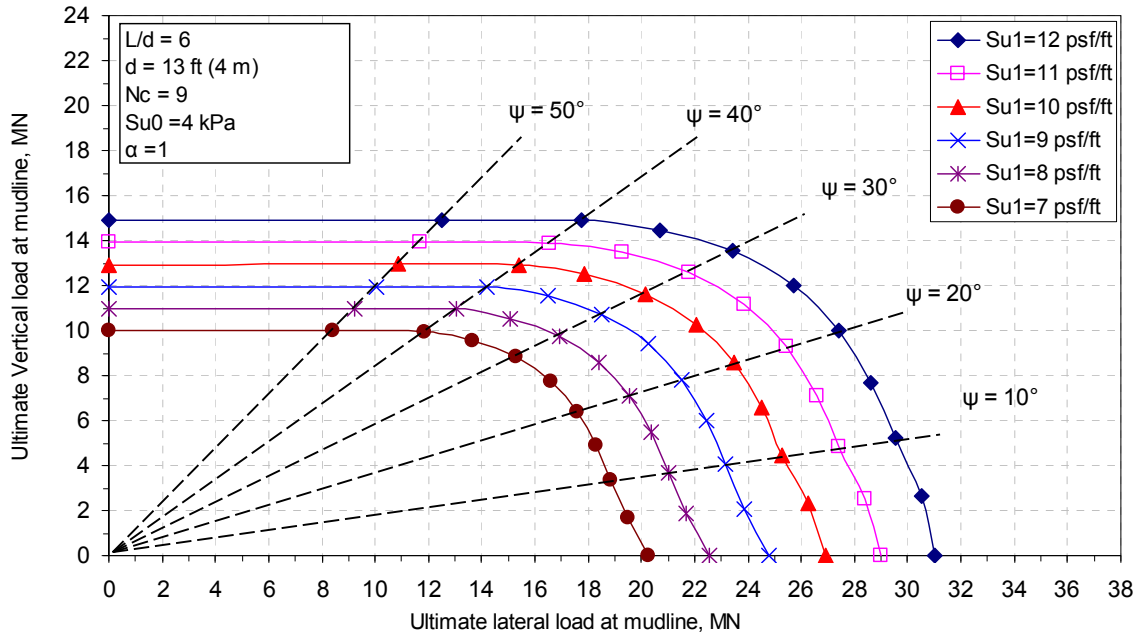


Figure 4.22: Effect of shear strength rate with depth on combined capacity at the mudline of a suction caisson ( $L/d = 6$  and  $d = 4$  m)

As in section 4.3.4, on the normalized interaction curve, a normalized interaction curve focusing on at the mudline is developed and plotted in Figure 4.23. The fitting curve was made using Equation 4.8. As may be seen in Figure 4.23, it is observed that the agreement of the curves is excellent over a wide angle range of 0 to 45 degrees.

$$\frac{V}{AS_{utip}} = -0.0716 \exp(0.1124 \frac{H}{AS_{utip}}) + 26.07 \exp(0.0034 \frac{H}{AS_{utip}}) \quad (4.8)$$

From Equation 4.9, a normalized curve in terms of the ultimate total load versus angle at the mudline is developed and presented in Figure 4.24. The curve fitting equation works excellent for a mudline angle less than or equal to 50 degrees. This is because the normalized ultimate total load corresponding to 90 degrees was excluded in the process of the curve fitting, due to difficulty in deriving the curve fitting equation.

However, because an angle at the mudline is always less than 50 degrees for the study spar structure (in all three water depths), this exclusion should not cause a problem.

$$\frac{T_a}{AS_{utip}} = -1.47 \times 10^{-4} (angle)^3 + 0.004315 (angle)^2 - 0.2431 (angle) + 53.98 \quad (4.9)$$

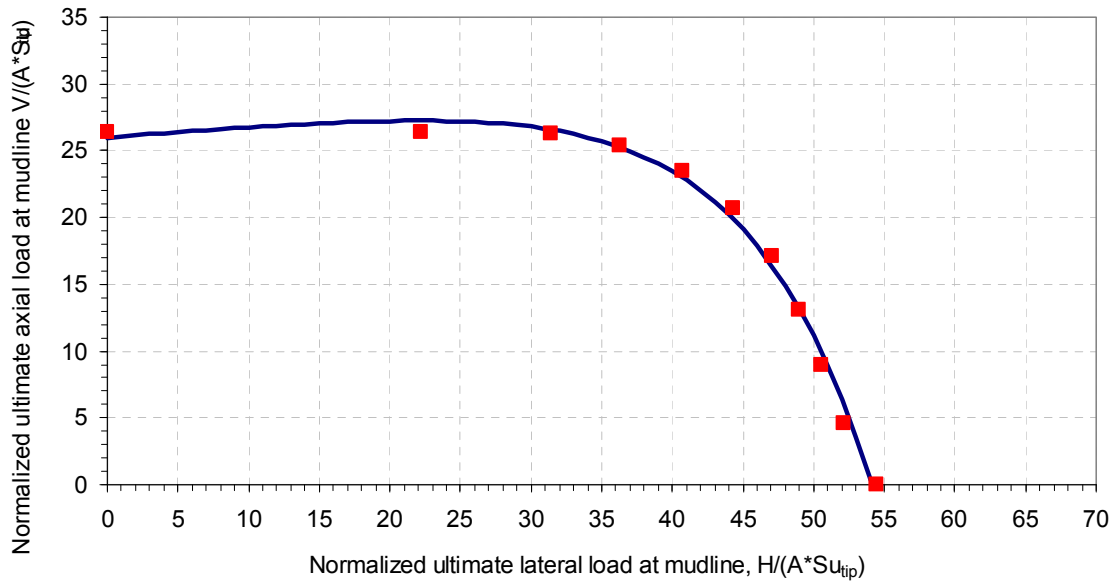


Figure 4.23: Comparison of the normalized and theoretical interaction curves for a suction caisson with  $L/d = 6$

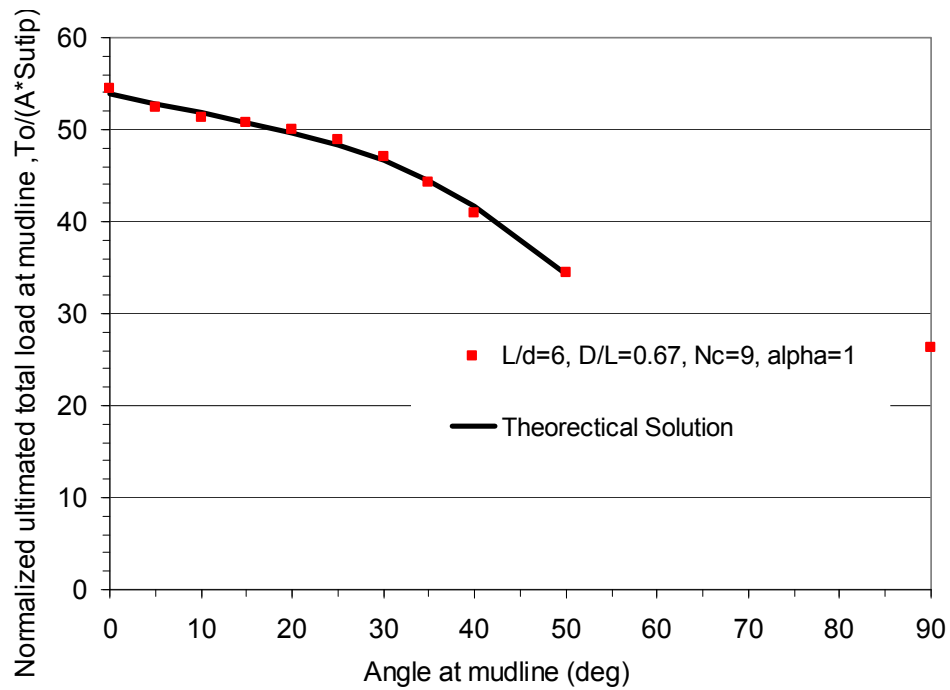


Figure 4.24: Comparison of the normalized and theoretical curves for ultimate total load at the mudline for a suction caisson with  $L/d = 6$

The interaction diagrams showing the wave load and the capacity of suction caissons at the mudline are presented in Figures 4.25 to 4.27. Anchor design is governed by axial failure mode in 2,000 m and 3,000 m of water while combined failure mode will govern anchor design in 1,000 m of water. The discrepancy in failure modes between at the padeye and at the mudline is attributed to the inverse catenary mooring line below the mudline as shown in Figure 3.28. Due to this reason, an additional analysis for foundation component reliability in 1,000 m based on combined failure mode is performed and compared with the results of reliability analysis of the foundation based on axial failure mode in Chapter 5. For the systems in deeper water depths, component reliability analyses are performed based on only axial failure mode. The interaction diagrams passing through the wave loads can be derived by reducing the undrained

shearing strength at the tip of the suction caisson. This is achieved by using reduction factors (RF), as indicated in the interaction diagram in Figures 4.27.

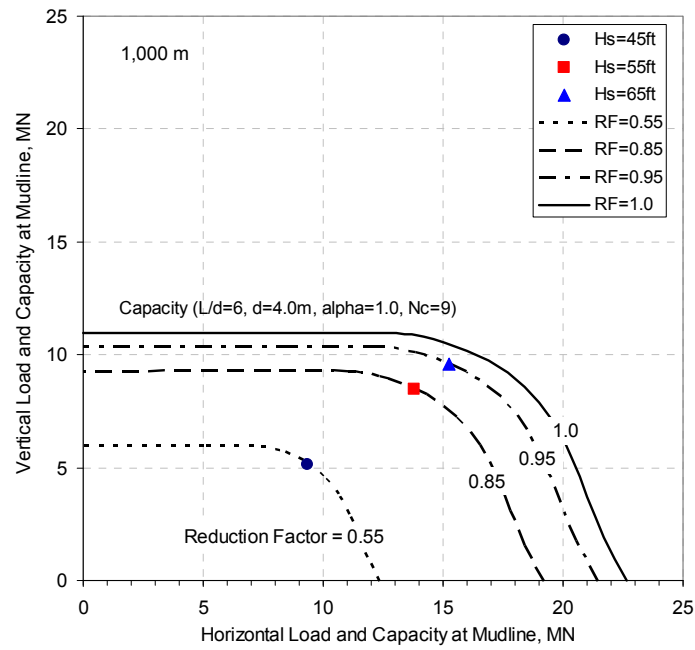


Figure 4.25: Interaction diagram showing wave load (line No. 8) and predicted capacity at the mudline of the suction caisson in 1,000 m of water



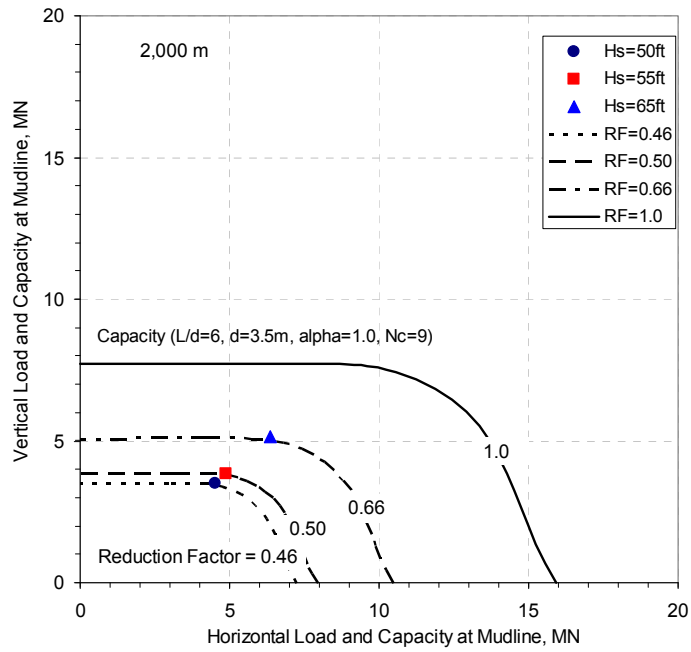


Figure 4.26: Interaction diagram showing wave load (line No. 8) and predicted capacity at the mudline of the suction caisson in 2,000 m of water

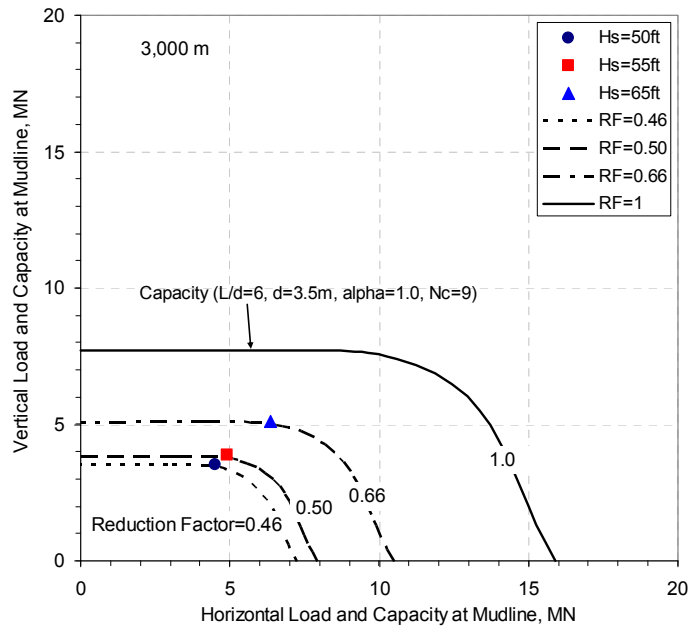


Figure 4.27: Interaction diagram showing wave load (line No. 8) and predicted capacity at the mudline of the suction caisson in 3,000 m of water

#### **4.4 DESIGN CHART FOR CAPACITIES OF SUCTION CAISSONS**

Using the SAIL that is based on the upper bound analysis, design charts have been developed for the lateral and axial capacities of caisson foundations installed in the soil profile in the Gulf of Mexico. The design charts that relate lateral and axial capacities to aspect ratio of a suction caisson being designed are shown in Figures 4.28 to 4.30. The ultimate load corresponding to any angle at the padeye, which is located two thirds of embedment length below the mudline, can also be estimated from Figure 4.28.  $N_c$  of 9 was held constant for Figure 4.28 while  $\alpha=1$  was used for Figure 4.28.  $N_c=9$  and  $\alpha=1$  were used for Figure 4.30. With these design charts, caisson design check is allowed to be generalized for any roughness between fully rough sides ( $\alpha=1$ ) and fully smooth sides ( $\alpha=0$ ), by interpolating between the two cases.

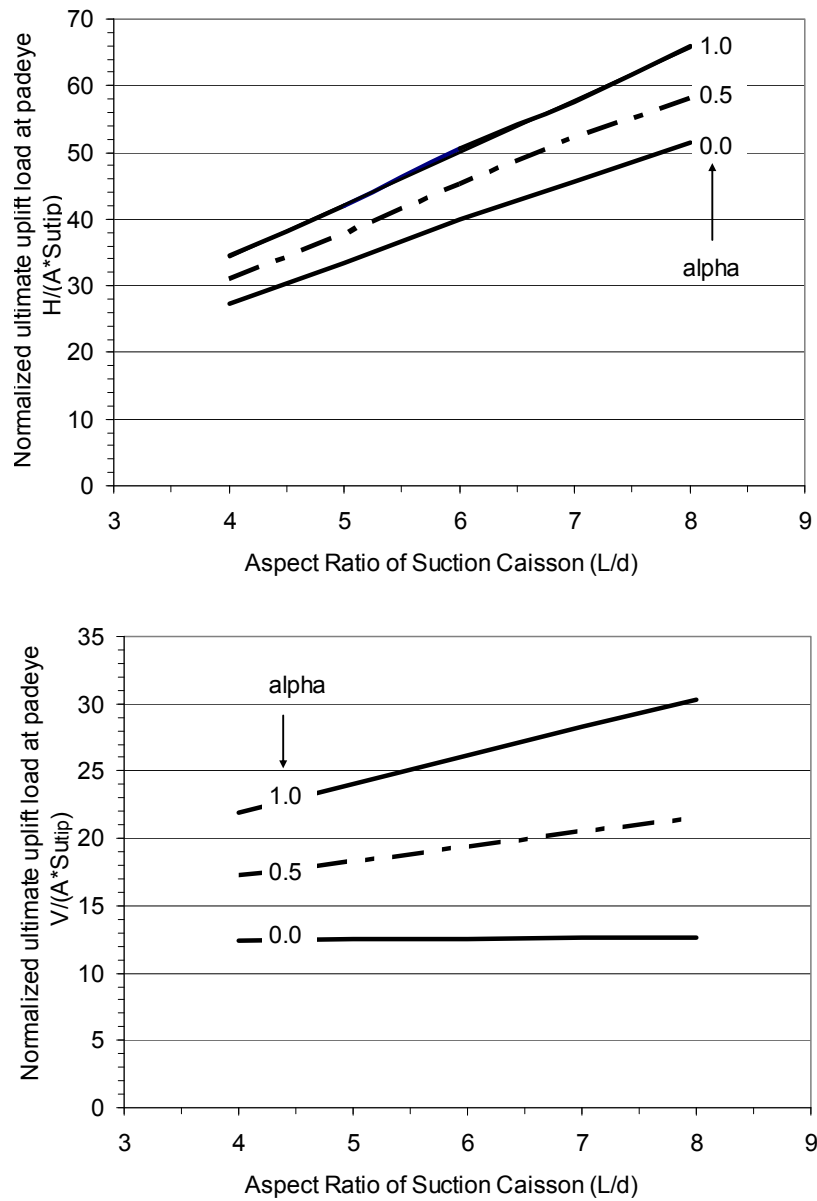


Figure 4.28: Design chart for lateral (top) and vertical (bottom) resistances of caisson foundations in normally consolidated clay (in case of  $N_c = 9$ )

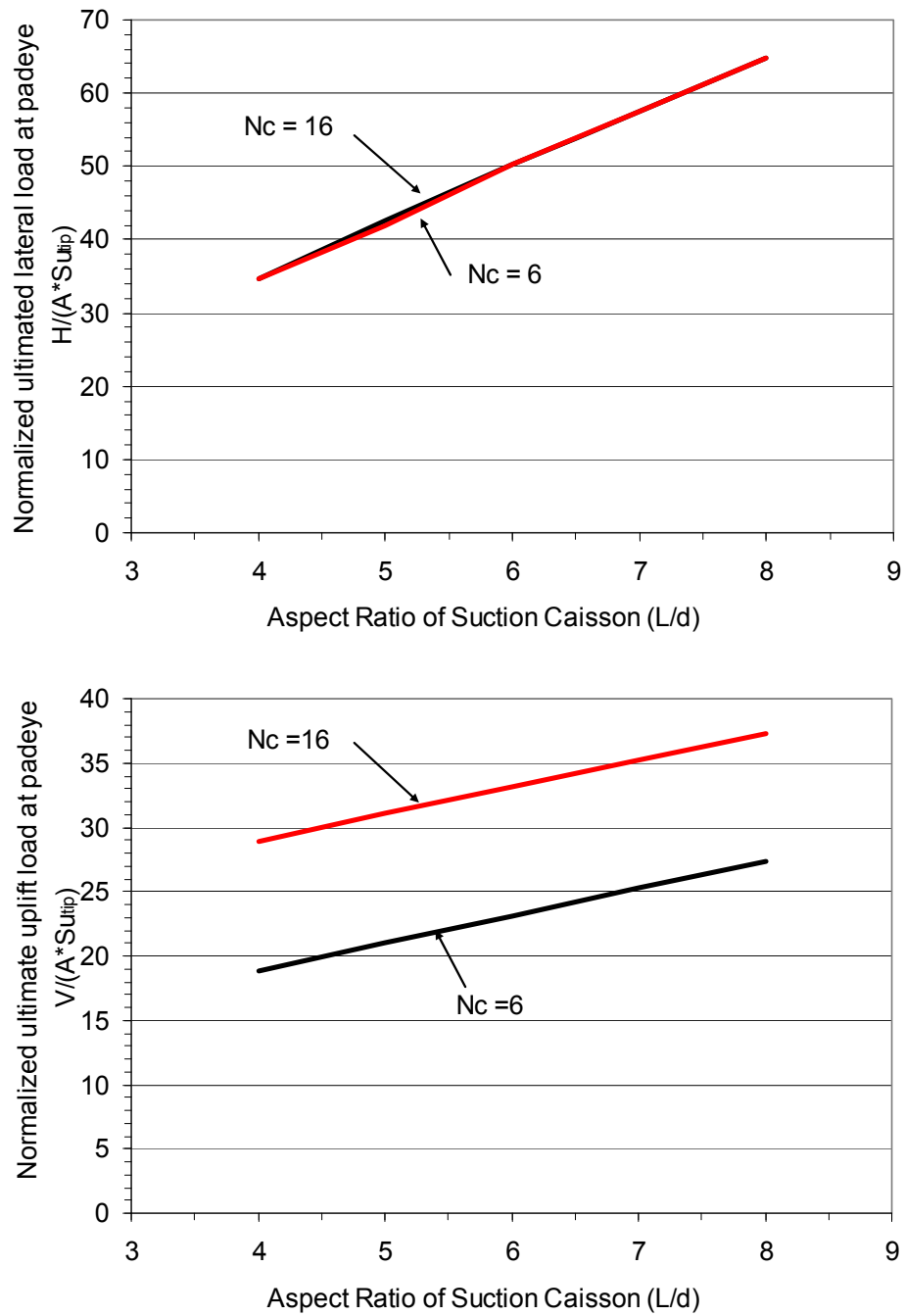


Figure 4.29: Design chart for lateral (top) and vertical (bottom) resistances of caisson foundations in normally consolidated clay (in case of  $\alpha = 1$ )

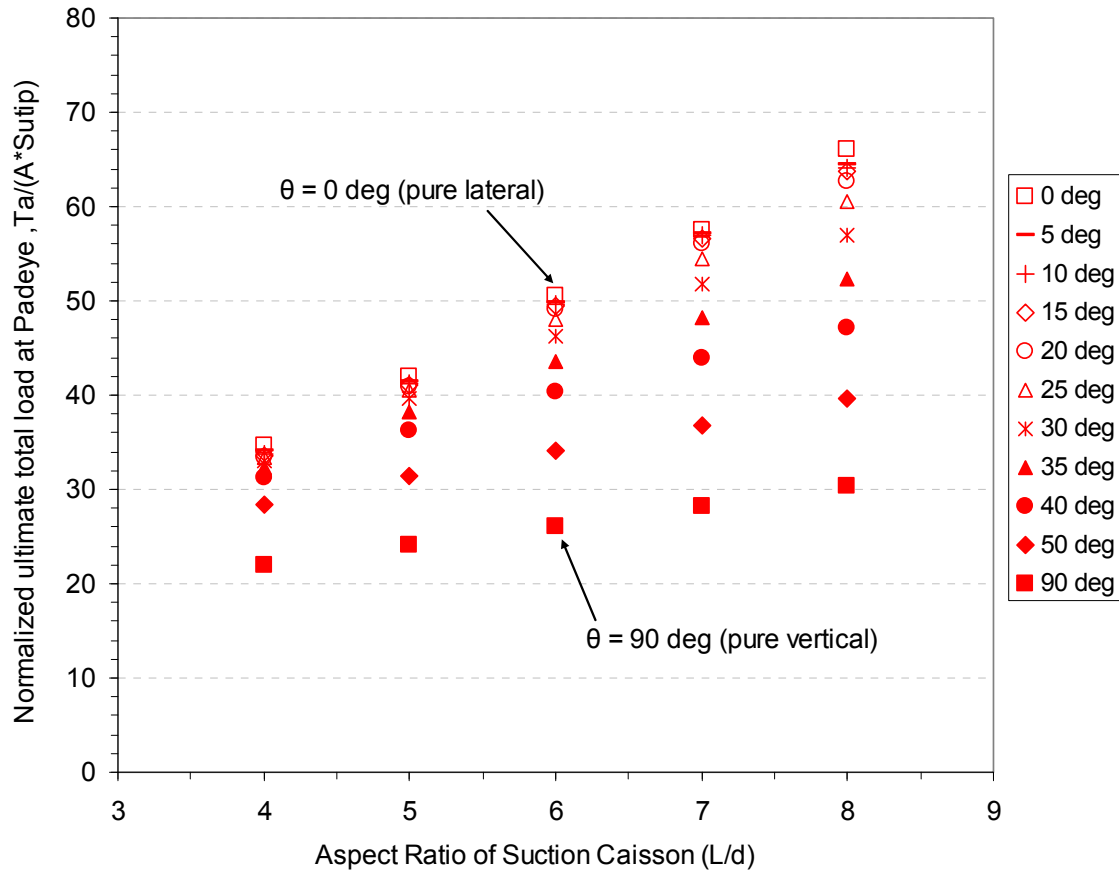


Figure 4.30: Design chart for total resistances at the mudline of caisson foundations in normally consolidated clay (in case of  $\alpha = 1$  and  $N_c = 9$ )

#### 4.5 BIAS AND C.O.V VALUES FOR THE PREDICTED FOUNDATION CAPACITIES

Bias and c.o.v values affect the median value and shape of a probabilistic distribution of foundation capacity, respectively.

“A database comprised of published load tests was assembled and used to evaluate biases and uncertainties in models for predicting the uplift capacity of suction caissons in normally consolidated clays. This database of 25 tests includes the following: laboratory-scale model tests (Luke et al., 2003), centrifuge tests (Clukey and

Morrison, 1993; House and Randolph, 2001; Randolph and House, 2002; Clukey and Phillips, 2002; and Clukey et al., 2004), and full-scale field tests (Cho et al., 2003).

For the purposes of an analysis, the predicted capacities in each test were calculated using the model developed by Aubeny et al., (2003a, 2003b) with an alpha value of 1.0 for side friction and a bearing capacity factor of 9.0 for the reverse end bearing. Shear strengths reported by each investigator were used directly. Refer to Najjar (2005) for details of this analysis. Ratios of measured to predicted capacities for the 25 tests in the database are plotted on Figure 4.31. The average value for the ratio of measured to predicted capacity on Figure 4.31 is 0.99, indicating an unbiased prediction model.” (Gilbert et al., 2005)

This finding has been proven by a set of laboratory-scale model tests performed by El-Sherbiny et al., (2005) supporting the use of an  $\alpha$  value of 1.0 and an  $N_c$  of 9.0 to produce unbiased predictions for capacity.

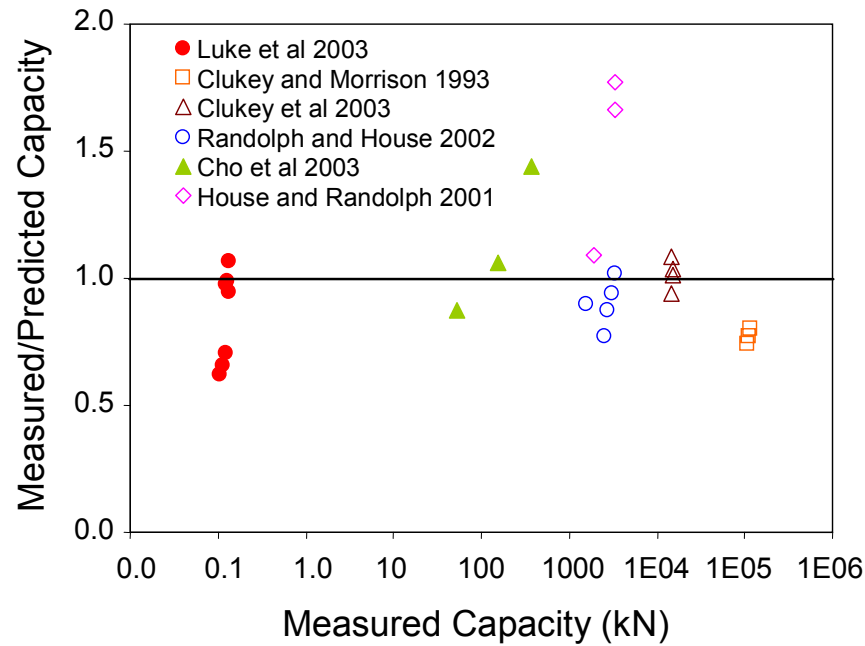


Figure 4.31: Measured versus predicted axial capacity for model tests on suction caissons in normally consolidated clays (from Najjar 2005)

“While there are variations in the design practice for suction caissons, typical values in practice for  $\alpha$  and  $N_C$  are 0.6 to 0.8 and 7 to 9, respectively. Therefore, there is a conservative bias that is introduced with these nominal values. To quantify this bias, the suction caisson design was considered for the study spar. The side friction contributes about 50 percent of the total capacity, and the reverse end bearing contributes about 35 percent of the total capacity. As an example, if there is a bias of 1.0/0.7 on the side friction and a bias of 9.0/7.0 on the end bearing, the composite bias on the total capacity is 1.3. For typical designs, the bias will range from about 1.2 to 1.4. Coincidentally, the design bias of about 1.3 for pile foundations on jacket platforms has been widely used as proposed in Tang and Gilbert (1993) and others.

The coefficient of variation in the ratio of measured to predicted capacity about the average on Figure 4.31 is 0.28. This value is very similar to the value of 0.3 that is

typically used for pile foundations on jacket platforms (Tang and Gilbert 1993).” (Gilbert et al., 2005)

In this study, the coefficient of variation in the vertical capacity of a suction caisson was assumed to be 0.3 based on these findings.

While lateral load tests on suction caissons installed in the offshore environments (full-scale field tests) may have been conducted, few results from such tests have been found in the published literature (e.g., El-Sherbiny 2005). In general, the available data suggest that the plasticity model works reasonably well for currently used sizes of suction caissons; however, the available experimental data are still insufficient for conclusive judgment, especially in the interaction zone. In addition, experiment test results are not sufficient enough to make sure that the plasticity model works especially in the interaction zone. Therefore, in this study, the coefficient of variation in the combined capacity is assumed to be 0.3 which is the same value for the axial capacity.

#### **4.6 LOWER BOUND FOUNDATION CAPACITY**

One consequence of the relatively large median factors of safety and small coefficients of variation in the applied loads for spar foundations is that the presence of a minimum or lower-bound capacity can have a large effect on the reliability (Gilbert et al., 2005). A simple estimate of the lower-bound capacity for a suction caisson in normally consolidated clay can be obtained using the remolded strength of the clay to calculate side friction and end bearing.

The database of load tests (Figure 4.31) was used to investigate the existence of a lower-bound capacity. For each test, a predicted lower-bound capacity was calculated using the remolded undrained shear strength with an alpha value of 1.0 and a bearing capacity factor of 9.0. Details for how the lower-bound capacity was calculated in each



test and a discussion of relevant assumptions are provided in Najjar (2005). The ratio of the calculated lower-bound capacity to the measured capacity is shown on Figure 4.32.

For all tests analyzed, the ratio of the calculated lower-bound capacity to the measured capacity is less than or equal to 1.0, providing compelling evidence for the existence of a lower-bound axial capacity. The ratio of lower-bound capacities to measured capacities ranges from 0.25 to 1.0 with an average value of 0.6. For foundations used for the study spar, the lower-bound capacity was calculated to be 0.43 times the median capacity.

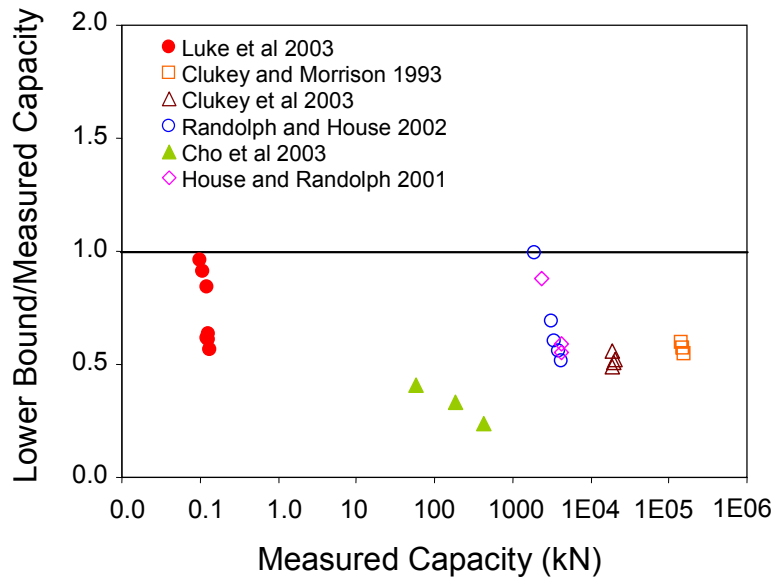


Figure 4.32: Calculated lower-bound versus measured axial capacity for suction caissons in normally consolidated clays (from Najjar 2005)

#### 4.7 PROBABILISTIC DESCRIPTION OF FOUNDATION CAPACITIES

Najjar (2005) found that mixed lognormal probability distributions, as shown on Figure 4.33, adequately represented the effect of a lower bound on the uncertainty in

axial capacity for driven piles. This same form of a probability distribution is used to model the lower bound capacity for reliability analysis of the offshore foundation.

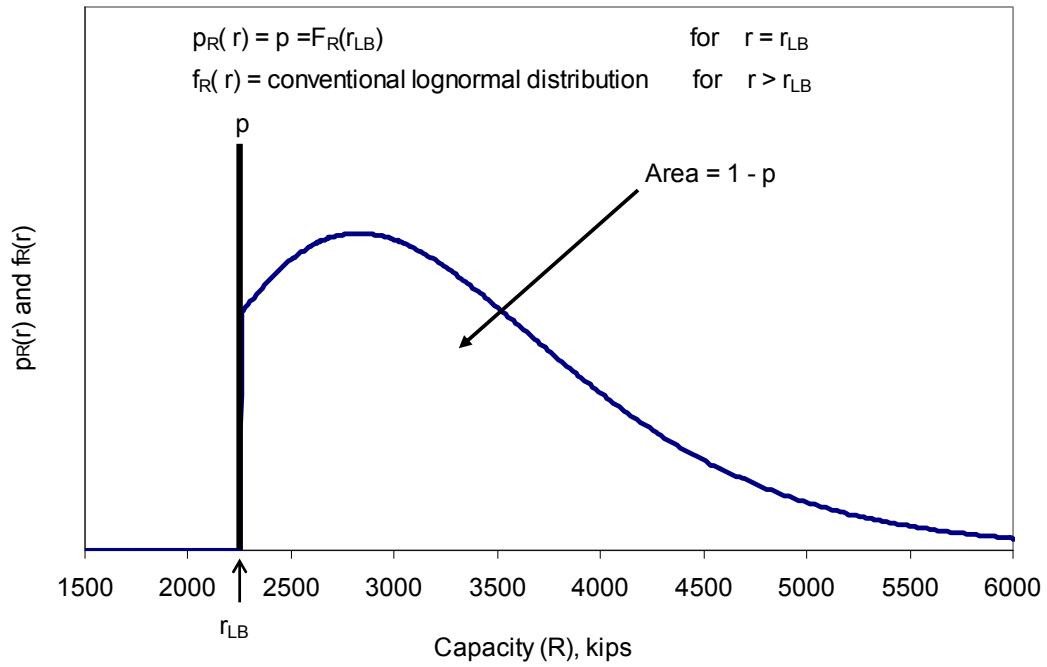


Figure 4.33: Mixed lognormal distribution for foundation capacity with a lower-bound

## Chapter 5: Framework for Reliability Analysis

### 5.1 INTRODUCTION

In this chapter, a framework to assess the reliabilities of component and system is adopted for the study spar. The framework for component reliability analysis is first described. The framework for system reliability is then discussed. This framework will be used to assess the mooring system foundation under extreme environmental events in Chapter 6.

### 5.2 FRAMEWORK FOR COMPONENT RELIABILITY CALCULATIONS

In this section, a framework for component reliability calculations is presented.

#### 5.2.1 Assessment of probability of failure with general distributions

If the capacity is assumed to be a constant with time, then the event of failure in the lifetime is the event that the maximum load over the lifetime is greater than or equal to the capacity. The event of failure in the lifetime is defined as  $R < S$  where the load is denoted as  $S$  and the capacity (or strength) is denoted as  $R$ . When  $R$  and  $S$  are random variables, the probability of failure can be calculated as (e.g., Ang and Tang, 1984):

$$P_F = P(R < S) = \iint_{R < S} f_{RS}(r, s) dr ds \quad (5.1)$$

where  $f_{RS}(r, s)$  = the joint density function of  $R$  and  $S$ . If  $R$  and  $S$  are statistically independent, Equation 5.1 becomes:

$$P_F = P(R < S) = \int_0^{\infty} F_R(s) f_S(s) ds \quad (5.2)$$

where  $F_R(s)$  is the cumulative distribution function (CDF) of the capacity evaluated at the load  $s$ ; and  $f_S(s)$  is the probability density function (PDF) of the load. As an example, random variable models for the capacity and the load are shown graphically with probability distributions in Figure 5.1. These distributions show all the possible values of load and capacity along x-axis, which occur in design life and along y-axis the likelihood of each of these values. Figure 5.1 also shows the region in which the capacity is less than the applied load, indicating the event of failure, for a given load.

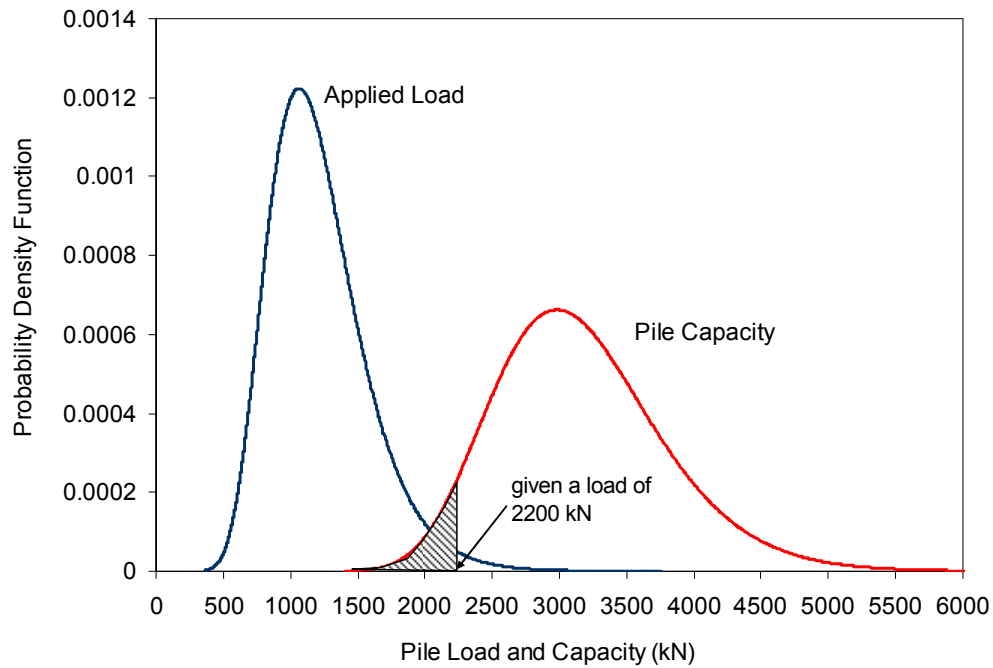


Figure 5.1: Example of probability distributions for caisson load and capacity

### 5.2.2 Assessment of probability of failure with normal or lognormal distributions

In cases where the load and capacity are both normally or lognormally distributed, closed form solutions for the probability of failure from Equation 5.2 can be obtained and expressed by Equation 5.3 and 5.4, respectively:

$$P_f = P(S > R) = \Phi \left( -\frac{(\mu_R - \mu_S)}{\sqrt{\sigma_R^2 + \sigma_S^2}} \right) = \Phi \left( -\frac{(FS_{\text{mean}} - 1)}{\sqrt{FS_{\text{mean}}^2 \delta_R^2 + \delta_S^2}} \right) = \Phi(-\beta) \quad (5.3)$$

$$P_f = P(S > R) = \Phi \left( -\frac{\ln(FS_{\text{median}})}{\sqrt{\ln[(1 + \delta_R^2)(1 + \delta_S^2)]}} \right) = \Phi(-\beta) \quad (5.4)$$

where  $\Phi(\cdot)$  is the normal cumulative distribution function;  $\mu_R$  and  $\mu_S$  are respectively the expected (or mean) capacity and the expected load in the design life, indicating the center of the distribution;  $\sigma_R$  and  $\sigma_S$  are respectively standard deviations of the capacity and the load, describing the amount of variability about the centers;  $FS_{\text{mean}}$  and  $FS_{\text{median}}$  are the mean and median factors of safety respectively, which are defined as the ratio of the mean or median capacity to the mean or median load;  $\delta_R$  and  $\delta_S$  are the coefficients of variation (c.o.v.), which are defined as the standard deviation divided by the mean value for the capacity and the load, respectively; and  $\beta$  is the reliability index.

“The coefficients of variation in Equation 5.4 represent uncertainty in the load and the capacity. For an offshore foundation, the uncertainty in the load is generally due to variations in the occurrence and strength of hurricanes at the platform site over the design life. The uncertainty in the capacity is due primarily to variations between the

actual capacity in a storm load compared to the capacity predicted using the design method.” (Gilbert et al., 2005)

For cases where the load and the capacity are assumed to follow both lognormal distributions, Equation 5.4 can be approximated to Equation 5.5.

$$P_f = P(\text{Load} > \text{Capacity}) \cong \Phi \left( -\frac{\ln(\text{FS}_{\text{median}})}{\sqrt{\delta_R^2 + \delta_S^2}} \right) = \Phi(-\beta) \quad (5.5)$$

This assumption has commonly been made in typical reliability analyses for offshore applications (e.g., Tang and Gilbert, 1993; Bea et al., 1999; Heredia-Zavoni et al., 2004). The difference between values from Equations 5.4 and 5.5 in the reliability calculation is essentially negligible as long as the coefficients of variation of the load and the capacity are relatively very small (Tables 5.1 and 5.2).

Table 5.1: Probability of failure for a case of  $\text{FS}_{\text{median}} = 4$  using Equation 5.4

		coefficient of variation of the capacity, $\delta_R$							
		0.05	0.1	0.15	0.2	0.25	0.3	0.4	0.5
coefficient of variation of the load, $\delta_S$	0.05	5.49E-86	9.48E-36	6.13E-19	5.71E-12	1.72E-08	1.62E-06	1.80E-04	1.76E-03
	0.1	9.48E-36	4.31E-23	5.57E-15	2.03E-10	9.03E-08	3.89E-06	2.47E-04	2.04E-03
	0.15	6.13E-19	5.57E-15	2.49E-11	1.13E-08	7.34E-07	1.28E-05	3.96E-04	2.57E-03
	0.2	5.71E-12	2.03E-10	1.13E-08	3.72E-07	5.74E-06	4.52E-05	6.86E-04	3.40E-03
	0.25	1.72E-08	9.03E-08	7.34E-07	5.74E-06	3.43E-05	1.48E-04	1.21E-03	4.63E-03
	0.3	1.62E-06	3.89E-06	1.28E-05	4.52E-05	1.48E-04	4.20E-04	2.10E-03	6.34E-03
	0.4	1.80E-04	2.47E-04	3.96E-04	6.86E-04	1.21E-03	2.10E-03	5.47E-03	1.15E-02
	0.5	1.76E-03	2.04E-03	2.57E-03	3.40E-03	4.63E-03	6.34E-03	1.15E-02	1.90E-02

Table 5.2: Probability of failure for a case of  $FS_{\text{median}} = 4$  using Equation 5.5

		coefficient of variation of the capacity, $\delta_R$							
		0.05	0.1	0.15	0.2	0.25	0.3	0.4	0.5
coefficient of variation of the load, $\delta_S$	0.05	6.99E-86	1.32E-35	9.12E-19	8.81E-12	2.70E-08	2.58E-06	2.92E-04	2.90E-03
	0.1	1.32E-35	5.49E-23	7.37E-15	2.83E-10	1.31E-07	5.83E-06	3.87E-04	3.28E-03
	0.15	9.12E-19	7.37E-15	3.18E-11	1.47E-08	9.92E-07	1.79E-05	5.87E-04	3.96E-03
	0.2	8.81E-12	2.83E-10	1.47E-08	4.76E-07	7.45E-06	6.03E-05	9.68E-04	5.02E-03
	0.25	2.70E-08	1.31E-07	9.92E-07	7.45E-06	4.41E-05	1.93E-04	1.65E-03	6.57E-03
	0.3	2.58E-06	5.83E-06	1.79E-05	6.03E-05	1.93E-04	5.42E-04	2.78E-03	8.72E-03
	0.4	2.92E-04	3.87E-04	5.87E-04	9.68E-04	1.65E-03	2.78E-03	7.13E-03	1.52E-02
	0.5	2.90E-03	3.28E-03	3.96E-03	5.02E-03	6.57E-03	8.72E-03	1.52E-02	2.50E-02

Based on the probability of failure, the reliability in the design life is calculated as follows:

$$\text{Reliability} = P(S < R) = 1 - \Phi(-\beta) \quad (5.6)$$

where  $P(S < R)$  is the probability that the capacity exceeds the load. The relationship between the reliability and the reliability index is shown in Table 5.3. For reference, typical values of 2.0 to 3.0 for the reliability index for offshore jacket platforms have been recognized (Tang and Gilbert, 1993). Tang and Gilbert (1993) found that, based on an analysis of three fixed-jacket offshore platforms, the reliability index for single piles over a 20-year lifetime ranged between 2.0 and 2.5. Note that the reliability index they found was based not on pile system but on single piles.

Table 5.3: Relationship between reliability index, reliability and probability of failure

Reliability Index, $\beta$	Reliability	Probability of Failure
1.5	0.933	0.067
2	0.977	0.023
2.5	0.9938	0.0062
3	0.9986	0.0014
3.5	0.99977	0.00023

The denominator in Equation 5.5 is referred to as the total coefficient of variation:

$$\delta_{\text{total}} = \sqrt{\delta_{\text{load}}^2 + \delta_{\text{capacity}}^2} \quad (5.7)$$

Figure 5.2 shows how the probability failure varies with the median factor of safety and the total coefficient of variation. An increase in the median factor of safety and a decrease in the total c.o.v. both reduce the probability of failure. As an example, the median factor of safety ranges from three to five for a pile in a typical jacket platform (Najjar and Gilbert, 2006). Given the range of the median factor of safety, the failure probabilities in lifetime for a pile in a typical jacket platform have a range of 0.005 to 0.05 as indicated in Figure 5.2. These reliabilities will be compared with those for the study spar in Chapter 6.



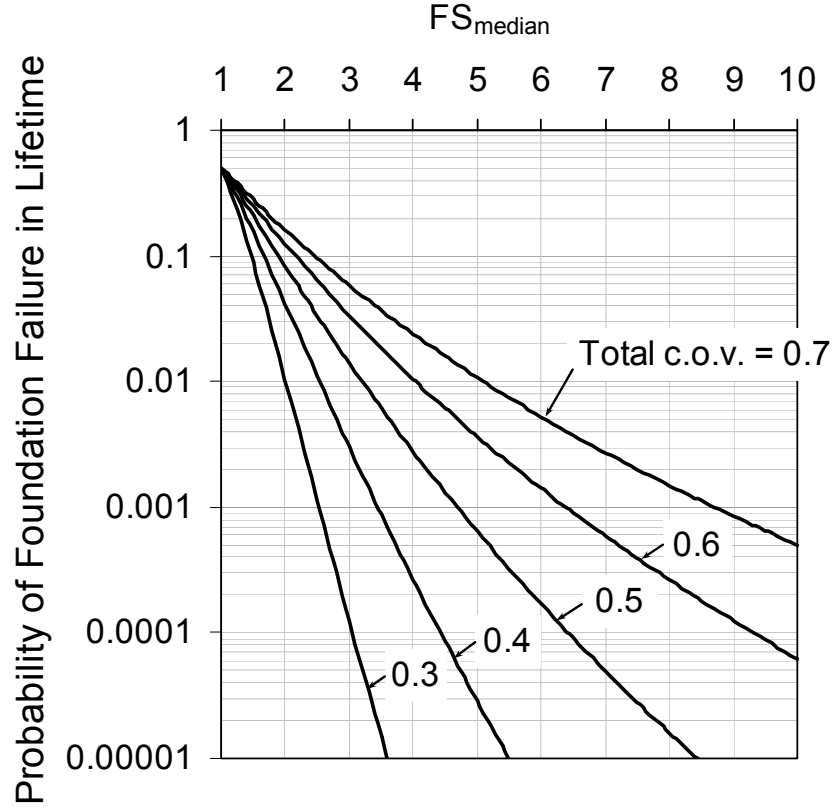


Figure 5.2: Component reliability from Equation 4.5

### 5.2.3 Relationship between the median and mean factors of safety

The median factor of safety in Equations 5.4 and 5.5 can be related to the factor of safety used in design:

$$FS_{\text{median}} = \frac{\text{capacity}_{\text{median}}}{\text{load}_{\text{median}}} = \frac{\text{capacity}_{\text{design}} b_R}{\text{load}_{\text{design}} b_S} = FS_{\text{design}} \times \frac{\left( \frac{\text{capacity}_{\text{median}}}{\text{capacity}_{\text{design}}} \right)}{\left( \frac{\text{load}_{\text{median}}}{\text{load}_{\text{design}}} \right)} \quad (5.8)$$

where the subscript “design” indicates the capacity or load used to design the mooring line or the suction caisson for the study spar (such as the 100-year storm load) and  $b_R$  and

$b_S$  are nominal bias factors that represent relationships between the median (or most likely) value in the design life and the value used in the design check via the factor of safety. The bias factors are used to convert the design values, which are typically conservative estimates, to the median values. For example, the median factor of safety can be estimated from typical values for the nominal bias factors and design factor of safety for piles in clay:  $b_S=0.7$ ,  $b_R=1.3$ ,  $FS_{\text{design}}=2.5$  (Gilbert et al., 1999). The median factor of safety turns out to be 4.64 [equal to  $(2.5 \times 1.3) / 0.7$ ]. Given the median factor of safety and typical coefficients of variation for load and capacity for piles in clay:  $\delta_S=0.4$ ,  $\delta_R=0.3$ , the probability of failure in lifetime for the pile is estimated to be 0.001 using Figure 5.2.

#### 5.2.4 Mooring line reliability

The component reliability calculation is extended to a complete line system consisting of the three line segments (i.e., steel chain-wire rope-chain in 1,000 m water and steel chain-polyester rope-chain in 2,000 m and 3,000 m water) and the corresponding anchor. The probability of failure of the line system can be expressed as follows:

$$\begin{aligned} P(\text{Line}) &= P(\text{Top} \cup \text{Middle} \cup \text{Bottom} \cup \text{Anchor}) \\ &= 1 - P(\overline{\text{Top}} \cap \overline{\text{Middle}} \cap \overline{\text{Bottom}} \cap \overline{\text{Anchor}}) \end{aligned} \quad (5.9)$$

where  $P(\text{Line})$  is the probability of failure of a line system;  $P(\text{Top})$ ,  $P(\text{Middle})$ ,  $P(\text{Bottom})$  and  $P(\text{Anchor})$  are the probabilities of failure of the top chain, wire rope (or polyester rope), bottom chain and anchor, respectively; and  $P(\overline{\text{Top}})$ ,  $P(\overline{\text{Middle}})$ ,  $P(\overline{\text{Bottom}})$ ,

and  $P(\overline{\text{Anchor}})$  are the reliabilities of the top chain, wire rope (or polyester rope), bottom chain and anchor, respectively.

Equation 5.9 describes the probability of a union of events, which signifies that a line breakage may occur anywhere along the mooring line. If the events Top, Middle, Bottom and Anchor are denoted as T, M, B and A, respectively, Equation 5.9 can be calculated using the probability theory as follows:

$$\begin{aligned}
 P(\text{Line}) = & [P(\overline{T}\overline{M}\overline{B}) + P(\overline{T}\overline{M}A) + P(\overline{T}M\overline{B}A) + P(\overline{T}MA)] \\
 & + [P(\overline{T}\overline{M}\overline{B}A) + P(\overline{T}M\overline{B}A) + P(\overline{T}MBA) + P(\overline{T}MBA)] \\
 & + [P(M\overline{B}A) + P(T\overline{B}A) + P(\overline{T}MB) + P(\overline{T}MA) + P(TMBA)]
 \end{aligned} \tag{5.10}$$

It is possible that a mooring line that is not the most heavily loaded during an extreme environmental event will fail before the most heavily loaded line. To account for this possibility, the probability of failure of any line can be expressed as follows:

$$P(\text{Any Line}) = P(L_1 \cup L_2 \cup L_3 \dots \cup L_{14}) \tag{5.11}$$

where  $L_1 \dots L_{14}$  represent the mooring lines corresponding to line No. 1 to No. 14. The probability of the union of fourteen failure events, which indicate that the first failure of fourteen line systems may occur in any line, can be estimated by summing the probability of the individual line system by assuming that the event of failure of the individual line is statistically independent.

### 5.3 RELIABILITY ASSESSMENT FOR DISTRIBUTIONS WITH A LOWER BOUND

One additional consideration in the reliability analysis of the foundations is the effect of a minimum or lower-bound capacity. A simple estimate of the lower-bound capacity for foundations in normally consolidated clay can be obtained using the remolded strength of the clay to calculate side friction and end bearing. Najjar (2005) found that mixed lognormal distributions, as shown on Figure 4.32, adequately represent the effect of a lower bound on the uncertainty in the axial capacity for driven piles. In mixed lognormal distributions, the distribution is the conventional lognormal distribution for capacities greater than the lower bound. For capacities at the lower bound, there is a finite probability that correspond to the probability being less than or equal to the lower bound in the non-truncated distribution (i.e., lognormal distribution).

Najjar (2005) also found that the first and second moments (i.e., mean and standard deviation) of the mixed lognormal distribution do not differ significantly from those of conventional non-truncated lognormal distribution given practical values of c.o.v of the capacity and practical ratios of lower-bound to median capacity. This indicates that the statistical properties of the raw data (in terms of the first and second moments) available in the literature can be incorporated directly into the mixed probability model without adjusting the statistical properties (Najjar 2005). Therefore, for this research, the same type of distribution for the capacity was adopted to model the lower bound capacity for suction caisson anchors.

In cases where the load is lognormally distributed and the capacity follows a mixed lognormal distribution in the presence of a lower bound capacity in the reliability analysis, closed form solutions for the probability of failure from Equation 5.2 can be obtained and expressed by Equation 5.11. This equation is based on the theorem of total probability (e.g., Ang and Tang, 1975).

$$P_F = P(R < S) = P(R < S | r = r_{LB})P(R = r_{LB}) + P(R < S | r > r_{LB})P(R > r_{LB}) \quad (5.11)$$

where,

$$P(R < S | r = r_{LB}) = 1 - \Phi \left( \frac{\ln(r_{LB}) - \ln(s_{\text{median}})}{\sqrt{\ln(1 + \delta_S^2)}} \right), \quad P(R = r_{LB}) = \Phi \left( \frac{\ln(r_{LB}) - \ln(r_{\text{median}})}{\sqrt{\ln(1 + \delta_R^2)}} \right)$$

$$P(R < S | r > r_{LB}) = \int_{r_{LB}}^{\infty} [1 - F_S(r)] f_R(r) dr$$

$$= \int_{r_{LB}}^{\infty} \left[ 1 - \Phi \left( \frac{\ln(r) - \ln(s_{\text{median}})}{\sqrt{\ln(1 + \delta_S^2)}} \right) \right] \frac{1}{\sqrt{2\pi} \sqrt{\ln(1 + \delta_R^2)} r} \exp \left[ -\frac{1}{2} \left( \frac{\ln(r) - \ln(r_{\text{median}})}{\sqrt{\ln(1 + \delta_R^2)}} \right)^2 \right] dr$$

$$P(R > r_{LB}) = 1 - \Phi \left( \frac{\ln(r_{LB}) - \ln(r_{\text{median}})}{\sqrt{\ln(1 + \delta_R^2)}} \right)$$

As indicated in the equation, the first part of Equation 5.11 can be evaluated analytically while the second part requires numerical integration.

#### 5.4 EXAMPLES OF COMPONENT RELIABILITY

As an example, for the spar in 1,000 m of water, the component reliabilities of the foundation in the uplift failure and combined failure modes are estimated using Equations 5.4 and 5.6 and the results are summarized in Table 5.4. For the combined failure mode, the capacity at the mudline is not independent of the load at the mudline because the normalized equation (Equation 4.9) is a function of angle of mooring lines at the mudline. In order to calculate the probabilities of failure for the combined failure mode, the angle at the mudline was calculated based on the damaged line loads at the mudline for the semi-taut mooring system (Figure 4.19). They are all on the same order of magnitude for the same factor of safety. As shown in Figure 5.3, the difference between

the reliabilities is essentially negligible, especially for the factor of safety of 2.5. Based on this finding, for simplicity, the component reliability analysis of the foundation will be performed with an assumption that the foundation is subjected to uplift failure in all three water depths hereafter. Note that foundations in deeper water depths are subjected to uplift failure.

Table 5.4: Comparison of reliabilities of foundations subject to uplift failure vs combined failure modes in 1,000 m of water under a hurricane event

	Uplift Failure Mode			Combined Failure Mode		
	1.5	2	2.5	1.5	2	2.5
$FS_{\text{design(damage)}}$						
$\text{load}_{\text{median}}/\text{load}_{\text{design}}$	0.41	0.41	0.41	0.44	0.44	0.44
$\text{capacity}_{\text{median}}/\text{capacity}_{\text{design}}$	1.30	1.30	1.30	1.25	1.27	1.29
$FS_{\text{median}}$	4.76	6.34	7.93	4.26	5.77	7.33
$\delta_{\text{load}}$	0.32	0.32	0.32	0.3	0.3	0.3
$\delta_{\text{capacity}}$	0.3	0.3	0.3	0.3	0.3	0.3
$\delta_{\text{total}}$	0.44	0.44	0.44	0.42	0.42	0.42
Reliability Index	3.56	4.21	4.72	3.42	4.13	4.69
Probability of Failure	1.89E-04	1.27E-05	1.18E-06	3.17E-04	1.80E-05	1.33E-06

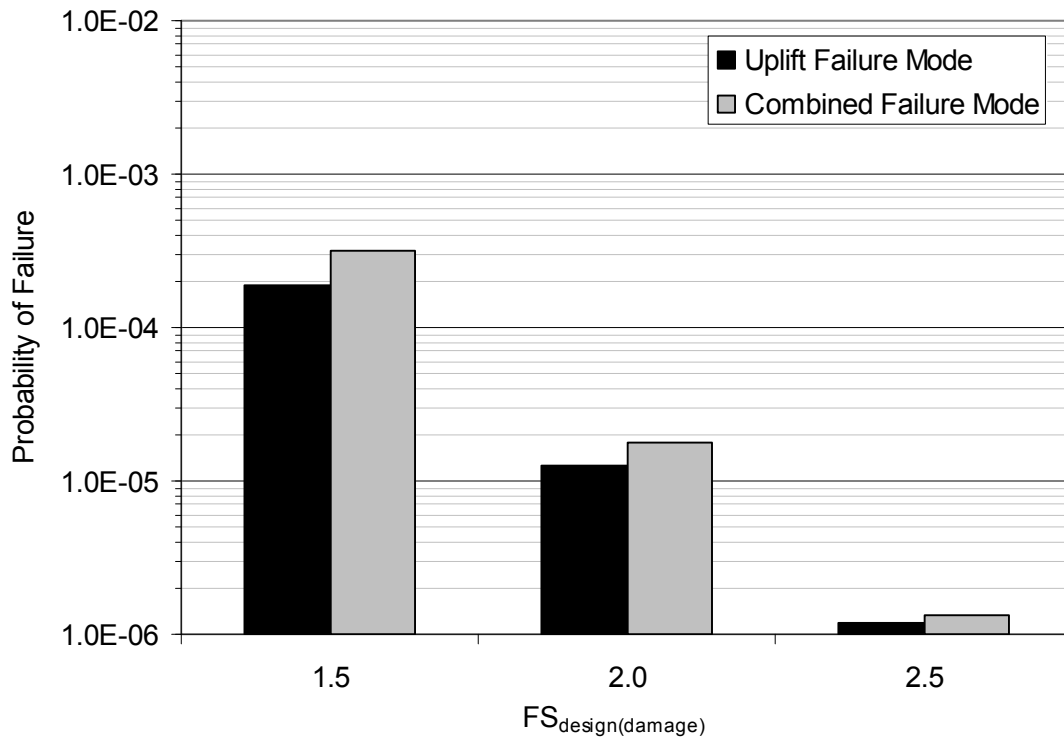


Figure 5.3: Comparison of probabilities of failure of foundations subject to uplift failure vs. combined failure modes in 1,000 m of water under a hurricane event

In addition, one of the outcomes of the component reliability analysis of the study spar under hurricane conditions is shown in Figures 5.4 and 5.5. Figure 5.4 shows the reliabilities of individual components of the most heavily loaded mooring line (line No. 8) for the hurricane events when the related mooring system is intact. Figure 5.5 shows the reliabilities of the most heavily loaded mooring line including the anchor under hurricane conditions. The intact safety factor of 2.5 for the anchor design, the safety factors of 1.67 (for intact condition) and 1.25 (for damaged condition) for the line design were used in calculating the probabilities of failure.

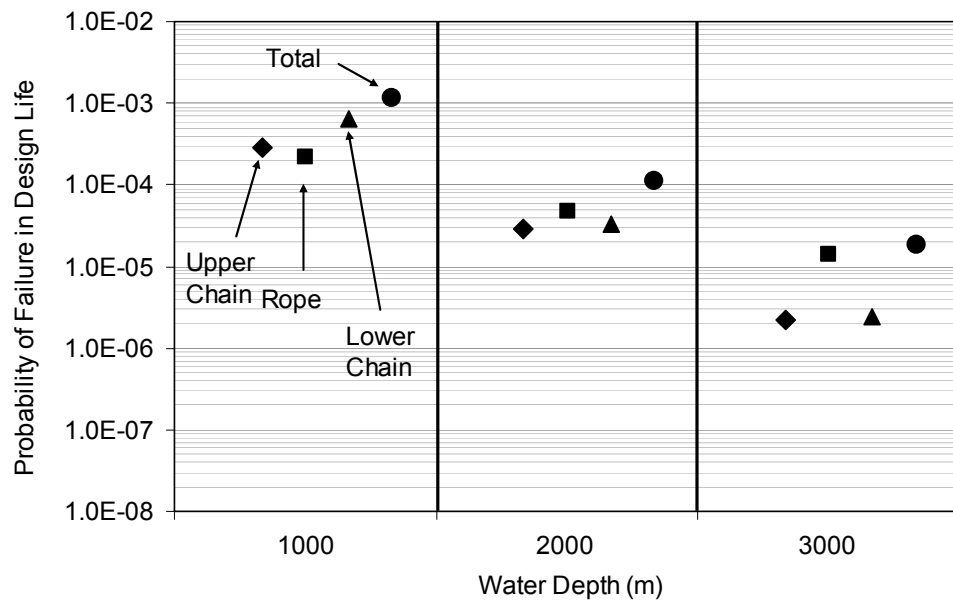


Figure 5.4: Example of reliabilities of individual components for most heavily loaded line of the study spar under hurricane conditions

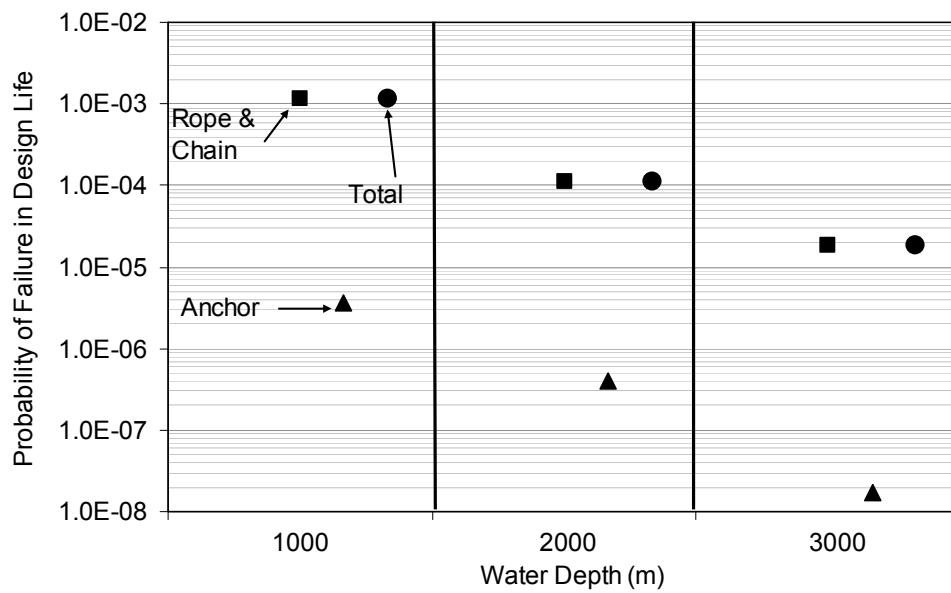


Figure 5.5: Example of complete line reliability of most heavily loaded line of the study spar under hurricane conditions



## **5.5 FRAMEWORK FOR SYSTEM RELIABILITY CALCULATIONS**

The event of a single component failure does not necessarily lead to collapse of the foundation or mooring system (Tang and Gilbert, 1993). Individual sequences of foundation and/or line failure are considered to identify the most likely modes of failure in extreme conditions and to quantify redundancy in the system.

### **5.5.1 Definition of system failure**

For the mooring systems, a system failure is defined as the failure of two mooring lines (either in the line itself or in the anchor), which will typically lead to a loss of station keeping. If the most heavily loaded line fails, the load will be redistributed to the adjacent lines of the spar. Individual sequences of line breakage and anchor failure are considered to identify the most likely modes of failure in extreme conditions and to quantify redundancy in the mooring system. For comparison, in cases where TLP (Tension Leg Platform) structure is considered in the system reliability analysis, failure of the TLP system is defined as failure of one tendon because a ruptured tendon falling to the ocean floor causes significant damage to adjacent risers and other tendons or foundations (Banon et al., 1994; Harding and Banon, 1989).

### **5.5.2 System reliability calculation**

The probability for a loss of station keeping is given by

$$P(\text{Second Line Fails}) = P(\text{Second Line Fails} | \text{First Line Fails}) \cdot P(\text{First Line Fails}) \quad (5.12)$$

where  $P(\text{Second Line Fails})$  is the probability of failure of a mooring system;  $P(\text{Second Line Fails} \mid \text{First Line Fails})$  is a conditional probability of failure of the second most heavily loaded line given that the most heavily loaded line has failed; and  $P(\text{First Line Fails})$  is the probability of failure of the most heavily loaded mooring line. For the study spar, the most heavily loaded line is line No. 8 under hurricane conditions and the second most heavily loaded line is line No. 9.  $P(\text{First Line Fails})$  can be calculated using the method discussed in section 5.2.

The methodology used to evaluate the system reliability involves: 1) updating the distribution for sea states given that one of the system components has failed during the storm; and 2) re-establishing the load on the next-most heavily loaded line (line No.9 for a hurricane event). In the first step in the methodology, since the maximum load is expected on line No. 8, the distribution for  $H_s$  is updated given that line No. 8 has failed using the Bayesian approach (Ang and Tang, 1975), as expressed in Equation 5.13.

$$f'_{H_s}(H_s) = f_{H_s|L8\text{ fails}}(H_s \mid L8\text{ fails}) = \frac{P(L > C \mid H_s)f_{H_s}(H_s)}{P(L8\text{ fails})} \quad (5.13)$$

where  $f_{H_s|L8\text{ fails}}(H_s \mid L8\text{ fails})$  is the updated probability distribution of  $H_s$ ;  $P(L8\text{ fails})$  is the probability of failure of the most heavily loaded line;  $f_{H_s}(H_s)$  is the prior probability distribution of  $H_s$ ; and  $P(L > C \mid H_s)$  is the probability that the load exceeds the capacity given a significant wave height. Figure 5.5 shows this approach. The thinner solid curve on Figure 5.6 is the prior probability distribution for  $H_s$  (i.e., the distribution before knowing that line No. 8 has failed). The thicker solid curve on Figure 5.6 is the probability that line No. 8 will fail as a function of  $H_s$ . These two curves are multiplied together to produce the updated probability distribution for  $H_s$  given that line No. 8 has failed (the hidden line curve on Figure 5.6). Note that the updated

probability distribution for  $H_s$  is shifted to the right to reflect the greater likelihood that a severe storm has occurred if line No. 8 has failed.

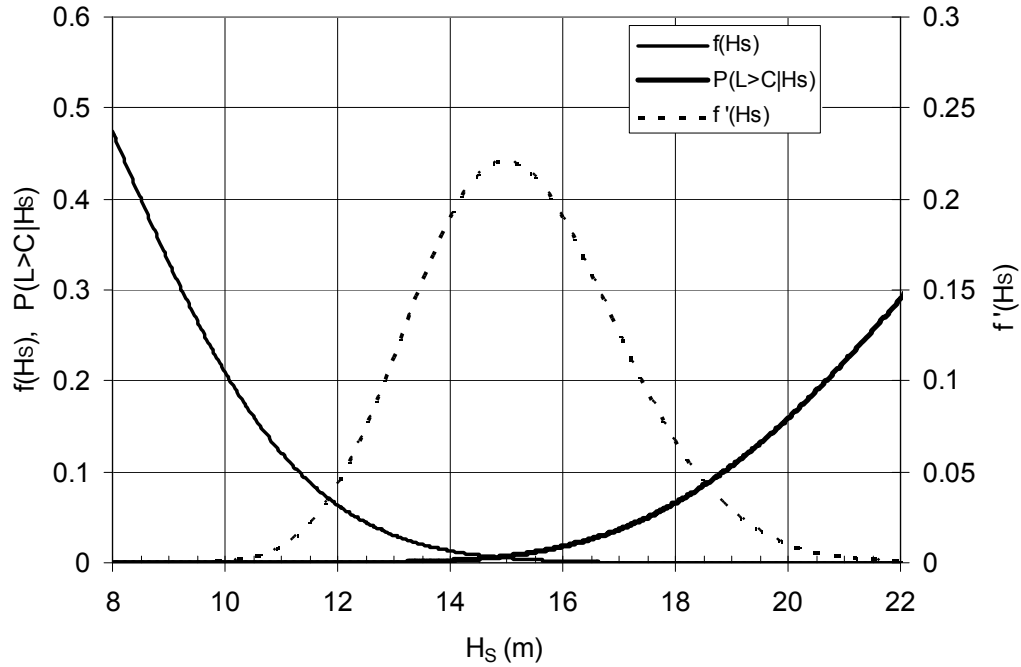


Figure 5.6: Probabilities of sea state and failure for mooring line No. 8

The second step in the methodology is to establish the distribution for the expected maximum load given that the most heavily loaded line has already failed as shown in Figure 5.7. This figure is a plot of the expected maximum mooring line loads at the fairlead for the most heavily loaded line and the second most heavily loaded line given that the first line has failed. It indicates that the load is linearly increasing with the significant wave height. Using two fitted lines, the expected line load can be estimated.  $P(L > C | H_s)$  in Equation 5.13 can then be calculated.

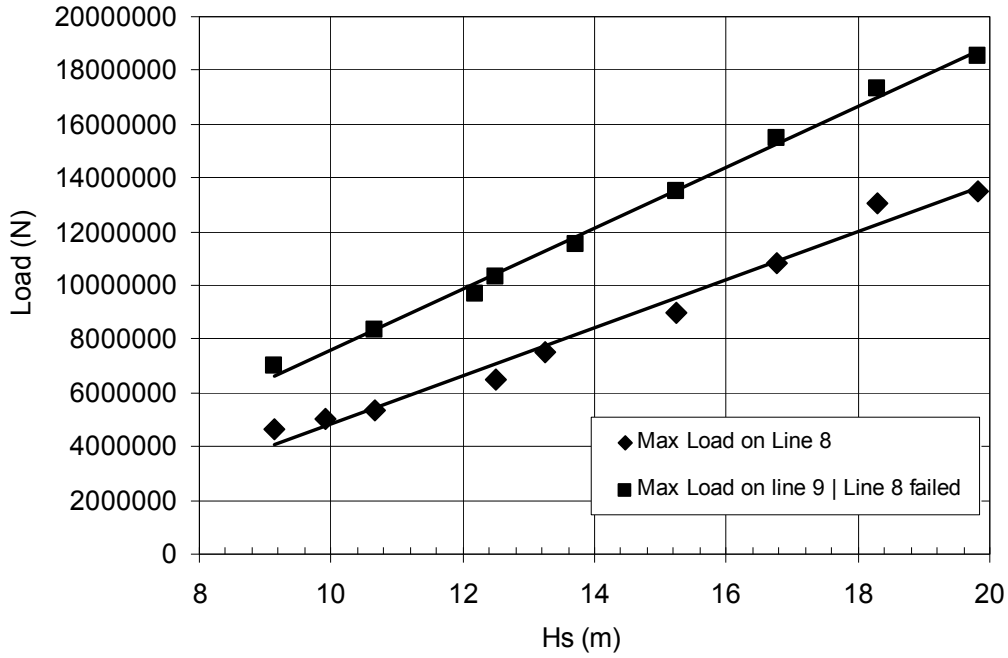


Figure 5.7: Expected maximum load at fairlead for mooring lines Nos. 8 and 9 plotted against the significant wave height

The updated probability distribution for the maximum load on line No. 9, given that line No. 8 has failed, can be obtained by combining the information shown in Figures 5.6 and 5.7. With this updated distribution for the maximum load on line No. 9, the probability that line No. 9 fails, given that line No. 8 has failed, can then be calculated. This probability provides an indication of the redundancy that is available in the mooring system.  $P(\text{Second Line Fails})$  can finally be calculated by multiplying the condition probability by the probability of failure of the most heavily loaded line.

### 5.5.3 System redundancy

The study spar consisting of fourteen mooring lines may be considered as a parallel system that is composed of redundant components. The reliability of a parallel

system depends on whether the redundant members are actively loaded, or only become loaded if a failure occurs (Ang and Tang, 1984). Redundant members that are not actively loaded are referred to as standby redundancies. In the case of standby redundancies, some of the redundant components are always inactive except when the active components have failed whereas for systems with active redundancies all the components of the system are carrying or sharing loads. Therefore, for an active redundant system, similar to the study spar, all subsequent component failure will involve conditional probabilities.

The redundancy in the mooring system is quantified in terms of a redundancy factor, which is defined as the inverse of this conditional probability. In other words, this is the conditional probability:  $P(\text{Second Line Fails} \mid \text{First Line Fails})$ . If this term is equal to 1.0, then there is no redundancy because line No. 9 will fail if line No. 8 fails and the spar will lose station keeping. This redundancy factor is shown on Figure 5.8 for illustrative purposes (the curve labeled “Active Redundancy”) as a function of the factor of safety used to design each individual mooring line. Also as an upper bound, the redundancy factor is shown on Figure 5.8 for a standby system where the most heavily loaded line is duplicated, so that if one fails then a second line is still present at that location (the curve labeled “Standby Redundancy”). Therefore, the standby redundancy is equal to the reciprocal of the conditional probability of failure,  $P(\text{Duplicated First Line Fails} \mid \text{First Line Fails})$ . In the calculation of the conditional probability, the updated distribution for sea states given that the most heavily loaded line has failed should be used while the prior probability distribution for the maximum load on line No. 8 should be used. This standby redundancy reflects the redundancy in the system when the effect of load redistribution due to line failure is neglected because the duplicated line carries the load of the failed line.

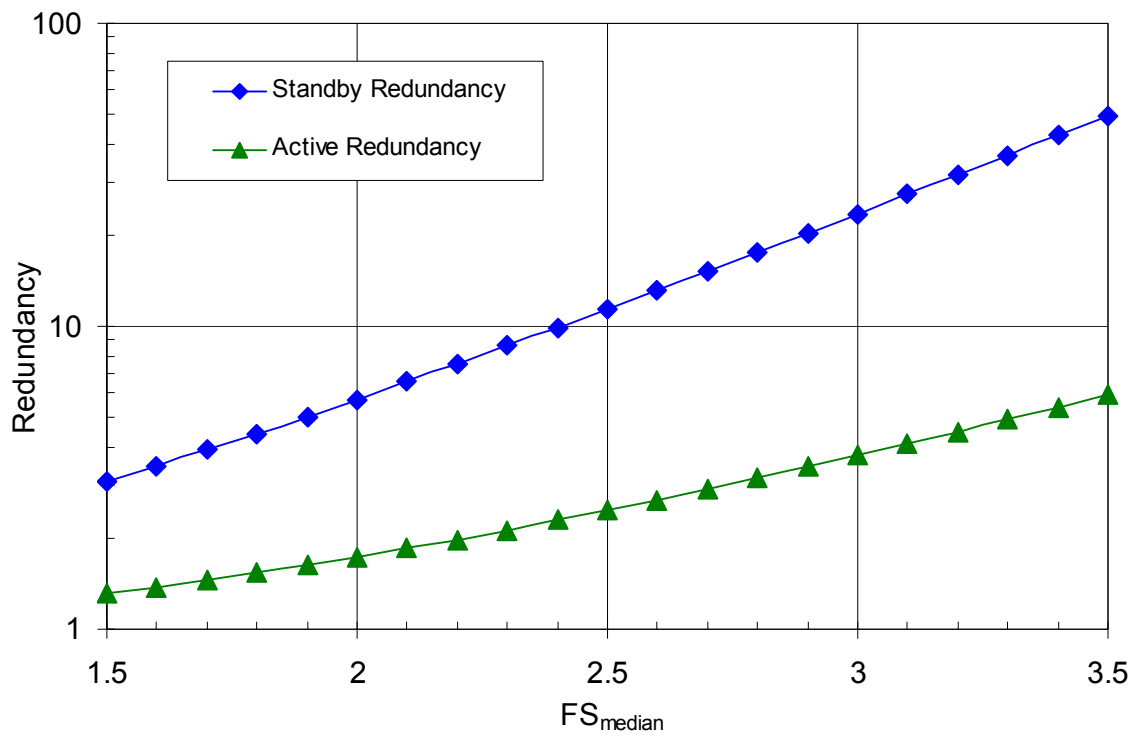


Figure 5.8: Mooring system redundancy factor

## 5.6 EXAMPLES OF SYSTEM RELIABILITY

Figure 5.9 shows an example of the total system reliability of station-keeping in the lifetime for the study spar at three water depths under a hurricane event.

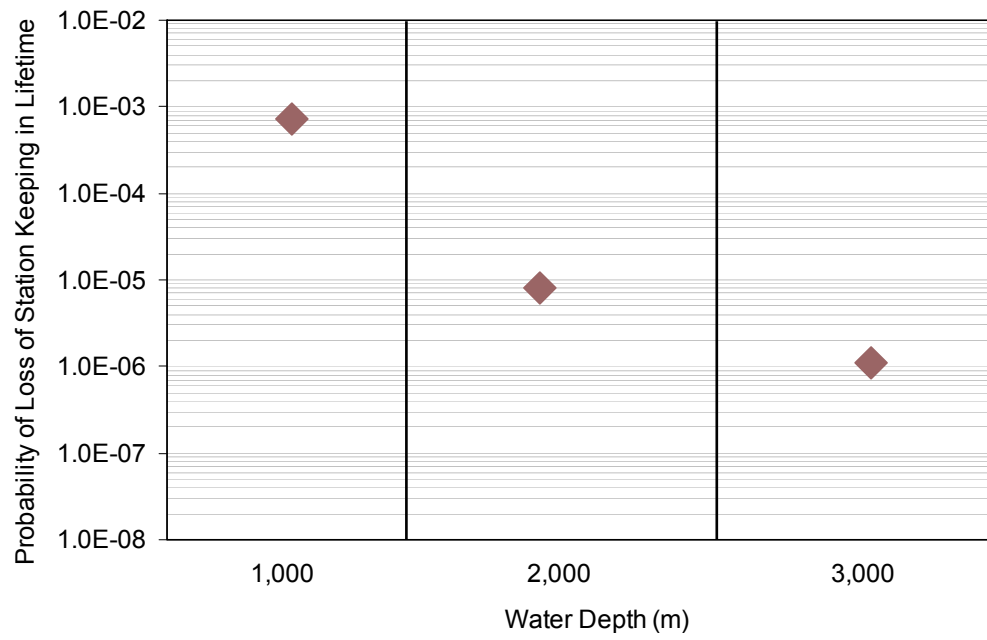


Figure 5.9: Example of system reliability of station keeping in 20-yr design life at three water depths under hurricane loading

## **Chapter 6: Results and Comparisons of Reliability Analysis of the Study Spar under Extreme Environmental Conditions**

### **6.1 INTRODUCTION**

The results of a reliability analysis of the mooring systems for the study spar are presented and discussed in this chapter. Finally, the results from this study are compared with the actual performance of floating structures that experienced Hurricanes Ivan, Katrina and Rita.

### **6.2 BIAS AND C.O.V VALUES FOR FOUNDATIONS**

As indicated in Figure 5.2, the reliability for a typical foundation in an offshore structure systems depends on the bias and c.o.v values for the load and capacity (Gilbert et al., 2005). Tables 6.1 and 6.2 summarize the bias and c.o.v values for the mooring line and foundation, respectively. The conservative bias in the median load versus the design load is greater for these spar foundations than for a pile in a typical jacket platform, where the ratio of the median to the design load is between 0.7 and 0.8 (Tang and Gilbert, 1993). This conservative bias is especially significant for the semi-taut mooring system (1,000-m water depth) due to the effect of removing a line in establishing the design load. The loads are shared more evenly between the lines in the taut mooring systems than in other mooring systems. This tends to minimize the impact of a failure of one line on the other lines. The difference between the bias values for the semi-taut versus taut mooring systems is smaller for a loop current event than that for a hurricane event. This result is mainly due to the characteristics of a loop current event in terms of loads along time histories. During a loop current event, loads on the most



loaded mooring line (i.e., No. 1, compared with No. 8 in the hurricane case) are relatively constant with time compared to loads in the hurricane case.

Table 6.1: Bias and c.o.v values for the heavily loaded mooring line in study spar in hurricane and current conditions

	Environmental Condition								
	Hurricane			Current (Weibull)			Current (Type II)		
	1000 m	2000 m	3000 m	1000 m	2000 m	3000 m	1000 m	2000 m	3000 m
$\text{load}_{\text{median}}/\text{load}_{\text{design}}$	0.5	0.73	0.75	0.7	0.72	0.72	0.63	0.69	0.71
$\text{capacity}_{\text{median}}/\text{capacity}_{\text{design}}$	1.0 – 1.2	1.0 – 1.2	1.0 – 1.2	1.0 – 1.2	1.0 – 1.2	1.0 – 1.2	1.0 – 1.2	1.0 – 1.2	1.0 – 1.2
$\text{FS}_{\text{design(damage)}}$	1.25	1.25-1.5	1.25-1.5	1.25	1.25-1.5	1.25-1.5	1.25	1.25-1.5	1.25-1.5
$\text{FS}_{\text{median}}$	2.5 – 3	2 – 2.5	2 – 2.5	2 – 2.5	2 – 3	2 – 3	2 – 2.5	2 – 3	2 – 3
$\delta_{\text{load}}$	0.25	0.13	0.1	0.09	0.1	0.09	0.11	0.12	0.11
$\delta_{\text{capacity}}$	0.15	0.15	0.15	0.15	0.15	0.15	0.15	0.15	0.15
$\delta_{\text{total}}$	0.29	0.20	0.18	0.17	0.18	0.17	0.19	0.19	0.19

Table 6.2: Bias and c.o.v values for the foundation for study spar in hurricane and current conditions

	Environmental Condition								
	Hurricane			Current (Weibull)			Current (Type II)		
	1000 m	2000 m	3000 m	1000 m	2000 m	3000 m	1000 m	2000 m	3000 m
$\text{load}_{\text{median}}/\text{load}_{\text{design}}$	0.41	0.7	0.71	0.6	0.69	0.7	0.59	0.68	0.69
$\text{capacity}_{\text{median}}/\text{capacity}_{\text{design}}$	1.2 – 1.4	1.2 – 1.4	1.2 – 1.4	1.2 – 1.4	1.2 – 1.4	1.2 – 1.4	1.2 – 1.4	1.2 – 1.4	1.2 – 1.4
$\text{FS}_{\text{design(damage)}}$	1.5 - 2.5	1.5 - 2.5	1.5 - 2.5	1.5 - 2.5	1.5 - 2.5	1.5 - 2.5	1.5 - 2.5	1.5 - 2.5	1.5 - 2.5
$\text{FS}_{\text{median}}$	4 – 8	3 – 5	3 – 5	3 – 6	3 – 5	3 – 5	3 – 6	3 – 5	3 – 5
$\delta_{\text{load}}$	0.32	0.14	0.11	0.11	0.1	0.1	0.14	0.13	0.13
$\delta_{\text{capacity}}$	0.3	0.3	0.3	0.3	0.3	0.3	0.3	0.3	0.3
$\delta_{\text{total}}$	0.44	0.33	0.32	0.32	0.32	0.32	0.33	0.33	0.33

Due to the geometry of the study spar and the metocean environment in deepwater, the uncertainty in the load is relatively small compared to c.o.v. values for a

jacket in shallow water, which are generally between 0.3 and 0.5 (Tang and Gilbert, 1993). There are several reasons for the smaller uncertainty in the loads on the spar. First, the line loads are less sensitive to wave height for a spar mooring system in deep water compared to a fixed jacket in shallow water (e.g., Banon and Harding, 1989). Therefore, variations in the sea states over the design life are less significant for the spar mooring system. Second, the mooring system is simpler to model than a jacket, meaning that there is less uncertainty in the loads predicted by the model. Finally, the spar line loads are dominated by pre-tension versus environmental loads; variations in the load due to variations in the sea states therefore have a smaller effect on the total line load. This effect of pre-tension is particularly significant for the taut mooring systems (2,000-m and 3,000-m water depths), which consequently have the smallest c.o.v. values (Tables 6.1 and 6.2).

For the loop current condition, the coefficients of variation in the foundation and line loads are nearly the same regardless of the type of the mooring systems. Also, the coefficients of variation in the foundation and line loads for the taut mooring systems are relatively independent of the environmental conditions. Note that the coefficient of variation in the foundation load is slightly greater than in the line load because of additional uncertainty in the soil properties.

### **6.3 COMPONENT RELIABILITY**

Figure 6.1 shows the component reliabilities for the mostly loaded mooring line for the hurricane condition. The probability that the component load will exceed the capacity of the component during a 20-year design life has a decreasing trend with greater water depth because a decrease in the total c.o.v with the water depth affects the probability. The decrease in the c.o.v arises from greater pretension and less variance in

the dynamic loading in the taut systems. In the taut systems, the levels of the reliability of the upper and lower chain are almost on the same order of magnitude whereas the level is not the same in the semi-taut system. The length of the bottom chain is greater in the semi-taut system than that in the taut systems, which affects the number of links for the asymptotic extreme value problem (Type I smallest).

The total line reliability including the reliability of the anchor was calculated using Equation 5.11 and is shown in Figures 6.1 and 6.2. The contribution of the anchor to the total line reliability can be found in Figure 6.2. For comparison, this anchor failure probability is more than two orders of magnitude smaller than that for any of the line components in all mooring systems. The difference between the total line and anchor probabilities becomes larger in 3,000-m water depth. The total line reliability is affected mainly by the line components not by the anchor as shown in Figure 6.2. Note that the proof load tests for the upper and bottom chains and the lower bound capacity of the foundation were considered in the calculation of the reliability.

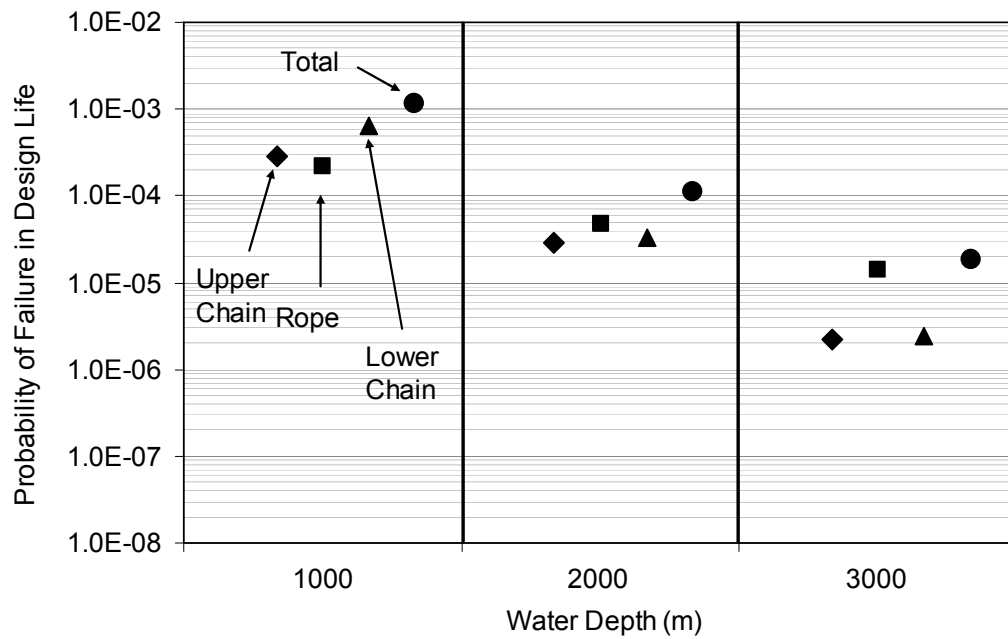


Figure 6.1: Reliability of components for the most heavily loaded line (No. 8) during hurricane events

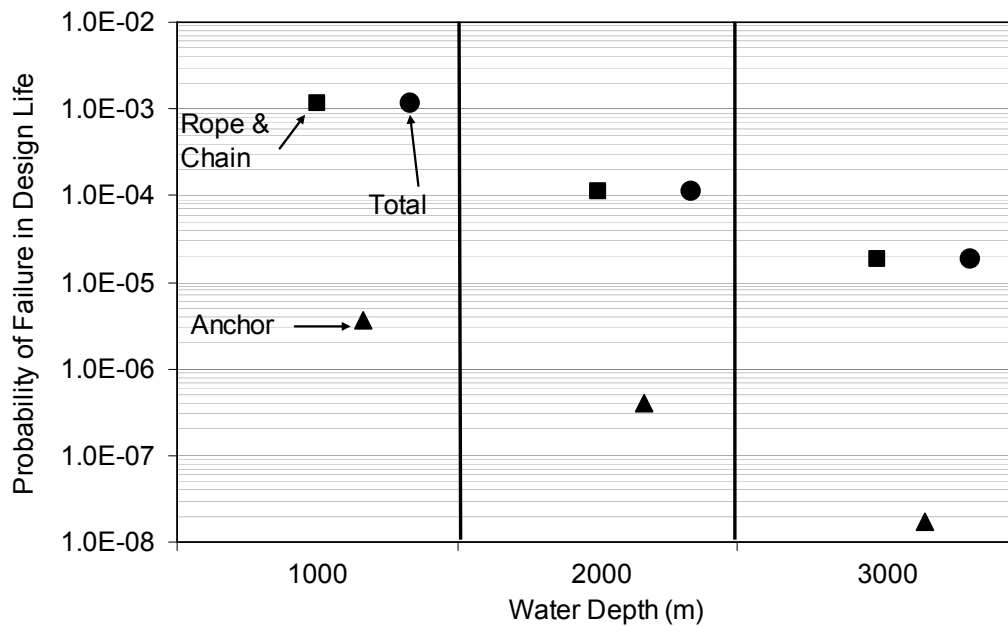


Figure 6.2: Complete line reliability of the mostly heavily loaded line during hurricane events

A calculation of the reliability has also been made without consideration of the proof load. The results are compared to those obtained when considering the proof load in Figures 6.3. For a 1000-m water depth, the effect of the proof load on the total line reliability becomes noticeable with water depths. This may be explained by the fact that the c.o.v in the line loads is smaller for the semi-taut system than that for the taut systems. The author will use all the reliability of the system with the proof load hereafter. It may be argued whether lower bounds on the chains exist, because there may be some quality difference between the manufacturing, handling, and installation processes.

Figure 6.4 illustrates the effect of the coefficients of variation in rope capacity (of 0.05 and 0.15) on the system reliabilities. The probability of failure of the total line is not reduced proportionally to the change of the probability of failure of the rope. This result occurs because the total line probability is controlled not by the smallest probability but by the largest of the component probabilities of failure. The anchor, which is designed conservatively, has a probability of failure that is about two orders of magnitude smaller than that of the line segments. Comparing the probabilities of anchors in three water depths, the difference in the probabilities of the total line with 0.05 and 0.15 becomes essentially negligible in all water depths, especially in 1000-m water. Therefore, the larger c.o.v is used for the remaining reliability analyses presented hereafter.

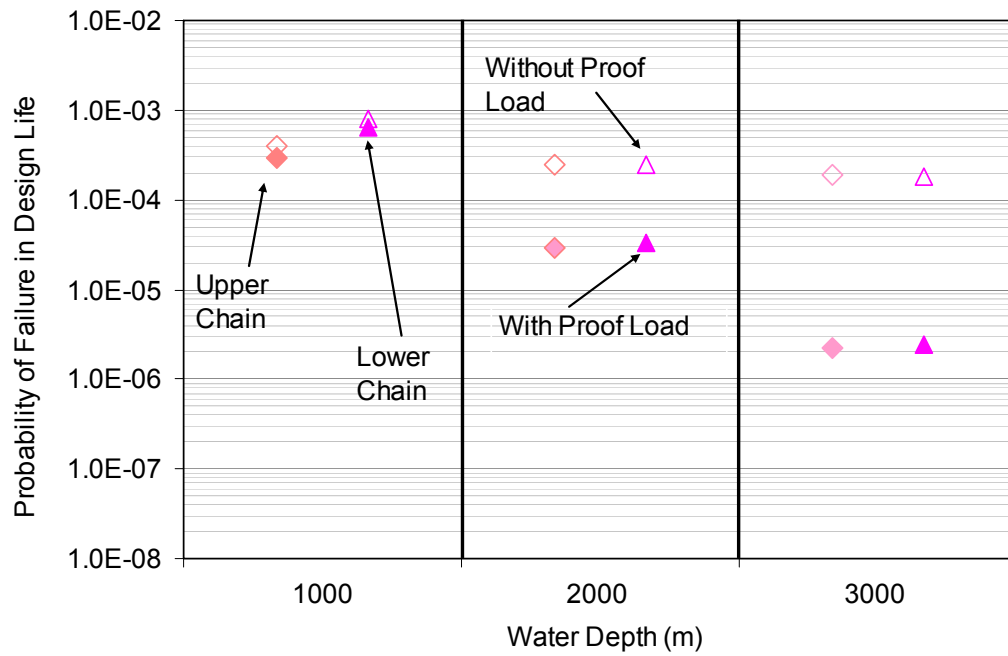


Figure 6.3: Effect of proof load on the reliabilities of the mostly heavily loaded mooring line in three water depths for the hurricane condition

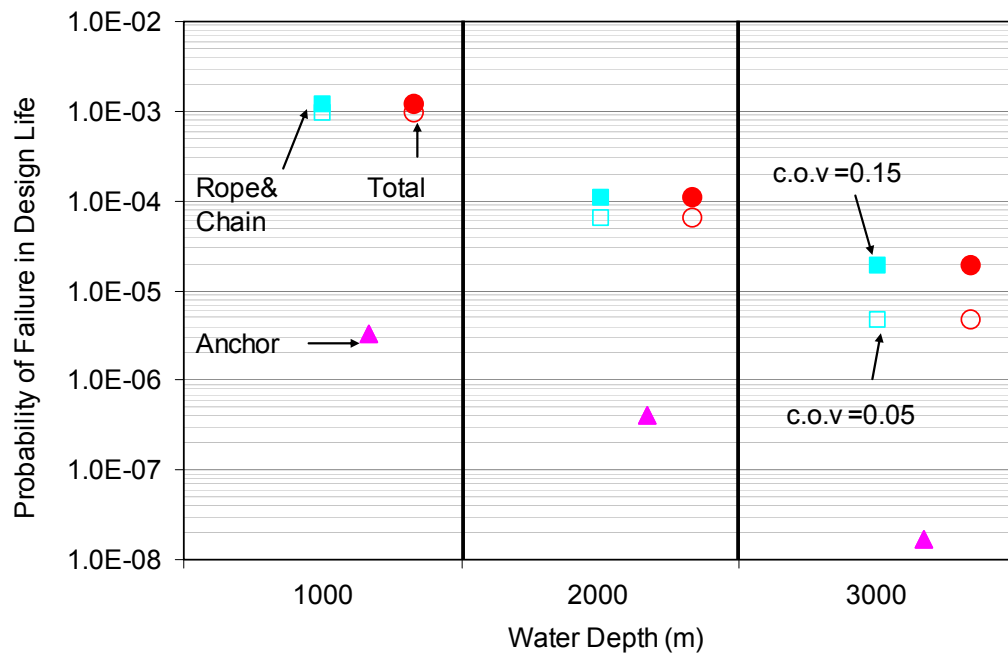


Figure 6.4: Comparison of total line and anchor reliability of No. 8 with two different coefficients of variation in rope capacity for hurricane conditions

The component reliabilities under the loop current condition are greater (in other words, the probability of failure is smaller) than those for the hurricane condition (Figure 6.5). This result occurs because the total c.o.v. values are smaller for the loop current condition (based on the Type II and Weibull distributions) than for the hurricane condition (Tables 6.1 and 6.2). The levels of the reliability are not consistent among the components in the case of both hurricane and loop current conditions because of the differences in the length of the mooring lines and the coefficients of variation in the line loads.

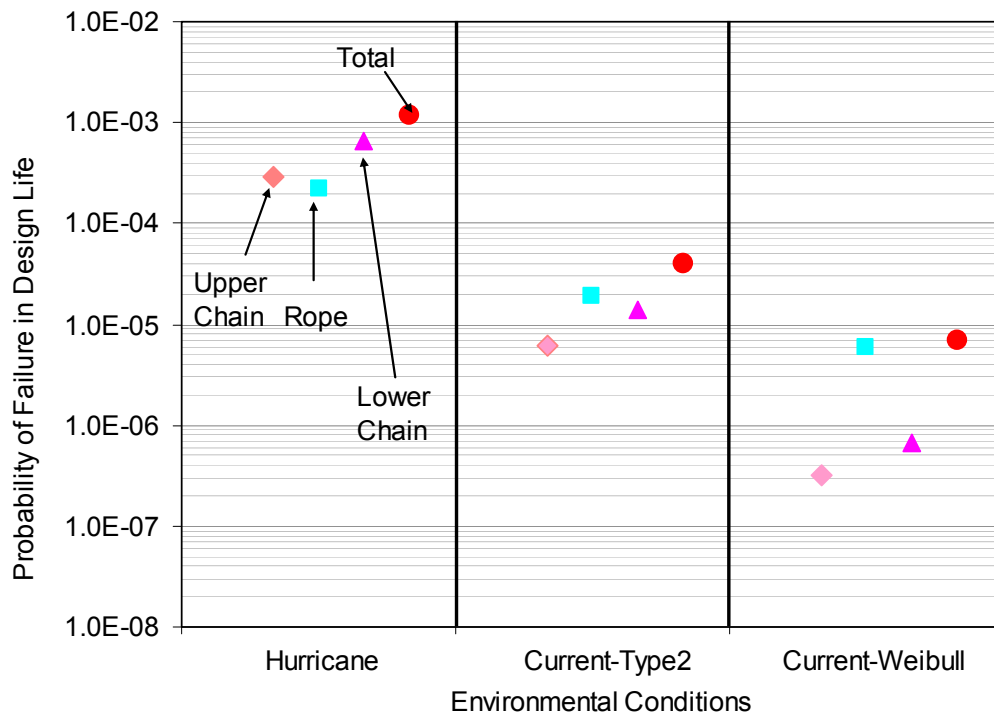


Figure 6.5: Comparison of failure probability of the components of the study spar under hurricane vs. loop current conditions in 1,000-m water depth

Figure 6.6 shows that the total line reliability of the mostly loaded line (i.e., line No. 8 for hurricane and line No. 1 for loop current) is affected mainly by the line

components and not by the anchor. The probabilities of failure for the anchor under the loop current conditions are less than  $10^{-8}$ .

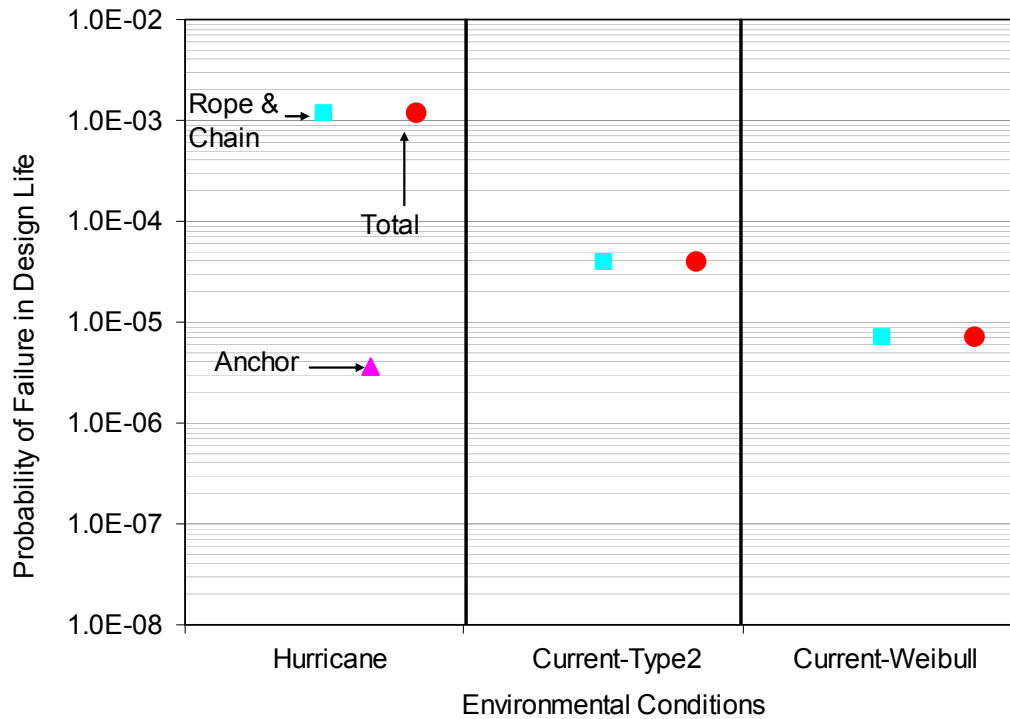


Figure 6.6: Comparison of total line and anchor reliability of the study spar under hurricane vs. loop current conditions in 1000-m water depth

#### 6.4 EFFECT OF LOWER BOUND CAPACITY ON RELIABILITY

One additional consideration in the reliability analysis of the foundation and the chain is the effect of a minimum or lower-bound capacity of the foundation system. In order to account for a lower bound in the probability distribution of the capacity, numerical integration is used to evaluate Equation 5.9.

The effect of a lower-bound capacity on the reliability of the foundation is emphasized on Figure 6.7 for the study spar in 2,000-m water depth. For context, the probability of failure associated with a lower bound ratio of 0.6 is more than 1,000 times



smaller with the lower-bound than without it for a factor of safety of 1.5 in the damage case. Moreover, the probability of failure is essentially zero for a lower-bound capacity of 0.6 times the median capacity for factors of safety of 2 or 2.5 in the damage case,

The effect of a lower bound capacity ratio of the foundation on the probability of failure is more emphasized in Figure 6.8. If there is no lower bound capacity of foundation, the lower-bound to median capacity ratio is zero. In the taut mooring systems, the effect on the probability of failure of the foundation is significantly larger than that in the semi-taut mooring system. For context, these probabilities for the lower-bound ratio of 0.43 in 2,000 and 3,000-m water depths are both more than two orders of magnitude smaller than that for a lower-bound ratio of zero.

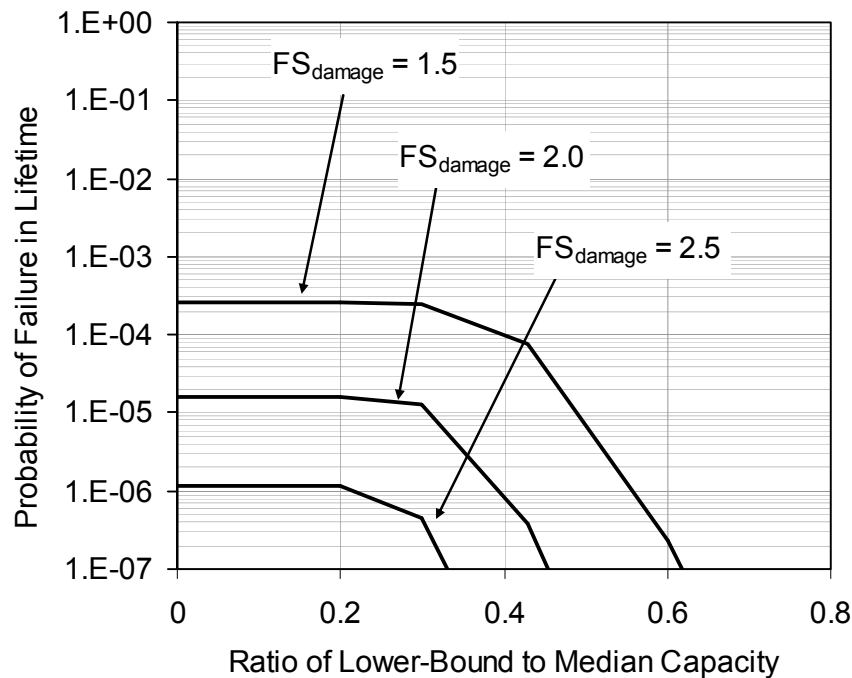


Figure 6.7: Effect of lower-bound capacity on probability of foundation failure (study spar in 2,000-m water depth)

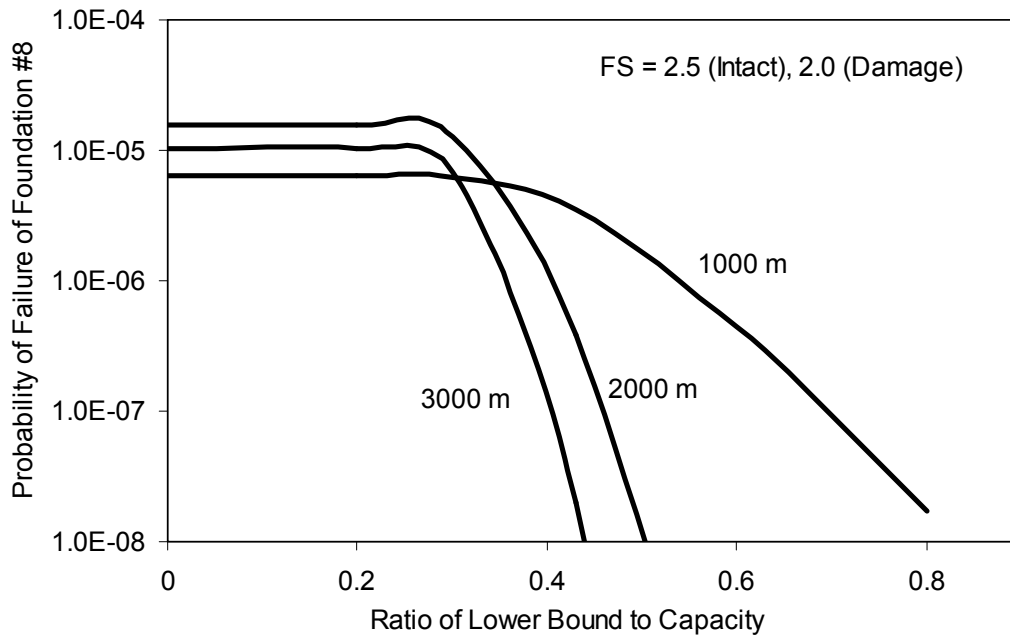


Figure 6.8: Effect of lower-bound capacity of foundation on probability of failure of foundation No. 8 in three water depths for the case of  $FS_{\text{intact}}=2.5$  and  $FS_{\text{damage}}=2.0$  for hurricane loading

One reason that the lower-bound capacity for the anchor has a significant effect is that the coefficient of variation in the foundation load is relatively small. The effect of the coefficient of variation of the line load on the reliability of the total line under the hurricane and current condition is shown in Figure 6.9. In Figure 6.9, the ratio of the probability of failure of the complete line system with lower bound to that without lower bound is shown along y-axis. If the line load has a coefficient of variation of smaller than about 0.25, the effect of lower-bound on the reliability of the study spar increases significantly.

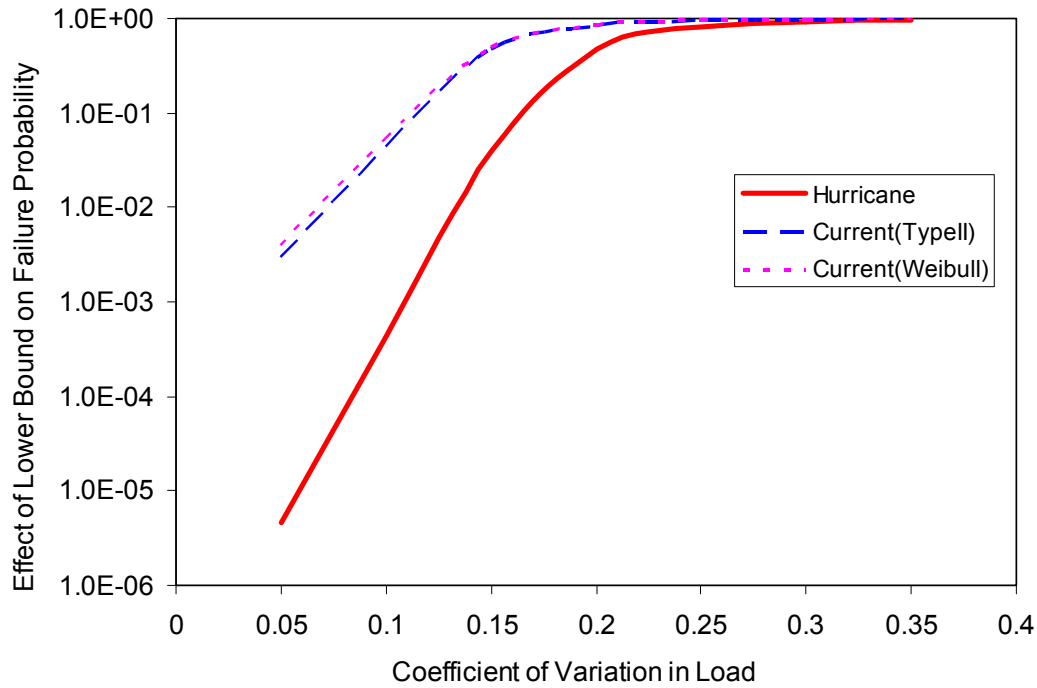


Figure 6.9: Effect of coefficient of variation in line load on reliability of total line

## 6.5 EFFECT OF FACTOR OF SAFETY ON RELIABILITY

The relationship between the probability of failure for line No.8 and the factor of safety for foundation in 2,000-m water depth is shown in Figure 6.10 for hurricane loading. The motivation for considering this factor of safety is that it is not yet well-established in practice (that is a range of values being used for the anchor factor of safety at present). The factor of safety for foundation has a great impact on the reliability of the anchor whereas the total line reliability is insensitive to this factor of safety. This insensitivity is observed because that the probability of failure of the line system (i.e., total line) is governed by the probability of failure of the line components instead of the probability of failure of the anchor. In these calculations, the lower-bound capacity was

calculated to be about 0.43 times the median capacity given the geometry of the suction caisson and the soil profile.

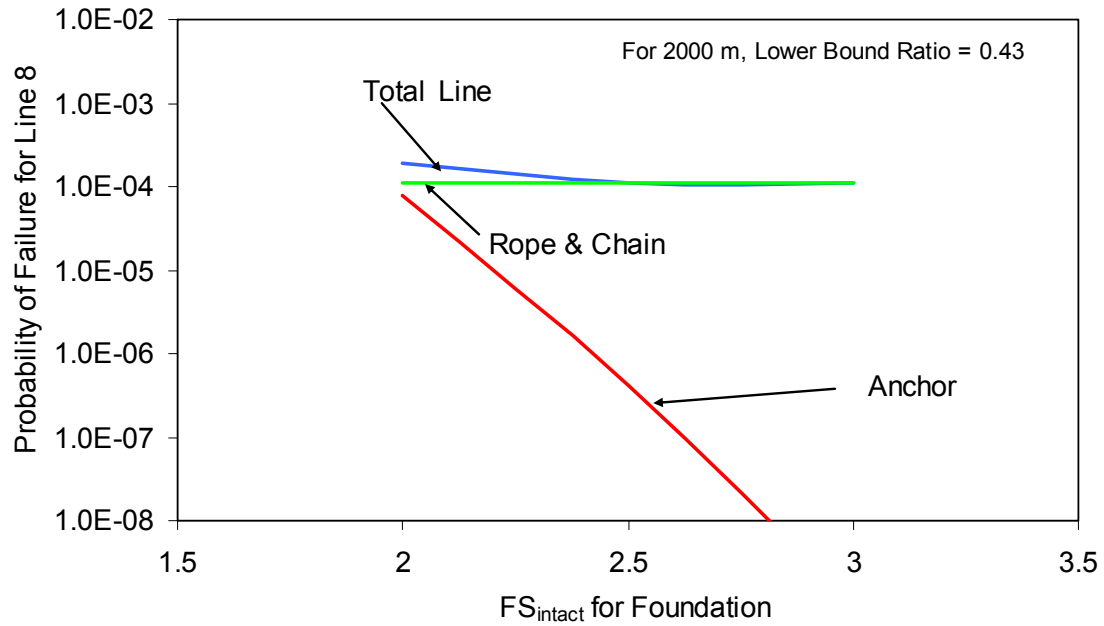


Figure 6.10: Effect of factors of safety on reliabilities of total line and its components in 2,000-m water depth with hurricane loading

The probabilities of failure of the mostly loaded line system for two additional water depths are shown in Figure 6.11. Figure 6.11 indicates that the total line reliability is relatively insensitive to the factor of safety for foundation.

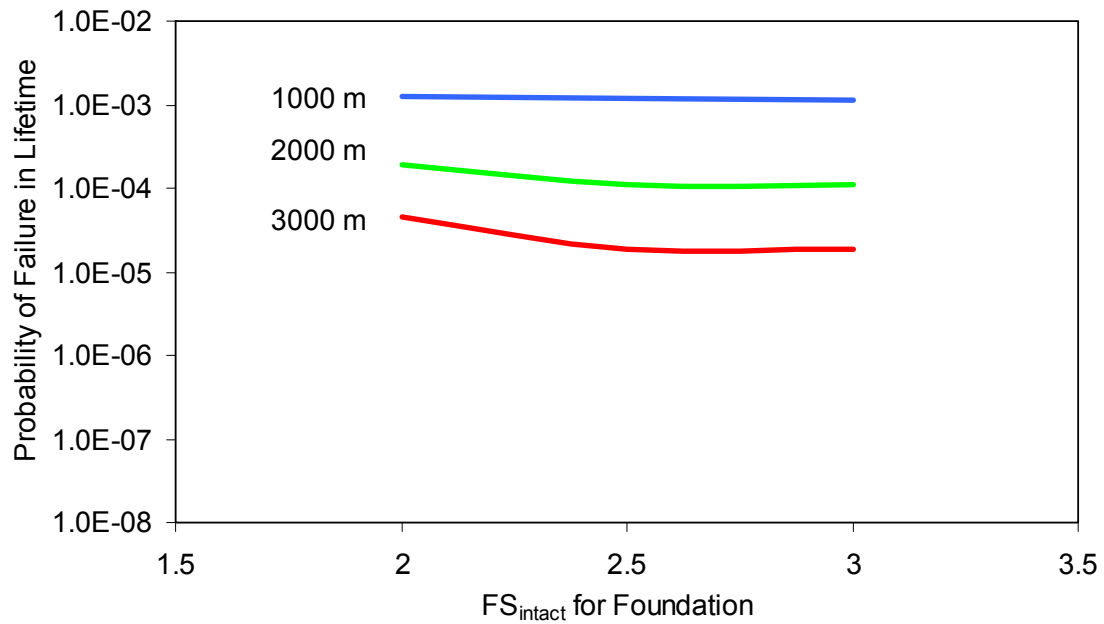


Figure 6.11: Effect of factors of safety on reliabilities of total line in three water depths for hurricane loading

Figure 6.12 shows the relationship between the factor of safety for the suction caisson foundation No. 8 and its probability of failure in three water depths for hurricane loading. The slopes of the three curves increase with increasing water depth. This is because the total c.o.v decreases with water depth because in Equation 5.5, a reciprocal of the total c.o.v value is approximately proportional to the level of the slope of each line.

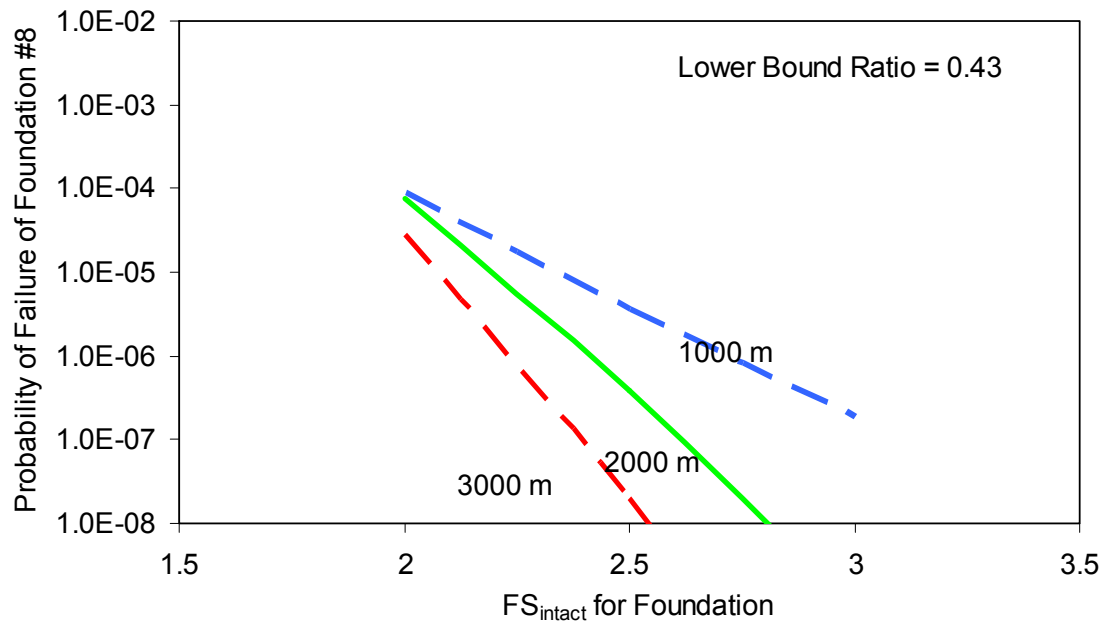


Figure 6.12: Variation in the probability of failure of foundation No. 8 with a lower bound ratio of 0.43 for hurricane loading

## 6.6 SYSTEM RELIABILITY

The results in this section are so significant both in the practice and in theory. For example, several temporary offshore structures in Hurricanes Ivan, Katrina and Rita drifted as many as several hundreds of miles from their original locations due to failure of the most heavily loaded lines. After failure of the most heavily loaded lines, the other mooring lines successively failed as a result of the excessive environmental loadings, resulting in complete failure of the system. Likewise, the performance of the floating production system depends more directly on the performance of the system of lines and anchors rather than on the performance of a single line or anchor. More discussion on some practical case histories is provided in Section 6.8.

Figures 6.13 and 6.14 show how the probability of failure for the most heavily loaded line contributes to the total probability of failure for at least one line in the system. The reliability for a single line is dominated by that for the most heavily-loaded line.

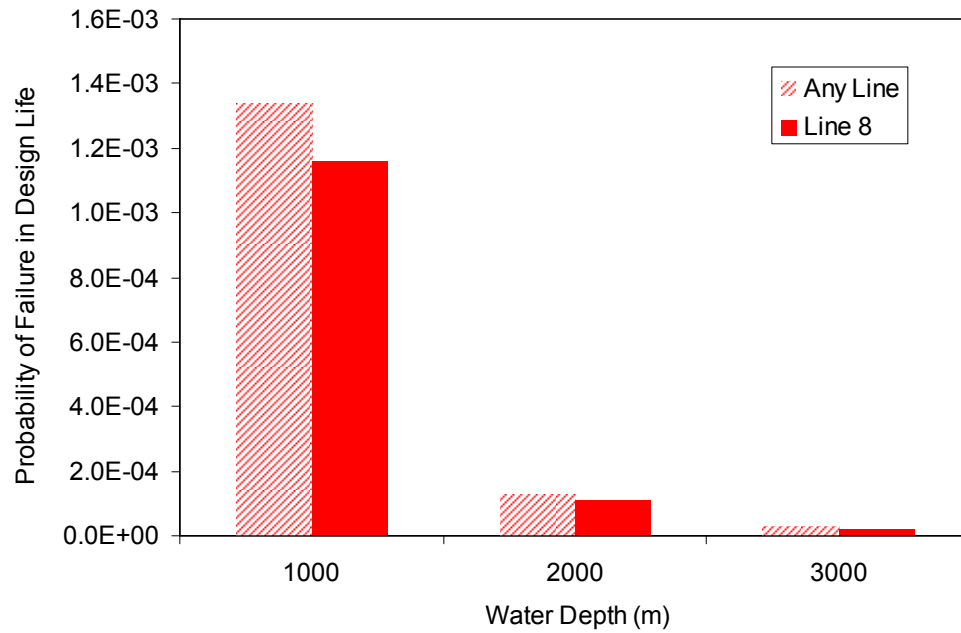


Figure 6.13: Comparisons of probabilities of failure of any line and the mostly loaded line in design life for three water depths under hurricane loading

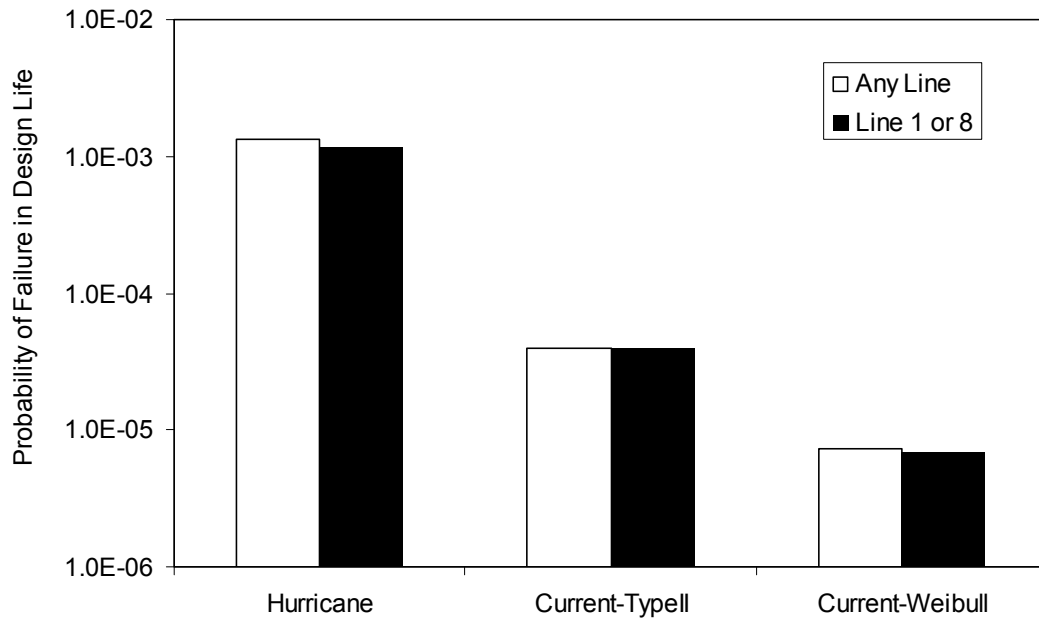


Figure 6.14: Comparisons of probabilities of failure of any line and the mostly loaded line in design life under hurricane versus loop current loading

The conditional probabilities that the second-most heavily loaded line (i.e., line No. 9) fails given that the most heavily loaded line (i.e., line No. 8) has failed for different water depths are shown in Figure 6.15 for hurricane loading. Three assumptions were made in this analysis: 1) the line load should be large enough to fail line No. 8 (i.e., storm must have big waves); 2) line No. 9 will be the most heavily loaded line if line No. 8 has failed; and 3) when line No. 8 fails, the failure point may be anywhere along the line (including the anchor). It should be noted that the failure of the anchor is very unlikely compared to that of the line due to reasons such as the lower-bound capacity of the soil and the setup effect.

For the conditional probability as shown in Figure 6.15, the redundancy factor can be calculated by reciprocal of this probability. The calculated redundancy factor is shown in Figures 6.16 through 6.19. For comparison, a general range for the



redundancy factor for conventional steel jacket systems is between 10 and 100 (e.g., Tang and Gilbert 1993).

The smallest level of redundancy is for the semi-taut system (1000-m of water) under hurricane loading. In this case, the redundancy factor is about 2. For the taut system (2000 and 3000-m of water), the redundancy factors are greater than 10 and similar to those for jackets. The reason why the redundancy factor is smaller for the semi-taut system than that for taut systems may be that there is the relatively small contribution of environmental loading to total loading in the mooring line versus pre-tension for the taut systems. Total loading consists of environmental loading and pre-tension. Also, the redundancy factors of loop current loading are greater than 10 for all water depths.

The total system reliability is shown on Figures 6.20 and 6.21 for hurricane and loop current loading conditions. The system reliability is greater for the taut versus the semi-taut designs under the hurricane loading while it is greater for the semi-taut system than those for the taut systems under the loop current loading. It is mainly because the relatively smaller and greater ratios of the bias factors in the line and foundation are expected for the taut systems and the semi-taut system, respectively (Tables 6.1 and 6.2). The effect of pre-tension on the system reliability becomes less important for the study spar under the loop current condition than for it under the hurricane condition.

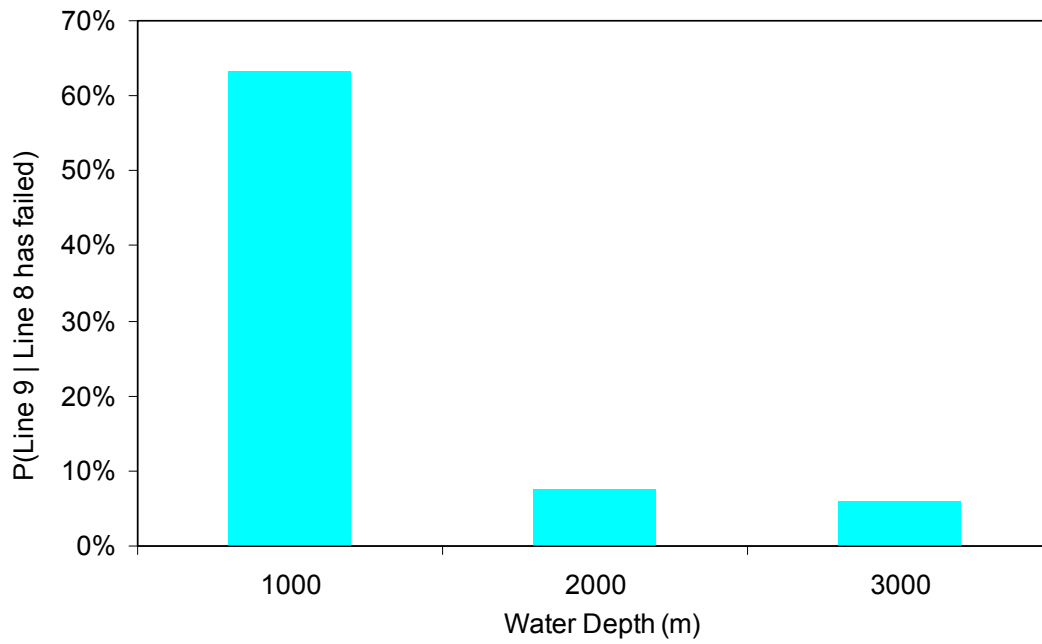


Figure 6.15: Conditional probability of failure of line No. 9 given that line No. 8 has failed at three water depths under hurricane loading

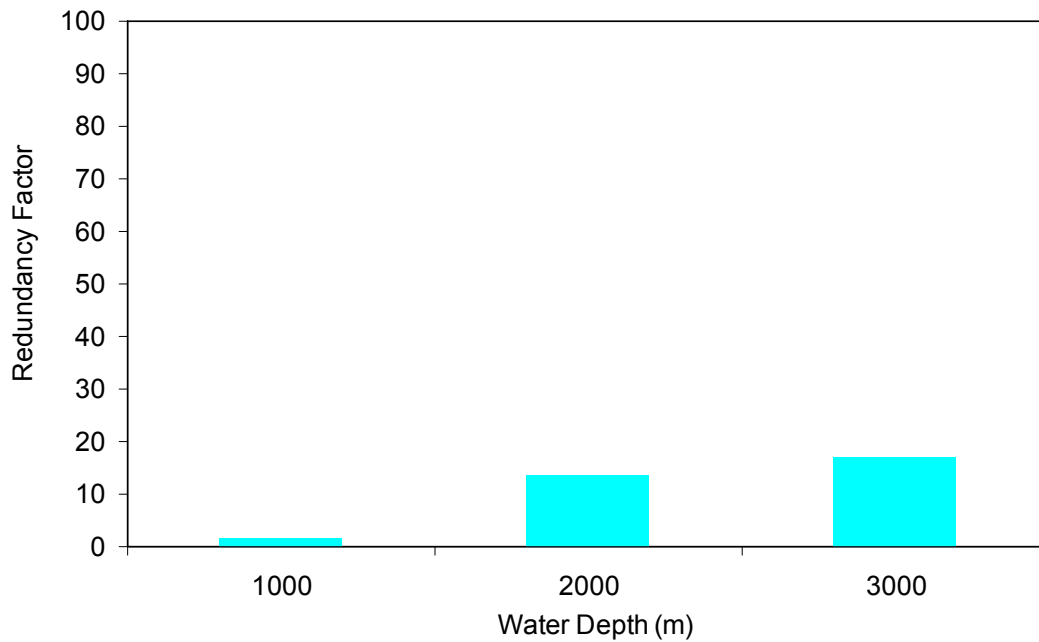


Figure 6.16: Redundancy factor for the study systems at three water depths for hurricane loading

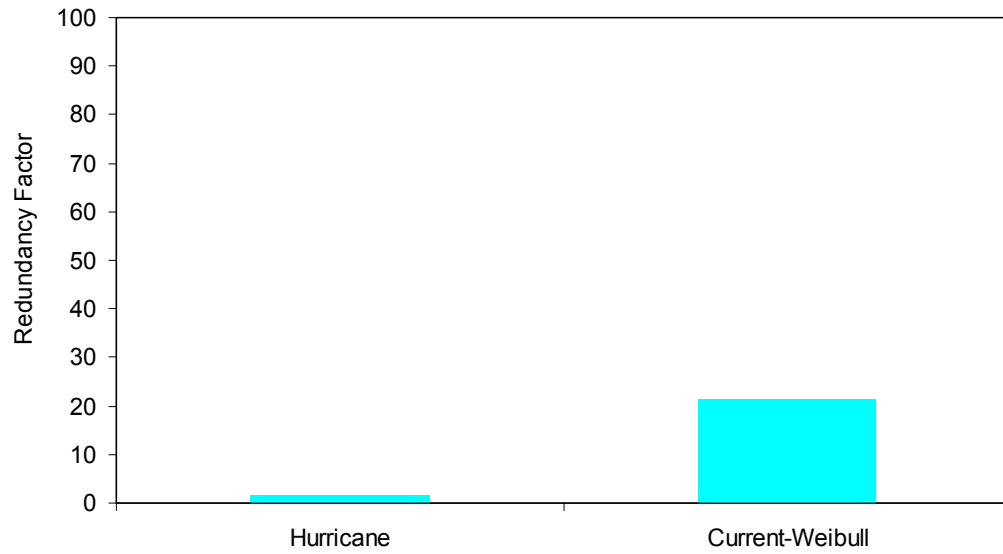


Figure 6.17: Redundancy factor for the study systems in 1000 m of water under hurricane and current conditions

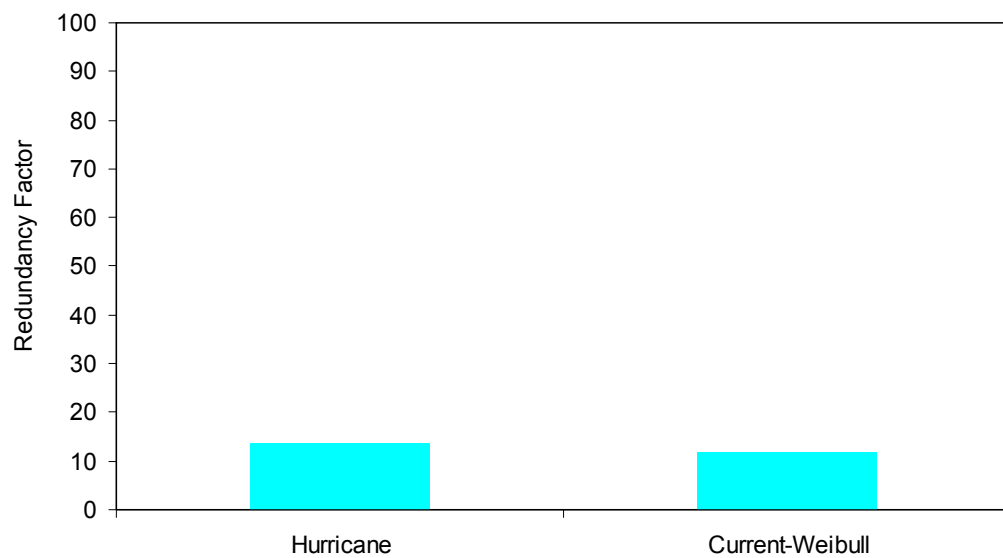


Figure 6.18: Redundancy factor for the study systems in 2000 m of water under hurricane and current conditions

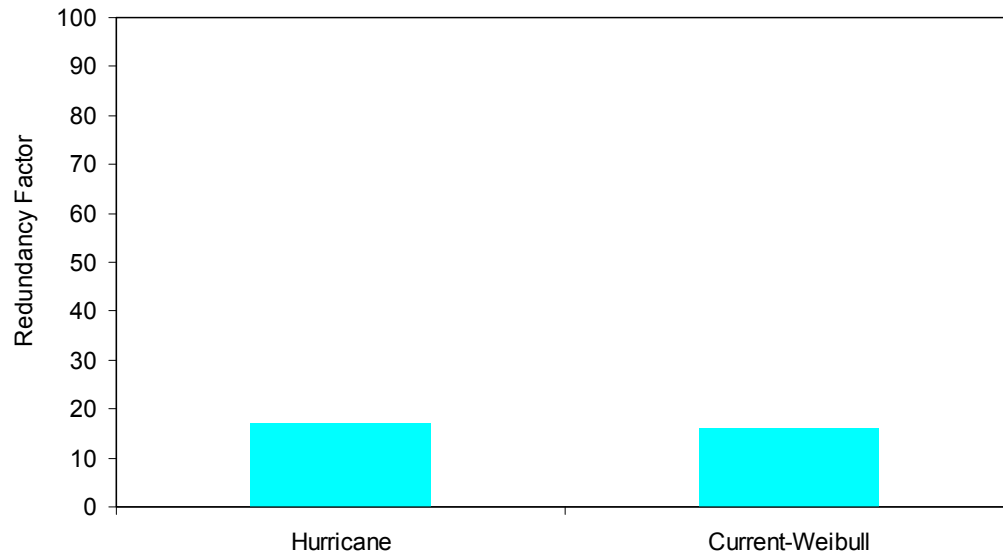


Figure 6.19: Redundancy factor for the study systems in 3000 m of water under hurricane and current conditions

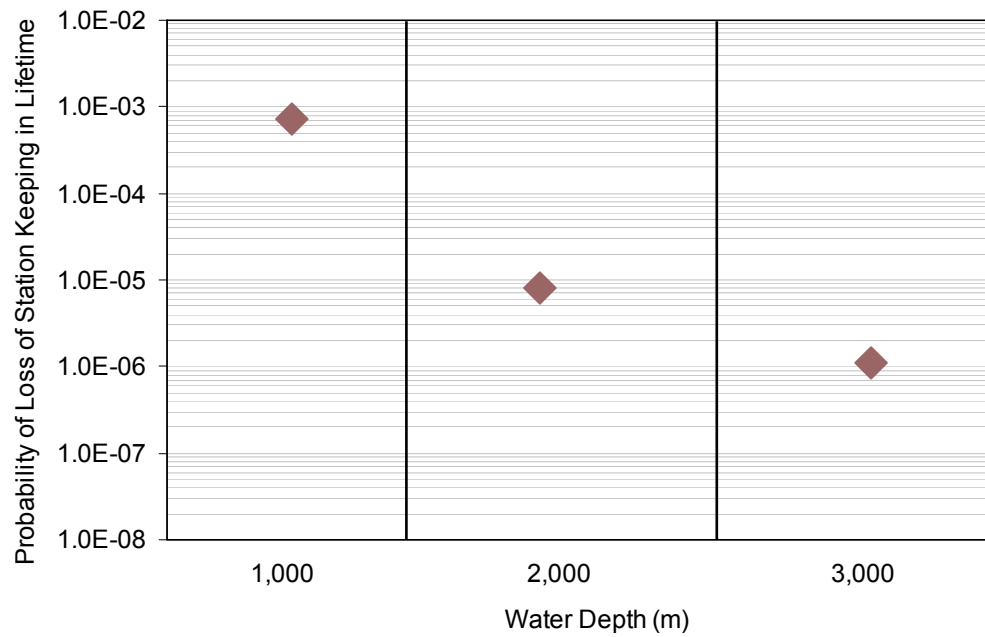


Figure 6.20: System reliability of station keeping in 20-yr design life at three water depths under hurricane loading

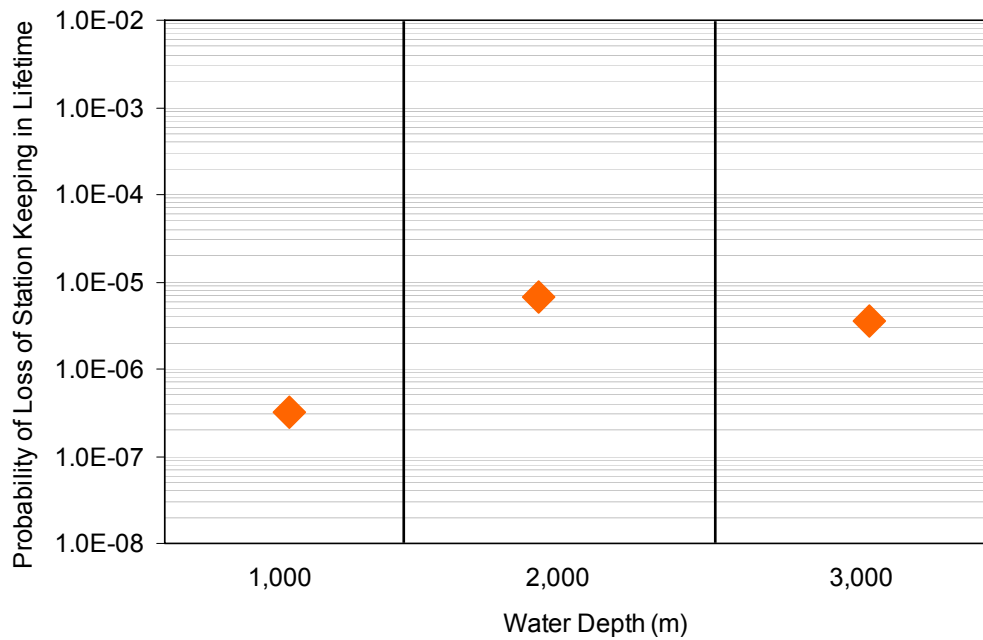


Figure 6.21: System reliability of station keeping in 20-yr design life at three water depths under loop current loading (Weibull)

One final consideration with respect to system reliability is that a single line could be missing for reasons other than failure during an extreme environmental event (e.g., maintenance or installation damage). Compared with the case where the conditional probability of failure of the second most heavily loaded line given that the most heavily loaded line has failed due to an extreme environmental event is estimated using Equation 5.13, one important thing should be considered in calculating system reliability. One does not need to update the probability distribution of  $H_s$  because the line is missing due not to an extreme environmental event but to other reasons. Other things are the same in calculating the system reliability. Figure 6.22 shows how the system reliability is affected by the probability that the most heavily loaded line is missing. Assuming that the possibility that the most heavily-loaded line is missing when the extreme

environmental event occurs is remote (e.g., less than 1 in 1000), then this possibility does not have a significant effect on the overall system reliability.

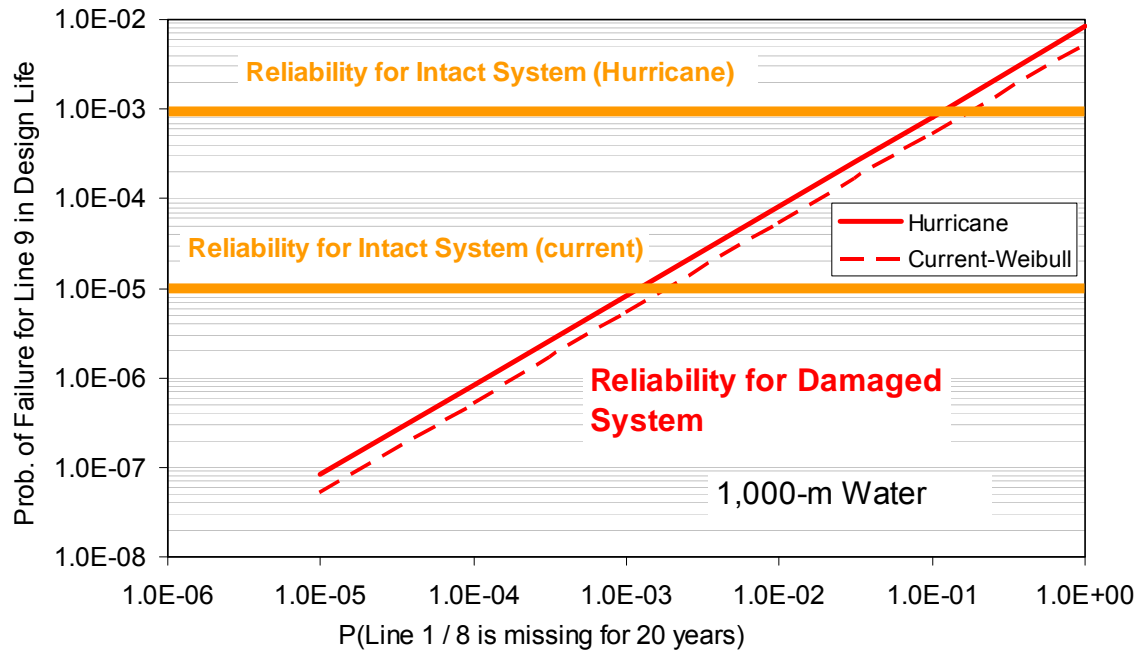


Figure 6.22: Effect of probability of one line missing on system reliability of station keeping in 20-yr design life in 1000-m water depth under hurricane loading condition

## 6.7 COMPARISON OF RESULTS TO INDUSTRY TARGETS

For cases of an event in offshore applications, many researchers generally present results from reliability analyses in terms of the annual probability of the event. As an example, Goodwin et al., (2000) recommend a target probability of failure of  $2 \times 10^{-4}$  per year for a single mooring line. Instead, for a foundation, the probability of failure during the lifetime of the structure is preferred to the annual probability. It is because “The motivation for using annual probabilities is that many events in offshore

applications, such as hurricanes and explosions, occur randomly with time. These annual probabilities of failure represent the rate of occurrence for high-consequence events. In contrast to an event that is dominated by a time varying load, the uncertainty in the failure of an offshore foundation is dominated by uncertainty in the capacity. This capacity does not vary randomly with time. Therefore, it is misleading to consider the probability of failure as a rate of failure. If the actual capacity is higher than expected, then the annual rate of failure due to storm loading may be very small. If the actual capacity is lower than expected, then the annual rate of failure may be larger. ” (Gilbert et al., 2005)

It is noted that this probability was calculated in Figures 6.1 to 6.6 by considering the time-varying component of the load to determine the distribution of the maximum load applied to the foundation over its lifetime.

The annual target probabilities, as recommended by Goodwin et al., (2000), should be converted to the target probabilities in a lifetime to compare failure probabilities in a design life with target probabilities of failure that are expressed as annual rates. Since it is implicit in published failure rates that event occurrences are statistically independent between years, the probability of failure in a lifetime,  $T$ , can be obtained from the following:

$$P(\text{Load} > \text{Capacity in } T \text{ years}) = 1 - (1 - p_{\text{annual}})^T \quad (6.6)$$

$$\cong T p_{\text{annual}}$$

where  $p_{\text{annual}}$  is the annual failure rate.

Based on Equation 6.6, a target probability of failure of 0.004 ( $= 2 \times 10^{-4}/\text{year} \times 20 \text{ year}$ ) in a 20-year design life is easily calculated for a single mooring line.

For the study spar foundation in the three water depths, Figure 6.23 shows the probability of failure in a lifetime along with the target probability of failure. The target reliability for all three water depths is achieved at a factor of safety of 1.3. In comparison, current practice has this factor of safety between 1.5 and 2.5.

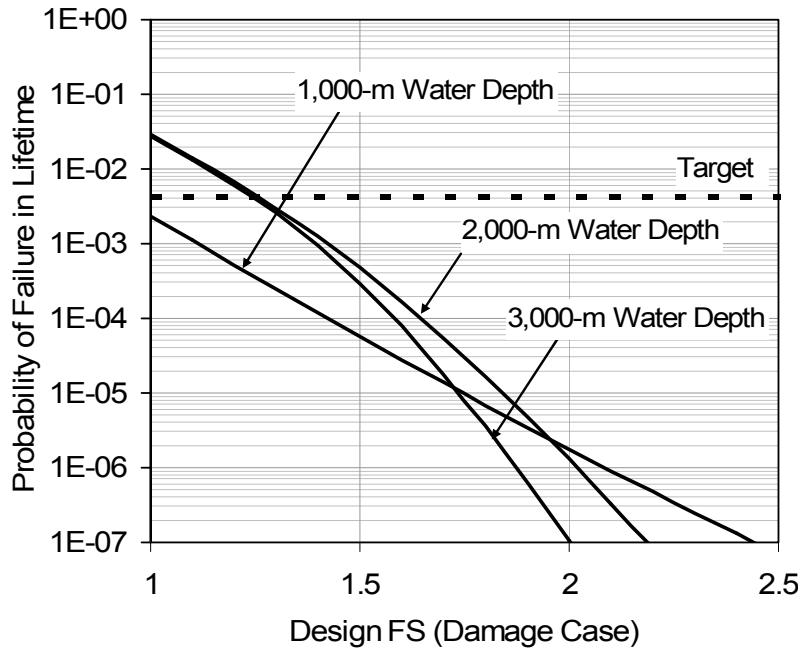


Figure 6.23: Reliability for study spar foundation versus design factor of safety (20-year design life)

The reliabilities of the mooring systems can also be compared with those of industrial facilities and nuclear power plants and dams that have been chosen and used in practice, as shown in Figure 6.24. Target frequencies are also shown in the figure for industrial facilities and nuclear power plants and dams as a function of consequences of failure: number of fatalities and equivalent cost. The acceptable frequencies are set based on the published data (Whitman 1984; Whitman 2000). In order to consider more general cases instead of just showing four single lines corresponding to the target



probability of 0.004 and the calculated probabilities for the mooring systems, bounds on the target probability for floating production systems and the total line probabilities for the semi-taut and the taut systems are shown in Figures 6.24 and 6.25.

The total line failure probabilities for the study spar for designs governed by hurricanes or loop currents are well below the target value. Furthermore, the designs governed by loop currents have probabilities of failure that are several orders of magnitude below the target value for all three water depths. Also, all of the taut systems (2000 and 3000-m water depths) have probabilities of failure that are several orders of magnitude below the target value for designs governed both by hurricane and loop currents. It should be noted that the level of reliability of the semi-taut system is much larger for the current condition than that for the hurricane condition. This result is mainly because of the smaller coefficients of variation in line and anchor loads and relatively larger median factors of safety for the current condition that were used in the calculations.

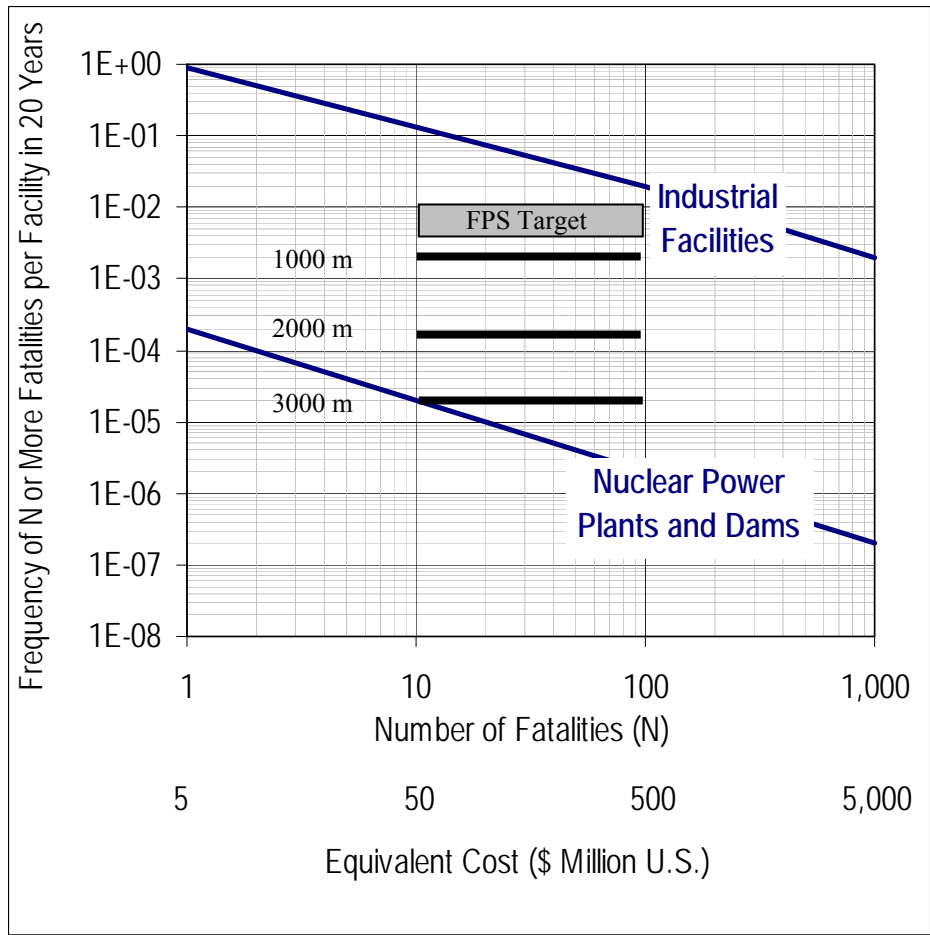


Figure 6.24: Comparison of target reliability and total line reliability of the mostly loaded line in three water depths in a design life of 20 years for hurricane conditions

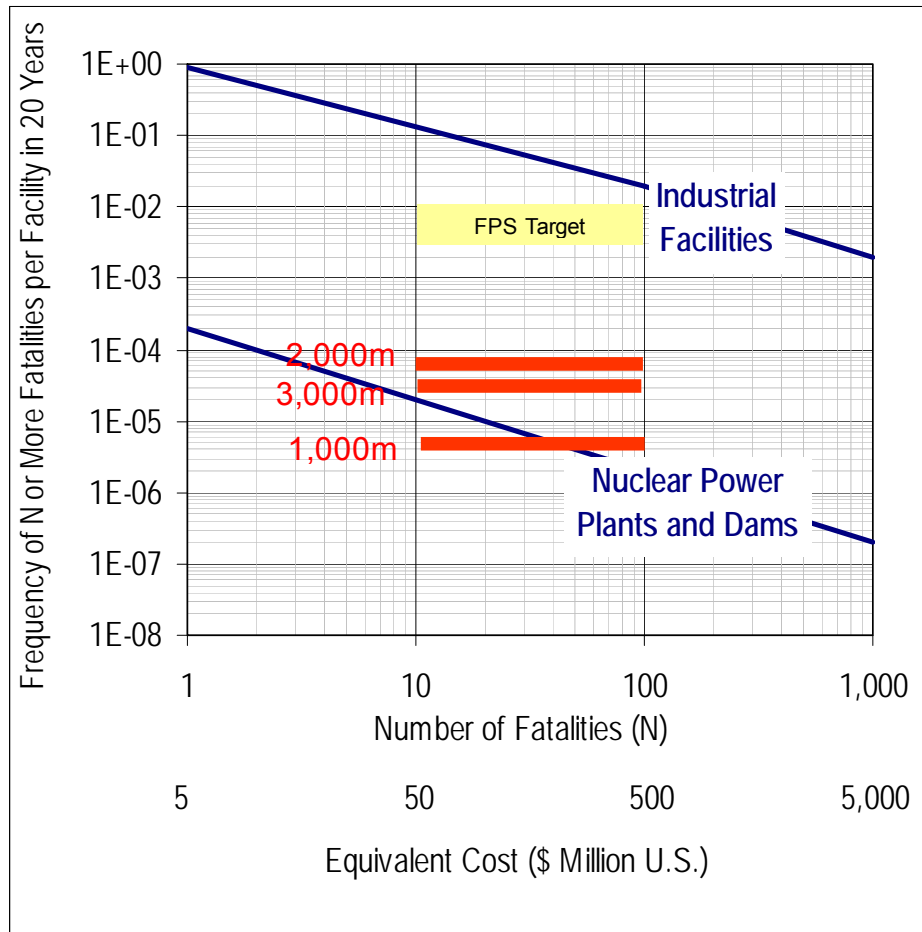


Figure 6.25: Comparison of target reliability with reliabilities of the semi-taut system and the taut systems in a design life of 20 years for current conditions (Weibull)

## **6.8 COMPARISONS OF THE ACTUAL PERFORMANCES OF FLOATING SYSTEMS IN HURRICANES**

The purpose of this section is to indicate that failures observed in the temporary floating structures in the field (such as MODUs) occurred due to failure in the mooring lines, but not in the foundations (as predicted in this study). Further, for permanent floating structures like spars, performance was satisfactory during hurricanes due to their high reliability (as predicted in this study).

During the 2004 and 2005 hurricane seasons, three of the most intense hurricanes in recorded history passed through the Gulf of Mexico: Ivan (2004), Katrina (2005) and Rita (2005). These hurricanes destroyed and damaged hundreds of shallow water fixed platforms and tens of deepwater temporary floating structures such as MODUs (Mobile Offshore Drilling Units). For example, according to an MMS (Minerals Management Service) news release from June 01, 2006, 19 moored rigs experienced a total loss of station-keeping ability due to Hurricanes Katrina and Rita. Among the rigs, many MODUs drifted as many as several hundred miles from their original locations due to failure of the most heavily loaded mooring lines. After failure of the most heavily loaded lines, the other mooring lines successively failed due to the excessive environmental loadings resulting in complete failure of the system.

Since 2005, many studies regarding assessment of deepwater floating structure performance during these hurricanes have been initiated. Published reports available to the public to date mostly focus on Hurricane Ivan. However, other studies focusing on Hurricanes Katrina and Rita are still underway. Based on an extensive search of mooring systems anchored to the seafloor using suction caissons, which have been reported to MMS, as having failed during these hurricanes, two moored rigs were found to have lost their station-keeping ability during Hurricane Ivan and are adopted to explain

how the system failed during Hurricane Ivan. These MODUs were anchored to suction caissons and are referred to as “NOBLE JIM THOMPSON” and “DEEPWATER NAUTILUS”. The actual performance of these floating systems during Hurricane Ivan is compared with the results of the model developed in this study. Specifically, the results presented by Sharples (2004) are presented in this section,

### **6.8.1 Noble Jim Thompson**

This MODU was moored in 1745-m of water to the seabed using nine mooring lines primarily consisting of wire rope although some chain was used. This MODU was a semi-taut steel mooring system. These mooring lines were connected to suction caissons having sizes of 2.9 m x 21.3 m (9.55' x 70') or 3.7 m x 18.3 m (12' x 60'). A picture of the MODU and its spread mooring lines at the time of the event are shown in Figures 6.26 and 6.27. The best possible sequence of failures determined by the layout of the broken lines on the seafloor after the storm is depicted in Figure 6.28. The sequence starts in order from view (1) with the failure of the 1<sup>st</sup> line through view (6). At the time of Ivan, the wind acted in the south-west direction, making Line No. 5 the mostly heavily loaded line. As predicted from this research, Line No. 5 failed first at the fairlead, Line No. 4 failed next (view (2)), followed by Line No. 6 (view (3)). After the first three lines had broken, a significant load was added on the padeyes of suction caissons 7, 8, 2 and 9, which resulted in failure of the padeyes (Sharples, 2004). Finally the vessel moved off to the south-west. The failure of this system during Hurricane Ivan is consistent with in the predictions made in Chapter 6 of this study. Specifically, the mooring system failed due to failure in mooring lines and not due to failure in foundations. However, this failure mode does not agree with current design philosophy (Balint and Orange, 2006). It is recommended by design procedures, such as API RP

2SK (1997), that foundations fail first prior to line breaking in order to redistribute line loads and reduce serious risk to pipeline damage due to the dragged anchors and the broken lines. It is because the damaged pipeline repairs are so expensive and time consuming resulting in production loss for a lengthy period.

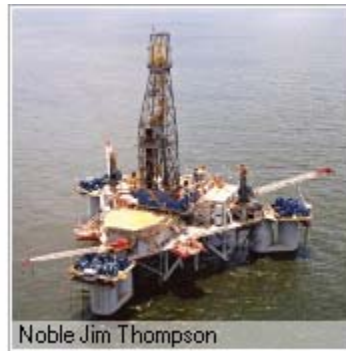


Figure 6.26: Nobel Jim Thompson (Image from [www.rigzone.com](http://www.rigzone.com))

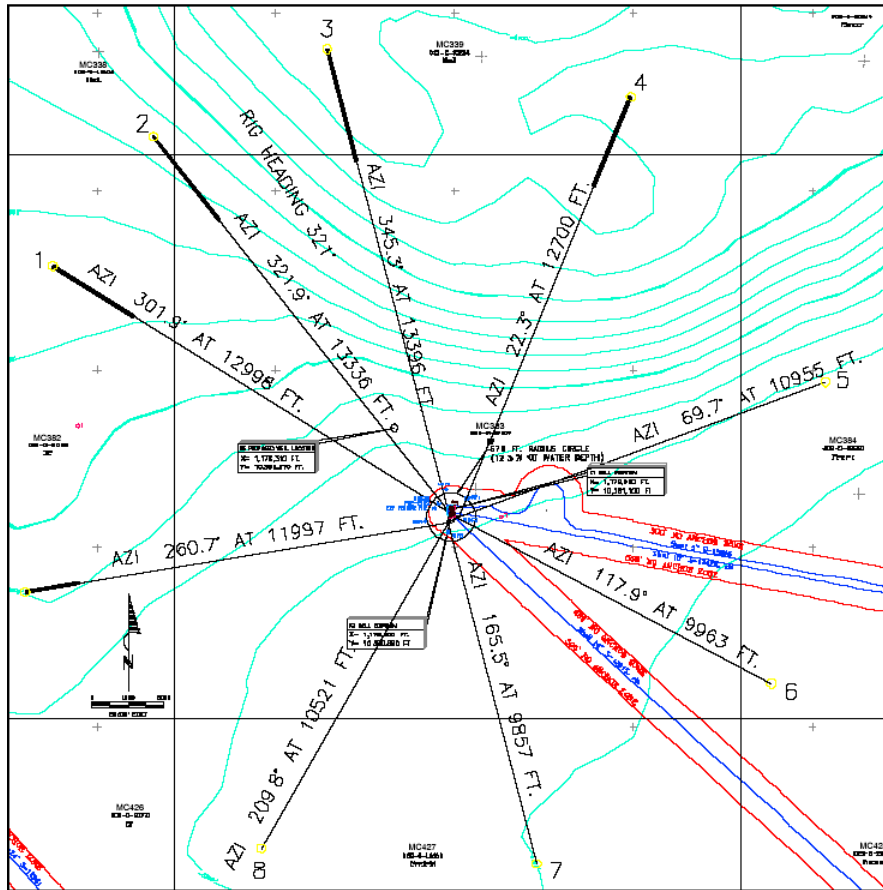


Figure 6.27: Mooring line pattern during Hurricane Ivan for Nobel Jim Thompson (Sharples 2004)

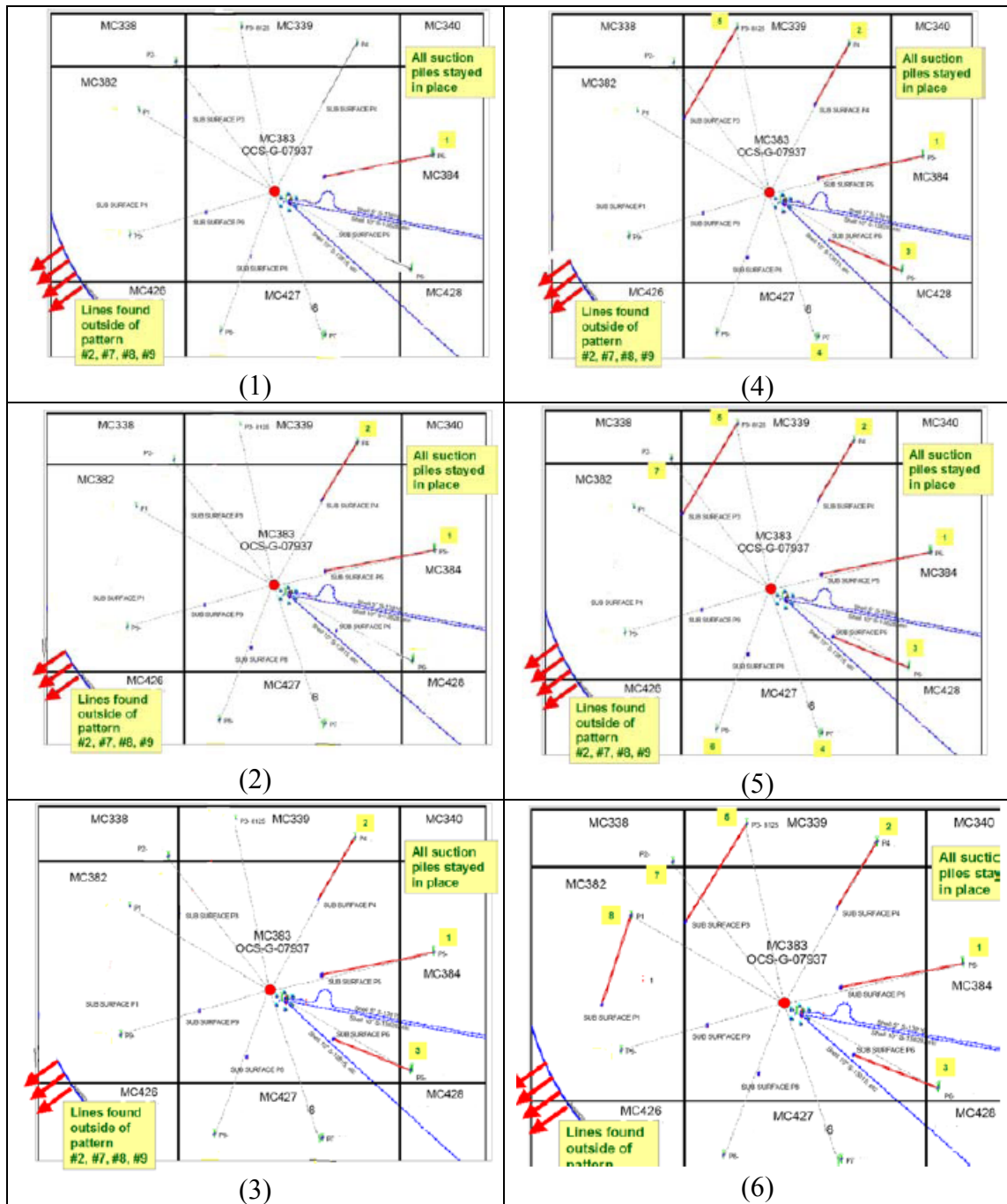


Figure 6.28: Diagrams showing the most probable sequence of line failure in order from (1) through (6) (Sharples 2004)



### **6.8.2 Deepwater Nautilus**

This MODU was moored using eight symmetrical mooring lines connected to suction caissons having a size of 2.9 m x 21.3 m (9.55' x 70'). This MODU was moored by a taut system, in which the mooring lines are a combination of wire rope-polyester rope-wire rope. A picture of this MODU and its spread mooring lines at the time of the event are shown in Figures 6.29 and 6.30. The best possible sequence of failures determined by the layout of the broken lines on the seafloor after the storm is depicted in Figure 6.31. The sequence starts in order from view (2) with the failure of the 1<sup>st</sup> line through view (8). At the time of Hurricane Ivan, the wind acted to the north, implying that the mostly heavily loaded line is Line No. 4. As predicted from this research, Line No. 4 failed first near the fairlead, followed by line Nos. 5, 3, 2, 6, 7, and 1. No foundation failures were reported except at anchor No. 8, which was observed to have traveled away with Line No. 8. The line No. 8 was still attached to the MODU at the time of recovery of the vessel. The failure of this system during Hurricane Ivan is also consistent with what is found in this study. This mooring system failed due to breakage of the mooring lines not due to failure in the foundations.



Figure 6.29: Deepwater Nautilus (Image from [www.rigzone.com](http://www.rigzone.com))

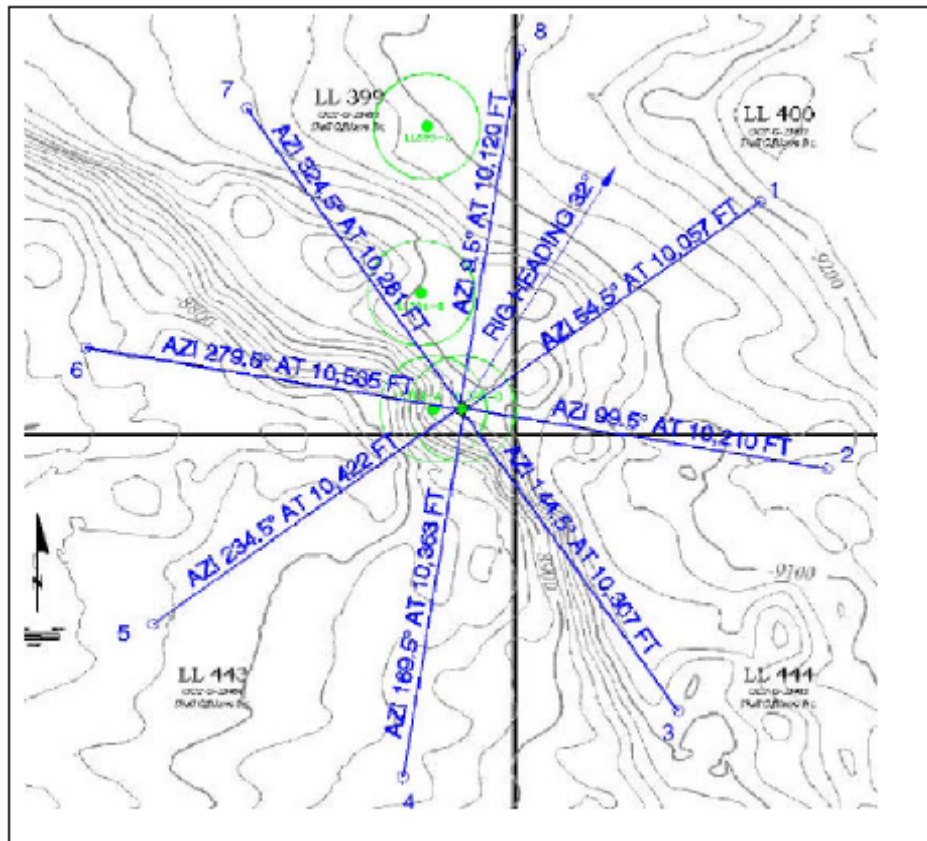


Figure 6.30: Mooring line pattern during Hurricane Ivan for Deepwater Nautilus (Sharples 2004)

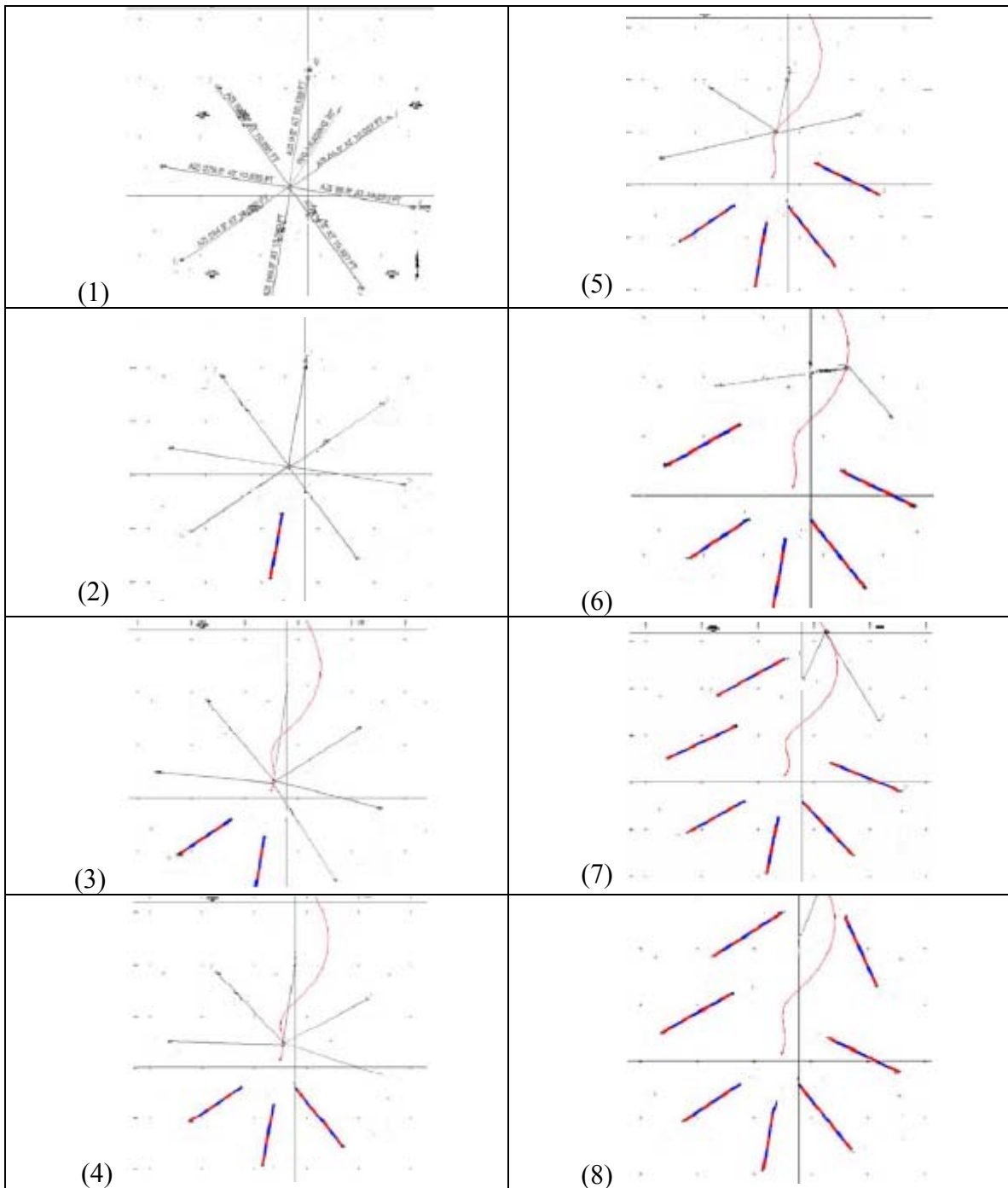


Figure 6.31: Diagrams showing the most probable sequence of line failure in order from (1) through (8) (Sharples 2004)

### **6.8.3 Comparisons of the predicted vs. actual performances of deepwater facilities**

Line Failure of these temporary floating structures is actually not surprising because, as prescribed in API RP-2SK (1997b), these MODU moorings were designed to commonly a 10-year return period hurricane. However, these three storms had very high wave heights which were much greater than the 100-year wave height (Sharples 2006). The mooring lines of these MODUs were also designed to the API standard with a factor of safety of 1.67 for the intact condition and a factor of safety of 1.25 for the damaged condition (Wisch 2006) which are the same as the factors of safety used for the reliability analysis in this study. Based on the presentation of the two moored rigs above, the systems had failed due to failure of the most heavily loaded lines at the fairlead and/or near the fairlead but not to failure of the foundations corresponding to the lines. The failure mode was predicted by the model in this study. Note that there were some cases where moored rigs during Hurricane Ivan were anchored to the mudline using drag anchors instead of suction caissons. They also failed due to the mooring lines at the fairlead (Sharples 2006).

In addition, based on the information that no major damage has been reported to deepwater permanent floating structures such as spars, they performed very well during these hurricanes (Wisch 2006). This would indicate that they had a very high reliability, as indicated in this study (Figure 6.24).

## **6.9 SUMMARY**

In this chapter, conducted were component and system reliabilities of the mooring systems in three different water depths using the information on the loads and capacities of the mooring lines and corresponding suctions under the extreme environmental loading conditions. The major conclusions found in this chapter are:

1. Mooring systems exhibit redundancy in that failure of the most heavily-loaded component during an extreme event does not necessarily lead to failure of the system. The redundancy is greater for the taut versus semi-taut systems and is greater during loop current events versus hurricane events.
2. Levels of reliability between mooring lines and anchors are not necessarily consistent; anchors have failure probabilities that are more than an order of magnitude smaller than those for lines under extreme loading.
3. The reliability for the taut systems is higher than that for the semi-taut system due to the relatively small contribution of environmental loading versus pre-tension for the taut systems.
4. Existing design guidelines provide for levels of system and component reliability against extreme loading that are above typical target levels that have been proposed by industry.
5. The reliability for a design that is governed by loop current events is greater than one that is governed by hurricane events due to smaller uncertainty in the environmental loading conditions during loop currents compared to hurricanes.
6. The failure mode of two moored systems during Hurricane Ivan is consistent with the results predicted from this study.
7. The deepwater permanent floating structures performed very well during Hurricanes Ivan, Katrina and Rita due to their high reliability.

## **Chapter 7: Summary, Conclusions and Implications**

### **7.1 SUMMARY**

Mooring systems for floating facilities that are used offshore to produce oil and gas, consisting of individual mooring lines and foundations, are currently designed on the basis of individual components. The most heavily loaded line and foundation are checked separately under extreme sea states, such as hurricanes and/or loop currents with the system of all lines intact and with one line removed. However, the station-keeping ability of the entire mooring system depends more directly on the reliability of the system consisting of lines and foundations rather than on the reliability of individual components. The main objective of this study is to assess and study the component and system reliabilities for the mooring system of a classical spar that is representative of existing practical technology in the Gulf of Mexico. Another objective is to assess the level of conservatism in the current design procedures of offshore foundations by comparing the predicted and actual performances of offshore deepwater mooring systems experienced during recent hurricanes such as Ivan, Katrina and Rita.

The spar chosen for this study was originally designed by the industry consortium, DeepStar. The mooring systems were designed for three different water depths: 1,000, 2,000 and 3,000 m (nominally, 3,000 ft, 6,000 ft and 10,000 ft, respectively). While steel wire ropes are used in 1,000 m of water depth, polyester ropes are employed in deeper depths.

A numerical model, known as COUPLE6D, was employed to simulate the interactions between the study spar and its mooring systems in three different water

depths under the impact of various storms or/and loop currents. The simulation predicts the global motion of the spar as well as tensions in the mooring lines as a function of time. The parameters of these storms and loop currents were chosen to represent a certain percentile of the probability distribution of their occurrence in the Gulf of Mexico during a 20-year design life span of the spar. From the resulting time histories and a probabilistic description of hurricanes and loop currents for the Gulf of Mexico, a probability distribution was developed for the maximum load in the most heavily loaded line during a hurricane and a loop current.

The vertical load at the anchor was then determined from the maximum load and corresponding angle in the mooring line at the mudline using the analytical model developed by Neubecker and Randolph (1995). The magnitude of the load at the padeye of a suction caisson was found to be smaller than that in the chain at the mudline due to the soil frictional resistance. Also, the angle of the load at the padeye was found to be steeper than that of the chain at the mudline because of the soil bearing resistance. The maximum vertical force on the foundation, which typically governs its design capacity, corresponds to the instant during a storm event of maximum tension and its associated angle in the chain at the mudline. Based on the vertical loads at the anchor, a probability distribution was developed for the expected maximum loads in foundations during a hurricane and a loop current as did for the maximum load in individual mooring lines. The related results are presented in Chapter 3. The results in this study indicate that the primary sources of the uncertainty in the expected maximum loads arise from uncertainty in occurrence and in magnitude of the storms and/or loop currents in the Gulf of Mexico.

In order to derive the capacity of a mooring system, the nominal design loads for a mooring line and its foundation were determined. Following the design practices used

by the offshore industry, the nominal design loads are selected to be equal to the expected maximum loads during extreme sea states, such as a 100-year hurricane or 100-year loop current. The nominal design capacity was set equal to the corresponding nominal design load multiplied by the factor of safety. Since the factor of safety in general was not unique but instead was bounded by a range, the design capacity depends on the choice of factors of safety even though the design load remains the same. Furthermore, the expected maximum loads and the design capacity depend on the type of extreme sea states, whether it is a 100-year hurricane or a 100-year loop current. Based on the design capacities of individual mooring components, such as top and bottom chains, middle steel wire or polyester ropes and suction caisson, their related strength models (or strength distribution) were established. The line and foundation capacities are described in Chapter 4.

Using these quantitative simulated results (i.e., loads related to line and foundation), capacities of the line and the foundation, and probability distributions of the extreme met-ocean conditions (hurricanes and loop currents) in the Gulf of Mexico, the probability of failure of individual mooring components was calculated first, then that of a complete mooring line which consists of top and bottom chains, a steel wire or polyester rope in the middle and a suction caisson buried in the seabed, and finally that of a mooring system. The probability of failure was calculated based on the load and capacity (strength) distributions. In this study, the reliability analysis was conducted based on a 100-year hurricane or a 100-year loop current.

In this study, a mooring system failure with respect to station-keeping was defined as the failure of two or more lines in the system. Individual sequences of line breakage and anchor pullout were considered to identify the most likely modes of failure in extreme conditions and to quantify redundancy in the system. The equations and



procedures for calculation of the probability of failure are described in Chapter 5. The results of the reliability analysis are presented in Chapter 6.

## **7.2 CONCLUSIONS**

The following conclusions are drawn from this study.

1. Levels of reliability between the mooring lines and anchors are not necessarily consistent. Specifically, anchors have failure probabilities that are more than an order of magnitude smaller than those for lines under extreme loading.
2. Mooring systems exhibit redundancy in that failure of the most heavily-loaded component during an extreme event does not necessarily lead to failure of the system. The redundancy was found to be greater for the taut versus semi-taut systems and is greater during loop current events versus hurricane events.
3. Existing design guidelines provide for levels of reliability against extreme loading for the system and components that are above typical target levels that have been proposed by industry.
4. The reliability for a design governed by loop current events was found to be greater than one governed by hurricane events. This difference was found to be due to the smaller uncertainty in the environmental loading conditions during loop currents compared to hurricanes.
5. The reliability for the taut systems is higher than that for the semi-taut system due to the relatively small contribution of environmental loading versus pre-tension for the taut systems.
6. The failure mode of two moored systems during Hurricane Ivan is consistent with the results predicted from this study.

7. The deepwater permanent floating structures performed very well during Hurricanes Ivan, Katrina and Rita indicating because of their high reliability.

### **7.3 IMPLICATIONS OF THIS RESEARCH**

Although this study focuses on the mooring systems of a classical spar structure, the methodology of the reliability analysis and the conclusions made in this study may have important implications on other mooring systems deployed in deep waters. This research provides several important contributions to the understanding of the component and system performances of the offshore foundations under extreme environmental loading conditions. The contributions include:

1. Existing foundations used for offshore structures in the Gulf of Mexico should be re-evaluated with the reliability methodology and the updated met-ocean criteria due to the recent hurricanes that are not yet available to the public.
2. More attention should be paid in a reliability assessment of deepwater floating structures to the effect of the lower-bound capacity on the reliability of foundation systems. This consideration of the lower-bound capacity will allow a more realistic management of risk in geotechnical engineering.
3. Through evaluation of the performance of the offshore production systems, this research identified the need for incorporating information on component and system reliabilities in reliability-based design methods for the mooring system to provide a more realistic and consistent level of reliability.
4. This study includes an investigation on how the performance of offshore foundations affects the performance of overall systems. Accordingly, the

performance of offshore structure systems can be understood in a more rational way by considering its reliability.

5. The current predictive models should be calibrated more with the real field performance database.
6. This study provides a good methodology to practitioners for design and analysis of future offshore foundations.
7. Insight is provided from this study into the current design practice in offshore foundations.

## References

- Ahilan, R. V., Cummins, I., Dyer, R. C., and Morris, W. D. M. (1996) "Reliability Analysis of FPSO Mooring Systems and the Interaction with Risers," Proceedings of the International Conference on Offshore Mechanics and Arctic Engineering Florence, Italy, Vol. 2, pp 287-302.
- Andersen, K. H., Murff, J. D., Randolph, M. F., Clukey, E. C., Erbrich, C. T., Jostad, H. P., Hansen, B., Aubeny, C. P., Sharma, P., and Supachawarote, C. (2005) "Suction Anchors for Deepwater Applications," Proceedings of the First International Symposium on Frontiers in Offshore Geotechnics (ISFOG), The University of Western Australia, Perth, pp 3-30.
- Ang, A. H. S., and Tang, W. H. (1975) Probability Concepts in Engineering Planning and Design, Volume 1 - Basic Principles: John Wiley & Sons, Inc.
- Ang, A. H. S., and Tang, W. H. (1984) Probability Concepts in Engineering Planning and Design, Volume 2 - Decision, Risk, and Reliability: John Wiley & Sons, Inc.
- API (1997a) "API Spec. 2F: Specification for Mooring Chain," American Petroleum Institute.
- API (1997b) "RP 2SK: Recommended Practice for Design and Analysis of Stationkeeping Systems for Floating Structures," American Petroleum Institute.
- API (2001) "RP 2FPS: Recommended Practice for Planning, Designing, and Constructing Floating Production Systems," American Petroleum Institute.
- API (2002) "RP 2A-WSD: Recommended Practice for Planning, Designing and Constructing Fixed Offshore Platforms - Working Stress Design," American Petroleum Institute.
- Aubeny, C. P., Han, S., and Murff, J. D. (2003a) "Refined Model for Inclined Load Capacity of Suction Caissons," Proceedings of the International Conference on Offshore Mechanics and Arctic Engineering, OMAE03-37502, Cancun, Mexico, Vol. 3, pp 883-887.
- Aubeny, C. P., Han, S. W., and Murff, J. D. (2003b) "Inclined Load Capacity of Suction Caissons," International Journal for Numerical and Analytical Methods in Geomechanics, Vol. 27, No. 14, pp 1235-1254.

- Aubeny, C. P., Murff, J. D., and Moon, S. K. (2001) "Lateral Undrained Resistance of Suction Caisson Anchors," *International Journal of Offshore and Polar Engineering*, Vol. 11, No. 3, pp 211-219.
- Balint, S. W., and Orange, D. (2006) "Panel Discussion: Future of the Gulf of Mexico after Katrina and Rita," *Offshore Technology Conference*, OTC18410, Houston, TX.
- Banon, H., Cornell, C. A., and Harding, S. J. (1991) "Probabilistic Combination of Forces in Tension Leg Platform Tethers," *Journal of Structural Engineering*, Vol. 117, No. 5, pp 1532-1548.
- Banon, H., and Harding, S. J. (1989) "Methodology for Assessing Reliability of Tension Leg Platform Tethers," *Journal of Structural Engineering*, Vol. 115, No. 9, pp 2243 - 2260.
- Banon, H., Toro, R. G., Jefferys, E. R., and De, R. S. (1994) "Development of Reliability-Based Global Design Equations for TLPs," *Proceedings of the International Conference on Offshore Mechanics and Arctic Engineering* Vol. 2, pp 335-344.
- Bea, R. G., Iversen, R., and Xu, T. (2001) "Wave-in-Deck Forces on Offshore Platforms," *Journal of Offshore Mechanics and Arctic Engineering*, Vol. 123, No. 1, pp 10-21.
- Bea, R. G., Jin, Z., Valle, C., and Ramos, R. (1999) "Evaluation of Reliability of Platform Pile Foundations," *Journal of Geotechnical and Geoenvironmental Engineering*, Vol. 125, No. 8, pp 696-704.
- Bea, R. G., and Mortazavi, M. M. (1995) "Simplified Evaluation of the Capacities of Template-Type Offshore Platforms," *Proceedings of the International Offshore and Polar Engineering Conference*. Hague, Neth, p 185.
- Bea, R. G., and Mortazavi, M. M. (1996) "ULSLEA: A Limit Equilibrium Procedure to Determine the Limit State Loading of Template-Type Platforms," *Journal of Offshore Mechanics and Arctic Engineering*, Vol. 118, No. 4, pp 267-275.
- Bhat, S. S., Cermelli, C. A., and Lo, K. H. (2002) "Polyester Mooring for Ultra-Deepwater Applications," *Proceedings of the International Conference on Offshore Mechanics and Arctic Engineering - OMAE*, Oslo, Norway, Vol. 1, pp 513-518.
- Billington, C. J., Bolt, H. M., and Ward, K. J. (1993) "Reserve, Residual and Ultimate Strength Analysis of Offshore Structures: State of the Art Review," *Singapore*, Singapore, pp 125-133.

- Bruen, F. J., Gordon, R. B., and Vyas, Y. K. (1991) "Reliability of a Deepwater Gulf of Mexico FPS Spread Mooring," Proceedings of the International Conference on Offshore Mechanics and Arctic Engineering Vol. 2, pp 179-186.
- Bush, R. B., Luo, Y., and Jack, R. L. (1992) "How Chain Cable Reliability Affects Mooring System Design, Part 2: A Mathematical Model of Mooring Chain Strength Provides a Useful Start toward Evaluating the Effects of Various Chain Cable Quality Control, Certification and Irm Procedures," Ocean Industry, Vol. 27, No. 4, pp 35-37.
- Byrne, B. W., and Houlsby, G. T. (1999) "Drained Behaviour of Suction Caisson Foundations on Very Dense Sand," Proceedings of the Annual Offshore Technology Conference, Vol. 1, pp 765-782.
- Cassidy, M. J., Byrne, B. W., and Randolph, M. F. (2004) "A Comparison of the Combined Load Behaviour of Spudcan and Caisson Foundations on Soft Normally Consolidated Clay," Geotechnique, Vol. 54, No. 2, pp 91-106.
- Chen, X., Zhang, J., Liagre, P., Niedzwecki, J., and Teigen, P. (2002) "Coupled Dynamic Analysis of a Mini TLP: Comparison with Measurements," 21st International Conference on Offshore Mechanics and Arctic Engineering-OMAE.
- Chiralaksanakul, A., and Mahadevan, S. (2004) "Reliability-Based Design Optimization Methods," Proceedings of the ASME Design Engineering Technical Conference, Salt Lake City, UT, United States, Vol. 1, pp 837-845.
- Cho, Y., Lee, T. H., Chung, E. S., and Bang, S. (2003) "Field Tests on Pullout Loading Capacity of Suction Piles in Clay," Proceedings of the International Conference on Offshore Mechanics and Arctic Engineering, OMAE, pp. 7.
- Choi, Y. J., Gilbert, R. B., Ding, Y., and Zhang, J. (2006) "Reliability of Mooring Systems for Floating Production Systems," OTRC, pp 114.
- Clukey, E. C. and Morrison, M. J. (1993) "A Centrifuge and Analytical Study to Evaluate Suction Caissons for TLP Applications in the Gulf of Mexico," Geotechnical Special Publication No. 38, ASCE, pp. 141-156.
- Clukey, E. C., Aubeny, C. P., and Murff, J. D. (2004) "Comparison of Analytical and Centrifuge Model Tests for Suction Caissons Subjected to Combined Loads," Journal of Offshore Mechanics and Arctic Engineering, Vol. 126, No. 4, pp 364-367.
- Clukey, E. C., Banon, H., and Kulhawy, F. H. (2000) "Reliability Assessment of Deepwater Suction Caissons," Proceedings of the Annual Offshore Technology Conference, Houston, TX, USA, Vol. 1, pp 777-785.

- Clukey, E. C., and Phillips, R. (2002) "Centrifuge Model Tests to Verify Suction Caisson Capacities for Taut and Semi-Taut Legged Mooring Systems," Proceedings of International Conference on Deepwater Offshore Technology.
- Dangayach, S. (2004) "Reliability Analysis for Mooring System of a Spar in Deepwater Gulf of Mexico," M.S. Thesis, The University of Texas at Austin, pp 85.
- Degenkamp, G., and Dutta, A. (1989) "Soil Resistances to Embedded Anchor Chain in Soft Clay," Journal of Geotechnical Engineering, Vol. 115, No. 10, pp 1420-1438.
- Ding, Y., Kim, M. S., Chen, X., and Zhang, J. (2003) "Coupled Analysis of Floating Production System," Deepwater Mooring Systems Concepts, Design, Analysis, and Material, Houston, TX, pp 152-167.
- El-Sherbiny, R. M., Olson, R. E., Gilbert, R. B., and Vanka, S. K. (2005) "Capacity of Suction Caissons under Inclined Loading in Normally Consolidated Clay," Proceedings of the First International Symposium on Frontiers in Offshore Geotechnics (ISFOG), The University of Western Australia, Perth, Australia.
- Faltinsen, O. M. (1990) Sea Loads on Ships and Offshore Structures, Cambridge Ocean Technology Series, Cambridge University Press.
- Gault, J. A., and Cox, W. R. (1974) "Method for Predicting Geometry and Load Distribution in an Anchor Chain from a Single Point Mooring Buoy to a Buried Anchorage," Houston, TX, pp 309-318.
- Gilbert, R. B., Choi, Y. J., Dangayach, S., and Najjar, S. S. (2005) "Reliability-Based Design Considerations for Deepwater Mooring System Foundations," Proceedings of the First International Symposium on Frontiers in Offshore Geotechnics (ISFOG), The University of Western Australia, Perth, pp 317-323.
- Gilbert, R. B., Gambino, S. J., and Dupin, R. M. (1999) "Reliability-Based Approach for Foundation Design without Site-Specific Soil Borings," Proceedings of the Annual Offshore Technology Conference, Houston, TX, Vol. 1, pp 631-640.
- Gilbert, R. B., and Murff, J. D. (2001a) "Design Methodologies and Criteria for Suction Caissons for Deepwater Mooring Applications," Workshop Report: Offshore Technology Research Center.
- Gilbert, R. B., and Murff, J. D. (2001b) "Identifying Uncertainties in the Design of Suction Caisson Foundations," Proceedings of International Conference on Geotechnical, Geological and Geophysical Properties of Deepwater Sediments Honoring Wayne A. Dunlap, Houston, TX, pp 231-242.
- Goodwin, P., Ahilan, R. V., Kavanagh, K., and Connaire, A. (1999) "Integrated Mooring and Riser Design: Reliability Analysis Methodology and Preliminary Results,"

- Proceedings of the Annual Offshore Technology Conference, Vol. 2 (I), pp 341-353.
- Goodwin, P., Ahilan, R. V., Kavanagh, K., and Connaire, A. (2000) "Integrated Mooring and Riser Design: Target Reliabilities and Safety Factors," Proceedings of the International Conference on Offshore Mechanics and Arctic Engineering New Orleans, LA, USA.
- Harding, S. J., and Banon, H. (1989) "Reliability of TLP Tethers under Maximum and Minimum Lifetime Loads," Offshore Technology Conference, Houston, TX, pp 519 - 528.
- Heredia-Zavoni, E., Campos, D., and Ramirez, G. (2004) "Reliability Based Assessment of Deck Elevations for Offshore Jacket Platforms," Journal of Offshore Mechanics and Arctic Engineering, Vol. 126, No. 4, pp 331-336.
- Houlsby, G. T., and Wroth, C. P. (1982) "Direct Solution of Plasticity Problems in Soils by the Method of Characteristics," Proceedings of the Fourth International Conference on Numerical Methods in Geomechanics, Alberta, Can, pp 1059-1071.
- House, A. R., and Randolph, M. F. (2001) "Installation and Pullout Capacity of Stiffened Suction Caissons in Cohesive Sediments," Proceedings of 11th International Offshore and Polar Engineering Conference.
- Larsen, K. (1996) "Efficient Reliability-Based Design of Mooring Systems," Proceedings of the International Conference on Offshore Mechanics and Arctic Engineering Vol. 2, pp 349-359.
- Larsen, K., and Mathisen, J. (1996) "Reliability-Based Fatigue Analysis of Mooring Lines," Proceedings of the International Conference on Offshore Mechanics and Arctic Engineering - OMAE, Florence, Italy, Vol. 2, pp 277-285.
- Li, H., and Foschi, R. O. (1998) "An Inverse Reliability Method and Its Application," Structural Safety, Vol. 20, No. 3, pp 257-270.
- Luke, A. M. (2002) "Axial Capacity of Suction Caissons in Normally Consolidated Kaolinite," M.S. Thesis, The University of Texas at Austin, p 227.
- Luke, A. M., Rauch, A. F., Olson, R. E., and Meacham, E. C. (2003) "Behavior of Suction Caissons Measured in Laboratory Pullout Tests," Proceedings of the International Conference on Offshore Mechanics and Arctic Engineering, OMAE, pp. 9.



- Luke, A. M., Rauch, A. F., Olson, R. E., and Meacham, E. C. (2005) "Components of Suction Caisson Capacity Measured in Axial Pullout Tests," *Ocean Engineering*, Vol. 32, No. 7, pp 878-891.
- Luo, Y., and Ahilan, R. V. (1992) "Probabilistic Chain Cable Strength and Mooring Reliability," *Offshore Technology Conference*, Houston, TX, pp 249-256.
- Ma, W., Webster, W. C., 1994. *An Analytical Approach to cable Dynamics: Theory and User Manual*. SEA GRANT PROJECT R/OE-26.
- Martin, C. M., and Houlsby, G. T. (2001) "Combined Loading of Spudcan Foundations on Clay: Numerical Modeling," *Geotechnique*, Vol. 51, No. 8, pp 687-699.
- Minguez, R., Castillo, E., and Hadi, A. S. (2005) "Solving the Inverse Reliability Problem Using Decomposition Techniques," *Structural Safety*, Vol. 27, No. 1, pp 1-23.
- Murff, J. D., and Hamilton, J. M. (1993) "P-Ultimate for Undrained Analysis of Laterally Loaded Piles," *Journal of Geotechnical Engineering*, Vol. 119, No. 1, pp 91-107.
- Murff, J. D., and Young, A. G. (2007) "Suction Caissons for Deepwater Moorings," *Geo-Strata*, pp 12-16.
- Murty, A. S. R., and Naikan, V. N. A. (1996) "Reliability Strength Design through Inverse Distributions-Exponential and Weibull Cases," *Reliability Engineering & System Safety*, Vol. 54, No. 1, pp 77-82.
- Najjar, S. S. (2005) "The Importance of Lower-Bound Capacities in Geotechnical Reliability Assessments," Ph.D. Dissertation, The University of Texas at Austin, p 347.
- Najjar, S. S., and Gilbert, R. B. (2006) "Suction Caissons: Seafloor Characterization for Deepwater Foundation Systems, " *Final Report prepared for the Minerals Management Service*, p 49.
- Neubecker, S. R., and Randolph, M. F. (1995) "Performance of Embedded Anchor Chains and Consequences for Anchor Design," *Offshore Technology Conference*, Houston, TX, pp 191-200.
- Olson, R. E. (2005) *Class Notes for Foundation Engineering Course: The University of Texas at Austin*.
- Petruska, D., Geyer, J., Macon, R., Craig, M., Ran, A., and Schulz, N. (2005) "Polyester Mooring for the Mad Dog Spar-Design Issues and Other Considerations," *Ocean Engineering*, Vol. 32, No. 7 SPEC ISS, pp 767-782.

- Randolph, M. F., and House, A. R. (2002) "Analysis of Suction Caisson Capacity in Clay," Proceedings of the Annual Offshore Technology Conference, Houston, TX, United States, pp 2145-2155.
- Reese, L. C., Cox, W. R., and Koop, F. D. (1974) "Analysis of Laterally Loaded Piles in Sand," Offshore Technology Conference, OTC 2080, Houston, Vol. 1, pp 473-483.
- Rosenblatt, M. (1952) "Remarks on a multivariate transformation," The Annals of Mathematical Statistics, 23(3), pp 470-472.
- Saranyasoonorn, K., and Manuel, L. (2004) "A Comparison of Wind Turbine Design Loads in Different Environments Using Inverse Reliability Techniques," Journal of Solar Energy Engineering, Transactions of the ASME, Vol. 126, No. 4, pp 1060-1068.
- Sharples, M. (2004) "Post Mortem Failure Assessment of Modus During Hurricane Ivan," Prepared for Minerals Management Service, p 97.
- Siddiqui, N. A., and Ahmad, S. (2000) "Reliability Analysis against Progressive Failure of TLP Tethers in Extreme Tension," Reliability Engineering and System Safety, Vol. 68, No. 3, pp 195-205.
- Skempton, A. W. (1951) "The Bearing Capacity of Clays," Building Research Congress, pp 180-189.
- Snell, R., and Versavel, T. (1999) "Reliability of Mooring Systems: Application to Polyester Moorings," Offshore Technology Conference, Houston, TX, USA, Vol. 3, pp 125-131.
- Stear, J., and Bea, R. (1997) "Ultimate Limit State Capacity Analyses of Two Gulf of Mexico Platforms," Offshore Technology Conference, Houston, TX, USA,
- Stear, J. D., and Bea, R. G. (1998) "Simplified Strength-Level Earthquake Assessment of Jacket-Type Platforms," Proceedings of the International Offshore and Polar Engineering Conference, Montreal, Can, Vol. 4, pp 492-503.
- Tang, W. H., and Gilbert, R. B. (1992) "Offshore Pile System Reliability," p 156.
- Tang, W. H., and Gilbert, R. B. (1993) "Case Study of Offshore Pile System Reliability," Proceedings - Annual Offshore Technology Conference, Houston, TX, USA, pp 677-683.
- Terzaghi, K., Peck, R. B., and Mesri, G. (1996) Soil Mechanics in Engineering Practice, New York: John Wiley and Sons, Inc.

- Vanmarcke, E. H. (1983) Random Fields: Analysis and Synthesis: The MIT Press (Cambridge, Massachusetts).
- VanShaar, S. R. (2002) "Dynamic Analysis for Suction Caissons and Geologic Model for Makassar Strait," M.S. Thesis, The University of Texas at Austin, p 171.
- Vivatrat, V., Valent, P. J., and Ponterio, A. A. (1982) "The Influence of Chain Friction on Anchor Pile Design," Houston, TX, pp 153-163.
- Ward, E. G. (2005) personal communication on loop current characteristics and models.
- Watson, P. G., Randolph, M. F., and Bransby, M. F. (2000) "Combined Lateral and Vertical Loading of Caisson Foundations," Proceedings of the Annual Offshore Technology Conference, OTC12195, Houston, TX, USA, Vol. 1, pp 797-808.
- Whitman, R. V. (1984) "Evaluating Calculated Risk in Geotechnical Engineering," J. Geotech. Engrg., Vol. 110, No. 2, pp 145-188.
- Whitman, R. V. (2000) "Organizing and Evaluating Uncertainty in Geotechnical Engineering," Journal of Geotechnical and Geoenvironmental Engineering, Vol. 126, No. 7, pp 583-593.
- Winterstein, S. R., and Kumar, S. (1995) "Reliability of Floating Structures: Extreme Response and Load Factor Design," Houston, TX, pp 569-578.
- Winterstein, S. R., Ude, T. C., Cornell, C. A., Bjerager, P., and Haver, S. (1993) "Environmental Parameters for Extreme Response. Inverse Form with Omission Factors," Innsbruck, Austria, Vol. 1, pp 551-557.
- Wisch, D. J. (2006) "Observations of Hurricane Impacts on Deepwater Facilities," Offshore Technology Conference, OTC18414, Houston, TX.

## **Vita**

Young Jae Choi was born to Yoon Ki Choi and Gui Ja Kim in Pusan, Korea in 1970. After graduating from Dong-A high school located in Pusan in 1989, he enrolled at Pusan National University and majored in civil engineering. After finishing sophomore study, he joined the Korean Army to finish a 1.5 year mandatory military service. He then reenrolled at the university and earned a Bachelor of Engineering degree in February 1995. Before he came to US in August 2000, he worked for one of major EPC companies in Korea, Daelim Engineering Co., Ltd., and later Daelim Industry Co., Ltd., for a total of 5.5 years including 1 year of experience as a field engineer in the Philippines. He began graduate studies at the University of Colorado at Boulder in the fall of 2000 and specialized in geotechnical engineering. After earning an MS degree in the spring of 2002, he entered The University of Texas at Austin in August 2002 to begin work on his Ph.D. degree in geotechnical engineering. During the period of his study at the school, he specially won an Outstanding Teaching Assistant/Assistant Instructor Award in March 2007.

Permanent address: 998-19 6/3 NamSan-Dong, KumJung-Ku, Pusan, Korea

This dissertation was typed by Young Jae Choi.